THERMODYNAMIC INVESTIGATIONS OF SOME AQUEOUS SOLUTIONS THROUGH CALORIMETRY AND DENSIMETRY

ROBERT A. MARRIOTT

B.Sc., University of Lethbridge, 1998

A Thesis

Submitted to the Council on Graduate Studies

of the University of Lethbridge in Partial Fulfilment of the

Requirements for the Degree

MASTER OF SCIENCE

LETHBRIDGE, ALBERTA

July, 1999

FOR GRAMPA BOLIVAR

ABSTRACT

Relative densities and heat capacity ratios have been measured for selected aqueous systems. These measurements have been used to calculate apparent molar volumes and heat capacities.

Densities of aqueous sodium bromide have been measured from 374 to 522 K and 10.00 to 30.00 MPa using a recently developed high temperature and pressure vibrating tube densimeter. These data have been used to test the utility of an automated high temperature and pressure densimetric data analysis program.

Apparent molar volumes and heat capacities of several aqueous rare earth sulphate systems at 298.15 K and 0.10 MPa have been reported, and discussed in terms of ionic contributions. Single ion partial molar volumes and heat capacities for aqueous trivalent rare earth species have been estimated in a review of apparent molar data from the literature and through the use of a semi-empirical Debye-Hückel equation. These single ion properties have subsequently been used to estimate the single ion properties of the monosulphate and disulphate rare earth complex species. Rigorous relaxation calculations are presented in a discussion of apparent molar heat capacities, where relaxation contributions are shown to be negative.

Apparent molar volumes and densities for aqueous L-histidine, L-phenylalanine, L-tyrosine, L-tryptophan, and L-dopa have been used to estimate reported partial molar properties at infinite dilution and at 288.15, 298.15, 313.15, and 328.15 K. These infinite dilution properties have been added to several reported properties for other amino acids and peptides to construct an additivity scheme that utilises the revised Helgeson, Kirkham, and Flowers (HKF) equations of state for neutral organic species.

A volumetric study of aqueous glycine, L-serine, and glycylglycine has been conducted at temperatures from 298 K to 423 K and pressures from 0.10 to 30.00 MPa. These data have been used to evaluate HKF coefficients in a discussion of peptide stability at elevated temperatures and pressures.

ACKNOWLEDGEMENTS

Leanne: Without your patience, encouragement, and understanding my studies would not be possible. Thank you.

I wish to sincerely thank my supervisor, Dr. Andrew Hakin, for his encouragement, patience, guidance, and friendship. Without exception, it was always a pleasure to work with Dr. Hakin.

I am thankful to Luis Delgado, Dave Daisley, Frank Klassen, and Greg Tompkins for their interest and patience in sharing their skills and experience. These combined talents complemented and made possible all high temperature and pressure investigations reported in Chapters 4 and 7.

I am grateful to Dr. Marc Roussel for the use of his computer systems and sharing his knowledge in the collaborative study contained in Chapter 4.

In connection with the rare earth sulphate investigations of Chapter 5, I'm grateful to Dr. Joe Rard for supplying chemicals and offering extensive guidance during the writing of this chapter. I would also like to thank Meg O'Shea for assisting with calculations.

A special word of appreciation is due to my friend Quintin for encouragement and listening, even when he may not have had any interest. I greatly appreciate the help of Jin Lian Liu for her assistance with measurements and helpful comments. Words of advice from Dr. René Boeré, Dr. Seamus O'Shea, Dr. Earl Woolley, and Bob McKay were also greatly appreciated. With regards to assistance with the NMR instrument, I am grateful to Dr. Kevin Smith and Dr. Peter Dibble.

Finally I wish to thank my parents, including inlaws, outlaws, and others.

TABLE OF CONTENTS

APPENDICES

LIST OF FIGURES

LIST OF TABLES

1) INTRODUCTION

The extent of any path independent process, such as a chemical reaction, can be elegantly described by thermodynamic relationships. Because most processes and chemical reactions occur in a diverse region of conditions, understanding the thermodynamic consequences of changing the temperature and/or pressure of the chemical system is of paramount importance. Following this theme, this thesis involves the measurement of heat capacities and densities. These properties provide insight into the manner in which chemical equilibria respond to changes in their environment. For many solution systems, these experimental properties also indicate how solutes interact with other solute and solvent molecules. Investigated aqueous solution systems have been identified by the lack of available experimental thermodynamic data within the literature, their importance to environmental issues, and their importance to the understanding of biochemical interactions. The thesis consists of 8 Chapters and encompasses 4 experimental studies.

The second Chapter introduces thermodynamic relationships and nomenclature for electrolyte and non-electrolyte solutions. Partial and apparent molar properties are defined in terms of theoretical and experimental relationships which are utilised in subsequent studies reported in the thesis. Some electrostatic theories useful in modelling the aforementioned properties are also discussed.

Chapter three describes the measurement techniques used throughout the thesis. This Chapter includes information on measuring heat capacities using a Picker microflow calorimeter, and measuring densities using a vibrating tube densimeter. The vibrating tube densimeters discussed include a commercially available Sodev O2D densimeter and an in-house built high temperature and pressure densimeter.

The fourth Chapter deals with improving the analysis of data produced by the high temperature and pressure densimeter. This improvement comes through an automated

computer analysis program that has been written specifically for the instrument, yet is comparable to other types of automated analysis.

The utility of experimental thermodynamics in describing equilibrium states is the focus of Chapters five through seven. In most cases, heat capacities and volumes for the various species investigated within this thesis are only available at 298.15 K and 0.10 MPa within the literature. In the case of the rare earth sulphate species investigated in Chapter five, data have been unavailable even at these ambient conditions. Thus Chapter five is an investigation into the partial molar heat capacities and densities of rare earth sulphates. These properties have been discussed in terms of the heat capacity and volume change associated with the extensive formation of complex aqueous monosulphate and disulphate species.

The thermodynamic characterisation of important biochemicals in water is the topic of Chapters six and seven. Apparent molar heat capacities and volumes for aqueous L-histidine, L-phenylalanine, L-tyrosine, L-tryptophan, and L-dopa are reported at 288.15, 298.15, 313.15, and 328.15 K (0.10 MPa) in Chapter six. These properties have been added to an ongoing data base of extensive thermodynamic data for aqueous amino acid and peptide systems and applied in an additivity model using the revised Helgeson, Kirkham, and Flowers equations of state for neutral organic species.

In Chapter seven, our interest in the thermodynamic properties of aqueous amino acids and peptides is further indulged with a volumetric investigation of aqueous solutions of L-serine, glycine, and glycylglycine at elevated temperature and pressure. These investigations have permitted the calculation of equilibrium properties over a large temperature and pressure range and complement the previous data set utilised in Chapter six.

Chapter eight is devoted to summarising some of the conclusions one can draw from the thesis and identifies several future directions for research in this area.

2) SOLUTION THERMODYNAMICS.

2.1 Introduction

Thermodynamics is a useful tool for describing equilibrium states of many systems through understanding equations of state. As a direct result of the first and second laws of thermodynamics, Duhem's law shows that fixed composition systems at equilibrium can be described in terms of a maximum of two fixed state variables (Anderson and Crerar, 1993). By Duhem's law the Gibbs energy of a system, G, can be described as the potential of a system to equilibrate under the conditions of constant temperature, T, and pressure, p. Although the state variables, T and p, can be measured, the Gibbs energy of the homogeneous system cannot; therefore, reversible changes in Gibbs energy for a system of fixed composition may be described by

$$dG = \left(\frac{\partial G}{\partial T}\right)_p dT + \left(\frac{\partial G}{\partial p}\right)_T dp = -S\,dT + V\,dp, \qquad (2.1)$$

where the entropy state variable, S, and volume, V, are defined through the first and second laws of thermodynamics. By definition $dG=0$ at equilibrium. Therefore any spontaneous process must involve a negative change in the Gibbs energy of the system (Anderson and Crerar, 1993; Pitzer and Brewer, 1961).

If a system has more than one component, the change in molar Gibbs energy can also be shown in terms of activity, a, which describes the extent of deviation from any defined standard state, denoted by ^{o}:

$$\begin{aligned}\Delta\bar{G} &= \Delta\bar{G}_{i,products} - \Delta\bar{G}_{i,reactants} \\ &= \Delta\bar{G}^{o}_{i,products} - \Delta\bar{G}^{o}_{i,reactants} + \sum_{products} RT \ln a_j - \sum_{reactants} RT \ln a_j \\ &= \Delta\bar{G}^{o} + RT \ln Q. \qquad (2.2)\end{aligned}$$

Equation 2.2 shows this relationship for any process, where the reaction quotient, Q, is defined as the ratio of activities, R is the gas constant (8.31451±0.00007 J mol^{-1} K^{-1}), i

refers to any path independent process, and j refers to any individual species involved in the process. Since at equilibrium, $\Delta\bar{G}=0$, an equilibrium constant, K, or the activity ratio at equilibrium is defined by the standard state Gibbs energy change:

$$\Delta\bar{G}^{o} = -RT \ln K. \tag{2.3}$$

As derived from equation 2.1, equation 2.4 shows that the pressure dependence of a Gibbs energy change is defined by the volume, V. The change in molar volume of a defined standard state is therefore related to the pressure dependence of the equilibrium constant using equation 2.5:

$$V = \left(\frac{\partial G}{\partial p}\right)_T \tag{2.4}$$

$$\left(\frac{\partial \ln K}{\partial p}\right)_T = -\frac{\Delta\bar{V}^{o}}{RT}. \tag{2.5}$$

Equation 2.5 shows the importance of volumetric data to the understanding of equilibrium changes over a range of pressures.

Through the definition of heat capacity at constant pressure, C_p, equation 2.6 shows the temperature dependence of the enthalpy, H. Application of the second law to equation 2.6 shows that the temperature dependence of entropy can also be described by the constant pressure heat capacity:

$$C_p = \left(\frac{\partial H}{\partial T}\right)_p = T\left(\frac{\partial S}{\partial T}\right)_p. \tag{2.6}$$

From equations 2.1 and 2.3 the heat capacity describes the temperature dependence of any equilibrium constant by equations 2.7 and 2.8:

$$\left(\frac{\partial \ln K}{\partial T}\right)_p = \frac{\Delta\bar{H}^{o}}{RT^2} \tag{2.7}$$

and

$$\Delta\bar{C}_p^{o} = \left(\frac{\partial \Delta\bar{H}^{o}}{\partial T}\right)_p. \tag{2.8}$$

If an equilibrium constant is known at one specific temperature, equations 2.4 and 2.7 can be used to describe the the same equilibrium over a range of temperatures and pressures. However, to describe equilibrium systems over a continuous temperature and pressure surface, the pressure dependence of the heat capacity and volumetric temperature dependence are also required. By using equation 2.1 to describe a Gibbs energy change, such that equilibrium is maintained, equation 2.9 can be derived. Equation 2.9 shows that volumetric temperature dependence is equivalent to the pressure dependence of the entropy:

$$-\left(\frac{\partial V}{\partial T}\right)_p = \left(\frac{\partial S}{\partial p}\right)_T . \tag{2.9}$$

It necessarily follows that the pressure dependence of the heat capacity can be calculated if the temperature dependence of the volume is known and *vice versa*:

$$-T\left(\frac{\partial^2 V}{\partial T^2}\right)_p = \left(\frac{\partial C_p^o}{\partial p}\right)_T . \tag{2.10}$$

Thus, with a temperature dependent description of the heat capacity, a pressure and temperature dependent description of volume, and knowledge of the thermodynamic relationships, equilibrium can be described over a continuous temperature and pressure surface.

Since most systems are composed of several species, the Gibbs energy must be described in terms of multiple components in addition to temperature and pressure variables. Therefore additional differentials must be applied to equation 2.1, yielding equation 2.11 for any reversible Gibbs energy change:

$$dG = \left(\frac{\partial G}{\partial T}\right)_{p,n_i} dT + \left(\frac{\partial G}{\partial p}\right)_{T,n_i} dp + \sum_i \left(\frac{\partial G}{\partial n_i}\right)_{n_{j\neq i},T,p} dn_i . \tag{2.11}$$

2.2 Partial molar and apparent molar properties

With complex multi-component systems such as solutions, it is often easier to describe the system in terms of the intrinsic or molar properties rather than the extensive properties. The partial molar Gibbs energy of any species, i, has been given its own name,

the chemical potential, μ_i, and can be used to describe individual component properties of macroscopic systems such as solvent and solute properties (Pitzer, 1991):

$$\mu_i = \left(\frac{\partial G}{\partial n_i}\right)_{n_{j\neq i},\, T,\, p}. \tag{2.11}$$

In general any partial molar property, $\bar{Y}$, can be defined by

$$\bar{Y}_i = \left(\frac{\partial Y}{\partial n_i}\right)_{n_{j\neq i},\, T,\, p}. \tag{2.12}$$

Furthermore, partial molar properties can be described by equations similar to those of the extensive properties, therefore defining partial molar volumes and heat capacities:

$$V = \left(\frac{\partial G}{\partial p}\right)_T \quad \Rightarrow \quad \bar{V}_i = \left(\frac{\partial \mu_i}{\partial p}\right)_T \tag{2.13}$$

and

$$C_p = \left(\frac{\partial H}{\partial T}\right)_p \quad \Rightarrow \quad \bar{C}_{pi} = \left(\frac{\partial \bar{H}_i}{\partial T}\right)_p. \tag{2.14}$$

Any extensive property of a system can now be calculated as the sum of the respective partial molar properties if all components have a known concentration. Although the additive definition of partial molar properties is convenient, direct measurements for these solution properties are difficult, because partial molar properties contain contributions from interactions with other species. When dealing with solutions it is more common to measure the apparent molar quantities, Y_ϕ, which can be defined as the change in property Y due to a known amount of solute in a known amount of solvent, assuming the solvent contributes the same as would its pure species. In other words, all changes in the state property can be attributed to the presence of the solute, even if those changes involve a change in the partial molar property of the solvent. The apparent molar property of any solute (i{solvent}=1 and i{solute}=2), $Y_{2,\phi}$, is defined by

$$Y_{2,\phi} = \frac{Y - n_1 \bar{Y}_1^o}{n_2}, \tag{2.15}$$

where n_1 defines the moles of solvent and n_2 defines the moles of solute in the system. $\bar{Y}_1^o$ defines the molar property of the pure solvent.

Because the solvent is assumed to contribute a constant quantity for all solute concentrations at fixed temperature and pressure, the partial derivative of the extensive property with respect to the moles of solute can be defined in terms of the apparent molar quantity:

$$\left(\frac{\partial Y}{\partial n_2}\right)_{n_1,T,p} = n_2 \left(\frac{\partial Y_{2\phi}}{\partial n_2}\right)_{n_1} + Y_{2,\phi} . \qquad (2.16)$$

Equation 2.16 and equation 2.12 show that if the apparent molar property and its derivative with respect to moles of solute are known[1], the partial molar property can be calculated. More importantly, if any good equation for the apparent molar property with respect to any concentration scale can be found from agreement with experimental data, the apparent molar property at infinite dilution can be also found. Theoretically as the concentration approaches zero the apparent molar volume approaches the partial molar volume of the solute at infinite dilution, because by definition the solvent is already assumed to be in a pure form. If the apparent molar property is assumed to reflect the apparent molar property of only the solute and not some solute-solvent complex, then the apparent molar property at infinite dilution, $Y_{2,\phi}^{\infty}$ would be equal to the standard state molar property of the solute, as defined by Henry's law. Without accepting the previous equality, equations of state developed for standard state partial molar variables have been used successfully to describe partial molar quantities at infinite dilution.

Apparent molar volume data as a function of concentration have been well represented by several equations (Millero, 1971; Robinson & Stokes, 1965). For non-electrolytes in solution it is common to choose a polynomial which best represents the data. Electrolyte solutions, however, are usually treated with various Debye-Hückel type equations, because Debye-Hückel theory can aid in predicting a reasonable slope for

---

[1]Any derivative with respect to moles of solute (e.g. equation 2.16) is equivalent to the derivative with respect to any scale which is directly proportional to the moles of solute. These scales include common concentration scales and if the valence factor is constant over a range of concentrations, ionic strength may also be used in equation 2.16.

electrolyte solutions near infinite dilution. This predicted slope increases the precision of the extrapolation to infinite dilution, because the infinite dilution value can never be measured. In practice the equation chosen is arbitrary if the only quantity sought is the infinite dilution molar quantity. In practice thermodynamics of solutions must be understood beyond infinite dilution. Therefore, for electrolytes extended Debye-Hückel theories are commonly used to make predictions at higher solute concentrations.

2.3 Electrolyte solutions

Prior to 1887, dissolved salts were thought to fill small voids in the solvent lattice and therefore could be treated as ideal solutions (Millero, 1971). Arrhenius' (1887) theory of complete ion dissociation prompted interest in explaining the phenomenon of solvation, as it was already pointed out that the addition of certain salts would decrease the volume of the solution.

Tammann (1895) developed the theory of internal pressure, where a dissolved salt caused the solvent, in this case water, to behave as if it were under an external pressure. He applied his theory to solution volumes (Tammann, 1895) by discussing apparent molar volumes in terms of the change in volume of the solute, solvent, and the mixture of the two, when changing the pressure from 1 atm to an internal pressure, π.

Drude and Nernst (1894) treated ions as hard sphere charges and developed an electrostatic theory, where hard sphere charges were placed in a continuous dielectric medium, such as any solvent. Born (1920) later developed calculation procedures which gave the size of the solvated ions and Webb (1926) calculated the magnitude of the effect charged ions have on water. Most of these theories are still used for describing standard state molar properties for ions; however, they do not address solute-solute or solute-solvent interactions.

Debye and Hückel (1923; 1924) proposed that long range coulombic effects cause a partially structured ionic atmosphere to form within a solution. The now widely accepted

Debye-Hückel theory describes the work involved in bringing a unit charge from infinity to the surface of a hard sphere. This work is made up of the energy required to charge the sphere in a dielectric medium and the interaction energy or long-range coulombic effects.

2.3.1 Activity coefficients and Debye-Hückel theory

The chemical potential for any individual ion can be described by

$$\mu_i = \mu_i^o + RT \ln a_i, \tag{2.17}$$

where a_i is the activity of the species (anion or cation) and μ_i^o is the partial molar Gibbs energy of any defined standard state. By application of equation 2.3 the chemical potential of a simple salt in solution can be described by equation 2.18 (Robinson & Stokes, 1965):

$$\begin{aligned}\mu_{M_{\nu 1}X_{\nu 2}} &= \mu^o_{M_{\nu 1}X_{\nu 2}} + \nu_1 RT \ln a_M + \nu_2 RT \ln a_X - RT \ln a_{MX} \\ &= \mu^o_{M_{\nu 1}X_{\nu 2}} + RT \ln a_M^{\nu 1} a_X^{\nu 2} - RT \ln a_{MX}.\end{aligned} \tag{2.18}$$

In equation 2.18 the standard state is defined such that there is no difference between the undissociated and dissociated species. Symbols ν_1 and ν_2 define the stoichiometric number of moles of cation M and anion X in one mole of the salt, $M_{\nu 1}X_{\nu 2}$.

Each individual concentration scale also affords a corresponding activity coefficient by division of the activity with the concentration. The molal activity coefficient is represented by γ and for a salt is more commonly represented by the mean ionic activity coefficient, $\gamma_\pm$, because individual ionic activity coefficients cannot be determined experimentally. A total stoichiometric ion concentration, $\nu=\nu_1+\nu_2$, may be defined, since any solution must be neutral and a charge balance, $\nu_1 Z_+ = \nu_1 Z_-$, will exist regardless of complete dissociation. Also due to the definition of the standard state, the equilibrium constant is at infinite dilution ($\gamma_\pm=1$), therefore we can define a mean activity:

$$\begin{aligned}a_\pm &= a_{MX}^{1/\nu} = (a_M^{\nu 1} a_X^{\nu 2})^{1/\nu} \\ &= (m_M^{\nu 1} m_X^{\nu 2} \gamma_M^{\nu 1} \gamma_X^{\nu 2})^{1/\nu}.\end{aligned} \tag{2.19}$$

Equation 2.19 also defines mean ionic activity coefficients, $\gamma_{\pm}=(\gamma_M^{\nu_1}\,\gamma_X^{\nu_2})^{1/\nu}$, and mean ionic molalities, $m_{\pm}=(m_M^{\nu_1}\,m_X^{\nu_2})^{1/\nu}$. Equation 2.18 can now be simplified by introducing the mean ionic activity in the following manner:

$$\mu_{MX} = \mu^{o}_{MX} + \nu\, RT \ln m_{\pm}\gamma_{\pm}$$

$$= \mu^{o}_{MX} + \nu\, RT \ln m_{\pm} + \nu\, RT \ln \gamma_{\pm}\,. \qquad (2.20)$$

By Henry's law, the defined standard state chemical potential would have a mean ionic activity of unity and would represent an ideal state with no ion-ion interactions; therefore the mean ionic activity coefficients describes the non-ideal contribution to the chemical potential of the solution. Interionic attraction theory assumes that the energy of a dilute salt may be separated into an electrostatic interaction contribution and an ideal contribution. This electrostatic contribution is contained in the last term of equation 2.20 (Pitzer & Brewer, 1961). Since the energy required to charge a sphere in a dielectric medium (self energy) is contained within the ideal pure chemical potential, Debye-Hückel theory suggests that mean ionic activity coefficients can be approximated with the electrical interaction energy. Equation 2.21 is the Debye-Hückel equation for predicting the mean ionic activity coefficients (Robinson & Stokes, 1965):

$$\log \gamma_{\pm} = -\frac{\mathbf{A}_{\gamma}\,|z_+ z_-|\sqrt{I}}{1 + \text{å}\mathbf{B}_{\gamma}\sqrt{I}}\,. \qquad (2.21)$$

where I is the ionic strength, z_+ and z_- are ionic valencies, and å is the Debye-Hückel distance of closest approach in angstroms. The constants $\mathbf{A}_{\gamma}$ and $\mathbf{B}_{\gamma}$ require a knowledge of the absolute temperature and the dielectric constant of the medium, ε. These constants are defined by equations 2.22 and 2.23 (Pitzer, 1979):

$$\mathbf{A}_{\gamma} = \sqrt{\frac{2\pi N_a \rho_o}{1000}}\,\frac{e^3}{(k\varepsilon T)^{3/2}} \qquad (2.22)$$

$$\mathbf{B}_{\gamma} = \sqrt{\frac{8\pi N_a e^2}{1000 k\varepsilon T}}\,, \qquad (2.23)$$

where N_a is Avogadro's number, ρ_o is the density of the solvent, e is the charge of one electron, k is Boltzmann's constant, and ε is the dielectric constant of the solvent medium. The ionic strength is defined with a valency factor, ω, using

$$I = \frac{1}{2}\sum m_i z_i^2 = \omega m \,. \tag{2.24}$$

At low values of $\sqrt{I}$ the B_γ term in the denominator of equation 2.21 becomes negligible and the equation takes a linear form, $\log \gamma_\pm = - A_\gamma | z_+ z_- | \sqrt{I}$. This is known as the Debye-Hückel limiting law, where the mean ionic activity coefficients become linear with respect to the square root of the ionic strength. Although this region of concentration is rarely approached in experimental investigations, the linear forms of Debye-Hückel equations are used in semi-empirical equations to aid in the fit to experimental data. As previously mentioned, this linear dependence aids in the extrapolation to infinite dilution where long-range coulombic effects are not a factor. Note that Debye-Hückel theory assumes that the second term in equation 2.20 containing the mean molality is absorbed into the standard state.

Partial molar heat capacities and volumes may be related to mean ionic activity coefficients by equations 2.25 and 2.26:

$$\begin{aligned} \bar{C}_{p2} &= \left(\frac{\partial \bar{H}_i}{\partial T}\right)_{m,\,p} \\ &= \bar{C}^{o}_{p2} - \nu R \left(T^2 \frac{\partial^2 \ln \gamma_\pm}{\partial T^2} + 2T \frac{\partial \ln \gamma_\pm}{\partial T} \right)_{m,p} \end{aligned} \tag{2.25}$$

and

$$\begin{aligned} \bar{V}_2 &= \left(\frac{\partial \mu_i}{\partial p}\right)_T \\ &= \bar{V}^{o}_2 - \nu R T \left(\frac{\partial \ln \gamma_\pm}{\partial p}\right)_{m,T} . \end{aligned} \tag{2.26}$$

At infinite dilution mean ionic activities approach unity therefore the standard state molar property is the only term left in equations 2.25 and 2.26. If Debye-Hückel limiting slopes are accepted in the dilute region, other partial molar properties can be derived with respect

to A_γ to reveal the limiting slopes for partial molar volumes, $\bar{A}_V$, and heat capacities, $\bar{A}_C$ (Pitzer and Brewer, 1961):

$$\bar{Y}_2 = \bar{Y}_2^o + \frac{v}{2}\bar{A}_Y |z_+z_-|\sqrt{I}$$

$$= \bar{Y}_2^o + \omega\,\bar{A}_Y\sqrt{I}\ , \tag{2.27}$$

$$\bar{A}_V = 2RT\left(\frac{\partial A_\gamma}{\partial p}\right)_T \tag{2.28}$$

and

$$\bar{A}_C = 2RT^2\left(\frac{\partial^2 A_\gamma}{\partial T^2}\right)_P\ . \tag{2.29}$$

Equation 2.30 is another expression of equation 2.16, using the ionic strength dependence of the apparent molar properties to reveal the partial molar property:

$$\bar{Y}_2 = Y_{2,\phi} + I\left(\frac{\partial Y_{2\phi}}{\partial I}\right)_{T,p}\ . \tag{2.30}$$

Multiplying by dI and integrating equation 2.30 by substitution of equation 2.27 leads to

$$\int_0^I \bar{Y}_2\,dI = \int_0^I Y_{2\phi}\,dI + \int_0^I I\,dY_{2\phi}$$

$$= \int_0^I \left(\bar{Y}_2^o + \omega\,\bar{A}_Y\sqrt{I}\right)dI$$

$$= I\,\bar{Y}^o + \omega\,\frac{2}{3}\bar{A}_Y\,I\sqrt{I}, \tag{2.31}$$

where the last integral term in the $dY_{2\phi}$ can be integrated by parts:

$$\int_0^I I\,dY_{2\phi} = \int_{Y_{2\phi}^\infty}^{Y_{2\phi}} I\,dY_{2\phi}$$

$$= I\,Y_{2\phi} - \int_0^I Y_{2\phi}\,dI. \tag{2.32}$$

Substituting equation 2.32 into equation 2.31 and rearranging leads to

$$Y_{2,\phi} = \bar{Y}^o + \omega\,\frac{2}{3}\bar{A}_Y\sqrt{I}$$

$$= \bar{Y}^o + \omega\,A_Y\sqrt{I}, \tag{2.33}$$

where $A_Y = \frac{2}{3}\bar{A}_Y$. Equation 2.33 is used to aid the goodness of fit of many semi-empirical equations to a group of experimental apparent molar property data.

Models using only the Debye-Hückel limiting law, such as equation 2.33, are referred to as non-extended Debye-Hückel equations. Güntelberg (1926) uses another simplification to equation 2.21 by setting the Debye-Hückel distance of closest approach to 3.04 Å at 298.15 K, and thus B_γ=1. Equation 2.35 is a commonly used extended Debye-Hückel equation for apparent molar properties, which has been derived in the same manner as before, except with Güntelberg's version of the extended Debye-Hückel equation, equation 2.34 (Pitzer & Brewer, 1961):

$$\log \gamma_\pm = -A_\gamma |z_+ z_-| \frac{\sqrt{I}}{1 + \sqrt{I}}, \tag{2.34}$$

therefore

$$Y_{2,\phi} = \bar{Y}_2^o + \frac{3}{2}\omega A_Y \left(\frac{1}{\Lambda} - \frac{\sigma}{3}\right)\sqrt{I} \tag{2.35}$$

where

$$\Lambda = 1 + \sqrt{I} \tag{2.36}$$

and

$$\sigma = 3\frac{\left(\Lambda - \frac{1}{\Lambda} - 2\ln\Lambda\right)}{\sqrt{I^3}}. \tag{2.37}$$

Equation 2.35 is applied in the same manner as the non-extended equation 2.33; however it can be utilized over a larger range of ionic strength. In summary various versions of the Debye-Hückel equation have been successfully utilized to better extrapolate partial molar properties to infinite dilution.

To a limited extent, variations of the Debye-Hückel equation can be used to estimate single ion activity coefficients. Because Debye-Hückel theory was developed for an ion in an atmosphere of oppositely charged ions, this approach can only be justified with very dilute solutions. This approach will be discussed further in Chapter 5. A more robust

method of estimating single ion activity coefficients, would be to use Pitzer's ion interaction model (Pitzer, 1991).

2.3.2 Pitzer ion interaction

Pitzer's ion interactions involve virial expansions of the Debye-Hückel equation. Virial equations take the form of any equation of state followed by a polynomial of one of the variables. The general virial equation was the expansion of the ideal gas law (Anderson & Crerar, 1993), where the reciprocal volume was the variable used in the expansion. In the latter expansion, the product of the temperature and the gas constant, RT, is the first virial coefficient representing the ideal state. Each coefficient, usually labeled B, C, D, etc., represents the contribution to the variable from all ascending interactions. In turn the coefficients may also be modelled by functions based on other variables, such as temperature and pressure. Hill (1960) shows a detailed derivation of the virial equation beginning with the ideal gas law from statistical mechanics. It starts by assuming that all molecular interaction potentials are known; however because there are far too many interactions to include, terms are collected in clusters which theoretically represent different particle groupings. Virial coefficients represent these clusters averaged over the volume of the system.

Pitzer added virial expansion terms to the excess Gibbs energy because it was a convenient form from which to derive most other thermodynamic properties. The non-ideal Gibbs energy of any mixture has already been given in equation 2.20. An excess energy can be defined as the non-ideal contribution to the energy and is easily shown as the difference between the observed and ideal energy. The excess partial molar Gibbs energy is therefore the contribution of the activity coefficient, as shown by

$$\bar{G}_i^{EX} = RT \ln \gamma_i. \qquad (2.38)$$

Therefore, Pitzer's ion interaction model is simply a virial expansion which models the mean ionic activity coefficient of any ionic solution:

$$\frac{G^{EX}}{RT} = n_w f(I) + \frac{1}{n_w}\sum_i\sum_j \lambda_{ij}(I)\, n_i n_j + \frac{1}{n_w^2}\sum_i\sum_j\sum_k \mu_{ijk}\, n_i n_j n_k. \qquad (2.39)$$

In equation 2.28 n_w defines the moles of solvent, n_i defines the moles of solute i, n_j defines the moles of solute j, etc.. $f(I)$ is used to define long-range coulombic effects with respect to ionic strength, therefore $f(I)$ is an extended Debye-Hückel equation which reduces to the Debye-Hückel limiting slope like all other extensions of this theory. The virial expansion coefficients are λ_{ij} and μ_{ijk} and represent short range doublet and triplet interactions respectively. Converting the total excess energy to partial molar excess energy, allows the derivation of molar excess volumes and heat capacities and finally the apparent molar volumes and heat capacities of a salt, $M_{\nu_M}X_{\nu_X}$:

$$V_{2,\phi} = \bar{V}_2^o + \nu\,|z_M z_X|\,\frac{A_V}{3.6}\ln(1+1.2\sqrt{I}) - 2\,\nu_M\nu_X RT\,(B^V_{MX}\,m + \nu_M z_M\, C^V_{MX}\, m^2) \qquad (2.40)$$

and

$$C_{p2,\phi} = \bar{C}_{p2}^o + \nu\,|z_M z_X|\,\frac{A_J}{3.6}\ln(1+1.2\sqrt{I}) - 2\,\nu_M\nu_X RT^2\,(B^J_{MX}\,m + \nu_M z_M\, C^J_{MX}\, m^2). \qquad (2.41)$$

In equations 2.40 and 2.41 the parameters B^V_{MX}, C^V_{MX}, B^J_{MX}, and C^J_{MX} are related to the second and third activity virial coefficients, B_{MX} and C_{MX}, by equations 2.42, 2.43, 2.44, and 2.45 respectively. Similarly the first virial coefficients A_V and A_J (equations 2.46 and 2.47) are derived from the extended Debye-Hückel equation, $f(I)$:

$$B^V_{MX} = \left(\frac{\partial\beta^{(o)}}{\partial p}\right)_T + \left(\frac{\partial\beta^{(1)}}{\partial p}\right)_T \frac{2}{\alpha^2 I}\left[1 - (1+\alpha\sqrt{I})e^{-\alpha\sqrt{I}}\right], \qquad (2.42)$$

$$C^V_{MX} = \left(\frac{\partial C_{MX}}{\partial p}\right)_T, \qquad (2.43)$$

$$B^J_{MX} = \left(\frac{\partial^2 B_{MX}}{\partial T^2}\right)_{p,\,I} + \frac{2}{T}\left(\frac{\partial B_{MX}}{\partial T}\right)_{p,\,I}, \qquad (2.44)$$

$$C^J_{MX} = \left(\frac{\partial^2 C_{MX}}{\partial T^2}\right)_p + \frac{2}{T}\left(\frac{\partial C_{MX}}{\partial T}\right)_p, \qquad (2.45)$$

$$A_V = -A_\gamma RT\left(\left(\frac{\partial \ln \varepsilon}{\partial p}\right)_T + \left(\frac{\partial V_I^o}{\partial p}\right)_T\right), \tag{2.46}$$

and

$$A_J = \left(\frac{\partial A_H}{\partial T}\right)_p \tag{2.47}$$

where

$$A_H = RT^2\left(\frac{\partial A_\phi}{\partial T}\right)_p . \tag{2.48}$$

A complete derivation and compilation of the Pitzer expressions can be found in Pytkowicz (1979) and Pitzer (1991).

Pitzer ion interaction is a convenient treatment, because the thermodynamics of any species in solution can be successfully calculated from known virial coefficients obtained from simple systems. It is therefore an empirical equation of state rather than only a theory required for extrapolation to infinite dilution. The difficulty with Pitzer ion interaction theory is the number of coefficients which must be found by fitting to experimental data. Many thermodynamic studies are limited by the data that can be generated. In complex solutions, and/or solutions containing ions of higher valence, the number of coefficients in Pitzer's equations can increase to the point of being statistically insignificant with respect to measured data. This concern is discussed further in Chapter 5.

Recall that other extended Debye-Hückel expressions were discussed as aiding the extrapolation to infinite dilution or standard state. Pitzer expressions can be used to extrapolate to infinite dilution just as other extended Debye-Hückel equations. There is no defined standard Debye-Hückel expression for extrapolation to infinite dilution. This is a problem, because each expression will produce different values at infinite dilution from the same experimental data. Selection of an appropriate equation is always a key consideration when evaluating partial molar properties at infinite dilution.

Other methods of obtaining standard state properties for interpretation or calculation, include using equations of state for standard state properties to extend the data

set beyond the investigated temperature and pressure investigated. Often these theoretical equations require semi-empirical corrections or portions which can be fit to experimental results. One popular semi-empirical equation of state was developed by Helgeson, Kirkham, and Flowers (HKF).

2.3.3 Born theory and the Helgeson, Kirkham, and Flowers model

Born (1920) advanced the Drude and Nernst (1894) treatment of solvated ions, by determining effective solvated ionic radii for hard sphere charges in a dielectric medium. Born calculated the Gibbs energy change involved in moving an ion of radius $r_{e,j}$ and charge $Z_j e$ from a vacuum to a medium with a dielectric constant, ε:

$$\Delta\bar{G}_{e,j} = \frac{N_a(Z_j e)^2}{2\, r_{ej}}\left(\frac{1}{\varepsilon} - 1\right). \tag{2.49}$$

In a series of studies in the late seventies and early eighties, Helgeson, Kirkham, and Flowers (Helgeson & Kirkham, 1976; Helgeson *et al.*, 1981) developed semi-empirical equations of state for partial molar properties at infinite dilution. Within these equations Born contributions described the non-empirical or theoretical portion of the standard state quantity, while the empirical contribution could be described by observing experimental data.

The HKF model considers the total differential of the partial molar Gibbs energy, equation 2.11, of ion j and then integrates to find changes in Gibbs energy with respect to changes in temperature, pressure, and concentration from some reference state ($T_r P_r n_o$):

$$\int_{T_r p_r n_o}^{T\, p\, n} d\bar{G}_j = -\int_{T_r}^{T} \bar{S}_{j p_r n_o}\, dT + \int_{p_r}^{p} \bar{V}_{j T_r n_o}\, dp + \int_{n}^{n_o} \mu_{j T_r p_r}\, dn_j \tag{2.50}$$

The temperature and pressure integrals in equation 2.50 require fixing the concentration or moles of ion j to n_o. If n_o is set to one mole, the entropy and volume terms describe an ideal system and therefore are the standard state partial molar entropy and volume. As discussed previously, the chemical potential, μ_j, describes the change in Gibbs energy with

respect to concentration and therefore requires knowing the activity of ion j with respect to solution composition. However, if ion j is fixed to one mole, equation 2.50 shows that only temperature and pressure changes are required to describe the changes in the standard state partial molar Gibbs energy, since at the standard state activity is at unity. Also, the entropy integral with respect to temperature change requires a knowledge of the standard state partial molar heat capacity as a function of temperature and pressure.

Because partial molar properties of individual ions cannot be measured, the convention is to refer to the partial molar properties of anions as their respective acids, where any standard state partial molar property of H^+ is assigned a value of zero. Therefore the Born equation used by HKF, contains a Born parameter ω_{ej} containing the correction for conventional single ion partial molar properties (Helgeson & Kirkham, 1976):

$$\Delta\bar{G}^{o}_{e,j} = \left(\frac{N_a(Z_j e)^2}{2\, r_{ej}} - \frac{N_a(Z_{H^+} e)^2\, Z_j}{2\, r_{eH^+}}\right)\left(\frac{1}{\varepsilon} - 1\right) = \omega_{ej}\left(\frac{1}{\varepsilon} - 1\right). \tag{2.51}$$

Through the additive convention of standard state partial molar properties, the Born parameters are also additive; therefore the Born coefficient of any salt can be obtained by the stoichiometric addition of the anion and cation contributions to the Born coefficient. Because the state variables are additive, the empirical parameters must also be additive. In equation 2.51 the ionic radius, r_e, is related to crystallographic ionic radii r_x by

$$r_{ej} = r_{xj} + |\, Z_j \,|\, [0.94 + g(T,p)] \tag{2.52}$$

and

$$r_{ek} = r_{xk} + |\, Z_k \,|\, g(T,p), \tag{2.53}$$

where subscripts j and k refer to cationic species and anionic species respectively. The original HKF model did not consider the ionic radii as a function of temperature and pressure; therefore the function g(T,p) was set to zero. Modern HKF theory utilizing the function g(T,p) is referred to as revised HKF theory (Tanger and Helgeson, 1988).

The electrostatic or solvation contribution to the standard state entropy and volume changes for solvation can be derived by differentiation of the Born equation:

$$\Delta\bar{S}^{o}_{e} = -\left(\frac{\partial \Delta\bar{G}^{o}_{e}}{\partial T}\right)_{p}$$

$$= -\omega_{e}\frac{\partial}{\partial T}\left(\frac{1}{\varepsilon} - 1\right) - \left(\frac{1}{\varepsilon} - 1\right)\left(\frac{\partial \omega_{e}}{\partial T}\right)_{p}$$

$$= \omega_{e}Y - \left(\frac{1}{\varepsilon} - 1\right)\left(\frac{\partial \omega_{e}}{\partial T}\right)_{p}, \tag{2.54}$$

$$\Delta\bar{V}^{o}_{e} = \left(\frac{\partial \Delta\bar{G}^{o}_{e}}{\partial p}\right)_{T}$$

$$= \omega_{e}\frac{\partial}{\partial p}\left(\frac{1}{\varepsilon} - 1\right) + \left(\frac{1}{\varepsilon} - 1\right)\left(\frac{\partial \omega_{e}}{\partial p}\right)_{T}$$

$$= -\omega_{e}Q + \left(\frac{1}{\varepsilon} - 1\right)\left(\frac{\partial \omega_{e}}{\partial p}\right)_{T}, \tag{2.55}$$

and

$$\Delta\bar{C}^{o}_{p_e} = T\left(\frac{\partial \Delta\bar{S}^{o}_{e}}{\partial T}\right)_{p}$$

$$= \omega_{e}T\left(\frac{\partial Y}{\partial T}\right)_{p} + 2TY\left(\frac{\partial \omega_{e}}{\partial T}\right)_{p} - T\left(\frac{1}{\varepsilon} - 1\right)\left(\frac{\partial^{2}\omega_{e}}{\partial T^{2}}\right)_{p}. \tag{2.56}$$

In equations 2.54, 2.55, and 2.56, Born functions Y and Q represent temperature and pressure derivatives of the dielectric constant of the solvent. In addition, the derivative of Y with respect to temperature is defined as the Born function X.

The HKF model chooses empirical equations that fit the differences between the theoretical Born solvation terms, equations 2.54-2.56, and experimental solvation values. Appropriately these contributions are termed the non-solvation contributions and are modeled by equations 2.57 and 2.58:

$$\Delta\bar{V}^{o}_{s} = a_{1} + \frac{a_{2}}{\Psi + p} + \frac{a_{3}}{T - \Theta} + \frac{a_{4}}{(T - \Theta)(\Psi + p)} \tag{2.57}$$

and

$$\Delta\bar{C}^{o}_{p_s} = c_{1} + \frac{c_{2}}{(T - \Theta)^{2}} + \left(\frac{2T}{(T - \Theta)^{3}}\right)\left[a_{3}\,(p - p_{r}) + a_{4}\ln\left(\frac{\Psi + p}{\Psi + p_{r}}\right)\right], \tag{2.58}$$

where a_1, a_2, a_3, a_4, c_1, and c_2 are solute dependent coefficients and Θ and Ψ are solvent dependent parameters. The solvent dependent parameters for water are 228 K and 2600 bars respectively (Tanger and Helgeson, 1988). Using equation 2.10, the pressure dependence of the non-solvation partial molar heat capacity is described by the temperature dependent parameters of the non-solvation partial molar volume equation. This dependency is shown in the last term of equation 2.58.

From the six empirical parameters obtained from fitting to experimental volumes and heat capacities and the Born solvation terms, all other standard state thermodynamic properties can be derived. It should be pointed out that HKF equations were derived for standard state partial molar properties which have previously been distinguished from partial molar properties at infinite dilution. Although these standard state properties may not be equivalent to infinite dilution properties, if all solute-solvent effects at infinite dilution are considered consistent, then HKF does enable the calculation of equilibrium constants, K, over a wide range of temperature and pressure.

Several studies presented within this thesis are concerned with aqueous non-electrolyte species. Although a great deal of theory presented here is for electrolyte solutions, it should be noted that another advantage of the HKF semi-empirical equation of state is a remarkable ability to model neutral aqueous species. This topic will be discussed further in Chapters 6 and 7.

3) METHODS OF MEASUREMENT USING PICKER MICROFLOW CALORIMETRY AND VIBRATING TUBE DENSIMETRY.

3.1 Introduction

The importance of heat capacity data to the understanding of the Gibbs energy of a solution system has been emphasised in Chapter 2. Knowledge of the heat capacity, and if possible the temperature dependence of the heat capacity, permits the calculation of enthalpy and entropy changes with respect to changes in temperature. The partial molar heat capacity, being related to the second derivative of the Gibbs energy, is also sensitive to the structure of interacting molecules.

Several different types of commercially available solution calorimeters can be used for the measurement of heats of mixing, heats of reaction, and heat capacities of aqueous solutions (Marsh & O'Hare, 1994). The calculation of apparent molar heat capacity changes due to the addition of a solute to a solvent, requires an instrument capable of precisely detecting the excess heat capacity of the solution. The excess heat capacity, as with most excess properties, is usually only about 1% of the total heat capacity of the system (Marsh & O'Hare, 1994). The traditional batch method has the disadvantage of lacking sensitivity in the dilute concentration region (Marsh & O'Hare, 1994) where measurements are required for extrapolation to infinite dilution. Also, experimental conditions often include the measurement of the heat capacity of the vapour above the solution of interest, thus introducing experimental error in the determined liquid heat capacity.

3.2 The Picker microflow calorimeter

The sensitivity of the Picker microflow calorimeter (Picker *et al.*, 1971) identifies it as an excellent instrument for the determination of heat capacities for aqueous and non-aqueous solutions. This sensitivity is achieved by measuring the heat capacity of a sample

Figure 3.1 Simplified diagram of a Picker microflow calorimeter.

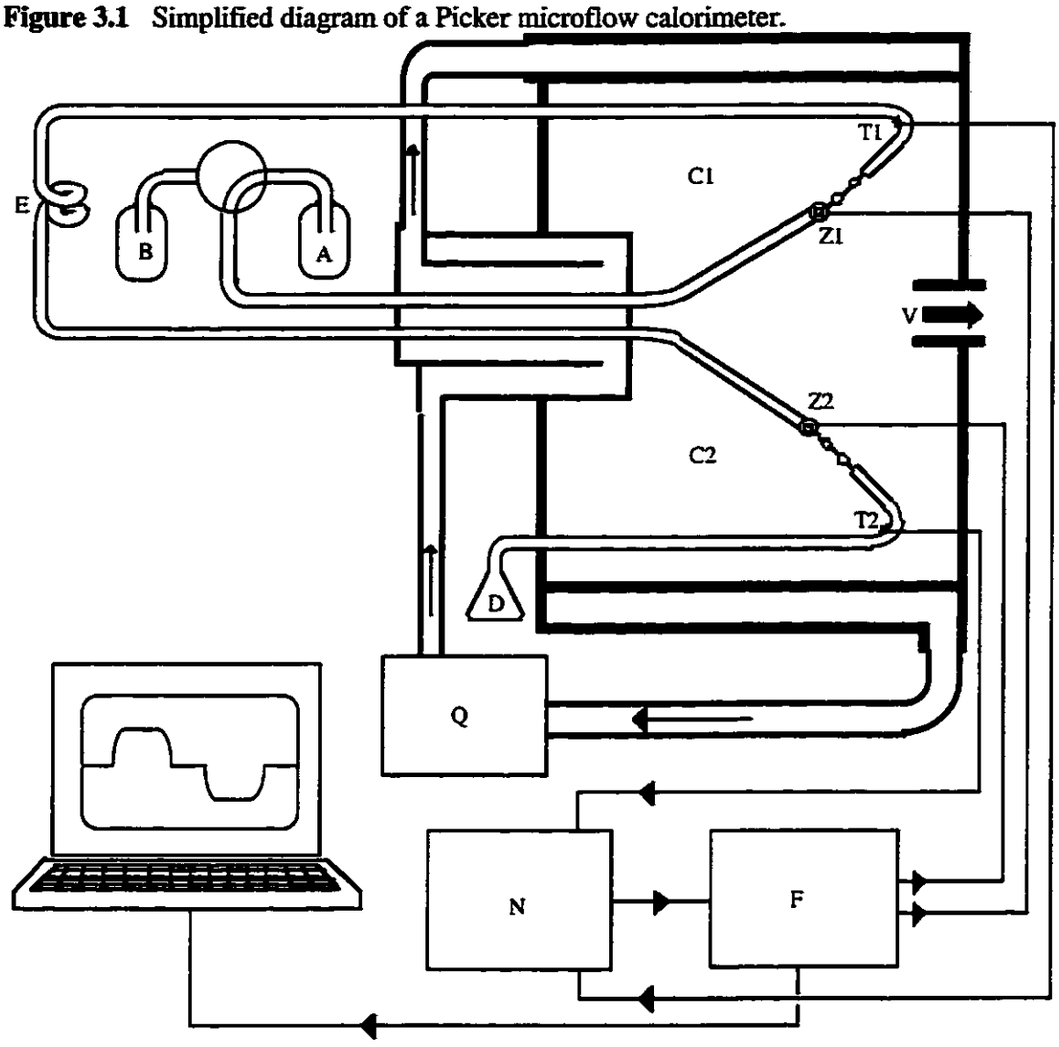

A and B) Solution reservoirs. C1 and C2) Calorimetric cells. D) Waste reservoirs. E) External sample delay loop. F) Feed back circuit. N) Null detector circuit. Q) Circulating thermostat. T1 and T2) Thermistors. V) Vacuum. Z1 and Z2) Zener diodes.

liquid relative to a liquid with a well known heat capacity. Another advantage of the Picker microflow calorimeter is that it removes the concern for correcting heat capacity measurements for the presence of vapour.

A diagram of the Picker microflow calorimeter used throughout the investigations reported in this thesis is shown in figure 3.1. The calorimeter consists of twin cells, C_I

and C_2. Zener diodes, Z_1 and Z_2, are used to heat the liquid within each cell and are positioned on a crimped portion of the tubing to facilitate complete heat exchange with the flowing liquid. Thermistors are attached to the tubing downstream of the Zener diodes and are used to measure the temperature of the liquid after heat exchange, T_1 and T_2. The volumetric heat capacity, σ, can be determined for the fluid in each cell, using equation 3.1:

$$\sigma = \frac{W}{\dot{f}\,\Delta T}, \qquad (3.1)$$

where ΔT defines a known temperature rise, $\dot{f}$ is the flow rate of the fluid through the cell, and W is a known amount of electrical energy supplied to the Zener diode.

The twin cell design of the Picker microflow calorimeter removes the necessity of using equation 3.1 in the calculation of heat capacities. The flow rate of each cell is the same, because the cells are in series separated by a small delay line. For the measurements described in this thesis, constant flow was maintained by gravity feed.

In figure 3.1 liquid A is shown flowing through the system. At the entrance of cells one and two the liquid is thermostated to the initial temperature T_O and then raised by ΔT_1 and ΔT_2 to the final temperatures T_1 and T_2 by the Zener diodes Z_1 and Z_2. The calorimeter is calibrated by nulling the final temperature when no heat is added, therefore $T_1=T_2=T_O$. With the transistors nulled, the power supplied to Z_1 and Z_2 is nulled at a given temperature increase based on the magnitude of the power supplied, (100 mW usually corresponds to rise in temperature of ~2 K). This temperature rise is used to calculate the initial temperature, causing the experimental temperature to be at half the temperature rise. Temperature calibrations of the instrument were performed on a daily basis.

When the system calibration is complete and a base power has been supplied to each zener diode, a feedback circuit is energised to maintain the same temperature change in each cell. This is achieved by regulating the power supplied to the Zener diodes. The difference in power supplied to the Zener diodes, in terms of a voltage difference,

Figure 3.2 An example of a typical output signal from a Picker microflow calorimeter; Aqueous; $La_2(SO_4)_3$ at 298.15 K.

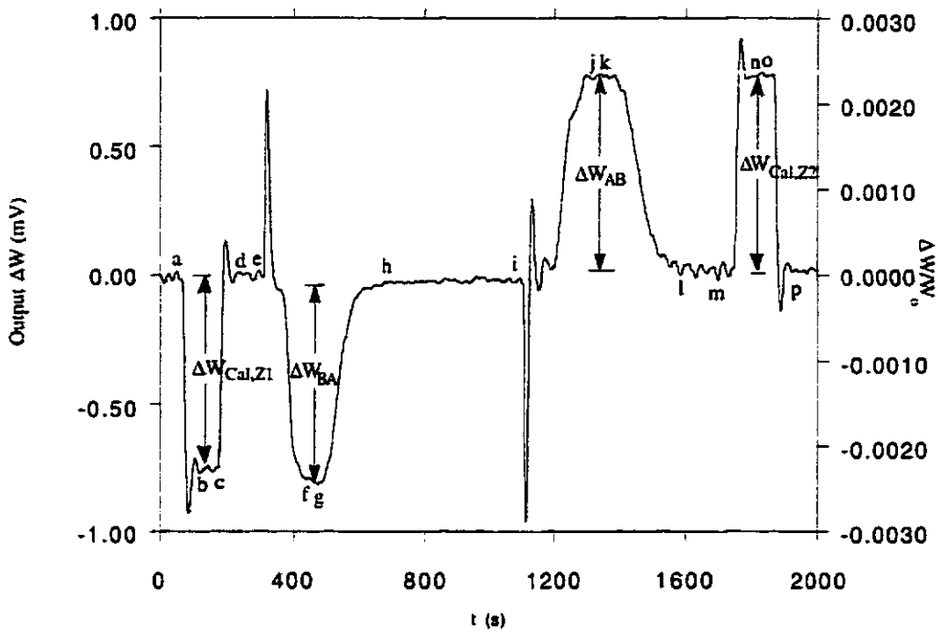

Points 'a' through 'p' are referenced within the text.

$\Delta W = W_1 - W_2$, is followed over the course of the experimental run. An example of the instrument's output is shown in figure 3.2.

A four way liquid chromatography valve is used to switch from the reference fluid A to the sample fluid B. As liquid B flows into cell one, the feedback adjusts the power supply to Z_1 to maintain T_1. With the differences in supplied power the output, ΔW, increases or decreases according to equation 3.2:

$$\frac{\Delta W_{BA}}{W_O} = \frac{\sigma_B - \sigma_A}{\sigma_A}, \qquad (3.2)$$

where W_O is the average power supplied to each diode. Assuming the volumetric heat capacity of liquid A is well known, the volumetric heat capacity of liquid B can be measured. The specific flow rate is no longer needed for calculating the heat capacity as long as it is constant and consistent in both cells. Because specific heat capacities are required for the calculation of partial and apparent molar heat capacities, equation 3.2 can be manipulated to define a relative specific heat capacity:

$$\frac{\Delta W_{BA}}{W_O} = \frac{C_{pB}\rho_B}{C_{pA}\rho_A} - 1. \tag{3.3}$$

Once the sample liquid B has continued through the delay loop and into cell two, the cells once again contain the same fluid at the same flow rate, therefore ΔW_{BB} is nulled. This portion of the output is labeled as 'h-i' in figure 3.2. The four way valve is then turned back to the first position, allowing the reference liquid A to flow into cell one. At this stage cell two still contains solution B, therefore, ΔW may now be defined by

$$\frac{\Delta W_{AB}}{W_O} = \frac{\sigma_A - \sigma_B}{\sigma_B}. \tag{3.4}$$

As the reference solution flows into cell two, the output will again return to zero. The differences in power supplies must be calibrated to reflect quantitative energy differences. Therefore when both cells contain reference fluid, electrical calibration peaks are measured by supplying a known amount of power to one diode. Figure 3.2 shows the calibration of the first Zener diode, 'b-c', before the sample solution flows through the calorimeter and the calibration peak for the second Zener, 'n-o', after the sample solution. The reason for this order is for consistency with flow rates; as the reservoirs are depleted the flow rate slows down slightly over the time of an experimental run. Experimental error is not likely to be influenced by a change of ordering; therefore, other studies have committed the calibration peaks to after the sample solution has followed through the calorimeter. The studies in chapter 6 use one calibration peak and therefore assume symmetrical calibration. Considering the magnitude of the relative volumetric heat capacities in chapter 6, this assumption is reasonable, because of large experimental error due to small peaks. Data in

the calibration Section of this Chapter were treated in a similar manner, and through a comparison with literature values, the results support the latter assumption.

Although the jacket surrounding the twin cells in a Picker type calorimeter is evacuated, there remains a small amount of heat loss (Desnoyers *et al.*, 1976) resulting in a less than 100% heat exchange with the solution. This heat leak can be corrected with the use of a heat loss correction factor, f, which is different for each calorimeter and is usually evaluated periodically over the life of the instrument:

$$f = \left(\frac{\sigma_B}{\sigma_A - \sigma_B}\right)^{\frac{\Delta W_{AB}}{W_O}} = \left(\frac{W_O}{\Delta W_{AB}^*}\right)^{\frac{\Delta W_{AB}}{W_O}} \qquad (3.5)$$

Since no two calorimeters are the same and the vacuum systems used to evacuate the jackets will differ, the heat loss correction factor can be evaluated by measuring a solution of known heat capacity, such as aqueous sodium chloride. In equation 3.5, $\frac{W_O}{\Delta W_{AB}^*}$ is the reciprocal of a standard relative heat capacity, determined by combining and evaluating several calorimetric studies (Desnoyers *et al.*, 1976). Because heat loss is associated with a slightly smaller ΔT, the heat loss correction factor is always slightly larger than one. The heat loss correction factor has been measured for the instrument utilised in this thesis, and is reported in the calibration Section 3.4.

Two different types of visual data analysis were studied throughout the course of this thesis. The analysis used with aqueous rare earth sulfates required the experimentalist to visually extrapolate values for points 'a' through 'p' as shown in figure 3.2. This allowed for the calculation of two heat capacity terms for each peak, therefore correcting for any asymmetry in the output signal. In most cases asymmetry is contained in the baseline on either side of the peak and not the peak itself. For measurements of aqueous sodium chloride and aqueous amino acids, only one value for each peak was extrapolated and one calibration peak was used. Uncertainties were calculated through theoretical equations derived hereafter (equations 3.13 and 3.14).

All heat capacity measurements were performed with a Sodev dynamic Picker

microflow calorimeter. The jacket vacuum was held at $1 \cdot 10^{-3}$ Pa with a Leybold Trivac D4A direct drive vacuum pump and an Edwards E050 air cooled diffusion pump. The vacuum was monitored with Penning CP25-K and Edwards PRM-10 vacuum gauges. Thermostating of the cells was achieved with a Technoeurope programmable circulating thermostat capable of controlling temperature to within ±0.001 K. All output data were collected by an IBM clone computer via an IEEE interface to either an HP 3456A Voltmeter or an HP 34401A Multimeter. The uncertainty in specific heat capacities, δC_p, obtained with this calorimeter has been estimated to be $7 \cdot 10^{-5}$ J K^{-1} mol^{-1}.

The measurement of precise heat capacities with a Picker microflow calorimeter requires density data for individual fluids. To reduce experimental error the Picker calorimeter was placed in series with a Sodev O2D vibrating tube densimeter. Therefore densities were measured in unison with calorimetric measurements.

3.3 The vibrating tube densimeter.

One of the more sensitive and by far the most popular types of modern instruments for measuring densities is the vibrating tube densimeter. Industrially, vibrating tube densimeters have long been used by brewers and distillers to quantify alcohol content (Strunk *et al.*, 1979). The first vibrating tube, used to measure the density of blood (Kratky *et al.*, 1969), was improved upon by Picker *et al.* (1974). Since Picker *et al.*'s improvements, vibrating U-tube densimeters have been the standard instrument for measuring densities of gases and fluids.

The basic theory supporting the operation of a vibrating tube densimeter can be easily described. Theoretically the undamped resonance frequency of any simple harmonic oscillator, ω_u, is given by

$$\omega_u = \sqrt{\frac{k}{m}}, \tag{3.6}$$

where k is the spring constant and m is the mass of the vibrating system. With respect to a

vibrating tube system, the mass is composed only of the mass of the fluid inside the tube, m_f, and the mass of the tube itself, m_t:

$$m_f + m_t = \frac{k}{\omega_u^2}. \tag{3.7}$$

Considering the difference between the tube containing one fluid, A, and the same tube containing another fluid, B, the difference in mass, $m_A - m_B$, is equal to the difference in density, $\rho_A - \rho_B$, since the volume within the tube is constant. Because the time period of oscillation is related to frequency, $\tau = 2\pi/\omega_u$, a relative density may be defined in terms of the time period of oscillation of the tube:

$$\begin{aligned} \rho_A - \rho_B &= k\left(\frac{1}{\omega_A^2} - \frac{1}{\omega_B^2}\right) \\ &= K\left(\tau_A^2 - \tau_B^2\right). \end{aligned} \tag{3.8}$$

Equation 3.8 is the fundamental equation for all vibrating tube densimeters, where K is a temperature dependent calibration constant for the system. K is determined by measuring the time periods for two systems of precisely known density. The calibration constants for this instrument were determined periodically throughout the course of work conducted in the series of studies presented in this thesis.

With a dynamic flow method and a sample of unknown density, a typical time period output would resemble figure 3.3, where regions a, b, and c represent the time period of the tube containing reference fluid, sample fluid, and reference fluid respectively. The reference fluid must have a well-known density, and for the purposes of systems studied in this thesis, the reference fluid was water. Similar to the calorimeter output, an experimentalist can visually extrapolate values for regions a, b, and c, however, it is often easier to simply average data points in each region.

The O2D vibrating tube densimeter was thermostated with a Technoeurope programmable circulating thermostat capable of controlling temperature to within ±0.001 K. Time period data were collected with an IBM clone computer via a serial interface with a Philips PM 6611 universal counter averaging every 10,000 counts. The uncertainty in

Figure 3.3 A plot of time period versus time for the Sodev O2D vibrating tube densimeter; Aqueous $La_2(SO_4)_3$ at 298.15 K.

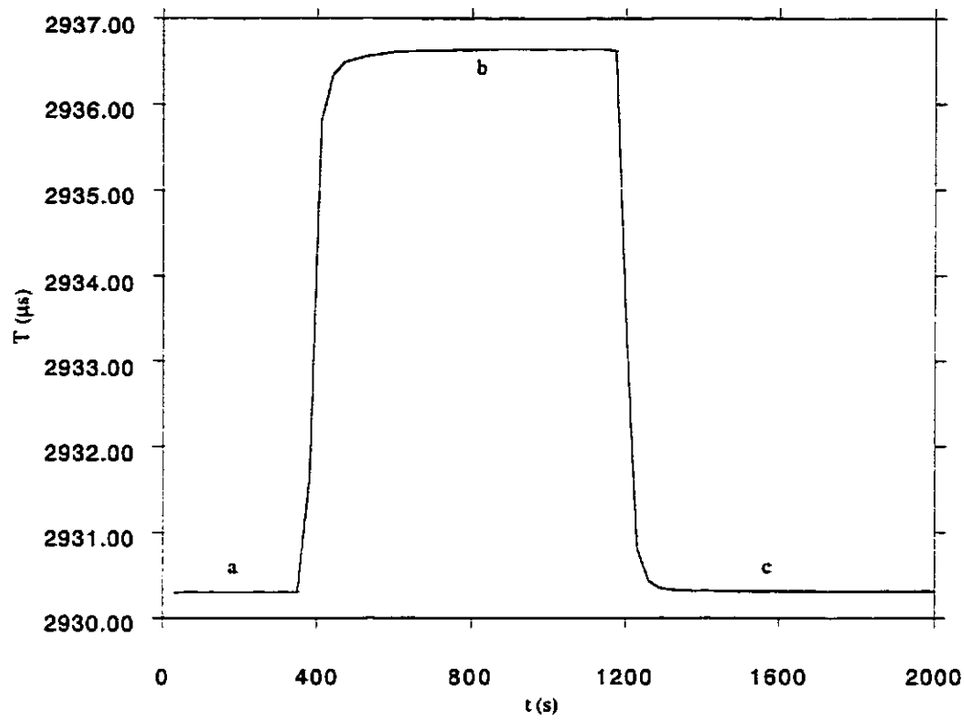

Points 'a','b', and 'c' are referenced within the text.

density data, $\delta\rho$, obtained with the densimeter is estimated to be $5 \cdot 10^{-6}$ g cm^{-3}.

3.4 Calibration[1]

An f-factor for the Picker flow calorimeter used in this thesis was obtained by measuring the relative heat capacities of aqueous solutions of sodium chloride. The standard empirical equation reported by Desnoyers *et al.* (1976) was used to calculate standard relative heat capacities for aqueous NaCl solutions at 298.15 K. These data were utilised in equation 3.5. The f-factor was assumed to be independent of temperature,

[1]A version of the calibration section has been published by Marriott et. al. (1998) with the remainder of this publication included in Chapter 6 of this thesis.

within the temperature range studied in this thesis.

Calibration constants for the vibrating tube densimeter were secured by obtaining the vibration time period of the tube containing pure water and dry nitrogen (or air) at 288.15, 298.15, 313.15, and 328.15 K.

3.4.1 Experimental

Water was obtained from an Osmonics model Aries High Purity D.I. Loop, capable of polishing to a resistance of 18.2 MΩ. Water was thoroughly degassed prior to experimental runs[2]. Sodium chloride was obtained from Sigma (Catalog No. S-7653) and used without further purification after being dried at 383 K for over 24 hours. All sodium chloride solutions were prepared by weight on the molality concentration scale.

The densities of water at 288.15, 298.15, 313.15, and 328.15 K used in equations 3.8 and 3.3 were 0.999101, 0.997047, 0.992219, and 0.985695 g cm^{-3} as reported by Kell (1967). The specific heat capacities for water used in equation 3.3, have been reported by Kell (1972) (4.1855, 4.1793, 4.1783, and 4.1821 J K^{-1} g^{-1} at 288.15, 298.15, 313.15, and 328.15 K respectively). The densities of dry nitrogen, ρ_{N_2}, were calculated using the ideal gas law and densities of moist air were calculated using the standard equations of Daniels *et al.* as reported in the CRC handbook (Weast, 1970).

3.4.2 Results and discussion

Calibration constants for the Sodev O2D densimeter were determined to be $7.192853 \cdot 10^{-7}$, $7.163983 \cdot 10^{-7}$, $7.107404 \cdot 10^{-7}$, and $7.058567 \cdot 10^{-7}$ g cm^{-3} μs^{-2} at 288.15, 298.15, 313.15, and 328.15 K respectively. These constants are in good agreement with previous values (Hakin *et al.*, 1991) and show the consistency of this instrument over time. The f-factor of the calorimeter was determined to be 1.0106±0.0076.

---

[2]The degassing of water was completed by vigorous mixing under a reduced pressure.

Apparent molar volumes and heat capacities were calculated by equations 3.9 and 3.10:

$$V_{2,\phi} = \frac{M}{\rho} - \frac{1000\,(\rho - \rho_o)}{m\rho\rho_o} \tag{3.9}$$

and

$$C_{p2,\phi} = MC_p + \frac{1000\,(C_p - C_{p_1}^o)}{m} \tag{3.10}$$

where M is the molar mass of the solute, m is the molality of the solution, C_p is the specific heat capacity of the solution, ρ is the density of the solution, $C_{p_1}^o$ is the specific heat capacity of pure water, and ρ_o is the density of pure water.

Apparent molar volumes and heat capacities at infinite dilution were obtained by fitting a non-extended Debye-Hückel equation to apparent molar heat capacities and volumes from experimentally determined data at 288.15, 298.15, 313.15, and 328.15 K respectively:

$$\begin{aligned} Y_{2,\phi} &= Y_{2,\phi}^{\infty} + \omega A_Y\sqrt{I} + \hat{B}_Y I \\ &= \bar{Y}_2^o + A_Y\sqrt{m} + \hat{B}_Y m \end{aligned} \tag{3.11}$$

The Debye-Hückel limiting slopes were obtained from Ananthaswamy and Atkinson (1984) and are shown in table 3.1. All equations were fitted using weighted linear regression, where the reciprocal squares of the uncertainties were used as weights. The uncertainties in each apparent molar property, $\delta Y_{2,\phi}$, were calculated from equations 3.12 and 3.13:

$$\begin{aligned} \delta V_{2,\phi} &= \left|\frac{\partial V_{2\phi}}{\partial \rho}\right| \delta\rho + \left|\frac{\partial V_{2\phi}}{\partial m}\right| \delta m \\ &= \left|M + \frac{1000}{m}\right| \frac{\delta\rho}{\rho^2} + \left|\frac{1000\,(\rho - \rho_o)}{m^2\rho\rho_o}\right| \delta m \end{aligned} \tag{3.12}$$

and

Table 3.1 Partial molar volumes and heat capacities at infinite dilution of aqueous NaCl solutions at 288.15, 298.15, 313.15, and 328.15 K.

$\bar{V}_2^o$ ($cm^3\ mol^{-1}$)	A_V^m ($cm^3\ kg^{1/2}\ mol^{-3/2}$)	$\bar{C}p_2^o$ ($J\ K^{-1}\ mol^{-1}$)	A_J^m ($J\ kg^{1/2}\ mol^{-3}\ K^{-1}$)
		T = 288.15 K	
15.49 ± 0.07 [15.60[a], 15.57[b], 15.62[c], 15.55[d], 15.63[e], 15.43[f], 15.68[k], 15.55[l]]	1.7150	-107.2 ± 1.7 [-107.5[d], -110.3[g], -109.7[l]]	29.882
		T = 298.15 K	
16.62 ± 0.01 [16.61[c], 16.62[d], 16.62[e], 16.63[h], 16.68[k], 16.62[l]]	1.8743	-85.7 ± 0.4 [-84.3[i], -84.6[j], -84.4[g], -85.0[l]]	32.783
		T = 313.15 K	
17.54 ± 0.01 [17.60[l]]	2.1540	-68.4 ± 0.4 [-65.7[l]]	37.446
		T = 328.15 K	
17.77 ± 0.02 [17.72[k], 17.76[c], 18.01[l], 17.92[a], 17.91[b]]	2.4946	-59.2 ± 1.2 [-58.8[l]]	42.699

[a](Lo Surdo *et al.*, 1982) [b](Millero, 1970) [c](Dunn, 1968) [d](Perron *et al.*, 1975) [e](Dessauges *et al.*, 1980) [f](Chen *et al.*, 1977) [g](Desnoyers *et al.*, 1976) [h](Vaslow, 1966) [i](Olofsson, 1979) [j](Singh *et al.*, 1976) [k](Connaughton *et al.*, 1986) [l](Archer, 1992) [m](Ananthaswamy & Atkinson, 1984)

$$\delta C_{p2,\phi} = \left|\frac{\partial C_{p2\phi}}{\partial C_p}\right| \delta C_p + \left|\frac{\partial C_{p2\phi}}{\partial m}\right| \delta m$$

$$= \left|M + \frac{1000}{m}\right| \delta C_p + \left|\frac{1000\,(C_p - C_{p1}^{o})}{m^2}\right| \delta m\,. \qquad (3.13)$$

For aqueous solutions of sodium chloride it is assumed that concentration errors are negligible, therefore $\delta m=0$.

Table 3.1 shows that partial molar properties at infinite dilution for aqueous sodium chloride, obtained using these instruments and current calibration constants, are in good agreement with previously published data.

3.5 High temperature and pressure densimetry

As discussed in Chapter 2 volumetric data can be related to the temperature dependence of the Gibbs energy and the pressure dependence of the entropy. This dependence requires volumetric data over a wide range of temperatures and pressures. Also, for aqueous solutions interesting thermodynamics occurs near the critical point of water and there are very few reliable sets of densimetric and volumetric data in this high temperature and pressure region. Indeed, this area of research is experimentally difficult. However, recent innovations in the design of vibrating tube densimeters has increased the availability of data in the elevated temperature and pressure region (Albert & Wood, 1984; Hakin *et al.*, 1998; Majer *et al.*, 1991; Simonson *et al.*, 1994).

Figure 3.4 shows a high temperature and pressure vibrating tube densimeter built at the University of Lethbridge, capable of reaching temperatures of 523 K and pressures of 30 MPa. A detailed description of this instrument has been published by Hakin *et al.* (1998). Basically, a stainless steel vibrating tube is housed in an aluminium block contained within two heat shields, which are secured inside a large iron can. A light beam is fed into the block through a 2 mm Pyrex glass rod and then fed to a detector by a 4 mm glass rod. Using the square wave signal produced by the vibrating tube chopping light, an optically coupled feedback amplifier circuit supplies an AC current to the vibrating tube.

Figure 3.4 Simplified diagram of the high temperature and pressure vibrating tube densimeter.

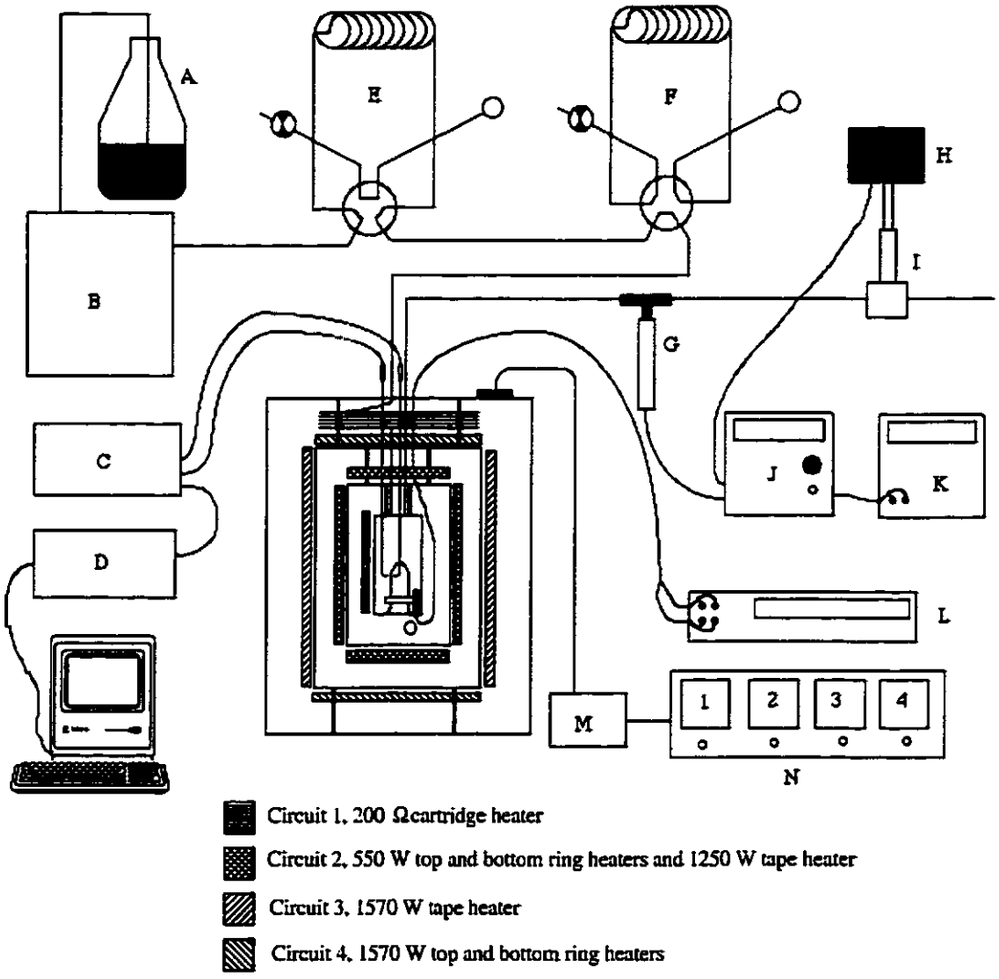

A) Reference solution reservoir (degassed water). B) HPLC pump C) Optically coupled feedback circuit. D) Frequency counter. E) Rheodyne injection valve 1 (inject position). F) Rheodyne injection valve 2 (load position). G) Pressure transducer. H) Stepping motor. I) Metering needle valve. J) PID pressure controller. K) Logging multimeter. L) Digital voltmeter. M) Relays. N) PID temperature controllers. O) 500 Ω platinum resistance thermometer.

There is a small permanent magnet attached to the side of the aluminium block. Hence the magnetic field combined with the AC current through the tube, forces the tube to vibrate according to the feedback frequency. The feedback amplifier has an output to an Optoelectronics 8040 TCXO time period counter that is interfaced to an IBM PS/2 computer. Data are collected as 1000 count averages and visually analysed using a commercial software package or another form of automated analysis (Chapter 4).

Temperature is controlled by four Omega model CN9000A PID controllers sampling from NiCr, type K, thermocouples. Control of strip heaters and ring heaters, associated with a particular shield and controller, is achieved through Omega model SSR240DC10 solid state relays. The temperature of the block is followed by a 500 Ω platinum resistance thermometer (Burns Engineering, Model No. XXPOG5-2-5B) connected to an HP 2456A digital voltmeter.

Perhaps one of the most innovative modifications to this vibrating tube densimeter is the PID pressure control. A high performance liquid chromatography pump (Waters model 501) is used to pump fluid through the system to a metering needle valve (Whitley SS-21RS2). The valve is controlled with a home-made PID feedback circuit, sampling from an Omega Model PX302-7.5KGV pressure traducer and outputting to an Intelligent Motion Systems Inc. model M2-2232-D stepping motor. The stepping motor is attached to the metering valve stem.

Samples are introduced via one of two sample loops attached to Rheodyne™ six port injection valves. Sample loops with an approximate volume of 3 mL were adequate for all studies within this thesis.

Calibration constants for this densimeter are obtained before and after every two sample runs. The time period stability is somewhat lower than the O2D densimeter described earlier; however, data produced by this machine still afforded thermodynamic discussion and interpretation, as its sensitivity is sufficient to determine excess and apparent molar volumes for several solutions.

4) AUTOMATED ANALYSIS OF DATA OBTAINED WITH A HIGH TEMPERATURE AND PRESSURE DENSIMETER.[1]

4.1 Introduction

This study features a method of automated analysis that addresses both data region, peak detection, and baseline prediction problems for time period data obtained from the high temperature and pressure vibrating tube densimeter discussed in Section 3.5. While optical coupled feedback driving and proportional-integral-differential pressure control contribute to acceptable time period stability, small temperature drifts correlated with smaller time period drifts are still observed within measurements made at extreme experimental conditions. In general, noise and baseline drifts are more significant problems for high temperature and pressure densimeters; therefore, these instruments provide a severe test of automated analysis methods.

Quantitative instrumental analysis generally requires overcoming two problems: First, significant regions in the data stream must be located; secondly, a baseline must be estimated either from separate measurements or, preferably, from the main data themselves. Both tasks can be performed adequately by trained personnel, although automated computer analysis is an attractive alternative, because it minimises the time required to perform tedious analyses and eliminates the possibility of experimenter bias. However, both data region detection and baseline correction pose a variety of challenges for a computer program. These topics have therefore generated considerable literature (Chiu, 1997; Clifton & Steiner, 1983; O'Sullivan, 1986; Phillips & Hamilton, 1996).

Because of the squared time period relationship within equation 3.8, uncertainties in measured periods have a large influence on the calculated relative density, both through sample measurement and in obtaining the calibration constant. The time periods used for

---

[1]A version of this chapter has been published by Marriott R. A., Hakin A. W., Liu J. L., and Roussel M. R. (1999) *Computers and Chemistry* , in press.

equation 3.8 can be obtained by either averaging the points in the reference and sample portion or by viewing expanded plots, which enable the experimenter to visually extrapolate to the time period axis (Hakin *et al.*, 1998). Both these methods are susceptible to experimenter bias. In particular both methods allow the experimenter to choose which points are considered to be part of the plateau or the baseline. In addition to experimenter bias, the squared time period differences can be influenced by many other instabilities within the instrument.

Our peak detection algorithm proceeds from a knowledge of the number of samples injected into the instrument. A statistical test is applied to the local slope to locate the sample regions within the data stream. The confidence level of the test is adjusted by the program to ensure that the correct number of peaks are detected. While this approach has been developed specifically for detecting sample regions in our densimetric data, it could be easily adapted to the detection of peaks or plateaus from other instruments where the number of interesting regions are fixed or known *a priori*.

Once the sample and baseline regions have been identified, the program proceeds to fit a polynomial in the temperature to the baseline regions. We have used multiple regression to partition temperature variance from the overall time period variance of the vibrating tube.

Several treatments for reducing the uncertainty in calibration constants have also been considered. Constants can be obtained each day, several times a day, or once at each temperature. Some studies have used a quadratic equation to model the calibration constant over some specified temperature range (Simonson *et al.*, 1994). Although the latter approach seems to address changes due to temperature drifts, the wear on the tube from mechanical ageing is assumed to be minimal. Also, where each sample run can be up to twenty minutes long, the squared time period difference, $\tau^2 - \tau_0^2$, may change due to small temperature fluctuations within the calibration samples. We have chosen to calibrate our instrument with concentrated aqueous sodium chloride before and after every two sample

solution measurements. With this method we are confident that error due to mechanical ageing has been eliminated from both analysis methods considered in this study.

To compare the two analysis methods, densities of aqueous sodium bromide were measured at temperatures from 373 to 523 K and pressures from 10 to 30 MPa. Measurements were analysed using a user specified baseline method, by three different experimentalists, and using the numerical baseline correction program. Densities were used to calculate apparent molar volumes, which in turn were used to compare the two methods to a standard semi-empirical model (Archer, 1991).

4.2 Experimental

For the purposes of this study, remote collection of time period data was performed in unison with the collection of temperature data via an IEEE interface. Temperature data were obtained using a 500 Ω platinum resistance thermometer (Burns Engineering, Model No. XXPOG5-2-5B) connected to a HP 3456A digital voltmeter, as shown in figure 3.4. Figure 4.1 shows a typical plot of time period versus time containing a calibration peak before and after every two sample runs. Each pair of sample solution peaks, between calibration solution peaks, corresponds to samples of the same concentration.

The reference fluid, corresponding to the baseline signal in figure 4.1, was pure water. Water was obtained from an Osmonics model Aries High-Purity DI loop, capable of polishing to a resistance of 18.2 MΩ. Standard solutions of sodium chloride and sample solutions of sodium bromide were prepared by weight on the molality concentration scale from high purity commercial samples (Sigma® Cat. No. S-7653 and S-9890) after being dried at 383 K for over 24 hours. Through Archer's (1992) Pitzer Ion Interaction program for sodium chloride and Hill's (1990) equation of state for water, the densities of sodium chloride and water were calculated at the mean temperature and pressure of each peak. Calibration solutions were prepared at an average concentration of 5.3 mol kg^{-1} and sample solutions of sodium bromide were prepared with a molality range of 0.2310 to

Figure 4.1 A plot of time period of the vibrating tube versus time while solution is continuously flowing through the tube at 521.60±0.07 K and 30.00±0.01 MPa.

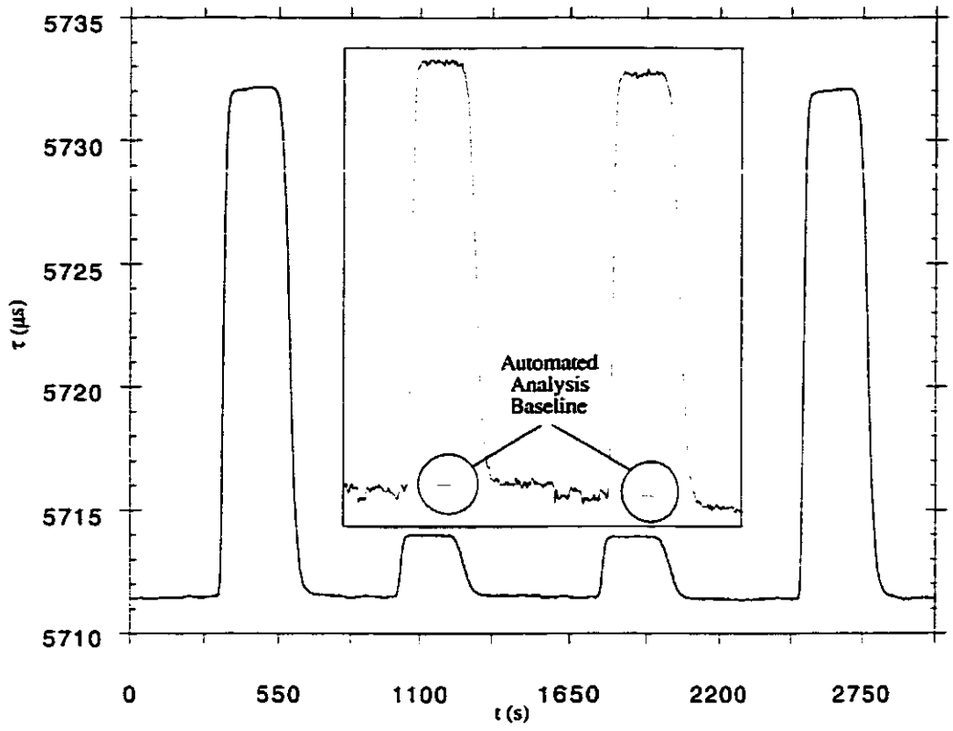

4.8903 mol kg^{-1}. All solutions were stored in sealable 100 mL Nalgene bottles.

4.3 Analysis

All code was written in C++ and is reported in Appendix A. The analysis program scanned the data files with moving windows of data, rather than inputting all the data at once. Small windows of data were used to fit straight lines and the slope or derivative was tested through a Student's t-test using a variable α value to distinguish plateau regions from sloped regions. The files were scanned and the α value increased until the number of sloped regions was equal to twice the number of samples specified by the user (figure 4.2).

Figure 4.2 Simplified flow diagram of the peak plateau and baseline identification Section of the automated analysis program.

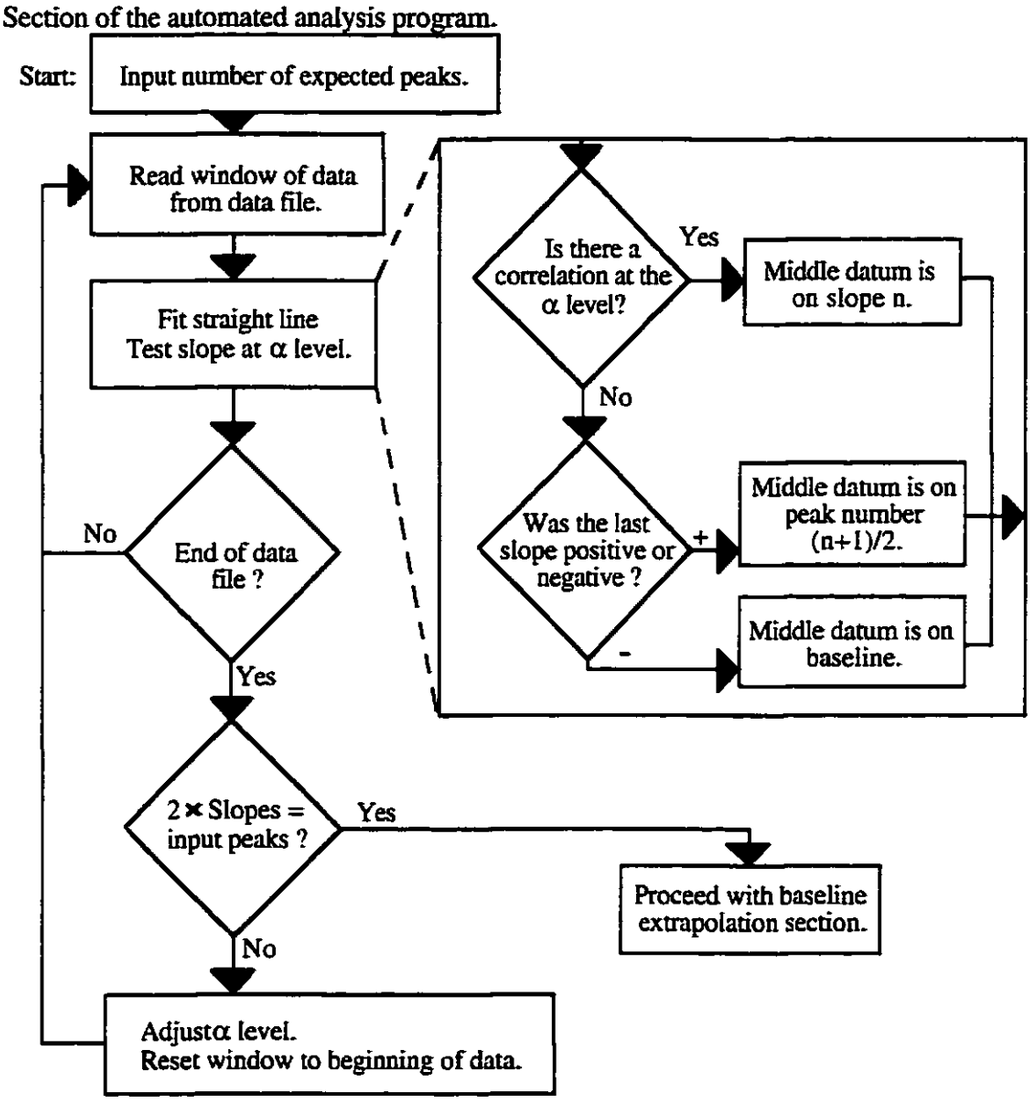

An adaptive method for peak detection has previously been described by Clifton and Steiner (1983), wherein the authors did not specify a constant threshold rejection region about the baseline, rather the threshold was adjusted according to the peak to noise ratio. Our analysis allows the peak to noise ratio, or straight line correlation, to predict the peaks by exceeding an acceptable probability. The acceptable value of the probability was

adjusted until the correct number of peaks were located. At this stage, our program simply scanned through the data, using a larger window (150 data points), and predicted baseline points corresponding to individual peak points in the middle of a given window.

Several forms of a temperature relationship equation were evaluated by fitting equations to baseline data obtained during stable and unstable temperature conditions. Through comparisons of the various F statistics, a quadratic form proved to be the most robust. Estimated baseline points, $\hat{t}_O$, used for the calculation of the squared time period difference, $\tau^2 - \hat{t}_O^2$, were predicted by fitting equation 4.1 to all baseline points within 75000 time period measurements of the peak point of interest:

$$\hat{t}_O = \hat{\beta}_O + \hat{\beta}_1 T + \hat{\beta}_2 T^2. \qquad (4.1)$$

The equation was refit for every point analysed, to reduce the influence of tube wear on baseline point predictions. Mean temperatures for peaks were calculated by the program using temperature points corresponding only to points on the peak of interest.

Probable error for densities calculated using the user specified baseline method, $\sigma\Delta\rho_{vis}$, have been calculated according to equation 4.2:

$$\sigma\Delta\rho_{vis} = \sqrt{\sigma\Delta\rho_e^2 + \sigma\Delta\rho_c^2}, \qquad (4.2)$$

where $\sigma\Delta\rho_e$ is the estimated error associated with the sample peaks and $\sigma\Delta\rho_c$ is the estimated error associated with the calibration peaks. Because two peaks exist for both sample solution and calibration, the user specified baseline method uses the difference between two densities of a given peak type, $\Delta\Delta\rho_i$, to estimate errors. This method of error calculation is consistent with previous studies (Hakin *et al.*, 1998).

The analysis program calculated squared time period differences for every point on any given peak, therefore standard deviations and standard errors were also calculated for each peak. These standard errors, calculated at the 95% confidence level, $t_{2.5\%}$, were used for the prediction of error values for densities calculated through the analysis program, $\sigma\Delta\rho_{prog}$. Equation 4.3 shows this relationship with relative error for each peak:

$$\sigma\Delta\rho_{prog} = \Delta\rho\sqrt{\left(\frac{t_{2.5\%}\sigma\Delta\tau^2}{\Delta\tau^2}\right)^2 + \left(\frac{t_{2.5\%}\sigma\Delta\tau_C^2}{\Delta\tau_C^2}\right)^2}. \quad (4.3)$$

Relative errors for the reference peaks, $t_{2.5\%}\sigma\Delta\tau_C^2/\Delta\tau_C^2$, were averaged for the closest reference solutions on either side of the sample peak. Where the user specified baseline errors required the analysis of two peaks containing the same sample, the automated analysis method needed only one peak to predict the relative error on a sample peak, $t_{2.5\%}\sigma\Delta\tau^2/\Delta\tau^2$, because of available standard deviations.

All spectra were analysed by three experimentalists (A. W. Hakin, J. L. Liu, and R. A. Marriott) with considerable experience with this vibrating tube densimeter and the user specified baseline method. Because the analysis program calculated an average temperature for each peak, a single temperature was used for each peak for all analysis methods and users. This single temperature ensured a consistent value for water density for individual calculations. With previous studies utilising the user specified baseline method, temperature was averaged from two resistance readings obtained before and after a sample solution measurement.

4.4 Results and Discussion

Relative densities for aqueous sodium bromide solutions, as calculated by the analysis program and the user specified baseline method, are reported in table 4.1. Relative densities were used to calculate apparent molar volumes, $V_{2,\phi}$, using equation 3.9 and uncertainties in apparent molar volumes have been calculated using equation 3.12. Calculated apparent molar volumes and their respective uncertainties for the user specified baseline method and the automated analysis method are shown in table 4.2 with those calculated from Archer's Pitzer Ion Interaction program for solutions of sodium bromide in water (Archer, 1991).

The data show that, even with low molalities and small peaks, the analysis program is able to detect the peak plateau region and calculate values which agree with the user

Table 4.1. Densities of aqueous sodium bromide as analysed by three different experimentalists at 374, 419, 473, and 522 K.

T (K)	m (mol kg^{-1})	ρ_0 [c] (kg m^{-3})	$\rho - \rho_0$ [d] (kg m^{-3})	$\rho - \rho_0$ [e] (kg m^{-3})	$\rho - \rho_0$ [f] (kg m^{-3})
		p = 10.00 ±0.01 MPa			
373.85	4.8552	962.46	309.19±0.53	309.20±0.60	309.35±0.49
373.86	4.8552	962.45	309.62±0.53	309.64±0.60	309.79±0.49
373.88	3.9614	962.43	259.31±0.36	259.49±0.37	259.35±0.31
373.91	3.9614	962.41	259.49±0.36	259.66±0.37	259.53±0.31
373.95	3.5195	962.39	233.79±0.33	233.67±0.29	233.87±0.20
373.99	3.5195	962.36	233.89±0.33	233.84±0.29	233.81±0.20
373.95	2.8240	962.38	191.55±0.58	191.58±0.53	191.58±0.49
373.92	2.8240	962.41	191.79±0.58	191.75±0.53	191.85±0.49
373.83	1.9939	962.47	138.84±0.27	138.85±0.41	138.83±0.36
373.82	1.9939	962.48	139.09±0.27	139.24±0.41	139.18±0.36
373.80	1.4730	962.50	104.42±0.27	104.38±0.45	104.45±0.23
373.80	1.4730	962.50	104.68±0.27	104.83±0.45	104.68±0.23
373.79	0.8033	962.50	58.16±0.20	58.04±0.34	58.14±0.25
373.78	0.8033	962.51	58.36±0.20	58.37±0.34	58.38±0.25
373.79	0.2310	962.50	17.28±0.04	17.21±0.02	17.25±0.08
373.76	0.2310	962.52	17.24±0.04	17.21±0.02	17.17±0.08
373.31	4.8552	962.84	309.74±0.53	310.47±0.35	310.14±0.46
373.43	4.8552	962.75	310.25±0.53	310.81±0.35	310.59±0.46
373.60	3.9614	962.63	259.54±0.67	260.13±0.61	259.58±0.69
373.65	3.9614	962.60	259.82±0.67	260.02±0.61	259.92±0.69
373.73	3.5195	962.54	233.50±0.30	233.60±0.61	233.54±0.52
373.76	3.5195	962.52	233.78±0.30	234.21±0.61	234.02±0.52
373.82	2.8240	962.50	191.62±0.58	191.73±0.68	191.76±0.44
373.80	2.8240	962.49	191.82±0.58	192.00±0.68	191.87±0.44
373.82	1.9939	962.48	139.16±0.29	139.23±0.22	139.06±0.21
373.88	1.9939	962.44	138.87±0.29	139.01±0.22	138.85±0.21
373.88	1.4730	962.43	105.10±0.73	105.09±0.61	105.05±0.79
373.87	1.4730	962.44	104.38±0.73	104.49±0.61	104.27±0.79
512.80	0.2942	807.85	24.89±0.27	24.94±0.40	24.81±0.19

Table 4.1 continued

521.73	0.2942	807.96	24.63±0.27	24.54±0.40	24.61±0.19
521.77	0.8281	807.91	66.37±0.27	66.42±0.30	66.40±0.25
521.77	0.8281	807.91	66.63±0.27	66.62±0.30	66.63±0.25
521.73	1.5015	807.96	116.21±0.08	116.19±0.15	115.98±0.11
521.74	1.5015	807.93	116.15±0.08	116.10±0.15	116.06±0.11
521.73	1.9324	807.96	146.58±0.36	146.54±0.51	146.66±0.57
521.76	1.9324	807.91	146.72±0.36	146.83±0.51	146.79±0.57
521.86	2.7693	807.76	202.13±0.46	202.44±0.63	202.25±0.78
521.92	2.7693	807.68	202.23±0.46	202.29±0.63	202.27±0.78
521.98	3.5340	807.59	250.56±0.03	250.46±0.13	250.57±0.05
522.02	3.5340	807.53	250.56±0.03	250.41±0.13	250.62±0.05
522.06	4.2692	807.48	294.15±0.41	294.51±0.50	294.21±0.33
522.11	4.2692	807.39	294.46±0.41	294.46±0.50	294.24±0.33
522.10	4.8903	807.42	328.83±0.72	328.86±0.55	328.87±0.55
522.07	4.8903	807.47	329.54±0.72	329.41±0.55	329.42±0.55
		p = 20.00 ±0.01 MPa			
418.37	0.2942	931.94	21.71±0.28	21.46±0.71	21.53±0.56
418.38	0.2942	931.94	21.99±0.28	22.17±0.71	22.09±0.56
418.37	0.8281	931.94	60.03±0.23	60.14±0.05	60.03±0.18
418.35	0.8281	931.96	60.26±0.23	60.19±0.05	60.20±0.18
418.45	1.5015	931.87	106.40±0.42	106.42±0.22	106.21±0.23
418.55	1.5015	931.78	106.24±0.42	106.22±0.22	106.23±0.23
418.66	1.9324	931.68	134.95±0.43	134.88±0.53	134.88±0.48
418.65	1.9324	931.69	135.00±0.43	135.39±0.53	135.18±0.48
418.66	2.7693	931.69	187.79±0.01	188.04±0.23	187.90±0.17
418.69	2.7693	931.67	187.80±0.01	187.99±0.23	187.78±0.17
418.78	3.5340	931.59	233.69±0.06	233.87±0.16	233.78±0.10
418.79	3.5340	931.57	233.73±0.06	234.02±0.16	233.87±0.10
418.75	4.2692	931.61	274.18±2.28	273.96±2.39	273.95±2.49
418.62	4.2692	931.73	275.86±2.28	275.47±2.39	275.41±2.49
472.47	0.2942	878.78	22.61±0.02	22.58±0.06	22.48±0.17
472.51	0.2942	878.74	22.68±0.02	22.64±0.06	22.65±0.17
472.61	0.8281	878.62	61.62±0.04	61.53±0.23	61.52±0.18
472.66	0.8281	878.57	61.71±0.04	61.76±0.23	61.70±0.18

Table 4.1 continued

472.75	1.5015	878.47	108.77±0.20	108.81±0.36	108.78±0.17
472.76	1.5015	878.47	108.80±0.20	108.69±0.36	108.68±0.17
472.76	1.9324	878.47	137.58±0.23	137.55±0.44	137.57±0.20
472.76	1.9324	878.47	137.81±0.23	137.78±0.44	137.56±0.20
472.84	2.7693	878.38	191.08±0.20	191.08±0.41	191.15±0.28
472.85	2.7693	878.37	191.35±0.20	191.49±0.41	191.33±0.28
472.90	3.5340	878.31	237.52±0.42	237.80±0.30	237.68±0.41
472.93	3.5340	878.27	237.85±0.42	237.69±0.30	237.92±0.41
472.87	4.2692	878.34	280.05±0.27	280.23±0.15	280.17±0.23
472.85	4.2692	878.36	280.13±0.27	280.20±0.15	280.20±0.23
472.86	4.8903	878.36	314.07±0.13	314.04±0.98	314.18±0.72
472.88	4.8903	878.34	314.75±0.13	315.02±0.98	314.89±0.72
		p = 30.00 ±0.01 MPa			
373.80	4.8552	971.40	309.96±0.20	309.47±0.44	309.73±1.07
373.74	4.8552	971.44	310.13±0.20	309.91±0.44	309.26±1.07
373.50	3.9614	971.60	259.91±0.58	259.93±0.92	260.17±0.72
373.19	3.9614	971.82	259.40±0.58	259.16±0.92	259.46±0.72
373.16	3.5195	971.84	233.30±0.28	233.22±0.46	233.41±0.24
373.17	3.5195	971.83	233.43±0.28	233.29±0.46	233.64±0.24
373.46	2.8240	971.63	190.96±0.46	191.16±0.40	191.11±0.30
373.47	2.8240	971.63	191.33±0.46	191.51±0.40	191.39±0.30
373.48	1.9939	971.62	138.41±0.43	138.73±0.49	138.55±0.39
373.50	1.9939	971.61	138.82±0.43	139.19±0.49	138.94±0.39
373.46	1.4730	971.63	104.32±0.08	104.40±0.29	104.24±0.33
373.46	1.4730	971.64	104.38±0.08	104.69±0.29	104.57±0.33
376.38	1.9939	969.61	138.11±0.24	138.24±0.72	138.07±0.38
376.41	1.9939	969.59	138.35±0.24	138.47±0.72	138.35±0.38
376.37	1.4730	969.63	104.38±0.33	104.46±0.23	104.33±0.32
376.35	1.4730	969.64	104.14±0.33	104.24±0.23	104.22±0.32
376.30	0.8033	969.67	58.23±0.05	58.20±0.14	58.24±0.13
376.30	0.8033	969.67	58.37±0.05	58.34±0.14	58.37±0.13
376.29	0.2310	969.68	17.21±0.02	17.15±0.06	17.08±0.04
376.28	0.2310	969.68	17.10±0.02	17.09±0.06	17.04±0.04
521.62	0.2942	827.65	23.79±0.25	23.87±0.20	23.83±0.16

Table 4.1 continued

521.59	0.2942	827.68	24.04±0.25	24.07±0.20	23.99±0.16
521.54	0.8281	827.77	64.90±0.65	65.13±0.71	65.25±0.86
521.52	0.8281	827.78	64.25±0.65	64.42±0.71	64.40±0.86
521.48	1.5015	827.84	113.07±0.22	113.10±0.25	113.05±0.40
521.35	1.5015	828.00	112.85±0.22	112.84±0.25	112.66±0.40
521.62	1.9324	827.67	142.47±0.45	142.51±0.22	142.52±0.41
521.63	1.9324	827.65	142.87±0.45	142.71±0.22	142.85±0.41
521.66	2.7693	827.60	198.29±0.51	198.13±1.36	198.15±1.39
521.72	2.7693	827.53	197.96±0.51	196.88±1.36	196.79±1.39
521.80	3.5340	827.42	244.15±0.84	244.19±0.85	244.24±0.75
521.77	3.5340	827.46	244.87±0.84	245.00±0.85	244.93±0.75
521.73	4.2692	827.51	286.37±0.31	286.02±0.89	286.48±0.39
521.74	4.2692	827.50	286.65±0.31	286.68±0.89	286.84±0.39
521.77	4.8903	827.47	322.20±0.61	322.18±0.75	322.46±0.14
521.78	4.8903	827.46	322.17±0.61	322.19±0.75	322.45±0.14

(c) Hill's equation of state for water (1990). (d) User specified baseline method (User A). (e) User specified baseline method (User B). (f) User specified baseline method (User C).

specified baseline method. Both methods give results which are, on average, lower than Archer's (1991) program predicts. This deviation is consistent with previous unpublished measurements and can be explained by the lack of data in this temperature and pressure range when the model was being constructed. The deviation increases with temperature, showing the difficulty in predicting properties removed from experimental temperatures near ambient.

On average the analysis program's baseline fit accounted for 21% of noise through correlation with temperature drift; however, through computed residuals from Archer's (1991) program, the results did not correlate with total temperature drift any better than the visual method. An analysis of variance from predicted values at an α-level of 0.05, suggests the automated analysis accounts for more variance than any individual user, yet cannot account for more variance than all users combined. Combining the data of all users for the user specified baseline method creates three times the number of samples as the

Table 4.2. A comparison of apparent molar volumes of aqueous sodium bromide at 374, 419, 473, and 522 K.

T (K)	m (mol kg^{-1})	$\rho - \rho_o$ [a] (kg m^{-3})	$V_{2,\phi}$ [a] (cm^3 mol^{-1})	$V_{2,\phi}$ [b] (cm^3 mol^{-1})	$V_{2,\phi}$ [c] (cm^3 mol^{-1})
		p = 10.00 ±0.01 MPa			
373.85	4.8552	309.53±0.71	28.82±0.13	28.87±0.10	28.80
373.86	4.8552	309.80±0.71	28.77±0.14	28.79±0.10	28.80
373.88	3.9614	258.86±0.49	28.66±0.12	28.54±0.08	28.55
373.91	3.9614	259.40±0.48	28.53±0.12	28.49±0.08	28.55
373.95	3.5195	233.63±0.40	28.37±0.11	28.32±0.07	28.40
373.99	3.5195	234.13±0.39	28.23±0.11	28.30±0.07	28.40
373.95	2.8240	191.87±0.30	27.99±0.10	28.09±0.18	28.15
373.92	2.8240	192.06±0.31	27.92±0.11	28.01±0.18	28.15
373.83	1.9939	139.04±0.28	27.64±0.14	27.74±0.17	27.77
373.82	1.9939	139.13±0.29	27.60±0.14	27.57±0.17	27.77
373.80	1.4730	104.30±0.40	27.50±0.27	27.42±0.22	27.46
373.80	1.4730	104.76±0.34	27.18±0.23	27.20±0.22	27.46
373.79	0.8033	57.84±0.34	27.53±0.43	27.17±0.34	26.89
373.78	0.8033	58.26±0.21	26.99±0.27	26.84±0.34	26.89
373.79	0.2310	17.04±0.16	26.83±0.75	25.88±0.20	25.97
373.76	0.2310	17.07±0.19	26.84±0.86	26.05±0.20	25.97
373.31	4.8552	310.13±0.92	28.72±0.18	28.72±0.09	28.80
373.43	4.8552	310.66±0.82	28.61±0.16	28.64±0.09	28.80
373.60	3.9614	259.74±0.82	28.46±0.20	28.46±0.16	28.55
373.65	3.9614	259.80±0.75	28.44±0.18	28.42±0.16	28.55
373.73	3.5195	233.65±0.71	28.37±0.19	28.40±0.13	28.41
373.76	3.5195	234.05±0.62	28.25±0.17	28.27±0.13	28.41
373.82	2.8240	191.82±0.33	28.01±0.11	28.05±0.19	28.15
373.80	2.8240	192.56±0.41	27.75±0.14	27.98±0.19	28.15
373.82	1.9939	139.28±0.47	27.52±0.24	27.59±0.12	27.77
373.88	1.9939	138.86±0.49	27.73±0.24	27.70±0.12	27.77
373.88	1.4730	104.95±0.52	27.05±0.36	26.96±0.49	27.45
373.87	1.4730	104.44±0.82	27.40±0.56	27.44±0.49	27.45
521.80	0.2942	24.91±0.25	-2.25±1.24	-2.12±1.47	-0.08

Table 4.2 continued

521.73	0.2942	24.50±0.20	-0.21±1.00	-0.65±1.47	-0.04
521.77	0.8281	66.54±0.32	3.94±0.55	4.18±0.47	5.15
521.77	0.8281	66.36±0.25	4.25±0.43	3.79±0.47	5.15
521.73	1.5015	116.74±0.46	7.22±0.42	7.77±0.10	8.77
521.74	1.5015	116.90±0.62	7.07±0.56	7.78±0.10	8.77
521.73	1.9324	147.24±0.57	9.00±0.39	9.44±0.33	10.45
521.76	1.9324	147.84±0.58	8.58±0.39	9.31±0.33	10.44
521.86	2.7693	202.33±0.42	12.33±0.19	12.35±0.29	12.95
521.92	2.7693	202.43±0.43	12.27±0.19	12.35±0.29	12.93
521.98	3.5340	250.15±0.59	14.42±0.20	14.29±0.02	14.75
522.02	3.5340	250.54±0.53	14.28±0.18	14.28±0.02	14.74
522.06	4.2692	294.76±0.67	15.84±0.19	15.91±0.11	16.23
522.11	4.2692	294.76±0.60	15.77±0.17	15.88±0.11	16.22
522.10	4.8903	329.69±0.72	17.06±0.17	17.26±0.14	17.34
522.07	4.8903	327.28±0.65	17.64±0.15	17.12±0.14	17.34
		p = 20.00 ±0.01 MPa			
418.37	0.2942	21.69±0.56	24.97±2.16	25.43±1.99	24.14
418.38	0.2942	21.69±0.53	23.98±2.04	23.45±1.99	24.14
418.37	0.8281	59.72±0.27	25.73±0.36	24.94±0.21	25.31
418.35	0.8281	60.11±0.42	25.21±0.56	25.07±0.21	25.31
418.45	1.5015	106.13±0.34	26.06±0.25	25.91±0.21	26.12
418.55	1.5015	106.07±0.49	26.10±0.35	25.98±0.21	26.12
418.66	1.9324	133.97±0.70	26.73±0.38	26.23±0.26	26.49
418.65	1.9324	134.93±0.40	26.21±0.22	26.07±0.26	26.49
418.66	2.7693	188.08±0.63	26.79±0.23	26.86±0.05	27.07
418.69	2.7693	187.78±0.49	26.91±0.18	26.88±0.05	27.07
418.78	3.5340	234.33±0.56	27.21±0.16	27.37±0.03	27.48
418.79	3.5340	233.92±0.68	27.32±0.19	27.34±0.03	27.48
418.75	4.2692	274.15±0.76	28.17±0.18	28.20±0.55	27.83
418.62	4.2692	275.83±0.85	27.79±0.20	27.85±0.55	27.83
472.47	0.2942	22.53±0.20	17.49±0.85	17.39±0.44	17.37
472.51	0.2942	22.51±0.17	17.59±0.71	16.95±0.44	17.37
472.61	0.8281	61.60±0.17	19.39±0.25	19.46±0.26	19.58
472.66	0.8281	61.73±0.29	19.21±0.42	19.21±0.26	19.58

Table 4.2 continued

472.75	1.5015	108.49±0.18	20.92±0.14	20.69±0.19	21.14
472.76	1.5015	108.22±0.21	21.13±0.16	20.74±0.19	21.14
472.76	1.9324	136.58±0.38	22.11±0.17	21.52±0.19	21.88
472.76	1.9324	136.93±0.27	21.90±0.16	21.43±0.19	21.88
472.84	2.7693	191.13±0.26	22.75±0.10	22.76±0.14	23.00
472.85	2.7693	191.33±0.29	22.66±0.12	22.64±0.14	23.00
472.90	3.5340	237.48±0.38	23.65±0.12	23.59±0.13	23.82
472.93	3.5340	237.90±0.33	23.52±0.10	23.55±0.13	23.82
472.87	4.2692	280.34±0.46	24.29±0.12	24.33±0.06	24.50
472.85	4.2692	280.14±0.40	24.34±0.10	24.33±0.06	24.50
472.86	4.8903	314.15±0.45	24.96±0.10	24.97±0.17	25.01
472.88	4.8903	314.72±0.52	24.84±0.11	24.80±0.17	25.01
		p = 30.00 ±0.01 MPa			
373.80	4.8552	309.81±0.81	29.04±0.15	29.06±0.10	29.15
373.74	4.8552	310.04±0.70	29.00±0.13	29.06±0.10	29.15
373.50	3.9614	259.82±0.69	28.74±0.16	28.70±0.08	28.93
373.19	3.9614	259.65±0.70	28.79±0.16	28.87±0.08	28.93
373.16	3.5195	233.41±0.74	28.76±0.20	28.79±0.07	28.81
373.17	3.5195	233.79±0.62	28.66±0.17	28.74±0.07	28.81
373.46	2.8240	190.99±0.66	28.64±0.22	28.61±0.18	28.58
373.47	2.8240	191.43±0.79	28.49±0.27	28.49±0.18	28.58
373.48	1.9939	138.49±0.51	28.30±0.25	28.26±0.17	28.24
373.50	1.9939	138.84±0.51	28.12±0.25	28.06±0.17	28.24
373.46	1.4730	104.53±0.45	27.75±0.30	27.89±0.22	27.96
373.46	1.4730	104.20±0.44	27.97±0.30	27.74±0.22	27.96
376.38	1.9939	138.19±0.24	28.36±.011	28.39±0.34	28.20
376.41	1.9939	138.46±0.26	28.23±0.13	28.26±0.34	28.20
376.37	1.4730	103.70±0.22	28.22±0.15	27.75±0.20	27.91
376.35	1.4730	104.11±0.23	27.95±0.16	27.89±0.20	27.91
376.30	0.8033	58.29±0.23	27.30±0.30	27.38±0.09	27.39
376.30	0.8033	58.27±0.25	27.33±0.32	27.21±0.09	27.39
376.29	0.2310	17.11±0.22	26.86±0.98	26.73±0.16	26.53
376.28	0.2310	16.99±0.18	27.43±0.82	27.04±0.16	26.53
521.62	0.2942	23.80±0.20	6.06±0.98	5.93±0.99	6.41

Table 4.2 continued

521.59	0.2942	23.75±0.29	6.30±1.41	4.96±0.99	6.42
521.54	0.8281	64.86±0.38	9.27±0.63	8.90±1.22	10.46
521.52	0.8281	64.25±0.54	10.28±0.88	10.11±1.22	10.46
521.48	1.5015	112.76±0.33	12.96±0.29	12.68±0.25	13.29
521.35	1.5015	113.63±0.79	12.22±0.69	12.95±0.25	13.32
521.62	1.9324	142.37±0.27	14.32±0.18	14.23±0.24	14.58
521.63	1.9324	143.12±0.40	13.82±0.26	14.02±0.24	14.58
521.66	2.7693	198.12±0.52	16.05±0.23	16.01±0.48	16.61
521.72	2.7693	196.83±0.74	16.61±0.33	16.44±0.48	16.60
521.80	3.5340	243.94±0.71	18.18±0.24	18.09±0.27	18.07
521.77	3.5340	244.21±0.55	18.09±0.18	17.84±0.27	18.08
521.73	4.2692	286.31±0.82	19.62±0.22	19.63±0.14	19.31
521.74	4.2692	286.96±0.68	19.45±0.18	19.51±0.14	19.31
521.77	4.8903	322.75±0.85	20.12±0.20	20.23±0.11	20.23
521.78	4.8903	322.78±0.71	20.11±0.16	20.22±0.11	20.23

(a) Automated analysis method. (b) User specified baseline method averaged over three users. (c) Calculated from Archer (1991).

automated analysis. Even with this large increase in sample number, the user specified baseline method fails to account for more variance than the automated analysis. Rather, the two methods account for equal amounts of variance. While the analysis program may not perform significantly better than the user baseline specified method, it clearly performs no worse.

Standard errors were calculated at the 95% confidence level using all four calculations for each sample solution. These standard errors showed 13.6% disagreement with the user specified baseline method and 8.2% disagreement with the automated analysis method. The two-sample format of the user specified baseline method averages error for two peaks and seems to exaggerate the error in one and underestimate the other. This effect contributes to slightly inferior error prediction, while the automated analysis is made more robust by determining errors for individual sample peaks.

Because of the direct standard deviation calculation for each peak, in the future, instead of running two solutions of the same concentration, two different concentrations can be run in between calibration solutions. Although replicates may be desired, there is no longer a constraint by the method of computing error. Not only can the number of runs be increased but the concentration range can be more densely sampled, providing for more robust models. If one event destroys a sample run, the previous sample peak may be usable, whereas with the alternative method either the standard error is exaggerated or both densities are thrown out.

During the study there were two shut-downs due to leaks within the instrument. The standard errors reported by the analysis program increased rapidly approximately one hour before data collection was abandoned. While the visual method allows the user to overlook small dips in the baseline due to instrumental problems, the standard errors calculated through the automated analysis program can be used as indicators of instrumental failure and of unreliable data. This feature may lead to future instrumental confidence testing.

Because it takes approximately two hours for an experimentalist to visually analyse 7 hours of experimental data and the analysis program is shown to perform as well as any experimentalist, efficiency is a factor. The automated analysis requires a maximum time of one minute to analyse seven hours worth of data.

This automated statistical approach to analysis of data could be adapted to other analytic instruments such as Picker microflow calorimeters, titration calorimeters, differential scanning calorimeters, and possibly to some applications within chromatography.

5) APPARENT MOLAR HEAT CAPACITIES AND VOLUMES OF THE AQUEOUS RARE EARTH SULPHATES.

5.1 Introduction

Thermal neutron fission of uranium or plutonium based fuels yields significant quantities of light rare earth metals and yttrium. Rare earth salts are also of interest because they represent a complete series of aqueous trivalent ions. Therefore the thermodynamic characterisation of aqueous rare earth salts may be used to learn more about trivalent ion-solvent and ion-ion interactions. With respect to nuclear waste management, americium, plutonium, and neptunium also have soluble trivalent ions; however problems with their radioactivity limit the extent to which experimentalists are able to safely handle them. By thermodynamic characterisation of a variety of trivalent rare earth ions, it may be possible to better understand the thermodynamic properties of these hazardous species. The importance of the thermodynamic characterisation of aqueous rare earth salts is therefore of interest to the nuclear industry in the treatment of radioactive waste containing fission products (Miodushi, 1998).

As discussed in Chapter 2, apparent molar heat capacities and volumes provide information with respect to the pressure and temperature dependence of any path independent Gibbs energy change involving rare earth ions and their complexes. Often the first data to become available are those at ambient temperature and pressure. Even without a knowledge of the temperature dependence of a heat capacity, ambient temperature heat capacities can still yield reasonable predictions of Gibbs energy changes below 423 K (Puigdomench *et al.*, 1997). Puigdomench *et al.* (1997) have also pointed out that previous extrapolations to infinite dilution from relatively high concentration experimental heat capacities of aqueous rare earth solutions obtained at ambient temperature are more positive than more recent measurements by as much as 75 J K^{-1} mol^{-1}.

While densimetric and thermochemical studies have reported volumetric and heat capacity data for aqueous rare earth chlorides, nitrates, and perchlorates, which exhibit negligible complexation, the heat capacities of aqueous rare earth sulphate species have yet to be studied. Aqueous rare earth sulphate solutions are good candidates for thermodynamic studies, because of their negligible hydrolysis (Baes & Mesmer, 1976). However, complex ion formation complicates characterisation (Fay & Purdie, 1969,1970; Fisher & Davies, 1967; Izatt *et al.*, 1969). Species currently described within the literature can be manipulated to provide single ion heat capacities and volumes, thus infinite dilution partial molar heat capacities and volumes can be calculated for the rare earth sulphates. The incomplete formation of complexes does however indicate that predictions beyond infinite dilution require an investigation into the experimental heat capacities and volumes over a wide concentration range. In addition, Rard (1996) has noted that osmotic coefficients, obtained from freezing point depression studies, require enthalpies of dilution and heat capacity data for their accurate conversion to ambient temperature. The presence of complex monosulphate and disulphate complex species indicate that infinite dilution heat capacities predicted through single ion heat capacities may not yield precise constant heat capacities in the concentration region required by the conversion mentioned above. In addition to the conversion of osmotic coefficients, heat capacities, being a second derivative of the Gibbs energy, convey a great deal of information about structural and electrostatic interactions (Woolley & Hepler, 1977).

Beyond infinite dilution the lack of knowledge concerning complex rare earth sulphate speciation is indicated by the diverse range of discussions within the literature (Chen & Millero, 1977; Fay & Purdie, 1969; Rard, 1996). Most studies have discussed the volumetric and thermodynamic properties of these solutions by considering one dominant complex species (RSO_4^+), therefore one could expect the concentration dependence of thermodynamic properties to be similar to those exhibited by 1:2 electrolytes. Considering that the monosulphate and disulphate ionic species may be

significant in solution, the concentration dependence of thermodynamic properties could also resemble those exhibited by 1:1 electrolytes. Rard (1996) has shown that the osmotic coefficients of aqueous lutetium sulphate resemble those of a lower valence charge type rather than those of a hypothetical fully dissociated 3:2 electrolyte.

Calorimetric and conductance methods have been used by various authors (Farrow & Purdie, 1973; Fay & Purdie, 1969; Izatt *et al.*, 1969; Spedding & Jaffe, 1954) to determine log K, ΔH^o, and ΔS^o for the formation of rare earth monosulphate complexes, where these properties pertain to infinite dilution. Without precisely knowing the ionic equilibria of aqueous rare earth sulphates, the average charge of all complex species is difficult to predict; hence, it is difficult to model the solutions as they approach infinite dilution.

Beyond infinite dilution, thermodynamic properties can be modelled by Debye-Hückel theory (Pitzer & Brewer, 1961) and the Pitzer ion interaction model (Pitzer, 1991). However, for solutions which exhibit extensive complexation both models require that contact ion speciation is known. Another simple method of modelling the approach to infinite dilution would be through the use of an empirical equation, such as those used by Rard (1996) or Millero (1971). However, choosing the correct form of equation when extrapolating to infinite dilution is crucial, because, as other authors have noted, different equations produce different values at infinite dilution (Hovey *et al.*, 1988; Millero, 1971). As the slope approaching infinite dilution for a trivalent ion is greater than for lower charge ions, errors in extrapolations become even more pronounced. In this study, properties for aqueous rare earth chlorides, nitrates, and perchlorates have been reviewed and infinite dilution properties have been extrapolated using a consistent extended Debye-Hückel equation. These infinite dilution values have been averaged to determine single aqueous trivalent rare earth partial molar volumes and heat capacities.

Apart from a poorly defined average valence for aqueous rare earth sulphates above infinite dilution, most Debye-Hückel equations assume a constant valence coefficient over

an extensive concentration range. To control the average valence of the solute species the ionic strength must be fixed. The fixing of ionic strength by the addition of another salt further complicates speciation and limits the experimental ionic strength to that of the most concentrated solution. Thus, by studying only aqueous rare earth sulphates, these contact ion pairs or complex ions impose non-constant average valence in solution as the concentration moves beyond infinite dilution.

Although Pitzer's ion interaction approach seems to be the model of choice when dealing with complex equilibria and unsymmetrical electrolytes, the downside of the model is the large number of parameters required for such an investigation (Rard, 1996). With a limited knowledge of both speciation and thermodynamic data, the parameters required in the Pitzer ion interaction model become statistically insignificant for many aqueous complex ionic species. Assuming *a priori* that at least two complex rare earth sulphate ions exist in the solution, requires the consideration of at least seven stable aqueous ions; R^{3+}, RSO_4^+, $R(SO_4)_2^-$, SO_4^{2-}, HSO_4^-, OH^-, and H^+. There is no closed-form solution to the complex equilibria involving the previous ions. Therefore, even with sufficient degrees of freedom for a Pitzer ion interaction model, continuous speciation equilibria calculations would be extremely challenging. Fortunately ionic activities can be estimated using less complex models, therefore providing a means of obtaining self-consistent estimations of speciation.

We have measured the relative densities and heat capacities of aqueous yttrium, lanthanum, praseodymium, neodymium, europium, dysprosium, holmium, and lutetium sulphate species over a wide concentration range at 298.15 K (0.10 MPa). Utilising the equilibrium constants for several association processes (reactions 5.12 - 5.15) and Debye-Hückel theory in an iterative fashion, we have numerically estimated the equilibrium concentrations for aqueous R^{3+}, RSO_4^+, $R(SO_4)_2^-$, SO_4^{2-}, HSO_4^-, OH^-, and H^+ ions for each solution investigated. Calculated speciation concentrations and single ion aqueous trivalent rare earth properties have been used to estimate properties for the rare earth sulphate complex ions. These estimates can be used to describe volumetric and heat

capacity changes arising from the association of ions. Subsequently, these changes can be shown to cause the concentration dependence of the apparent molar properties to deviate significantly from the Debye-Hückel slope for the hypothetical fully dissociated 3:2 electrolyte.

5.2 Experimental

Water was double distilled, polished to a resistance of 18.2 MΩ using an Osmonics model Aries High Purity D.I. Loop, and then thoroughly degassed prior to solution preparation.

Rare earth sulphate salts were prepared by Dr. Joe Rard at the Geosciences and Environmental Technologies Division of Lawrence Livermore National Laboratories, University of California. All impurities were assumed to exist as their respective sulphate. Impurity mole fraction calculations indicate the following data: $Ho_2(SO_4)_3$ (99.984 mol-% $Ho_2(SO_4)_3$; 0.015 mol-% $CaSO_4$; 0.001 mol-% $Fe_2(SO_4)_3$) and $Lu_2(SO_4)_3$ (99.978 mol-% $Lu_2(SO_4)_3$; 0.005 mol-% $Yb_2(SO_4)_3$; 0.001 mol-% $Pr_2(SO_4)_3$; 0.012 mol-% $Al_2(SO_4)_3$; 0.003 mol-% Ag_2SO_4; < 0.001 other impurities). For $La_2(SO_4)_3$, $Pr_2(SO_4)_3$, and $Eu_2(SO_4)_3$, analysis was performed on the oxides (La_2O_3, Pr_2O_{3+x}, and Eu_2O_3) used to synthesise the sulphates and indicated purities of 99.98 mol-% and greater. The purity of $Y_2(SO_4)_3$, as determined by analysis of the Y_2O_3 from which is was prepared, was approximately 99.73 mol-%, with $CaSO_4$ being identified at the most abundant impurity. Neither $Nd_2(SO_4)_3$, $Dy_2(SO_4)_3$, nor their respective oxides were analysed; however, since all oxide purities were obtained at 99.9 %+, it was assumed that their purities would be greater than or equal to 99.9 %.

Following the preparation of stock solutions and prior to dilution, solutions of rare earth sulphates were microfiltered using 0.20 μm Nalgene polycarbonate membranes. Molalities of stock solutions were obtained by dehydration, where multiple crucibles containing aliquots of stock solution were dried over a hot plate and then heated to ~773 K

in a muffle furnace for over 3 hours. Aliquots ranged from 2 to 10 mL depending on the compound solubility. All samples were cooled in an evacuated desiccater and weighed the same day. The relative humidity within the laboratory, during dehydration analyses, never exceeded 30 %. Therefore, corrections for water vapour absorption were not used (Rard, 1996).

For every solution series, except $Lu_2(SO_4)_3$, only one stock solution was prepared. Due to the higher solubility of $Lu_2(SO_4)_3$ and the small amount of high purity salt available, the densities of five solutions in the higher concentration range were first measured. The concentration of the stock solution used to prepare the first series was determined by dehydration analysis. The salt from the first series solutions was collected after measurements and a second stock solution was prepared to extend the concentration range investigated. The molality of the second stock solution was determined from a polynomial equation fit to the density data from the first series.

All measurements took place in less than 48 hours from the preparation of the respective stock solutions. Relative densities were measured with the Sodev O2D vibrating tube densimeter described in Section 3.3. Calibration constants were obtained each day by measuring the time period of oscillation, when the tube contained pure water and air. Calibration measurements were performed three times during the course of a series of rare earth solution measurements. The density of water at 298.15 K used in all calculations was 0.997047 g cm^{-3} as reported by Kell (1967). Densities of air were calculated from standard equations (Weast, 1970).

Calibration of the Picker microflow calorimeter has been described in Section 3.4.

5.3 Results and discussion

Relative densities and heat capacity ratios for aqueous $Y_2(SO_4)_3$, $La_2(SO_4)_3$, $Pr_2(SO_4)_3$, $Nd_2(SO_4)_3$, $Eu_2(SO_4)_3$, $Dy_2(SO_4)_3$, $Ho_2(SO_4)_3$, and $Lu_2(SO_4)_3$ have been reported in tables 5.1 to 5.8 respectively.

Calculation of apparent molar properties for aqueous electrolytes which do not completely dissociate or partially complex requires the use of 'experimental' apparent molar properties as defined by equation 5.1:

$$Y_{2,\phi}^{exp} = \frac{Y - n_1 \bar{Y}_1^o}{n_{2i}}, \tag{5.1}$$

where n_{2i} is now defined as the stoichiometric number of moles of salt added to the solution. Note the distinct difference between this equation and equation 2.15 that describes apparent molar properties. In equation 2.15 n_2 defines the number of moles of solute in the solution. If the salt is assumed to completely dissociate (e.g. NaCl and NaBr), equation 5.1 is redundant because $n_2=n_{2i}$, hence equation 2.15 could be used. However, with the incomplete complex speciation of the aqueous rare earth sulphates each mole of $R_2(SO_4)_3$ does not yield three moles of SO_4^{2-} and two moles of R^{3+} upon dissociation. Similarly equations 3.9 and 3.10 are now expressed as experimental apparent molar volumes and experimental apparent molar heat capacities by

$$V_{2,\phi}^{exp} = \frac{M}{\rho} - \frac{1000\ (\rho - \rho_o)}{m_{2i}\rho\rho_o} \tag{5.2}$$

and

$$C_{p2,\phi}^{exp} = MC_p + \frac{1000\ (C_p - C_{p1}^o)}{m_{2i}}. \tag{5.3}$$

In equations 5.2 and 5.3 m_{2i} defines a stoichiometric molality. Experimental apparent molar properties are often preferred by experimentalists, because they do not require equilibrium calculations.

Uncertainties in experimental apparent molar volumes and experimental apparent molar heat capacities were calculated using equations 5.4 and 5.5 respectively:

$$\delta V_{2,\phi}^{exp} = \left| M + \frac{1000}{m_{2i}} \right| \frac{\delta\rho}{\rho^2} + \left| \frac{1000\ (\rho - \rho_o)}{m_{2i}^2\rho\rho_o} \right| \delta m_{2i} \tag{5.4}$$

and

$$\delta C_{p2,\phi}^{exp} = \left| M + \frac{1000}{m_{2i}} \right| \delta C_p + \left| \frac{1000\ (C_p - C_{p1}^o)}{m_{2i}^2} \right| \delta m_{2i}, \tag{5.5}$$

where the uncertainties in density, $\delta\rho$, and heat capacity measurements, δC_p, have been reported in Chapter 3. Relative uncertainties in stoichiometric concentration, $\delta m_{2i}/m_{2i}$, were estimated to be 0.1% for all solutions.

Table 5.1. Relative densities, experimental apparent molar volumes, heat capacity ratios, and experimental apparent molar heat capacities of aqueous $Y_2(SO_4)_3$ at 298.15 K.

m (mol kg^{-1})	$(\rho - \rho_o)$ (kg m^{-3})	$V_{2,\phi}^{exp}$ (cm^3 mol^{-1})	$10^3\left(\frac{c_p\rho}{c_p^o\rho_o}-1\right)$	$C_{p2,\phi}^{exp}$ (J K^{-1} mol^{-1})
0.01346	6.182	5.41±0.83	-0.297	-70.7±7.2
0.01594	7.309	6.12±0.77	-0.318	-58.7±6.4
0.04031	18.259	11.49±0.57	-0.410	4.9±3.7
0.04097	18.561	11.48±0.57	-0.409	5.6±3.6
0.05437	24.529	13.25±0.53	-0.387	25.1±3.2
0.07088	31.839	15.01±0.51	-0.310	44.0±2.9
0.06878	30.913	14.78±0.51	-0.292	43.6±2.9
0.08035	36.050	15.50±0.50	-0.224	52.8±2.7
0.09120	40.796	16.71±0.49	-0.066	66.6±2.6
0.09910	44.268	17.28±0.48	-0.038	73.6±2.5
0.01346	6.192	4.65±0.83	-0.315	-79.4±7.2
0.01594	7.317	5.61±0.77	-0.332	-64.6±6.4
0.04031	18.276	11.08±0.57	-0.376	6.8±3.7
0.04097	18.573	11.18±0.57	-0.438	1.5±3.7
0.05437	24.545	12.97±0.53	-0.390	23.8±3.2
0.07088	31.876	14.50±0.51	-0.300	42.5±2.9
0.06878	30.941	14.38±0.51	-0.312	40.7±2.9
0.08035	36.045	15.56±0.50	-0.213	53.7±2.7
0.09120	40.882	15.80±0.49	-0.041	63.9±2.6

Table 5.2. Relative densities, experimental apparent molar volumes, heat capacity ratios, and experimental apparent molar heat capacities of aqueous $La_2(SO_4)_3$ at 298.15 K.

m (mol kg^{-1})	$(\rho - \rho_O)$ (kg m^{-3})	$V_{2,\phi}^{exp}$ (cm^3 mol^{-1})	$10^3\left(\frac{c_p\rho}{c_{pl}^{o}\rho_O}-1\right)$	$C_{p2,\phi}^{exp}$ (J K^{-1} mol^{-1})
0.005332	2.965	8.35±1.50	-0.423	-300.6±15.8
0.009480	5.249	10.65±1.08	-0.661	-250.4±10.0
0.01355	7.465	13.39±0.92	-0.887	-220.9±7.8
0.02025	11.132	14.47±0.79	-1.220	-194.2±6.0
0.02591	14.199	16.22±0.73	-1.436	-166.5±5.2
0.03226	17.637	17.40±0.69	-1.667	-145.9±4.7
0.02871	15.712	16.97±0.71	-1.550	-157.4±5.0
0.04052	22.101	18.53±0.66	-2.023	-133.9±4.2
0.04378	23.863	18.95±0.65	-2.132	-126.8±4.1
0.04896	26.627	20.05±0.63	-2.352	-119.6±3.9
0.005332	2.969	7.53±1.50	-0.390	-277.5±15.8
0.009480	5.252	10.32±1.08	-0.681	-260.2±10.0
0.01355	7.476	12.60±0.92	-0.872	-219.4±7.8
0.02025	11.132	14.50±0.79	-1.181	-186.0±6.0
0.02591	14.199	16.19±0.74	-1.454	-169.7±5.2
0.03226	17.640	17.31±0.69	-1.685	-148.7±4.7
0.02871	15.721	16.68±0.71	-1.540	-157.2±5.0
0.04052	22.097	18.64±0.66	***	***
0.04378	23.859	19.04±0.65	-2.119	-125.2±4.1
0.04896	26.627	20.04±0.63	-2.313	-116.2±3.9

Table 5.3. Relative densities, experimental apparent molar volumes, heat capacity ratios, and experimental apparent molar heat capacities of aqueous $Pr_2(SO_4)_3$ at 298.15 K.

m (mol kg^{-1})	$(\rho - \rho_o)$ (kg m^{-3})	$V_{2,\phi}^{exp}$ (cm^3 mol^{-1})	$10^3\left(\frac{c_p\rho}{c_p^o\rho_o}-1\right)$	$C_{p2,\phi}^{exp}$ (J K^{-1} mol^{-1})
0.08830	48.596	17.22±0.58	-2.152	-31.4±3.1
0.07876	43.404	16.61±0.59	-2.029	-39.7±3.2
0.06762	37.338	15.63±0.61	-1.916	-54.7±3.4
0.05990	33.158	14.33±0.62	-1.767	-65.0±3.6
0.05133	28.487	12.98±0.64	-1.662	-82.8±3.8
0.04408	24.498	12.32±0.66	***	***
0.03568	19.872	11.21±0.69	-1.285	-105.4±4.4
0.02543	14.224	8.82±0.75	-1.030	-134.4±5.3
0.01522	8.565	5.58±0.89	-0.694	-169.5±7.2
0.008265	4.682	1.83±1.17	-0.424	-209.3±11.1
0.008265	4.671	3.16±1.17	-0.434	-208.5±11.1
0.01522	8.563	5.75±0.89	-0.689	-167.2±7.2
0.02543	14.228	8.64±0.75	-1.024	-134.1±5.3
0.03568	19.874	11.16±0.69	-1.321	-109.9±4.4
0.04408	24.493	12.44±0.66	-1.572	-98.8±4.0
0.05133	28.521	12.33±0.64	-1.675	-86.5±3.8
0.05990	33.156	14.36±0.62	-1.851	-70.8±3.6
0.06762	37.355	15.39±0.61	-1.957	-58.3±3.4
0.07876	43.417	16.46±0.59	-2.115	-45.0±3.3
0.08830	48.603	17.15±0.58	-2.265	-37.1±3.1

Table 5.4. Relative densities, experimental apparent molar volumes, heat capacity ratios, and experimental apparent molar heat capacities of aqueous $Nd_2(SO_4)_3$ at 298.15 K.

m (mol kg^{-1})	$(\rho - \rho_o)$ (kg m^{-3})	$V_{2,\phi}^{exp}$ (cm^3 mol^{-1})	$10^3\left(\frac{c_p\rho}{c_p^o \rho_o} - 1\right)$	$C_{p2,\phi}^{exp}$ (J K^{-1} mol^{-1})
0.01843	10.384	11.39±0.83	-0.640	-99.3±6.3
0.02642	14.817	13.92±0.74	-0.806	-71.0±5.1
0.03244	18.146	15.46±0.70	-0.922	-55.7±4.6
0.04646	25.890	17.35±0.65	-1.103	-28.1±3.9
0.06140	24.093	19.16±0.62	-1.249	-6.2±3.5
0.07260	40.216	20.35±0.60	-1.353	6.0±3.3
0.08045	44.541	20.49±0.59	-1.348	14.5±3.2
0.08983	49.627	21.54±0.58	-1.405	23.6±3.1
0.09836	54.247	22.36±0.57	-1.372	34.1±3.0
0.1175	64.552	23.95±0.56	-1.330	51.8±2.8
0.01843	10.378	11.74±0.83	-0.633	-96.3±6.3
0.02642	14.819	13.85±0.74	-0.798	-70.0±5.1
0.03244	18.156	15.16±0.71	-0.903	-54.4±4.6
0.04646	25.898	17.19±0.65	-1.122	-30.4±3.9
0.06140	34.086	19.27±0.62	-1.244	-5.4±3.5
0.07260	40.211	20.40±0.60	-1.312	8.6±3.3
0.08045	44.504	20.94±0.59	-1.341	16.7±3.2
0.08983	49.584	22.00±0.58	-1.319	29.5±3.1
0.09836	54.213	22.69±0.57	-1.329	37.3±3.0
0.1175	64.577	23.75±0.56	-1.331	51.0±2.8

Table 5.5. Relative densities, experimental apparent molar volumes, heat capacity ratios, and experimental apparent molar heat capacities of aqueous $Eu_2(SO_4)_3$ at 298.15 K.

m (mol kg^{-1})	$(\rho - \rho_o)$ (kg m^{-3})	$V_{2,\phi}^{exp}$ (cm^3 mol^{-1})	$10^3\left(\frac{c_p\rho}{c_p^o\rho_o}-1\right)$	$C_{p2,\phi}^{exp}$ (J K^{-1} mol^{-1})
0.006816	4.042	-2.67±1.33	-0.263	-174.0±12.9
0.008558	5.064	-1.41±1.18	-0.342	-174.4±10.9
0.01024	6.049	-0.65±1.08	-0.415	-173.8±9.5
0.01321	7.795	0.40±0.97	-0.522	-165.4±8.0
0.01455	8.577	1.02±0.93	-0.553	-156.2±7.5
0.01641	9.653	2.01±0.89	-0.598	-145.7±6.9
0.01851	10.887	2.30±0.85	-0.654	-139.5±6.4
0.02116	12.430	2.92±0.82	-0.723	-132.2±5.9
0.02267	13.320	2.79±0.80	-0.741	-126.3±5.7
0.02513	14.713	4.70±0.78	-0.812	-117.0±5.4
0.006816	4.041	-2.43±1.33	-0.294	-192.5±13.0
0.008558	5.070	-2.11±1.18	-0.332	-172.8±10.9
0.01024	6.048	-0.49±1.08	-0.411	-171.8±9.5
0.01321	7.795	0.44±0.97	-0.486	-153.4±7.9
0.01455	8.576	1.14±0.93	-0.526	-148.0±7.5
0.01607	9.659	1.61±0.91	-0.586	-144.1±7.0
0.01851	10.889	2.19±0.85	-0.642	-137.3±6.4
0.02116	12.431	2.92±0.82	-0.681	-123.8±5.9
0.02267	13.296	3.85±0.80	-0.698	-114.0±5.7
0.02513	14.714	4.68±0.78	-0.753	-107.0±5.4

Table 5.6. Relative densities, experimental apparent molar volumes, heat capacity ratios, and experimental apparent molar heat capacities of aqueous $Dy_2(SO_4)_3$ at 298.15 K.

m (mol kg^{-1})	$(\rho - \rho_o)$ (kg m^{-3})	$V_{2,\phi}^{exp}$ (cm^3 mol^{-1})	$10^3\left(\frac{c_p\rho}{c_{pl}^o\rho_o}-1\right)$	$C_{p2,\phi}^{exp}$ (J K^{-1} mol^{-1})
0.005773	3.497	5.62±1.48	-0.235	-148.1±14.9
0.01054	6.359	8.35±1.08	-0.287	-80.1±9.3
0.01762	10.578	10.80±0.77	-0.383	-47.0±6.1
0.02218	13.286	12.13±0.82	-0.405	-26.5±5.8
0.03044	18.186	13.80±0.75	-0.476	-8.6±4.9
0.03660	21.817	14.98±0.72	-0.518	2.6±4.5
0.04420	27.300	15.81±0.72	-0.524	17.6±4.1
0.04586	26.304	15.87±0.67	-0.529	15.6±4.0
0.05176	30.739	17.08±0.67	-0.529	28.0±3.9
0.05988	35.509	17.85±0.66	-0.535	36.6±3.6
0.005773	3.503	4.62±1.48	-0.189	-118.8±14.8
0.01054	6.369	7.41±1.08	-0.255	-71.4±9.3
0.01762	10.576	10.94±0.77	-0.365	-41.9±6.1
0.02218	13.288	12.04±0.82	-0.414	-28.8±5.8
0.03044	18.195	13.50±0.75	-0.438	-4.5±4.9
0.03660	21.844	14.23±0.72	-0.461	6.1±4.5
0.04420	27.301	15.77±0.72	-0.489	20.6±4.1
0.04586	26.308	15.77±0.67	-0.467	21.1±4.0
0.05176	30.761	16.67±0.67	-0.490	29.5±3.9
0.05988	35.521	17.66±0.66	-0.526	36.5±3.6

Table 5.7. Relative densities, experimental apparent molar volumes, heat capacity ratios, and experimental apparent molar heat capacities of aqueous $Ho_2(SO_4)_3$ at 298.15 K.

m (mol kg^{-1})	$(\rho - \rho_o)$ (kg m^{-3})	$V_{2,\phi}^{exp}$ (cm^3 mol^{-1})	$10^3\left(\frac{c_p\rho}{c_p^o\rho_o}-1\right)$	$C_{p2,\phi}^{exp}$ (J K^{-1} mol^{-1})
0.009765	5.945	7.38±1.12	-0.233	-70.1±9.8
0.01566	9.489	10.22±0.92	-0.265	-28.9±7.1
0.02263	13.668	12.03±0.82	-0.315	-8.6±5.7
0.03116	18.768	13.68±0.75	-0.344	10.3±4.8
0.03807	22.889	14.79±0.72	-0.296	28.8±4.4
0.04680	28.078	15.95±0.69	-0.298	39.5±4.0
0.05072	30.397	16.52±0.68	-0.274	46.0±3.9
0.06501	38.856	17.95±0.65	-0.176	63.3±3.5
0.06855	40.945	18.29±0.65	-0.123	68.6±3.5
0.07875	46.943	19.35±0.63	-0.035	78.7±3.3
0.009765	5.946	7.28±1.12	-0.216	-62.9±9.8
0.01566	9.493	10.01±0.92	-0.261	-28.6±7.1
0.02263	13.668	12.04±0.82	-0.293	-4.5±5.7
0.03116	18.784	13.18±0.75	-0.331	10.0±4.8
0.03807	22.904	14.41±0.72	-0.322	24.3±4.4
0.04680	28.080	15.93±0.69	-0.277	41.3±4.0
0.06501	38.866	17.81±0.65	-0.127	66.0±3.5
0.06855	40.943	18.30±0.65	-0.144	67.4±3.5
0.07327	43.715	18.89±0.64	-0.032	76.9±3.4

Table 5.8. Relative densities, experimental apparent molar volumes, heat capacity ratios, and experimental apparent molar heat capacities of aqueous $Lu_2(SO_4)_3$ at 298.15 K.

m (mol kg^{-1})	$(\rho - \rho_O)$ (kg m^{-3})	$V_{2,\phi}^{exp}$ (cm^3 mol^{-1})	$10^3\left(\frac{c_p\rho}{c_{pl}^o\rho_O}-1\right)$	$C_{p2,\phi}^{exp}$ (J K^{-1} mol^{-1})
0.4345	262.525	24.46±0.49	22.123	323.5±2.0
0.1161	72.592	10.40±0.63	3.305	163.7±3.0
0.07570	47.536	7.94±0.67	1.658	125.7±3.4
0.05301	33.435	5.36±0.71	0.948	97.9±3.9
0.03752	23.749	3.15±0.75	0.502	69.7±4.4
0.02424	15.416	0.15±0.83	0.230	40.6±5.5
0.01374	8.780	-2.93±1.00	0.070	9.2±7.8
0.007321	4.707	-6.77±1.33	-0.041	-52.0±12.3
0.3858	234.143	23.92±0.51	18.997	309.6±2.1
0.3296	201.115	21.84±0.52	15.104	285.9±2.2
0.2617	160.744	19.14±0.55	10.646	252.4±2.4
0.2010	124.301	16.04±0.58	7.212	218.8±2.6
0.1551	96.500	13.03±0.60	5.017	191.1±2.7

Experimental apparent molar volumes and heat capacities, $V_{2,\phi}^{exp}$ and $C_{p2,\phi}^{exp}$, for species investigated within this study are also shown in tables 5.1 to 5.8 with their respective stoichiometric molalities. These experimental properties can be used for fitting Debye-Hückel equations or Pitzer ion interaction equations. However, rare earth sulphates exhibit substantial complexation over the range of molalities investigated within this study, therefore, infinite dilution values for apparent molar volumes and heat capacities have been extrapolated from data within the literature. From these properties single ion partial molar properties at infinite dilution, $\bar{Y}^o$(ion), have been calculated at 298.15 K and 0.10 MPa.

5.3.1 Single ion partial molar properties at infinite dilution.

By defining value of a thermodynamic property for one ion (usually H^+(aq)) the thermodynamic properties of all other single ions can be calculated through the simple

additive nature of infinite dilution ionic properties. For single ion partial molar heat capacities, a popular convention is to set $\bar{C}_p^o(H^+)$ equal to zero. Zana and Yeager (1966, 1967) report a value of $\bar{V}^o(H^+)$=-5.4 $cm^3\ mol^{-1}$ that was determined from ionic vibration potential measurements. Several values for the single ion partial molar volume for the aqueous ion H^+ have been suggested within the literature. However, only that of Zana and Yeager (1966, 1967) has been determined directly from experimental data (Millero, 1971).

The semi-empirical extended Debye-Hückel equation,

$$Y_{2,\phi} = \bar{Y}_2^o + \frac{3}{2}\omega A_Y \left(\frac{1}{\Lambda} - \frac{\sigma}{3}\right)\sqrt{I} + \sum_{i=2} B_{Yi}\, I^{i/2}, \qquad (5.6)$$

has been fit to available experimental apparent molar volumes and heat capacities for aqueous rare earth chlorides, nitrates, and perchlorates. In equation 5.6 B_{Yi} is a fitting coefficient representing correlation with the ionic strength raised to the power of i/2 and the valence factor, ω, was fixed at 6. Λ and σ have been defined in Subsection 2.3.1. Limiting slopes, A_V=1.8305 $cm^3\ kg^{1/2}\ mol^{-3/2}$ and A_C/R=3.8360 $mol^{1/2}\ kg^{-1/2}$, have been reported by Archer and Wang (1990).

Apparent molar volumes for aqueous rare earth solutions have been reported by Spitzer *et al.* (1979), Spedding *et al.* (1966, 1974, 1975a, 1975b), Rard and Spedding (1982), Leipziger and Roberts (1958), and more recently by Xiao and Tremaine (1996, 1997). Xiao and Tremaine (1996, 1997) have used a vibrating tube densimeter, similar to the O2D instrument described in Section 3.3. Most of Xiao and Tremaine's (1996, 1997) apparent molar property data have been calculated through the use of Young's rule (Young & Smith, 1954). This approach corrects for the excess perchloric acid utilised in those investigations to prevent hydrolysis. As data for individual aqueous species were combined in our analyses, apparent molar volume data for $Eu(ClO_4)_3$ in the absence of excess acid show good agreement with data measured in the presence of acid. Therefore, we have assumed other rare earth perchlorates treated in a similar manner by Xiao and Tremaine (1996, 1997) should yield reasonably precise apparent molar properties.

Table 5.9. Empirical coefficients for extended Debye-Hückel equations modeling apparent molar volumes of the rare earth chlorides, nitrates, and perchlorates at 298.15 K.

Rare earth ion	Anion	$\bar{V}^o$ ($cm^3\ mol^{-1}$)	B_V^1 ($cm^3\ kg\ mol^{-2}$)	B_V^2 ($cm^3\ kg^{3/2}\ mol^{-5/2}$)	Ref.
Y^{3+}	Cl^-	13.19±0.12	-0.923±0.256	0.594±0.117	h
	NO_3^-	45.63±0.05	0.179±0.070	0.172±0.030	i
La^{3+}	Cl^-	13.90±0.09	0.632±0.078		c, d, e
	NO_3^-	49.16±0.14	1.226±0.075		a, b, d
	ClO_4^-	93.22±0.13	-2.486±0.397	1.236±0.205	e, g
Pr^{3+}	Cl^-	10.93±0.03	0.075±0.053		d
	NO_3^-	46.03±0.23	3.335±0.773		a, g
Nd^{3+}	Cl^-	10.16±0.03	-0.468±0.173	0.536±0.124	d
	NO_3^- *	45.53±0.10	7.397±0.667	-5.746±0.769	a, d
	ClO_4^-	88.38±0.11	-2.101±0.292	1.132±0.147	f, g
Sm^{3+}	Cl^-	11.15±0.04	-2.110±0.412	1.800±0.407	d
	NO_3^-	46.57±0.20	2.770±0.698	-0.812±0.338	a, g
Eu^{3+}	Cl^-	12.00±0.03	-1.624±0.345	1.366±0.366	g
	NO_3^-	46.85±0.06	3.981±0.576	-2.667±0.571	g
	ClO_4^-	90.20±0.06	-1.167±0.144	0.592±0.072	f
Gd^{3+}	Cl^-	13.08±0.04	-1.796±0.447	1.494±0.433	d
	NO_3^-	47.22±0.05	0.687±0.031		a, g
	ClO_4^-	91.45±0.13	-2.125±0.335	0.985±0.167	e, g
Tb^{3+}	Cl^-	13.15±0.08	-0.182±0.149		d
	NO_3^-	47.35±0.09	-0.231±0.231		a, g
Dy^{3+}	Cl^-	12.70±0.06	-1.603±0.650	1.412±0.658	d
	NO_3^-	46.64±0.06	0.496±0.029		a, g
Ho^{3+}	Cl^-	11.72±0.02	-1.086±0.195	1.050±0.194	d
	NO_3^-	45.54±0.10	-0.302±0.338	0.415±0.163	a, g
Er^{3+}	Cl^-	10.58±0.03			d
	NO_3^-	45.11±0.12	-0.772±0.313	0.556±0.147	a, d
	ClO_4^-	88.98±0.10	-0.764±0.190	0.473±0.084	f
Tm^{3+}	Cl^-	9.24±0.05			g
	NO_3^-	43.85±0.03	-0.254±0.059		g

Table 5.9 Continued

Yb^{3+}	Cl^-	9.22±0.06	-1.072±0.513	0.887±0.410	d
	NO_3^-	42.98±0.22	-0.502±0.523	0.425±0.237	a, d
	ClO_4^-	87.45±0.08	-0.915±0.182	0.553±0.089	f
Lu^{3+}	Cl^-	7.73±0.04	-0.128±0.083		g
	NO_3^-	42.22±0.04	-0.493±0.104	0.478±0.052	a, g
	ClO_4^-	86.10±0.05	-4.337±0.467	3.148±0.463	g

All uncertainties have been calculated from the regression variance-covariance matrix. *Requires B_V^3= 1.375±0.222 (cm^3 kg^2 mol^{-3}) (a) Spedding *et al.* (1975a). (b) Leipziger & Roberts (1958). (c) Spitzer *et al.* (1979). (d) Spedding *et al.* (1966). (e) Xiao & Tremaine (1996). (f) Xiao & Tremaine (1997). (g) Spedding *et al.* (1974). (h) Spedding (1975b) (i) Rard & Spedding (1982)

Because our primary interest is in infinite dilution properties, apparent molar volume data reported by Spedding *et. al.* (1975a,b) and Leipziger and Roberts (1958) were only utilised at solution concentrations of less than 1 mol kg^{-1}. In addition, all apparent molar volume data reported by Spedding (1966, 1974, 1975a,b) and Leipziger and Roberts (1958) were converted to units of cm^3 mol^{-1} from the outdated mL mol^{-1} as suggested by Kell (1972). Most literature data obtained using a pycnometer exhibited more uncorrelated variance than those obtained using either a magnetic float method or vibrating tube densimetry. No weighting was applied in the fitting of equation 5.6 as data obtained using the magnetic float method was predominantly in the lower concentration region where the Debye-Hückel contribution is a good model of the data. The empirical B_{Yi} coefficients simply model the data at higher concentrations where contributions from the Debye-Hückel terms alone fail to model the data well. Coefficients obtained from these fits are reported in table 5.9.

Conventional single ion partial molar volumes ($\bar{V}^o(H^+)=0$) for $Cl^-(aq)$, $NO_3^-(aq)$ and $ClO_4^-(aq)$ have been reported by Millero (1971) (17.83, 29.00, and 44.12 cm^3 mol^{-1}

respectively). Using $\bar{V}^{o}(H^{+}) = -5.4$ cm^3 mol^{-1} yields single ion partial molar volumes of 23.23, 34.40, and 49.52 cm^3 mol^{-1} respectively for the aforementioned species. These data have been used to calculate single ion partial molar volumes for the aqueous trivalent rare earth ions. The results of our single ion partial molar volume calculations are reported in table 5.10 and shown in figure 5.1. The general agreement of single ion partial molar volumes calculated using infinite dilution partial molar volumes from chloride, nitrate, and perchlorate salts is satisfactory and consistent over the full range of species investigated. Volumes derived from volumetric data for aqueous nitrate salts are less negative, and those from the perchlorate salts are more negative, relative to those from the chloride salts. With the exception of lanthanum, deviations in the single ion properties derived from chloride and perchlorate salts differ by 0.58±0.09. This low variance in deviation is an indication of the internal consistency of our extrapolations. The variance of single ion volumes derived from nitrate salts is not as satisfying. This large variance is most likely due to partial complexation at slightly dilute concentrations (Rard & Spedding, 1975). Average single ion partial molar volumes at infinite dilution have been calculated by weighting individual single ion properties by the reciprocal of the uncertainty in the respective infinite dilution extrapolation. We note that the uncertainty in the extrapolations for the nitrate salts is on average twice that of the chloride salts.

A critical review of the partial molar heat capacities of aqueous trivalent rare earth species has been completed by Hovey (1988). In this review equation 5.6 has been fit to apparent molar heat capacities within the literature. We have used these extrapolations to determine single ion heat capacities for most of the rare earth series. However, we did not include any extrapolations from measurements obtained using batch calorimetry, as batch calorimetry does not provide the sensitivity required for precise apparent molar heat capacities at low concentrations (Marsh & O'Hare, 1994). More precise measurements on aqueous solutions of $La(ClO_4)_3$, $LaCl_3$, $Gd(ClO_4)_3$, $Nd(ClO_4)_3$, $Eu(ClO_4)_3$, $Er(ClO_4)_3$, and $Yb(ClO_4)_3$ species have recently been reported by Xiao and Tremaine (1996, 1997).

Table 5.10. Single ion partial molar volumes at infinite dilution for aqueous trivalent rare earth ions at 298.15 K.

Rare earth ion	$\bar{V}^o$(ion) (a) ($cm^3\ mol^{-1}$)	$\bar{V}^o$(ion) (b) ($cm^3\ mol^{-1}$)	$\bar{V}^o$(ion) (c) ($cm^3\ mol^{-1}$)	$\bar{V}^o$(ion) (Avg) ($cm^3\ mol^{-1}$)
Y^{3+}	-56.50 (0.12)	-57.57 (0.05)		-57.04±0.76
La^{3+}	-55.79 (0.09)	-54.04 (0.14)	-55.34 (0.13)	-55.17±0.92
Pr^{3+}	-58.76 (0.03)	-57.17 (0.23)		-58.58±1.42
Nd^{3+}	-59.53 (0.03)	-57.67 (0.10)	-60.18 (0.11)	-59.29±1.32
Sm^{3+}	-58.54 (0.04)	-56.63 (0.20)		-58.22±1.62
Eu^{3+}	-57.69 (0.03)	-56.35 (0.06)	-58.36 (0.06)	-57.52±1.03
Gd^{3+}	-56.61 (0.04)	-55.98 (0.05)	-57.11 (0.13)	-56.44±0.59
Tb^{3+}	-56.64 (0.08)	-55.85 (0.09)		-56.27±0.56
Dy^{3+}	-56.99 (0.06)	-56.56 (0.06)		-56.78±0.36
Ho^{3+}	-57.97 (0.02)	-57.66 (0.10)		-57.92±0.26
Er^{3+}	-59.11 (0.03)	-58.09 (0.12)	-59.58 (0.10)	-59.04±0.77
Tm^{3+}	-60.45 (0.05)	-59.35 (0.03)		-59.76±0.80
Yb^{3+}	-60.47 (0.06)	-60.22 (0.22)	-61.11 (0.08)	-60.67±0.47
Lu^{3+}	-61.96 (0.04)	-60.98 (0.04)	-62.46 (0.05)	-61.75±0.76

(a) Extrapolations from aqueous RCl_3 solutions. (b) Extrapolations from aqueous $R(NO_3)_3$ solutions. (c) Extrapolations from aqueous $R(ClO_4)_3$ solutions. Weighted averages have been calculated using the reciprocal of the uncertainty for the infinite dilution property of the salt. The uncertainties are shown in brackets.

Equation 5.6 has been fit to apparent molar heat capacities reported in these studies. For aqueous $LaCl_3$, apparent molar heat capacity data reported by Spitzer *et al.* (1979) were combined with the data from Xiao and Tremaine (1996) as these data were measured using a similar Picker microflow system yielding similar measurement precision. Coefficients to equation 5.6 obtained using these data are reported in table 5.11.

Single ion partial molar heat capacities at infinite dilution for Cl^-(aq), NO_3^-(aq) and ClO_4^-(aq) have been reported by Hovey (1988) (-126.9,-71.8, and -26.0 $J\ K^{-1}\ mol^{-1}$

Figure 5.1 Single ion partial molar volumes at infinite dilution of some aqueous trivalent rare earth species as a function of atomic number at 298.15 K.

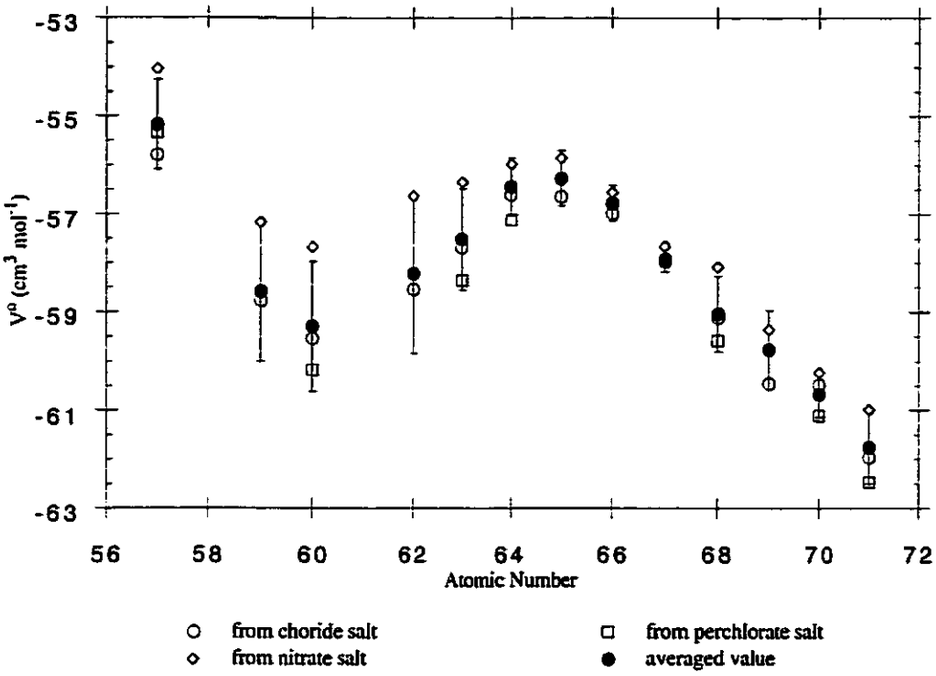

Table 5.11 Empirical coefficients for extended Debye-Hückel equations modeling apparent molar heat capacities of the rare earth perchlorates and lanthanum chloride at 298.15 K.

Species	$\bar{C}_p^o$ (cm^3 mol^{-1})	B_{Cp}^1 (cm^3 kg mol^{-2})	B_{Cp}^2 (cm^3 kg$^{3/2}$ mol$^{-5/2}$)
$LaCl_3$	-466.4±1.9	-43.4±6.4	24.9±3.3
$La(ClO_4)_3$	-182.9±4.0	-14.9±8.8	11.0±4.3
$Nd(ClO_4)_3$	-191.1±2.4	-5.1±5.1	7.5±2.4
$Eu(ClO_4)_3$	-156.1±1.7	-8.3±3.8	7.7±1.9
$Gd(ClO_4)_3$	-164.5±2.9	8.1±1.4	
$Er(ClO_4)_3$	-144.5±1.7	3.6±3.0	2.4±1.3
$Yb(ClO_4)_3$	-141.7±1.9	-1.5±4.1	5.3±2.0

All uncertainties have been calculated from the regression variance-covariance matrix. All apparent molar property data was taken from Xiao & Tremaine (1996, 1997) excepting $LaCl_3$ that also contains data from Spitzer *et al.* (1979).

Table 5.12. Single ion partial molar heat capacities at infinite dilution for aqueous trivalent rare earth ions at 298.15 K.

Rare earth ion	$\bar{C}_p^o$(ion) [a] (J K^{-1} mol^{-1})	$\bar{C}_p^o$(ion) [b] (J K^{-1} mol^{-1})	$\bar{C}_p^o$(ion) [c] (J K^{-1} mol^{-1})	$\bar{C}_p^o$(ion) [d] (J K^{-1} mol^{-1})	$\bar{C}_p^o$(ion) [avg] (J K^{-1} mol^{-1})
Y^{3+}	-37.3				-37.3±20.2**
La^{3+}	-112.2(-85.7)*	-101.2	-133.7	-104.9 (4.0)	-104.0±18.0
Pr^{3+}	-119.3	-102.0	-154.6		-125.3±26.8
Nd^{3+}	-108.0	-87.1	-145.0	-113.1 (2.4)	-113.3±23.9
Sm^{3+}	-108.4	-77.8	-139.1		-108.4±30.7
Eu^{3+}	-80.4	****	-117.0	-78.1 (1.7)	-88.4±22.2
Gd^{3+}	-92.9	-67.3	-111.1	-86.5 (2.9)	-88.9±18.1
Tb^{3+}	-73.3	-79.9	-109.4		-87.5±19.2
Dy^{3+}	-70.3	-76.7	-96.9		-81.3±13.9
Ho^{3+}	-76.6	-86.6	-97.7		-87.0±10.6
Er^{3+}	-72.0	-95.6	-104.4	-66.5 (1.7)	-81.0±18.7
Tm^{3+}	-66.0	-91.9	-94.4		-84.1±15.7
Yb^{3+}	-68.2	-92.4	-117.8	-63.7 (1.9)	-81.2±25.4
Lu^{3+}	-68.2	-99.9	-104.8		-91.0±19.9

(a) Extrapolations from aqueous RCl_3 (Hovey, 1988). (b) Extrapolations from aqueous $R(NO_3)_3$ (Hovey, 1988). (c) Extrapolations from aqueous $R(ClO_4)_3$ (Hovey, 1988). (d) Extrapolations from aqueous $R(ClO_4)_3$ reported in table 9.11 *Extrapolations from aqueous $LaCl_3$ using the data of Xiao and Tremaine (1996) and Spitzer *et al.* (1979). Weighted averages have been calculated using a weight of two for infinite dilution properties which have been extrapolated from data obtained using a Picker microflow calorimeter ((d) & *). **Uncertainty has been estimated by an average of all other predicted uncertainties.

Figure 5.2 Single ion partial molar heat capacities at infinite dilution of some aqueous trivalent rare earth species as a function of atomic number at 298.15 K.

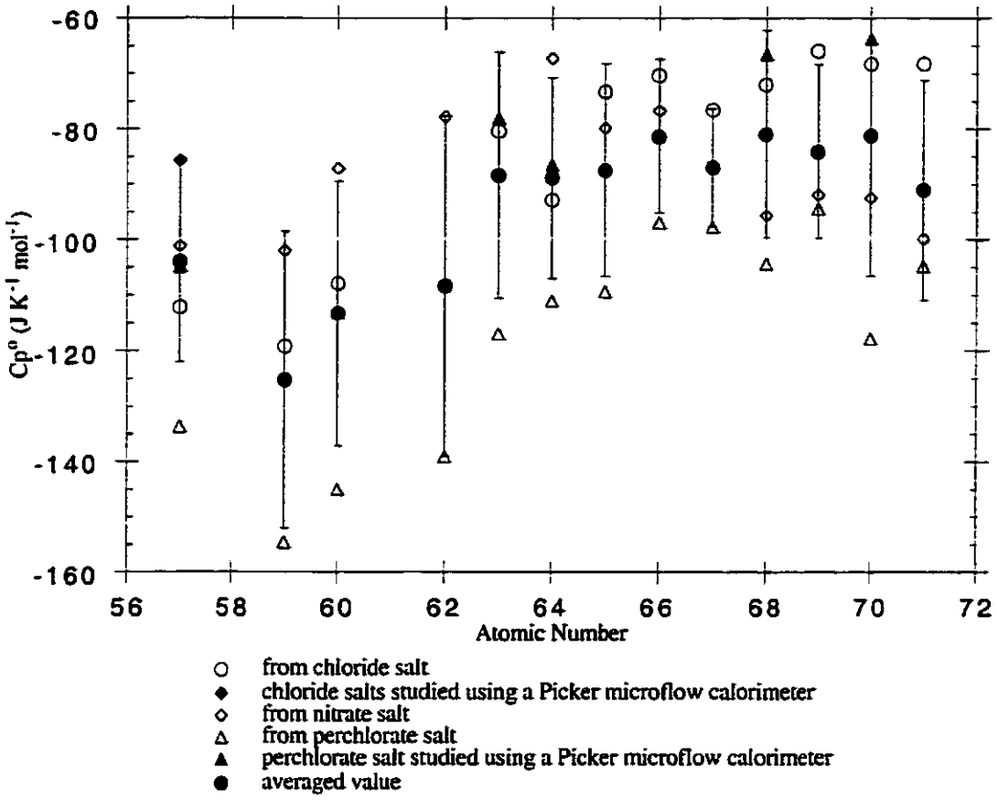

respectively). These values were obtained using the same extended Debye-Hückel equation (equation 5.6) and the most precise data from within the literature. Single ion heat capacities for the aqueous trivalent rare earth species, calculated using the previous anion heat capacities, are reported in table 5.12 and shown in figure 5.2. Most values in table 5.12 have been calculated from infinite dilution extrapolations made by Hovey (1988). Apparent molar heat capacities obtained using a Picker microflow calorimeter are thought to be more reliable. Therefore, these data have been doubly weighted in calculating the average single ion property. Heat capacity properties measured using a Picker microflow calorimeter correspond to the coefficients in table 5.11 and come from the data of Xiao and Tremaine (1996, 1997) and Spitzer *et al.* (1979). Figure 5.2 indicates poor agreement

between the various data sets within the literature; however, there are few modern data sets to correct and update these single ion heat capacities.

One would expect the variance of a second derivative property, such as the heat capacity, to be even greater than the variance of a first derivative property, such as the volume. Indeed, infinite dilution values for La^{3+} have been extrapolated from data reported in Xiao and Tremaine (1996), and show substantial disagreement among their respective predictions as derived from the aqueous perchlorate and chloride species (-104.9 versus -85.7 J K^{-1} mol^{-1}). As discussed by Xiao and Tremaine (1996) the disagreement is due to the uncertainty of the extrapolation to infinite dilution combined with three times the uncertainty in the single ion heat capacities for the anions.

5.3.2 Apparent molar volumes and heat capacities of some aqueous rare earth sulphates.

We have used the single ion volumes and heat capacities to calculate the partial molar volume and heat capacity at infinite dilution for species investigated within this study. Millero (1971) has reported a conventional partial molar volume ($\bar{V}^o(H^+)$ = -5.4 cm^3 mol^{-1}) of 13.98 cm^3 mol^{-1} for the aqueous sulphate ion, corresponding to a single ion partial molar volume ($\bar{V}^o(H^+)$ = -5.4 cm^3 mol^{-1}) of 24.78 cm^3 mol^{-1}. Once again, for internal consistency we have taken the single ion heat capacity from Hovey (1988) $\bar{C}_p^o(SO_4^{2-})$ = -280 J K^{-1} mol^{-1}. Using these single anion apparent molar properties and the single cation properties described previously, aqueous rare earth sulphate apparent molar properties can be calculated at infinite dilution. Using the latter values, the Debye-Hückel term for the completely dissociated salt does not even begin to approach the property of the lowest concentration for any species investigated herein. The large difference between the lowest concentration property and the predicted infinite dilution property is due to a large change in volume or heat capacity for any association of ions within the solution. While any empirical equation would present a

simple calculation for predicting the experimental apparent molar properties in the range of concentrations investigated, there are some fundamental problems with its predictions between the lowest concentration and infinite dilution. With single ion partial molar volumes and heat capacities for the complexed ions, it may be possible to model this large change, by calculating the changes associated with the formation of any complex.

Consider Young's rule (Young & Smith, 1954) for the additivity of single ion apparent molar properties:

$$Y_{2,\phi}^{exp} = \sum_{i=2}^{n} \frac{\hat{m}_i}{m} Y_{i\phi} + \delta, \qquad (5.7)$$

where $\hat{m}_i$ is a predicted species molality for ion i, $Y_{i\phi}$ is any single ion apparent molar property evaluated at the total ionic strength of the solution, and δ is an excess mixing term arising from any association reaction. In addition every single ion property will be modelled by some form of equation 5.8:

$$Y_{i\phi} = \bar{Y}_i^o + f(I), \qquad (5.8)$$

where f(I) is a function describing the ionic strength dependence of the single ion apparent molar property. Debye-Hückel theory attempts to predict this dependence for all ions in solution, through the use of a constant valence factor, ω. From our experience with the completely dissociating rare earth salts, a conservative assumption is that if the ionic strength after association is less than 0.5 mol kg^{-1}, then the extended Debye-Hückel term from equation 5.6 is a good function for this purpose. If this assumption is reliable for most of the concentrations investigated in this study, then the B_Y terms of equation 5.6 are approximately zero. Therefore substituting equation 5.8 into equation 5.7 and using the extended Debye-Hückel term from equation 5.6 yields

$$Y_{2,\phi}^{exp} = \sum_{i=2}^{n} \frac{\hat{m}_i}{m} (\bar{Y}_i^o + f(I)) + \delta$$

$$= \sum_{i=2}^{n} \frac{\hat{m}_i}{m} (\bar{Y}_i^o) + \frac{3}{2} \omega A_Y \left(\frac{1}{\Lambda} - \frac{\sigma}{3} \right) \sqrt{I} + \delta \,. \qquad (5.9)$$

As discussed previously, at infinite dilution there is no ion association in solution. However, as ions begin to associate into complex ions, their infinite dilution partial molar property becomes a contributing factor to the property of the system. Thus, equation 5.9 can be rearranged to show these contributions:

$$Y_{2,\phi}^{exp} - \frac{3}{2} \omega A_Y \left(\frac{1}{\Lambda} - \frac{\sigma}{3} \right) \sqrt{I} - \delta = \sum_{i=2}^{n} \frac{\hat{m}_i}{m} (\bar{Y}_i^o). \qquad (5.10)$$

Equation 5.10 has the distinct disadvantage of requiring predicted equilibrium concentrations for each ionic species. If these concentrations can be predicted with some degree of precision, equation 5.10 can be rearranged to show the contributions from infinite dilution partial molar properties of rare earth sulphate complex species:

$$Y_{2,\phi}^{exp} - \frac{3}{2} \omega A_Y \left(\frac{1}{\Lambda} - \frac{\sigma}{3} \right) \sqrt{I} - \delta - \hat{\alpha}_{R3+} \bar{Y}^o\{R^{3+}\} - \hat{\alpha}_{SO_4^{2-}} \bar{Y}^o\{SO_4^{2-}\}$$

$$= \hat{\alpha}_{RSO_4^+} \bar{Y}^o\{RSO_4^+\} + \hat{\alpha}_{R(SO_4)_2^-} \bar{Y}^o\{R(SO_4)_2^-\}. \qquad (5.11)$$

In equation 5.11 $\hat{\alpha}_i = \hat{m}_i/m$ and only the noncomplexed ions, the monosulphate, and disulphate species are considered to contribute to the apparent molar property. Both assumptions made here require some investigation into speciation equilibria over the range of concentrations studied. As discussed in the introduction, equilibrium concentrations have been computed by considering seven aqueous species present in solution.

5.3.3 Equilibria calculations

To better define aqueous speciation equilibria among our experimental solutions, we have utilised Debye-Hückel theory in speciation calculations for individual solution concentrations. We have considered the following equilibria reactions in all calculations, regardless of the very small concentrations of some of the species present in solutions:

$$R^{3+} + SO_4^{2-} \rightleftharpoons RSO_4^+ \,, \qquad (5.12)$$

$$RSO_4^+ + SO_4^{2-} \rightleftharpoons R(SO_4)_2^-, \quad (5.13)$$

$$H^+ + SO_4^{2-} \rightleftharpoons HSO_4^-, \quad (5.14)$$

and

$$H^+ + OH^- \rightleftharpoons H_2O. \quad (5.15)$$

Equilibrium constants at ambient temperature for reactions 5.12 and 5.13 ($K\{RSO_4^+\}$ and $K\{R(SO_4)_2^-\}$) have been reported by Izatt *et al.* (1969) and for reaction 5.14 ($K\{RSO_4^-\}$) by Hovey (1988). Mass balance equations have been related to stoichiometric molalities reported in tables 5.1 to 5.8. Equilibrium equations, mass balance equations, and a charge balance equation were all numerically solved using release 4 of the software package Maple V. Ionic activity coefficients were calculated using the Davies revision of the Debye-Hückel equation (Robinson & Stokes, 1965):

$$\log \gamma_i = -\frac{z_i^2 A_\gamma \sqrt{I}}{1 + \sqrt{I}} + 0.2\, z_i^2 A_\gamma I. \quad (5.16)$$

Initial concentrations were predicted by assuming all activity coefficients were unity. These concentrations were used to calculate the ionic strength and then new ionic activity coefficients were calculated. Concentrations were then predicted using the new activity coefficients. This process was repeated in an iterative manner until the ionic strength varied less than 0.0000001 between successive cycles.

Appendix B shows speciation calculations for all species investigated in this study. As expected, the concentrations of OH^-, HSO_4^-, and H^+ ions are very small and not large enough to affect the thermodynamic properties of the solutions investigated. This was also the case for all speciation calculations performed at higher ionic strengths. Although the concentrations of RSO_4^+ and SO_4^{2-} ions are clearly the dominant species at the lower concentration range investigated, the concentrations of R^{3+} and $R(SO_4)_2^-$ are large enough to contribute to the total concentration of all ionic species. Therefore, although R^{3+} and $R(SO_4)_2^-$ concentrations were small at low stoichiometric concentration, they should have an effect on the experimental apparent molar properties. The $R(SO_4)_2^-$ concentration also

increased rapidly with increasing salt concentration. These equilibrium calculations support the speciation suggested by previous authors (Fay and Purdie, 1970; Izatt et al., 1969). They also show nonsymmetrical complexation.

The results of our equilibrium calculations support the assumption of four significant ionic species and have supplied us with estimates of their concentrations over the investigated stoichiometric concentration range. Therefore equation 5.11 can be used to investigate the single ion properties for the monosulphate and disulphate complex species. If our equilibrium calculations are fairly robust and our measurements are precise, we should observe good correlation between the corrected apparent molar properties and the relative concentrations of the complex species. With respect to correcting apparent molar volumes these calculations are straightforward, since the excess mixing term for the association equations 5.12 and 5.13 are considered to be equal to zero. The excess mixing term for heat capacities is not as simple. Fortunately, Woolley and Hepler (1977) have outlined a method for calculating such contributions for weak electrolytes.

5.3.4 Relaxation contributions to the apparent molar heat capacities.

For any system the total enthalpy is defined by

$$H = n_i \bar{H}_i, \tag{5.17}$$

where n_i and $\bar{H}_i$ are the moles and partial molar enthalpies of any species i. Differentiation of this enthalpy with respect to temperature is by definition the system's heat capacity (equation 2.6):

$$C_p = \sum_n n_i \left(\frac{\partial \bar{H}_i}{\partial T}\right)_p + \sum_n \bar{H}_i \left(\frac{\partial n_i}{\partial T}\right)_p \tag{5.18}$$

However this differential shows that the total heat capacity has a contribution from all species present and from the changing of species present. For systems in which there is no change in relative concentrations, this latter contribution is eliminated. Woolley and Hepler

(1977) have discussed this 'relaxation contribution' to apparent molar heat capacities in detail. The heat capacity of a solution system containing one kilogram of water (molality concentration scale) can be defined by

$$C_p = \left(\frac{\partial H^{sp}}{\partial T}\right)_p + \left(\frac{\partial H^{rel}}{\partial T}\right)_p, \tag{5.19}$$

where 'sp' represents all species and 'rel' represents the heat capacity relaxation contribution arising from an association or dissociation reaction. Since the heat capacity of water is fixed in the experimental apparent molar property, it is possible to express the experimental apparent molar heat capacity (equation 2.15) with the heat capacity of the system defined by equation 5.19:

$$C_{p2,\phi}^{exp} = \frac{\left[\left(\frac{\partial \bar{H}^{sp}}{\partial T}\right)_p + \left(\frac{\partial \bar{H}^{rel}}{\partial T}\right)_p - C_{p\,1}^{o}\right]}{m_{2i}}. \tag{5.20}$$

Therefore the apparent molar heat capacity arising from only the solutes can now be calculated using

$$C_{p2,\phi} = C_{p2,\phi}^{exp} - \frac{\left(\frac{\partial \bar{H}^{rel}}{\partial T}\right)_p}{m_2}. \tag{5.21}$$

For any single association or dissociation reaction among the solutes, the derivative of the enthalpy with respect to temperature can be expressed by

$$\left(\frac{\partial \bar{H}^{rel}}{\partial T}\right)_p = \left(\frac{\partial \bar{H}^{rel}}{\partial \alpha m}\right)_p \left(\frac{\partial \alpha m}{\partial T}\right)_p, \tag{5.22}$$

where α represents the extent of the reaction and therefore the relative concentration as defined previously. Equation 5.23 corresponds to the definition of the enthalpy of such a reaction at any ionic strength:

$$\Delta \bar{H}_{rxn} = \left(\frac{\partial \alpha m}{\partial T}\right)_p \tag{5.23}$$

therefore

$$C_{p2,\phi} = C_{p2,\phi}^{exp} - \sum_{rxn\ i} \Delta\bar{H}_{rxn\ i} \left(\frac{\partial \alpha_i}{\partial T}\right)_{p,m} . \qquad (5.24)$$

The latter term in equation 5.24 corresponds to δ in equation 5.11. Derivation of the $(\partial\alpha_i/\partial T)$ term in the above equation is evaluated only at the constant molality of the species involved in the given reaction. In most studies constant molality of one salt does not imply constant speciation; therefore, any derivative with respect to temperature must be also be evaluated with respect to ionic strength.

Using our predicted equilibrium data we have calculated the concentration quotients for reactions 5.12 and 5.13 for each sample:

$$Q_{RSO_4^+} = \frac{[RSO_4^+]}{[R^{3+}][SO_4^{2-}]} = \frac{\hat{\alpha}}{(2-\hat{\alpha}-\hat{\beta})(3-\hat{\alpha}-2\hat{\beta})m} \qquad (5.25)$$

and

$$Q_{R(SO_4)_2^-} = \frac{[R(SO_4)_2^-]}{[RSO_4^+][SO_4^{2-}]} = \frac{[\hat{\beta}]}{(\hat{\alpha})(3-\hat{\alpha}-2\hat{\beta})m}, \qquad (5.26)$$

where $\hat{\alpha}$ and $\hat{\beta}$ are the predicted extents of reactions 5.12 and 5.13 or $\hat{\alpha}_{RSO_4^+}$ and $\hat{\alpha}_{R(SO_4)_2^-}$. Because our predicted equilibrium calculations rely on the Debye-Hückel equation 5.16, we have chosen to use the same equation to define the ionic strength dependence of the concentration quotients. Equations 5.27 and 5.28 relate concentration quotients 5.25 and 5.26 to their respective infinite dilution equilibrium constants by substituting equation 5.16 for the prediction of the activity coefficients:

$$\log (Q_{RSO_4^+}) = \log (K_{RSO_4^+}) - \frac{12A_\gamma\sqrt{I}}{1+\sqrt{I}} + 2.4A_\gamma I \qquad (5.27)$$

and

$$\log (Q_{R(SO_4)_2^-}) = \log (K_{R(SO_4)_2^-}) - \frac{4A_\gamma\sqrt{I}}{1+\sqrt{I}} + 0.8A_\gamma I. \qquad (5.28)$$

As previously discussed we require the temperature derivative of these quotients at constant pressure and molality. Thus the total differential of this function which is dependent on temperature, pressure, and ionic strength is applicable to the relaxation calculations:

$$Q = Q\,(I, T, p) \tag{5.29}$$

therefore

$$dQ = \left(\frac{\partial Q}{\partial I}\right)_{T,p} dI + \left(\frac{\partial Q}{\partial T}\right)_{I,p} dT + \left(\frac{\partial Q}{\partial p}\right)_{T,I} dp\,. \tag{5.30}$$

By definition pressure is constant for apparent molar heat capacities; therefore the last term in equation 5.30 is equal to zero. Dividing by dT yields equation 5.31:

$$\left(\frac{\partial Q}{\partial T}\right)_p = \left(\frac{\partial Q}{\partial I}\right)_{T,p} \left(\frac{\partial I}{\partial T}\right)_p + \left(\frac{\partial Q}{\partial T}\right)_{I,p}. \tag{5.31}$$

The ionic strength of aqueous rare earth sulphate solutions may be given by

$$I = m(15 - 6\hat{\alpha} - 8\hat{\beta}), \tag{5.32}$$

therefore

$$\left(\frac{\partial Q}{\partial T}\right)_p = \left[-6m\left(\frac{\partial \hat{\alpha}}{\partial T}\right)_p - 8m\left(\frac{\partial \hat{\beta}}{\partial T}\right)_p\right]\left(\frac{\partial Q}{\partial I}\right)_{T,p} + \left(\frac{\partial Q}{\partial T}\right)_{I,p}. \tag{5.33}$$

Therefore, equation 5.33 in combination with equations 5.25 and 5.26 have been used to calculate the $(\partial\hat{\beta}/\partial T)_{p,m}$ and $(\partial\hat{\alpha}/\partial T)_{p,m}$ derivatives required for the relaxation contribution. These calculations are defined by the following relatively complicated series of equations:

$$\left(\frac{\partial \hat{\alpha}}{\partial T}\right)_{p,m} = \frac{F_I m\,(c + 8b)}{a} \tag{5.34}$$

and

$$\left(\frac{\partial \hat{\beta}}{\partial T}\right)_{p,m} = \frac{F_I m\,(d - 6b)}{a} \tag{5.35}$$

where

$$a = F_4 [\, \hat{\alpha}F_4 + 2m^2F_1\left(\frac{\partial Q_{RSO_4^+}}{\partial I}\right)_{T,p}(3\hat{\alpha}F_2+4F_5) + 2m^2F_1\left(\frac{\partial Q_{R(SO_4)_2^-}}{\partial I}\right)_{T,p}(3\hat{\alpha}F_3+4F_6)], \quad (5.36)$$

$$b = 8m^2F_1[\left(\frac{\partial Q_{R(SO_4)_2^-}}{\partial T}\right)_{I,p}\left(\frac{\partial Q_{RSO_4^+}}{\partial I}\right)_{T,p}(F_5F_3-F_6F_2) + \left(\frac{\partial Q_{RSO_4^+}}{\partial T}\right)_{I,p}\left(\frac{\partial Q_{R(SO_4)_2^-}}{\partial I}\right)_{T,p}(F_6F_2-F_5F_3)\,], \quad (5.37)$$

$$c = \hat{\alpha}F_4 [\, F_2\left(\frac{\partial Q_{RSO_4^+}}{\partial T}\right)_{I,p} + F_3\left(\frac{\partial Q_{R(SO_4)_2^-}}{\partial T}\right)_{I,p}\,], \quad (5.38)$$

$$d = F_4 [\, F_5\left(\frac{\partial Q_{RSO_4^+}}{\partial T}\right)_{I,p} - F_6\left(\frac{\partial Q_{R(SO_4)_2^-}}{\partial T}\right)_{I,p}\,], \quad (5.39)$$

$$F_1 = 3 - 2\hat{\beta} - \hat{\alpha}\,, \quad (5.40)$$

$$F_2 = \hat{\alpha}\hat{\beta}^2 - 3\hat{\beta}^2 + 12\hat{\beta} + 2\hat{\alpha}^2\hat{\beta} - 10\hat{\alpha}\hat{\beta} + \hat{\alpha}^3 - 7\hat{\alpha}^2 + 16\hat{\alpha} - 12\,, \quad (5.41)$$

$$F_3 = 7\hat{\alpha}^2 - 4\hat{\alpha}^2\hat{\beta} - 3\hat{\alpha}^3\,, \quad (5.42)$$

$$F_4 = 4\hat{\beta}^2 + 4\hat{\alpha}\hat{\beta} - 4\hat{\beta} + \hat{\alpha}^2 - 6\,, \quad (5.43)$$

$$F_5 = 2\hat{\beta}^4 - 11\hat{\beta}^3 + 6\hat{\alpha}\hat{\beta}^3 - 22\hat{\alpha}\hat{\beta}^2 + 6\hat{\alpha}^2\hat{\beta}^2 + 20\hat{\beta}^2 - 11\hat{\alpha}^2\hat{\beta} + 20\hat{\alpha}\hat{\beta} - 12\hat{\beta} + 2\hat{\alpha}^3\hat{\beta}\,, \quad (5.44)$$

and

$$F_6 = 7\hat{\alpha}^2\hat{\beta} + \hat{\alpha}^4 - 6\hat{\alpha}^2 - 2\hat{\alpha}^2\hat{\beta}^2 \quad (5.45)$$

Derivatives with respect to ionic strength required values for $(\partial A_\gamma/\partial T)_p$. These values were obtained directly from the Debye-Hückel limiting slope for apparent molar enthalpy, as reported by Archer and Wang (1990).

The relaxation contribution to the heat capacities of the rare earth sulphates is given by

$$C_{p2,\phi}^{rel} = \Delta\bar{H}\{RSO_4^+\}\left(\frac{\partial\hat{\alpha}}{\partial T}\right)_{p,m} + \Delta\bar{H}\{R(SO_4)_2^-\}\left(\frac{\partial\hat{\beta}}{\partial T}\right)_{p,m}. \quad (5.46)$$

Partial molar enthalpy changes at any given ionic strength, $\Delta\bar{H}$, would be better calculated through enthalpy of dilution and infinite dilution data. However, while infinite dilution enthalpies were available (Izatt *et al.*, 1969) enthalpy of dilution data for the species

investigated were not complete. Therefore, once again for internal consistency, enthalpies were predicted directly from our predicted reaction quotients and a Debye-Hückel expression consistent with equations 5.27 and 5.28, $(\partial \ln Q/\partial T)_p$.

Aqueous lutetium sulphate is more soluble than all other species investigated in this study. In most cases, when fitting equation 5.6 to apparent molar properties for fully dissociated rare earth species, we have found the extended Debye-Hückel approximations to be relatively robust up to approximately I=0.5 mol kg^{-1}. Because of the applicable ionic strength limitations of the extended Debye-Hückel equation, we did not compute relaxation contributions for $Lu_2(SO_4)_3$ (aq) where the ionic strength was predicted to be in excess of 0.5 mol kg^{-1}.

All calculated relaxation contributions, ionic strengths, $(\partial \hat{\alpha}/\partial T)_{p,m}$ values, and $(\partial \hat{\beta}/\partial T)_{p,m}$ values are reported in tables 5.13 to 5.20.

Table 5.13. Estimated ionic strength and relaxation contributions to experimental heat capacities of aqueous $Y_2(SO_4)_3$ at 298.15 K.

m	$\hat{I}$	$10^3\left(\frac{\partial \hat{\alpha}}{\partial T}\right)_{p,m}$	$10^3\left(\frac{\partial \hat{\beta}}{\partial T}\right)_{p,m}$	$C_{p2,\phi}^{rel}$
(mol kg^{-1})	(mol kg^{-1})	(K^{-1})	(K^{-1})	(J K^{-1} mol^{-1})
0.01346	0.06738	3.87	-2.82	39.4
0.01594	0.07828	3.62	-3.02	34.7
0.04031	0.1793	2.68	-3.43	20.1
0.04097	0.1818	2.67	-3.43	19.9
0.05437	0.2323	2.50	-3.38	18.0
0.07088	0.2901	2.38	-3.27	17.1
0.06878	0.2830	2.39	-3.29	17.1
0.08035	0.3210	2.35	-3.19	16.9
0.09120	0.3549	2.32	-3.07	16.9
0.09910	0.3785	2.31	-2.96	17.0

Table 5.14 Estimated ionic strength and relaxation contributions to experimental heat capacities of aqueous $La_2(SO_4)_3$ at 298.15 K.

m	$\hat{I}$	$10^3\left(\frac{\partial\hat{\alpha}}{\partial T}\right)_{p,m}$	$10^3\left(\frac{\partial\hat{\beta}}{\partial T}\right)_{p,m}$	$C_{p2,\phi}^{rel}$
(mol kg^{-1})	(mol kg^{-1})	(K^{-1})	(K^{-1})	(J K^{-1} mol^{-1})
0.005332	0.02711	3.75	-0.41	48.1
0.00948	0.04431	2.60	-1.51	28.2
0.01355	0.06060	2.01	-2.08	19.0
0.02025	0.08676	1.50	-2.48	12.1
0.02591	0.1084	1.27	-2.62	9.3
0.03226	0.1321	1.10	-2.69	7.4
0.02871	0.1189	1.18	-2.66	8.3
0.04052	0.1622	0.96	-2.73	6.0
0.04378	0.1738	0.92	-2.75	5.6
0.04896	0.1918	0.86	-2.76	5.2

Table 5.15 Estimated ionic strength and relaxation contributions to experimental heat capacities of aqueous $Pr_2(SO_4)_3$ at 298.15 K.

m	$\hat{I}$	$10^3\left(\frac{\partial\hat{\alpha}}{\partial T}\right)_{p,m}$	$10^3\left(\frac{\partial\hat{\beta}}{\partial T}\right)_{p,m}$	$C_{p2,\phi}^{rel}$
(mol kg^{-1})	(mol kg^{-1})	(K^{-1})	(K^{-1})	(J K^{-1} mol^{-1})
0.08830	0.2943	0.95	-3.89	-1.7
0.07876	0.2675	0.96	-3.86	-1.6
0.06762	0.2348	0.98	-3.83	-1.4
0.05990	0.2114	1.00	-3.82	-1.3
0.05133	0.1845	1.04	-3.81	-1.1
0.04408	0.1610	1.09	-3.81	-0.8
0.03568	0.1331	1.18	-3.82	-0.4
0.02543	0.09799	1.38	-3.77	1.0
0.01522	0.06191	1.86	-3.46	6.3
0.008265	0.03640	2.82	-2.39	23.3

Table 5.16 Estimated ionic strength and relaxation contributions to experimental heat capacities of aqueous $Nd_2(SO_4)_3$ at 298.15 K.

m	$\hat{I}$	$10^3\left(\frac{\partial\hat{\alpha}}{\partial T}\right)_{p,m}$	$10^3\left(\frac{\partial\hat{\beta}}{\partial T}\right)_{p,m}$	$C_{p2,\phi}^{rel}$
(mol kg^{-1})	(mol kg^{-1})	(K^{-1})	(K^{-1})	(J K^{-1} mol^{-1})
0.01843	0.08775	2.51	-1.32	22.1
0.02642	0.1231	1.94	-1.74	11.2
0.03244	0.1483	1.66	-1.95	6.5
0.04646	0.2038	1.25	-2.26	0.5
0.06140	0.2586	0.99	-2.52	-3.0
0.07260	0.2968	0.87	-2.70	-4.8
0.08045	0.3222	0.80	-2.82	-5.8
0.08983	0.3512	0.74	-2.97	-6.8
0.09836	0.3765	0.70	-3.10	-7.7
0.1175	0.4295	0.66	-3.39	-9.3

Table 5.17 Estimated ionic strength and relaxation contributions to experimental heat capacities of aqueous $Eu_2(SO_4)_3$ at 298.15 K.

m	$\hat{I}$	$10^3\left(\frac{\partial\hat{\alpha}}{\partial T}\right)_{p,m}$	$10^3\left(\frac{\partial\hat{\beta}}{\partial T}\right)_{p,m}$	$C_{p2,\phi}^{rel}$
(mol kg^{-1})	(mol kg^{-1})	(K^{-1})	(K^{-1})	(J K^{-1} mol^{-1})
0.006816	0.03269	3.62	-0.81	46.3
0.008558	0.03977	6.11	-1.31	33.6
0.01024	0.04648	2.74	-1.68	24.9
0.01321	0.05820	2.23	-2.19	14.2
0.01455	0.06343	2.07	-2.35	11.0
0.01641	0.07060	1.89	-2.51	7.7
0.01851	0.07868	1.71	-2.67	4.7
0.02116	0.08877	1.53	-2.81	2.0
0.02267	0.09447	1.45	-2.87	0.9
0.02513	0.1037	1.34	-2.95	-0.6

Table 5.18 Estimated ionic strength and relaxation contributions to experimental heat capacities of aqueous $Dy_2(SO_4)_3$ at 298.15 K.

m	$\hat{I}$	$10^3\left(\frac{\partial\hat{\alpha}}{\partial T}\right)_{p,m}$	$10^3\left(\frac{\partial\hat{\beta}}{\partial T}\right)_{p,m}$	$C_{p2,\phi}^{rel}$
(mol kg^{-1})	(mol kg^{-1})	(K^{-1})	(K^{-1})	(J K^{-1} mol^{-1})
0.005773	0.03165	5.34	0.13	84.9
0.01054	0.05357	4.00	-0.92	51.2
0.01762	0.08493	3.03	-1.76	28.3
0.02218	0.1047	2.65	-2.07	20.7
0.03044	0.1395	2.21	-2.42	12.6
0.03660	0.1646	1.99	-2.59	9.1
0.04420	0.1945	1.78	-2.75	6.1
0.04586	0.2009	1.74	-2.79	5.5
0.05176	0.2230	1.63	-2.90	3.9
0.05988	0.2524	1.51	-3.03	2.3

Table 5.19 Estimated ionic strength and relaxation contributions to experimental heat capacities of aqueous $Ho_2(SO_4)_3$ at 298.15 K.

m	$\hat{I}$	$10^3\left(\frac{\partial\hat{\alpha}}{\partial T}\right)_{p,m}$	$10^3\left(\frac{\partial\hat{\beta}}{\partial T}\right)_{p,m}$	$C_{p2,\phi}^{rel}$
(mol kg^{-1})	(mol kg^{-1})	(K^{-1})	(K^{-1})	(J K^{-1} mol^{-1})
0.009765	0.05454	4.41	0.62	65.9
0.01566	0.08393	3.47	0.16	45.3
0.02263	0.1178	2.77	-0.23	30.7
0.03116	0.1577	2.20	-0.57	19.9
0.03807	0.187	1.86	-0.79	14.0
0.04680	0.2260	1.54	-1.03	8.8
0.05072	0.2421	1.42	-1.13	7.0
0.06501	0.2973	1.09	-1.48	1.9
0.06855	0.3101	1.03	-1.56	1.0
0.07327	0.3269	0.95	-1.67	-0.2
0.07875	0.3458	0.88	-1.79	-1.4

Table 5.20 Estimated ionic strength and relaxation contributions to experimental heat capacities of aqueous $Lu_2(SO_4)_3$ at 298.15 K.

m	$\hat{I}$	$10^3\left(\frac{\partial\hat{\alpha}}{\partial T}\right)_{p,m}$	$10^3\left(\frac{\partial\hat{\beta}}{\partial T}\right)_{p,m}$	$C_{p2,\phi}^{rel}$
(mol kg^{-1})	(mol kg^{-1})	(K^{-1})	(K^{-1})	(J K^{-1} mol^{-1})
0.1551	0.4949	1.17	-3.94	0.0
0.1161	0.4002	1.13	-3.61	0.4
0.07570	0.2855	1.21	-3.29	1.5
0.05301	0.2112	1.37	-3.13	2.7
0.03752	0.1556	1.58	-3.00	4.7
0.02424	0.1049	1.95	-2.77	8.9
0.01374	0.06292	2.66	-2.16	19.9
0.007321	0.03625	3.76	-1.05	42.5

We note the total relaxation contribution to the heat capacity becomes negative as the ionic strength is increased. The total contribution becomes negative due to the negative calculated values for $(\partial\hat{\beta}/\partial T)_{p,m}$. At first glance it seems counterintuitive for values of $(\partial\hat{\beta}/\partial T)_{p,m}$ to be negative if the enthalpy change is positive. There appears to be no previous literature investigations which have described negative relaxation contributions, since for most reactions a positive ΔH implies a positive temperature derivative and *vice versa*. However, with aqueous rare earth sulphate solutions there are two coupled association reactions, which make this situation possible. Note that the extent of reaction 5.13 is not only dependent on temperature but also on the extent of reaction 5.12, therefore $\beta(T,\alpha)$. The total differential of $\beta(T,\alpha)$ yields

$$d\beta = \left(\frac{\partial\beta}{\partial T}\right)_{p,\alpha} dT + \left(\frac{\partial\beta}{\partial\alpha}\right)_{p,T} d\alpha \,. \tag{5.47}$$

Dividing by dT yields

$$\left(\frac{\partial\beta}{\partial T}\right)_{p,m} = \left(\frac{\partial\beta}{\partial T}\right)_{p,\alpha} + \left(\frac{\partial\beta}{\partial\alpha}\right)_{p,T}\left(\frac{\partial\alpha}{\partial T}\right)_{p,m}, \tag{5.48}$$

from which it can be observed that $(\partial\beta/\partial T)_{p,m}$ depends on $(\partial\beta/\partial\alpha)_T$. Since $(\partial\hat{\alpha}/\partial T)_\beta$ is large with respect to $(\partial\hat{\beta}/\partial T)_\alpha$ (ΔH^o(reaction 5.12) >> ΔH^o(reaction 5.13)) the latter term is dominant. Also $(\partial\hat{\beta}/\partial\hat{\alpha})$ is negative for the coupled reactions 5.12 and 5.13 in the concentration ranges of our solutions. This term does become positive at lower concentration ranges. Therefore although $(\partial\beta/\partial T)_\alpha$ must be positive, there is no such restriction placed on $(\partial\beta/\partial T)_{p,m}$ for a coupled reaction.

5.3.5 Single ion partial molar volumes and heat capacities at infinite dilution for some rare earth sulphate complex species.

Single ion apparent molar volumes and heat capacities at 298.15 K for selected aqueous RSO_4^+ and $R(SO_4)_2^-$ species have been predicted by multiple regression of equation 5.11 with our predicted relative concentrations, $\hat{\alpha}$ and $\hat{\beta}$. These single ion apparent molar properties are reported in table 5.21. The uncertainties in these predictions come from the regression variance-covariance matrix combined with the predicted uncertainties in the single ion trivalent rare earth partial molar properties. Although these uncertainties are large, the R^2 values for all apparent molar volume fits indicate that over 99% of the variance has been accounted for. For heat capacities, R^2 values are slightly lower at an average of 88±7%. Heat capacities without relaxation contribution corrections significantly reduced the R^2 values for all species. This good correlation appears to support the validity of our attempt to model some portion of the apparent molar properties through calculated relaxation contributions and the extended Debye-Hückel terms from equation 5.6.

The combination of single ion properties and the extended Debye-Hückel contribution, allows for the calculation of the apparent molar properties by equation 5.9. Figures 5.3 through 5.6 show the apparent molar volumes of aqueous $La_2(SO_4)_3$, $Pr_2(SO_4)_3$, $Eu_2(SO_4)_3$, and $Ho_2(SO_4)_3$. Figures 5.7 through 5.10 show the apparent molar heat capacities of aqueous $Y_2(SO_4)_3$, $Nd_2(SO_4)_3$, $Dy_2(SO_4)_3$, and $Lu_2(SO_4)_3$. At the lower portion of these figures the predicted Debye-Hückel curve for a completely

Table 5.21 Single ion partial molar heat capacities and volumes for aqueous monosulphate and disulphate rare earth ions at 298.15 K.

Complex ion	$\bar{V}^o$ (cm^3 mol^{-1})	$\bar{C}_p^o$ (J K^{-1} mol^{-1})
YSO_4^+	-12.8 ± 0.8	81.3 ± 20.7
$Y(SO_4)_2^-$	38.3 ± 0.8	138 ± 21
$LaSO_4^+$	-8.05 ± 0.95	-29.0 ± 18.5
$La(SO_4)_2^-$	42.1 ± 1.0	171 ± 20
$PrSO_4^+$	-14.5 ± 1.5	14.8 ± 26.9
$Pr(SO_4)_2^-$	42.2 ± 1.5	131 ± 27
$NdSO_4^+$	-7.11 ± 1.34	96.3 ± 24.2
$Nd(SO_4)_2^-$	44.2 ± 1.4	181 ± 25
$EuSO_4^+$	-14.9 ± 1.1	26.3 ± 18.9
$Eu(SO_4)_2^-$	36.2 ± 1.4	179 ± 24
$DySO_4^+$	-7.87 ± 0.42	73.8 ± 15.9
$Dy(SO_4)_2^-$	41.5 ± 0.6	279 ± 21
$HoSO_4^+$	-5.47 ± 0.31	140 ± 12
$Ho(SO_4)_2^-$	43.0 ± 0.5	281 ± 17
$LuSO_4^+$	-17.0 ± 0.9	141 ± 22
$Lu(SO_4)_2^-$	37.9 ± 0.8	227 ± 24

dissociated 3:2 electrolyte is shown. These Debye-Hückel contributions illustrate the inadequacy of using such a model to aid in extrapolating from apparent molar properties of aqueous rare earth sulphates. The poor modelling of the rare earth species by the constant average valence terms is clearly due to the partial molar volume and heat capacity changes due to the formation of their respective monosulphate and disulphate species. These properties are much more positive in comparison to the fully noncomplexed ions, thus, figures 5.3 to 5.10 also show the predicted apparent molar properties as predicted from equation 5.9. The species dependent equation 5.9 is much more robust by reflecting the change in volume or heat capacity as a function of complexation and thus ionic strength.

Figure 5.3 The concentration dependence of the experimental apparent molar volume of aqueous $La_2(SO_4)_3$ at 298.15 K.

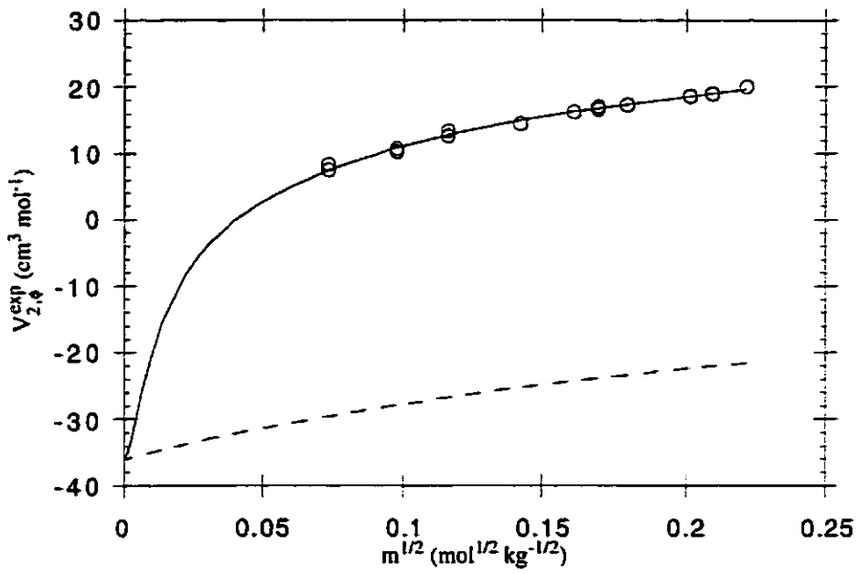

—— equation 5.9. – – – – Debye-Hückel contribution for a completely dissociated 3:2 electrolyte.

Figure 5.4 The concentration dependence of the experimental apparent molar volume of aqueous $Pr_2(SO_4)_3$ at 298.15 K.

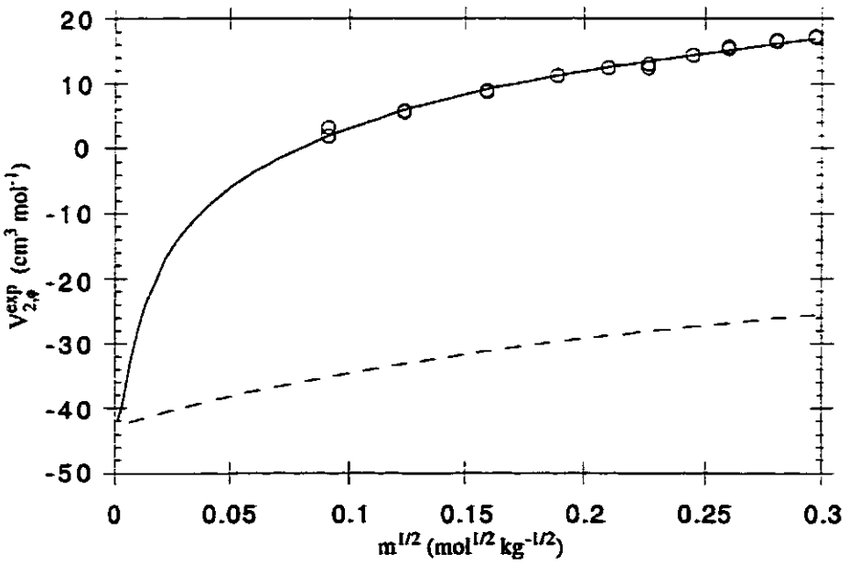

—— equation 5.9. – – – – Debye-Hückel contribution for a completely dissociated 3:2 electrolyte.

Figure 5.5 The concentration dependence of the experimental apparent molar volume of aqueous $Eu_2(SO_4)_3$ at 298.15 K.

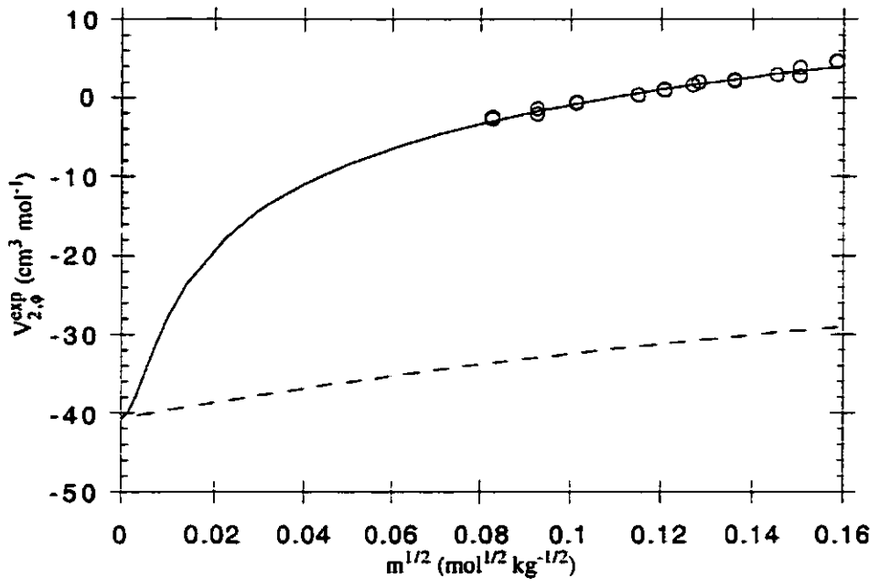

—— equation 5.9. – – – – Debye-Hückel contribution for a completely dissociated 3:2 electrolyte.

Figure 5.6 The concentration dependence of the experimental apparent molar volume of aqueous $Ho_2(SO_4)_3$ at 298.15 K.

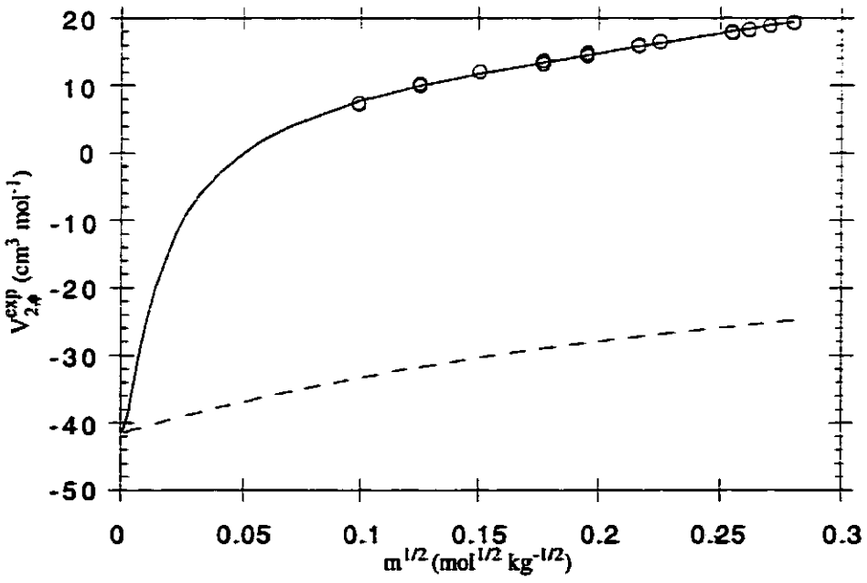

—— equation 5.9. – – – – Debye-Hückel contribution for a completely dissociated 3:2 electrolyte.

Figure 5.7 The concentration dependence of the experimental apparent molar heat capacity of aqueous $Y_2(SO_4)_3$ at 298.15 K.

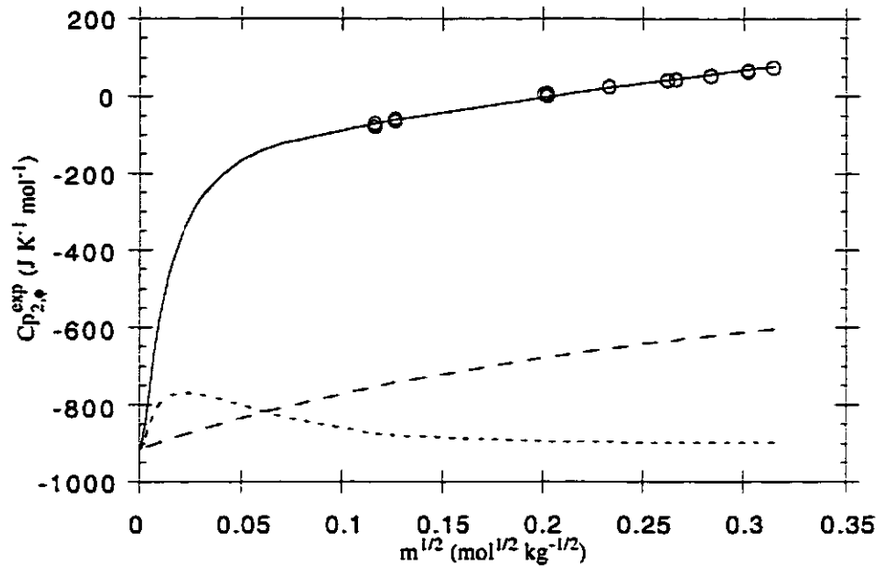

—— equation 5.9. - - - $C^{rel}_{p2,\phi}$ ——— Debye-Hückel contribution for a completely dissociated 3:2 electrolyte.

Figure 5.8 The concentration dependence of the experimental apparent molar heat capacity of aqueous $Nd_2(SO_4)_3$ at 298.15 K.

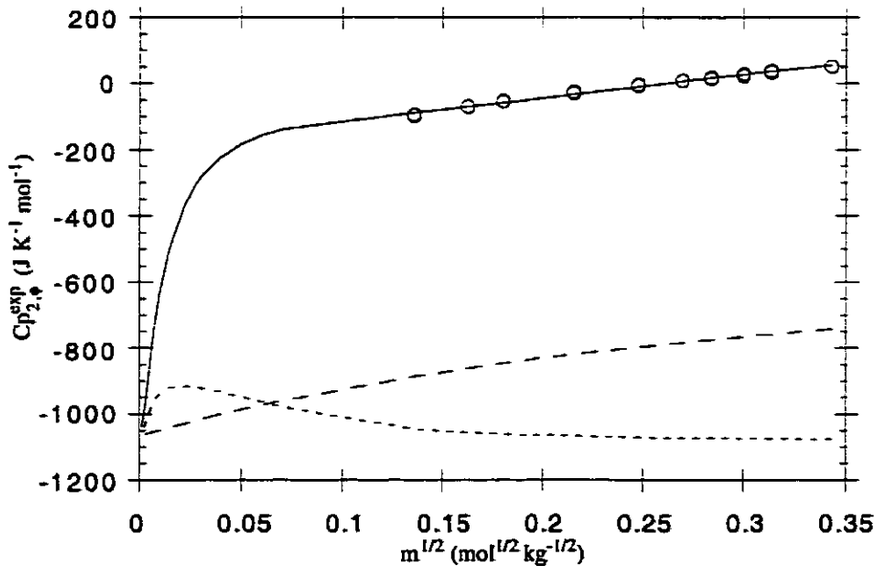

—— equation 5.9. - - - $C^{rel}_{p2,\phi}$ ——— Debye-Hückel contribution for a completely dissociated 3:2 electrolyte.

Figure 5.9 The concentration dependence of the experimental apparent molar heat capacity of aqueous $Dy_2(SO_4)_3$ at 298.15 K.

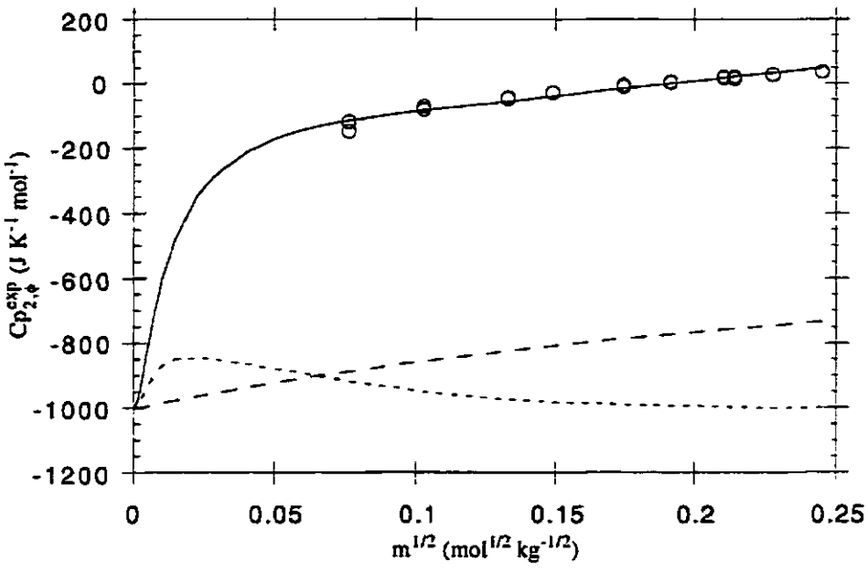

—— equation 5.9. - - - $C_{p2,\phi}^{rel}$ ——— Debye-Hückel contribution for a completely dissociated 3:2 electrolyte.

Figure 5.10 The concentration dependence of the experimental apparent molar heat capacity of aqueous $Lu_2(SO_4)_3$ at 298.15 K.

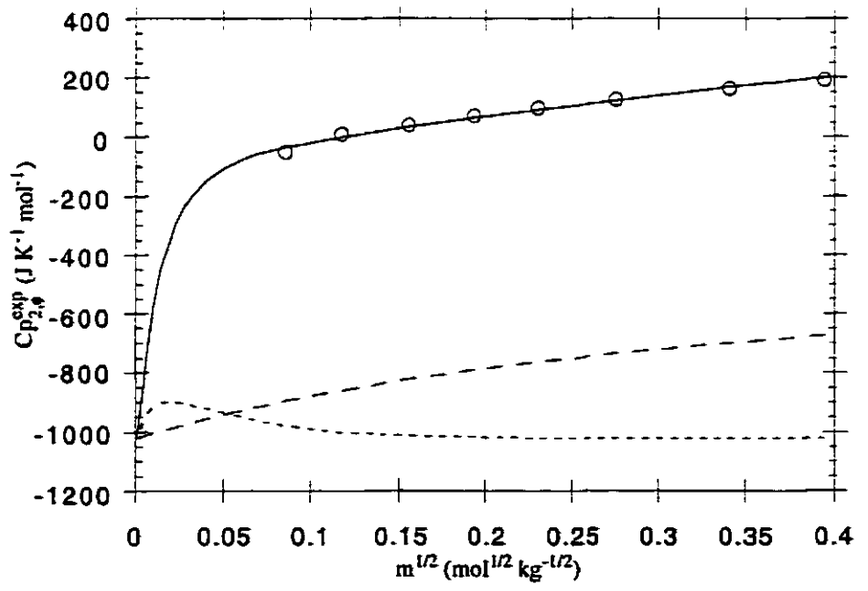

—— equation 5.9. - - - $C_{p2,\phi}^{rel}$ ——— Debye-Hückel contribution for a completely dissociated 3:2 electrolyte.

In figures 5.7 through 5.10, relaxation contributions have also been shown. This relaxation contribution is clearly the major contributing factor as concentrations approach infinite dilution. The maxima in these relaxation contributions also indicate where $(\partial\beta/\partial\alpha)$ changes sign.

From single ion properties reported in this study, $\Delta\bar{V}^o$ and $\Delta\bar{C}_p^o$ for association reactions 5.12 and 5.13 can be calculated.

$$\Delta\bar{Y}^o = \bar{Y}^o(\text{complex ion}) - \bar{Y}^o(\text{free ions}) \qquad (5.49)$$

These are the principal properties of interest with respect to extending equilibrium calculations beyond 298.15 K and 0.10 MPa. Equations 2.5 and 2.8 show these relationships. With respect to both association reactions 5.12 and 5.13, $\Delta\bar{V}^o$ and $\Delta\bar{C}_p^o$ are large. Chen and Millero (1977) have reported $\Delta\bar{V}^o = 22.8\pm1$ cm^3 mol^{-1} for the formation of the RSO_4^+ species. This value is in good agreement with our calculated value of 22.34 ± 0.95 cm^3 mol^{-1}.

In spite of our extensive reliance on Debye-Hückel theory, our analysis has indicated that the relaxation approach provides a very good working model of experimentally determined apparent molar properties. Although our relaxation contributions have been estimated in a region of ionic strength where Debye-Hückel theory is not able to provide precise predictions of activity coefficients, our analyses appear to provide a first attempt at modelling the heat capacity properties of these species. We are also confident in the precision of our apparent molar properties which may be used by future authors, with perhaps more insight into aqueous rare earth sulphate behaviour.

6) A VOLUMETRIC AND CALORIMETRIC STUDY OF SEVERAL AQUEOUS AMINO ACID SYSTEMS AT TEMPERATURES REMOVED FROM AMBIENT[1].

6.1 Introduction

The discovery of organisms which thrive at elevated temperatures and pressures, for example within hydrothermal vent habitats (Aono *et al.*, 1989; Baross & Deming, 1995; Brown & Kelly, 1989; Burggraf *et al.*, 1990), has prompted research into the thermodynamics of aqueous biochemical systems under elevated temperature and pressure conditions. Historically, the thermodynamics of aqueous solutions of biologically important molecules, such as amino acids and peptides, have been studied at temperatures and pressures close to ambient (298.15 K and 0.1 MPa) (Iqbal & Verall, 1989; Jolicoeur *et al.*, 1986; Millero *et al.*, 1978). This is in part due to the considerable number of experimental difficulties one encounters when attempting to measure thermodynamic properties at elevated temperatures and pressures. Hence, there is a growing interest in the use of semi-empirical models to estimate extensive thermodynamic properties of these aqueous systems under extreme conditions (Amend & Helgeson, 1997a; Shock, 1992; Amend & Shock, 1998).

Of particular note within the modelling of geochemical systems, are the semi-empirical equations of state of Helgeson, Kirkham, and Flowers (HKF) (Helgeson & Kirkham, 1976). As discussed in Chapter 2 these semi-continuous equations have been found to accurately model the partial molar properties at infinite dilution of many aqueous electrolyte systems (Amend & Helgeson, 1997b; Helgeson & Kirkham, 1976). More recently, the revised equations have been used to estimate thermodynamic parameters at infinite dilution for neutral organic species in aqueous solution (Amend & Helgeson,

---

[1]. A version of this chapter has been published by Marriott R. A., Hakin A. W., and Liu J. L. (1998) *J. Solution Chem.* **27**, 771-802.

1997a,b; Hakin *et al.*, 1995; Shock, 1992; Shock & Helgeson, 1990). With the aid of parameter correlation techniques (Shock, 1992; Shock & Helgeson, 1990) and additivity techniques (Amend & Helgeson, 1997a,b), the HKF model has been used to estimate thermodynamic parameters for equilibrium processes at temperatures and pressures beyond those within the experimental literature. However, in spite of its apparent success, several authors (Amend & Helgeson, 1997a,b; Hakin *et al.*, 1994b; Shock, 1992) have criticised the HKF model on the grounds that most of its parameters are estimated from limited and variable input data sets which may compromise the utility of predicted properties.

Additivity schemes have also been used to model the thermodynamic properties of aqueous amino acids and peptides (Amend & Helgeson, 1997a; Hakin *et al.*, 1994b, 1995). One aim of this study has been to construct an additivity scheme that could be used to estimate the partial molar volumes and heat capacities at infinite dilution of aqueous biochemical solutions over an extended temperature range. To achieve this goal we have defined three basic requirements which must be met by any model under consideration: i) the model must be constructed with a consistent and carefully measured experimental data set obtained over a range of temperatures; ii) the data set must be large enough to ensure statistical confidence in estimated parameters; iii) the model must be simple, and yet robust, so that it can be of use to a wide range of researchers. The basic HKF model meets the latter three requirements.

In their most simple form the HKF equations compliment an additive approach by splitting partial molar properties at infinite dilution into structural (non-solvation) and electrostatic (solvation) contributions (Shock, 1992). In our past work with the model (Hakin *et al.*, 1994b, 1995), we reported structural contributions to partial molar volumes and heat capacities at infinite dilution for a limited number of functional groups at temperatures of 288.15, 298.15, 313.15, and 328.15 K. In this study we have caused the HKF parameters, themselves, to be additive in terms of functional group contributions. This treatment removes the isothermal constraint that was placed on our data in our

previous investigations.

Amend and Helgeson (1997a,b) have recently utilised a similar approach in which the electrostatic and the structural terms of the HKF model are treated as additive with respect to group contributions. They have used this approach to look at equilibrium processes which may be significant to the chemistry of hydrothermal vent systems. However, in this study each of the empirical HKF parameters was considered as a sum of temperature-independent functional group contributions.

The present study extends the data base of volumetric and thermochemical properties of aqueous amino acid and peptide systems obtained by this laboratory (Duke *et al.*, 1994; Hakin *et al.*, 1994a,b, 1995, 1997), by reporting relative densities, $(\rho - \rho_O)$, heat capacity ratios, $[(C_p\rho/C_p^o\rho_O) - 1]$, apparent molar volumes, $V_{2,\phi}$, and apparent molar heat capacities, $C_{p2,\phi}$, for aqueous L-histidine, L-phenylalanine, L-tyrosine, L-tryptophan, and L-2,3-dihydroxyphenylalanine (L-dopa) at 288.15, 298.15, 313.15, and 328.15 K (0.1 MPa). These data have been used to estimate partial molar properties at infinite dilution, which have been compared, where possible, to available literature values. The input data set to our HKF model consists of partial molar volumes and heat capacities at infinite dilution for 24 aqueous biochemical species which cover a temperature range of 40 K about ambient temperature. The structures of the 24 aqueous biochemical species are given in Appendix C. The results of our HKF analyses are a set of parameters which permit us to obtain the contributions to partial molar volumes and heat capacities at infinite dilution of a large number of functional groups as a function of temperature. These group contributions can, in turn, be used to estimate thermochemical and volumetric properties of aqueous amino acid and peptide systems.

6.2 Experimental

L-histidine, L-phenylalanine, L-tyrosine, L-tryptophan, and L-dopa, of the highest purity, were obtained from the Sigma Chemical Company (catalog numbers H-8000,

P-2126, T-0254, T-8649, and D-9628). All chemicals were further purified by repeated recrystallisation from ethanol + water mixtures and were then dried and stored under vacuum at 328 K over phosphorus pentoxide. Purification of L-dopa took place in a nitrogen environment to prevent oxidation. Infrared spectra of the five investigated species were obtained using a Bomem BM100 series IR spectrophotometer. Proton NMR spectra were obtained using a Brüker 250 MHz instrument in which D_2O was used as an internal standard. Postpurification characterizations were in good agreement with data in the literature (Pouchert, 1981; Pouchert & Campbell, 1974).

Water was obtained from an Osmonics model Aries High Purity D. I. Loop, capable of polishing to a resistance of 18.2 MΩ. All solvent was thoroughly degassed prior to use. Solutions were prepared by weight, using the molality concentration scale, and stored, in an unbuffered state, in 100 mL and 50 mL Nalgene bottles.

Densities were measured relative to water with the Sodev O2D vibrating tube densimeter (Picker *et al.*, 1974) described in Section 3.3 and heat capacity ratios were measured with the Picker microflow calorimeter (Picker *et al.*, 1971) described in Section 3.2. The calibration of both these instruments have been previously discussed in Section 3.4.

6.3 Results

Relative densities for all sample solutions were calculated using equation 3.8 where ρ_A is the density of pure water. The densities of pure water used in this investigation are those reported by Kell (1967). Densities of water are reported in the calibration Subsection 3.4.1 and the respective calibration constants used in this study are reported in Subsection 3.4.2.

Apparent molar volumes and apparent molar heat capacities were calculated from relative densities and heat capacity ratios using equations 3.9 and 3.10. The specific heat

Table 6.1. Relative densities, apparent molar volumes, heat capacity ratios, and apparent molar heat capacities of aqueous L-dopa at 288.15, 298.15, 313.15, and 328.15 K.

m (mol kg^{-1})	$(\rho - \rho_o)$ (kg m^{-3})	$V_{2,\phi}$ (cm^3 mol^{-1})	$10^3\left(\frac{c_p\rho}{c_{pl}^o\rho_o}-1\right)$	$c_{p2,\phi}$ (J K^{-1} mol^{-1})
		T = 288.15 K		
0.004498	0.332	123.35±1.11	----	----
0.004498	0.328	124.17±1.12	-0.212	319.8±15.7
0.004892	0.361	123.40±1.02	-0.241	307.9±14.3
0.004892	0.348	126.11±1.02	-0.255	307.1±14.3
0.005371	0.384	125.74±0.93	-0.238	338.1±13.0
0.005371	0.393	123.98±0.93	-0.267	308.0±13.0
0.005948	0.436	123.82±0.84	-0.270	325.7±11.8
0.005948	0.436	123.92±0.84	-0.267	328.2±11.8
0.006268	0.459	123.90±0.80	-0.306	311.3±11.2
0.006268	0.461	123.68±0.80	-0.301	313.8±11.2
0.007398	0.546	123.40±0.68	-0.382	297.3±9.5
0.007398	0.543	123.73±0.68	-0.369	306.5±9.5
		T = 298.15 K		
0.002417	0.172	126.04±2.08	-0.099	351.7±29.0
0.002885	0.205	126.16±1.74	-0.137	324.5±24.3
0.003292	0.233	126.72±1.53	-0.137	352.2±21.3
0.004077	0.290	126.20±1.23	----	----
0.004556	0.325	125.93±1.10	-0.193	346.0±15.4
0.005144	0.364	126.59±0.98	-0.242	328.6±13.6
0.005639	0.403	125.83±0.89	-0.242	343.1±12.4
0.006345	0.451	126.15±0.79	-0.275	342.4±11.0
0.006934	0.494	126.03±0.73	-0.312	334.7±10.1
0.007479	0.432	126.47±0.67	-0.339	335.0±9.4
0.002417	0.169	127.64±2.08	-0.103	351.4±29.0
0.002885	0.201	127.58±1.74	-0.143	322.5±24.3
0.003292	0.234	126.29±1.53	-0.154	328.9±21.3
0.004077	0.287	126.79±1.23	----	----
0.004556	0.322	126.56±1.10	-0.194	347.7±15.4

Table 6.1 Continued

0.005144	0.367	125.93±0.98	-0.236	331.1±13.6
0.005639	0.399	126.61±0.89	-0.239	348.3±12.4
0.006345	0.451	126.25±0.79	-0.297	328.5±11.0
0.006934	0.494	126.01±0.73	-0.316	332.2±10.1
0.002417	0.168	127.97±2.08	-0.108	344.0±29.0
0.002316	0.166	125.56±2.17	-0.108	327.1±30.2
0.002851	0.202	126.34±1.76	-0.127	338.1±24.6
0.003221	0.229	126.20±1.56	-0.150	329.4±21.7
0.003889	0.275	126.63±1.29	----	----
0.004293	0.306	125.93±1.17	----	----
0.004688	0.334	126.07±1.07	-0.215	332.0±14.9
0.005150	0.368	125.80±0.98	-0.212	349.9±13.6
0.005708	0.407	126.00±0.88	-0.254	337.1±12.3
0.006602	0.471	125.95±0.76	-0.291	338.3±10.6
0.007044	0.501	126.20±0.71	-0.300	345.8±10.0
		T = 313.15 K		
0.002392	0.172	125.54±2.12	-0.071	394.7±29.3
0.002392	0.169	126.81±2.12	-0.056	----
0.002827	0.204	125.54±1.80	-0.090	386.7±24.8
0.002827	0.201	126.46±1.80	-0.086	396.4±24.8
0.003283	0.234	126.27±1.55	-0.147	334.6±21.3
0.003283	0.232	126.88±1.55	-0.112	382.5±21.3
0.004039	0.286	126.66±1.26	----	----
0.004039	0.287	126.54±1.26	-0.134	384.7±17.3
0.004613	0.326	126.83±1.10	----	----
0.004613	0.326	126.92±1.10	-0.185	356.4±15.2
0.005209	0.375	125.67±0.98	-0.222	340.6±13.5
0.005209	0.369	126.79±0.98	-0.226	342.0±13.5
0.006048	0.433	125.88±0.84	-0.233	359.4±11.6
0.006048	0.435	125.69±0.84	-0.244	350.4±11.6
0.006621	0.472	126.25±0.77	----	----
0.006621	0.469	126.71±0.77	----	----
0.007021	0.499	126.54±0.72	-0.251	373.6±10.0
0.007021	0.503	125.92±0.72	-0.305	338.3±10.0

Table 6.1 Continued

0.007285	0.520	126.18±0.70	-0.273	364.5±9.6
0.007285	0.519	126.30±0.70	-0.318	339.1±9.6
0.007336	0.522	126.45±0.69	----	----
0.007336	0.518	126.91±0.69	----	----
0.005674	0.405	126.15±0.90	----	----
		T = 328.15 K		
0.002210	0.147	131.75±2.33	----	----
0.002210	0.152	129.38±2.33	----	----
0.002819	0.200	126.94±1.83	----	----
0.002819	0.194	129.01±1.83	----	----
0.003530	0.247	127.95±1.46	----	----
0.003530	0.244	128.81±1.46	----	----
0.003964	0.271	129.76±1.30	----	----
0.003964	0.276	128.26±1.30	----	----
0.004560	0.315	128.91±1.13	----	----
0.004560	0.315	128.87±1.13	----	----
0.005178	0.363	127.74±0.99	----	----
0.005178	0.360	128.37±0.99	----	----
0.005674	0.394	128.47±0.91	----	----
0.005674	0.394	128.51±0.91	----	----
0.006324	0.440	128.45±0.81	----	----
0.006324	0.439	128.51±0.81	----	----
0.006921	0.482	128.34±0.74	----	----
0.007336	0.505	129.19±0.70	----	----
0.007336	0.511	128.26±0.70	----	----

capacity of pure water is also shown in the calibration Subsection 3.4.1 as reported by Kell (1972).

Uncertainties in calculated apparent molar volumes, $\delta V_{2,\phi}$, and heat capacities, $\delta C_{p2,\phi}$, were calculated using equations 3.12 and 3.13. Uncertainties arising from errors in solution preparation, δm, have been considered to be negligible.

Table 6.2. Relative densities, apparent molar volumes, heat capacity ratios, and apparent molar heat capacities of aqueous L-phenylalanine at 288.15, 298.15, 313.15, and 328.15 K.

m (mol kg^{-1})	$(\rho - \rho_O)$ (kg m^{-3})	$V_{2,\phi}$ (cm^3 mol^{-1})	$10^3\left(\frac{c_p\rho}{c_p^O\rho_O}-1\right)$	$c_{p2,\phi}$ (J K^{-1} mol^{-1})
		T = 288.15 K		
0.04209	1.872	120.57±0.12	-1.234	379.6±1.7
0.04969	2.207	120.57±0.10	-1.456	379.5±1.4
0.05253	2.330	120.61±0.10	-1.568	377.4±1.3
0.05671	2.510	120.69±0.09	-1.628	382.5±1.2
0.06482	2.868	120.66±0.08	-1.863	382.1±1.1
0.07744	3.427	120.59±0.07	-2.303	377.3±0.9
0.08698	3.845	120.59±0.06	-2.583	377.4±0.8
0.03269	1.452	120.65±0.15	-1.037	369.9±2.2
0.04477	1.987	120.65±0.11	-1.322	378.9±1.6
0.05988	2.648	120.71±0.08	-1.744	380.7±1.2
0.06598	2.917	120.69±0.08	-1.940	379.4±1.1
0.07811	3.448	120.70±0.06	-2.314	378.2±0.9
0.08893	3.918	120.73±0.06	-2.623	378.8±0.8
0.1004	4.426	120.66±0.05	-2.969	378.0±0.7
0.1114	4.897	120.72±0.04	-3.282	378.6±0.6
0.1212	5.320	120.73±0.04	-3.551	379.1±0.6
0.1338	5.864	120.71±0.04	-3.920	378.9±0.5
		T = 298.15 K		
0.03269	1.415	121.98±0.15	-0.905	390.9±2.2
0.04477	1.929	122.10±0.11	-1.231	392.0±1.6
0.05988	2.575	122.10±0.08	-1.644	392.0±1.2
0.06598	2.835	122.11±0.08	-1.796	392.9±1.1
0.07811	3.353	122.09±0.06	-2.145	391.7±0.9
0.08893	3.808	122.14±0.06	-2.445	391.6±0.8

Table 6.2 Continued

0.1004	4.300	122.09±0.05	-2.777	390.5±0.7
0.1114	4.770	122.04±0.05	-3.049	391.4±0.6
0.1212	5.178	122.08±0.04	-3.325	391.1±0.6
0.1338	5.706	122.08±0.04	-3.690	390.3±0.5
0.04209	1.819	121.99±0.12	-1.130	394.3±1.7
0.04969	2.142	122.05±0.10	-1.360	392.2±1.4
0.05253	2.265	122.03±0.10	-1.459	390.4±1.3
0.05671	2.442	122.06±0.09	-1.565	391.2±1.2
0.06482	2.792	122.01±0.08	-1.797	390.4±1.1
0.07744	3.330	122.02±0.07	-2.110	392.3±0.9
0.08698	3.744	121.92±0.06	-2.619	390.9±0.8
		T = 313.15 K		
0.03269	1.368	123.80±0.16	-0.919	394.0±2.2
0.04477	1.878	123.64±0.11	-1.191	399.7±1.6
0.05988	2.491	123.93±0.09	-1.598	400.3±1.2
0.06598	2.745	123.89±0.08	-1.713	403.1±1.1
0.07811	3.240	123.94±0.07	-2.057	401.6±0.9
0.08893	3.691	123.86±0.06	-2.345	401.0±0.8
0.1004	4.172	123.77±0.05	-2.636	400.9±0.7
0.1114	4.609	123.89±0.05	-2.935	400.9±0.6
0.1212	5.001	123.95±0.04	-3.197	400.9±0.6
0.1338	5.515	123.92±0.04	-3.532	400.4±0.5
0.04912	6.894	123.12±0.10	-1.315	399.3±1.4
0.05672	7.190	123.50±0.09	-1.483	403.5±1.2
0.06261	7.435	123.47±0.08	-1.647	402.5±1.1
0.06835	7.670	123.50±0.07	-1.769	404.4±1.0
0.07217	7.823	123.56±0.07	-1.907	402.3±1.0
0.07669	8.001	123.66±0.07	-2.023	402.8±0.9
0.07168	8.215	123.55±0.07	-2.134	403.3±1.0
0.09415	8.719	123.62±0.05	-2.497	401.8±0.8
0.1020	9.037	123.64±0.05	-2.667	403.4±0.7
0.1506	11.005	123.65±0.03	-3.928	403.1±0.5

Table 6.2 Continued

		T = 328.15 K		
0.03193	1.307	125.29±0.16	-0.738	418.5±2.2
0.05340	2.166	125.57±0.10	-1.144	426.5±1.3
0.06262	2.573	125.48±0.08	-1.507	414.7±1.1
0.07249	2.944	125.43±0.07	-1.866	407.3±1.0
0.08583	3.475	125.48±0.06	-1.942	420.6±0.8
0.09547	3.858	125.51±0.05	-2.323	413.4±0.7
0.1084	4.378	125.48±0.05	-2.638	413.1±0.7
0.1142	4.604	125.50±0.05	-3.039	403.3±0.6
0.1327	5.345	125.45±0.04	-3.415	406.6±0.5

Heat capacity ratios, relative densities, apparent molar volumes, heat capacities, and the uncertainties in the apparent molar properties for L-dopa, L-phenylalanine, L-tryptophan, L-histidine, and L-tyrosine are reported in tables 6.1, 6.2, 6.3, 6.4, and 6.5 respectively.

Equation 6.1 has been fit, using weighted linear regression analysis, to the calculated apparent molar properties of L-phenylalanine, L-histidine, and L-tryptophan, to determine the extensive thermodynamic property of interest at infinite dilution, $Y^{\infty}_{2,\phi}$. The latter quantity is equal to the partial molar property at infinite dilution, $\bar{Y}^{o}_{2}$:

$$Y_{2,\phi} = Y^{\infty}_{2,\phi} + S_Y m. \qquad (6.1)$$

In equation 6.1 the symbol S_Y defines the calculated slope. The weights used in the regression analyses were calculated as the reciprocal squares of the uncertainties.

Estimated partial molar properties at infinite dilution are compared to available literature data in table 6.6. Table 6.6 also contains estimates of experimental slopes and the standard errors associated with each fit.

Due to their low solubilities, calculated apparent molar properties for aqueous L-tyrosine and L-dopa were found to be independent of concentration. Following the lead

Table 6.3. Relative densities, apparent molar volumes, heat capacity ratios, and apparent molar heat capacities of aqueous L-tryptophan at 288.15, 298.15, 313.15, and 328.15 K.

m (mol kg^{-1})	$(\rho - \rho_o)$ (kg m^{-3})	$V_{2,\phi}$ (cm^3 mol^{-1})	$10^3\left(\frac{c_p\rho}{c_p^o\rho_o}-1\right)$	$c_{p2,\phi}$ (J K^{-1} mol^{-1})
		T = 288.15 K		
0.008071	0.506	141.57±0.62	-0.360	405.2±8.7
0.01137	0.717	141.10±0.44	-0.515	400.3±6.2
0.01314	0.817	142.05±0.38	-0.620	396.1±5.3
0.01652	1.022	142.26±0.30	-0.771	399.1±4.3
0.01935	1.200	142.11±0.26	-0.889	401.4±3.6
0.03280	2.031	142.10±0.15	-1.569	393.1±2.1
0.03829	2.369	142.08±0.13	-1.800	396.3±1.8
0.04429	2.736	142.15±0.11	-2.099	394.9±1.6
0.008631	0.536	142.11±0.58	-0.383	406.4±8.1
0.01282	0.791	142.53±0.39	-0.608	395.1±5.5
0.01557	0.968	141.98±0.32	-0.752	388.8±4.5
0.01941	1.203	142.13±0.26	-0.898	398.2±3.6
0.02620	1.627	142.00±0.19	-1.242	392.6±2.7
0.02973	1.844	142.01±0.17	-1.412	392.1±2.4
0.02184	1.356	142.02±0.23	-1.047	390.5±3.2
0.03255	2.017	142.05±0.15	-1.573	388.6±2.2
0.04474	2.768	142.04±0.11	-2.161	388.4±1.6
		T = 298.15 K		
0.008071	0.490	143.73±0.62	-0.360	410.3±8.7
0.01137	0.689	143.75±0.44	-0.529	402.1±6.2
0.01314	0.796	143.78±0.38	-0.606	403.9±5.3
0.01652	1.000	143.77±0.30	-0.724	413.6±4.3
0.01935	1.170	143.82±0.26	-0.887	405.2±3.6
0.02545	1.539	143.78±0.20	-1.139	409.4±2.7
0.02933	1.773	143.77±0.17	-1.323	407.7±2.4
0.008285	0.502	143.77±0.61	-0.384	403.2±8.5
0.01107	0.668	144.02±0.45	-0.497	410.2±6.3

Table 6.3 Continued

0.01549	0.936	143.89±0.33	-0.690	411.1±4.5
0.03280	1.983	143.71±0.15	-1.490	406.1±2.1
0.03829	2.305	143.93±0.13	-1.759	404.6±1.8
0.04429	2.672	143.76±0.11	-1.969	410.1±1.6
0.01848	1.123	143.54±0.27	-0.812	412.0±3.8
0.02284	1.385	143.65±0.22	-1.043	405.0±3.1
0.02507	1.515	143.83±0.20	-1.148	405.2±2.8
0.02915	1.762	143.76±0.17	-1.350	402.6±2.4
0.03898	2.354	143.76±0.13	-1.750	408.3±1.8
0.04475	2.702	143.71±0.11	-2.044	404.6±1.6
		T = 313.15 K		
0.01137	0.667	146.13±0.45	-0.499	420.3±6.2
0.01314	0.774	145.85±0.39	-0.553	426.5±5.3
0.01652	0.968	146.16±0.31	-0.632	443.8±4.3
0.01935	1.137	145.95±0.26	-0.775	435.5±3.6
0.02545	1.493	146.03±0.20	-1.013	436.7±2.8
0.02933	1.722	145.96±0.17	-1.218	429.1±2.4
0.03280	1.925	145.93±0.16	-1.341	431.6±2.1
0.04428	2.596	145.90±0.12	-1.820	430.2±1.6
0.008071	0.466	147.07±0.63	-0.332	435.9±8.7
0.008285	0.484	146.37±0.61	-0.446	379.3±8.5
0.01107	0.653	145.82±0.46	-0.377	460.8±6.3
0.01549	0.906	146.30±0.33	-0.646	429.9±4.5
0.01848	1.085	146.06±0.28	-0.796	423.3±3.8
0.02284	1.340	146.06±0.22	-1.023	415.8±3.1
0.02507	1.474	145.92±0.20	-1.065	424.9±2.8
0.02915	1.711	145.96±0.17	-1.263	421.4±2.4
0.03427	2.009	145.98±0.15	-1.478	422.2±2.1
0.03898	2.288	145.89±0.13	-1.703	419.3±1.8
0.04475	2.627	145.81±0.11	-1.926	421.5±1.6
		T = 328.15 K		
0.008071	0.467	147.56±0.64	-0.308	446.8±8.7
0.01137	0.655	147.78±0.45	-0.491	426.4±6.2
0.03829	2.199	147.74±0.13	-1.590	432.5±1.8

Table 6.3 Continued

0.04428	2.540	147.77±0.12	-1.968	420.1±1.6
0.01314	0.756	147.85±0.39	-0.503	447.4±5.3
0.01652	0.949	147.91±0.31	-0.598	456.4±4.3
0.02933	1.686	147.77±0.18	-1.140	444.1±2.4
0.03280	1.881	147.88±0.16	-1.259	446.6±2.1
0.008285	0.475	148.14±0.62	-0.322	446.4±8.5
0.01107	0.635	148.10±0.47	-0.455	436.7±6.3
0.01549	0.889	148.00±0.33	-0.596	447.0±4.5
0.02284	1.316	147.70±0.23	-0.926	436.9±3.1
0.02915	1.676	147.75±0.18	-1.160	440.1±2.4
0.03427	1.969	147.77±0.15	-1.328	444.6±2.1
0.03898	2.245	147.59±0.13	-1.506	444.2±1.8
0.04475	2.566	147.79±0.12	-1.829	435.3±1.6

of previous authors (Jolicoeur *et al.*, 1986; Kikuchi *et al.*, 1995) partial molar properties at infinite dilution for these systems were estimated by averaging the apparent molar properties. Heat capacity ratios for L-tyrosine could not be determined at 313.15 and 328.15 K and heat capacity ratios for L-dopa could not be determined at 328.15 K, because of low signal to noise ratios, caused by their extremely low solubilities in water. Where heat capacity ratios for L-tyrosine and L-dopa have been reported, oversized data sets were used to increase our confidence in the average limiting properties. These estimated partial molar properties at infinite dilution are also shown in table 6.6 together with calculated standard deviations.

Data reported in table 6.6 consistently show the absence of previously published experimental thermodynamic properties for amino acids beyond ambient temperature. With the exceptions of the studies conducted by Kikuchi *et al.* (1995) and Kharakoz (1989), $\bar{V}_2^0$ values for these systems could not be located in the literature for temperatures removed from 298.15 K.

Table 6.4. Relative densities, apparent molar volumes, heat capacity ratios, and apparent molar heat capacities of aqueous L-histidine at 288.15, 298.15, 313.15, and 328.15 K.

m (mol kg^{-1})	$(\rho - \rho_O)$ (kg m^{-3})	$V_{2,\phi}$ (cm^3 mol^{-1})	$10^3\left(\frac{c_p\rho}{c_p^O\rho_O}-1\right)$	$c_{p2,\phi}$ (J K^{-1} mol^{-1})
		T = 288.15 K		
0.02115	1.218	97.48±0.24	-0.969	213.6±3.3
0.03812	2.188	97.60±0.13	-1.739	314.5±1.8
0.05318	3.041	97.72±0.09	-2.453	212.6±1.3
0.07134	4.068	97.78±0.07	-3.234	215.8±1.0
0.08664	4.932	97.79±0.06	-3.983	212.8±0.8
0.1062	6.031	97.84±0.05	-4.878	212.9±0.7
0.1232	6.981	97.87±0.04	-5.648	213.1±0.6
0.1503	8.184	97.91±0.03	-6.895	212.5±0.5
0.2017	11.307	98.02±0.03	-9.099	215.3±0.4
0.2509	13.989	98.07±0.02	-11.305	214.8±0.3
		T = 298.15 K		
0.02115	1.191	98.86±0.24	-0.902	231.6±3.3
0.03812	2.138	98.99±0.13	-1.672	226.5±1.8
0.05318	2.977	99.01±0.09	-2.228	234.7±1.3
0.07134	3.983	99.07±0.07	-2.969	235.8±1.0
0.08664	4.823	99.15±0.06	-3.640	234.2±0.8
0.1062	5.906	99.11±0.05	-4.416	235.6±0.7
0.1232	6.832	99.17±0.04	-5.106	236.1±0.6
0.1503	8.304	99.20±0.03	-6.190	236.8±0.5
0.2017	11.074	99.28±0.03	-8.232	237.9±0.4
0.2509	13.696	99.34±0.02	-10.159	238.7±0.3
		T = 313.15 K		
0.02115	1.165	100.33±0.24	-0.750	265.9±3.3
0.03812	2.092	100.42±0.13	-1.396	261.1±1.8
0.05318	2.907	100.55±0.10	-1.987	258.3±1.3
0.07134	3.890	100.59±0.07	-2.633	260.1±1.0
0.08664	4.714	100.64±0.06	-3.248	257.6±0.8
0.1062	5.766	100.67±0.05	-3.891	261.1±0.7

Table 6.4 Continued

0.1232	6.677	100.67±0.04	-4.511	260.9±0.6
0.1503	8.111	100.73±0.03	-5.539	259.6±0.5
0.2017	10.827	100.74±0.03	-7.313	261.5±0.4
0.2509	13.383	100.83±0.02	-9.016	262.5±0.3
		T = 328.15 K		
0.02115	1.148	101.44±0.24	-0.696	278.8±3.3
0.03812	2.070	101.32±0.14	-1.300	273.0±1.8
0.05318	2.867	101.63±0.10	-1.806	274.6±1.3
0.07134	3.833	101.72±0.07	-2.501	270.1±1.0
0.08664	4.647	101.73±0.06	-2.937	274.9±0.8
0.1062	5.689	101.71±0.05	-3.657	272.2±0.7
0.1232	6.581	101.78±0.04	-4.173	274.7±0.6
0.1503	8.003	101.77±0.03	-4.979	277.3±0.5
0.2017	10.675	101.83±0.03	-6.619	278.2±0.4
0.2509	13.197	101.91±0.02	-8.346	275.9±0.3

There appears to be no previous volumetric or calorimetric studies of aqueous L-dopa solutions in the literature. This is somewhat surprising, considering the importance of L-dopa to the medical sciences and the recent interest in its equilibrium state during the treatment of Parkinson's disease (Okabe *et al.*, 1991; Rao *et al.*, 1989).

Our reported $\bar{V}_2^0$, for L-phenylalanine at 298.15 K (122.03 ± 0.05 cm^3 mol^{-1}) is in good agreement with Jolicoeur *et al.*'s (1986) value of 121.92 cm^3 mol^{-1} and Mishra and Ahluwalia's (1984) value of 122.2 cm^3 mol^{-1}. Also, it is in reasonable agreement with values reported by Kikuchi *et al.* (1995) and Millero *et al.* (1978). Our $\bar{V}_2^0$ value at 288.15 K (120.58 ± 0.05 cm^3 mol^{-1}) is in good agreement with Kikuchi *et al.*'s (1995) value of 120.43 cm^3 mol^{-1}. Acceptable agreement is observed between our data and those reported by Kharakoz (1989) at all temperatures.

Table 6.5. Relative densities, apparent molar volumes, heat capacity ratios, and apparent molar heat capacities of aqueous L-tyrosine at 288.15, 298.15, 313.15, and 328.15 K.

m (mol kg^{-1})	$(\rho - \rho_O)$ (kg m^{-3})	$V_{2,\phi}$ (cm^3 mol^{-1})	$10^3\left(\frac{c_p\rho}{c_p^o\rho_O}-1\right)$	$c_{p2,\phi}$ (J K^{-1} mol^{-1})
		T = 288.15 K		
0.001458	0.084	123.74±3.44	-0.095	241.8±48.0
0.001782	0.101	124.45±2.81	-0.079	333.0±39.3
0.002094	0.121	123.27±2.39	-0.100	313.1±33.4
0.002455	0.140	124.28±2.04	-0.130	295.2±28.5
0.001458	0.083	124.52±3.44	-0.059	349.3±48.0
0.001782	0.103	123.70±2.81	-0.072	346.7±39.3
0.001782	0.104	123.04±2.81	-0.070	349.5±39.3
0.002094	0.123	122.64±2.39	-0.079	353.1±33.4
0.002094	0.120	123.85±2.39	-0.090	336.2±33.4
0.002094	0.120	123.93±2.39	-0.093	330.6±33.4
0.002455	0.142	123.46±2.04	-0.122	306.2±28.5
0.002455	0.141	123.81±2.04	-0.116	318.7±28.5
0.002455	0.141	123.76±2.04	-0.103	339.8±28.5
0.001458	0.082	124.65±3.43	-0.061	345.8±48.0
0.001458	0.084	123.52±3.44	-0.069	317.6±48.0
0.001782	0.101	124.38±2.81	-0.076	339.2±39.3
0.001782	0.101	124.30±2.81	-0.086	315.1±39.3
0.002094	0.122	123.05±2.39	-0.096	321.0±33.4
0.002094	0.118	124.72±2.39	-0.101	318.0±33.4
0.002455	0.140	124.17±2.04	-0.135	286.9±28.5
0.002455	0.143	123.03±2.04	-0.112	320.8±28.5
0.002376	0.144	120.47±2.11	-0.129	274.5±29.5
0.002376	0.140	122.31±2.11	-0.107	321.7±29.5
0.002376	0.144	120.63±2.11	-0.113	303.0±29.5
0.002376	0.136	124.04±2.11	-0.129	289.3±29.5
0.002440	0.143	122.69±2.05	-0.144	263.3±28.7
0.002440	0.147	120.80±2.05	-0.131	278.8±28.7

Table 6.5 Continued

0.002440	0.149	120.18±2.05	-0.115	302.5±28.7
0.002440	0.141	123.45±2.05	-0.129	292.5±28.7
0.002440	0.146	121.45±2.05	-0.140	266.0±28.7
0.002440	0.145	121.76±2.05	-0.142	263.7±28.7
0.002440	0.143	122.47±2.05	-0.133	281.6±28.7
0.002440	0.144	122.35±2.05	-0.139	270.5±28.7
0.002376	0.143	120.88±2.11	-0.115	300.4±29.5
0.002376	0.139	122.76±2.11	-0.091	352.1±29.5
0.002376	0.140	122.25±2.11	-0.117	302.2±29.5
0.002376	0.139	122.84±2.11	-0.117	304.9±29.5
0.002434	0.142	122.69±2.06	-0.124	298.2±28.7
0.002434	0.141	123.28±2.06	-0.119	309.5±28.7
0.002434	0.142	122.85±2.06	-0.112	320.0±28.7
0.002434	0.141	123.31±2.06	-0.116	314.9±28.7
0.002440	0.146	121.38±2.05	-0.138	268.5±28.7
0.002440	0.146	121.50±2.05	-0.143	260.4±28.7
0.002440	0.144	122.39±2.05	-0.132	282.1±28.7
0.002440	0.147	120.95±2.05	-0.130	280.4±28.7
0.002376	0.141	121.74±2.11	-0.120	295.9±29.5
0.002376	0.138	122.97±2.11	-0.117	306.2±29.5
0.002376	0.142	121.57±2.11	-0.116	301.3±29.5
0.002376	0.141	121.99±2.11	-0.118	299.4±29.5
		T = 298.15 K		
0.001458	0.082	125.29±3.45	-0.069	322.5±48.0
0.001782	0.099	125.56±2.82	-0.088	314.0±39.3
0.002094	0.117	125.53±2.40	-0.083	354.8±33.4
0.002455	0.135	126.37±2.05	-0.129	304.6±28.5
0.001458	0.081	126.01±3.45	-0.050	381.5±48.0
0.001458	0.081	125.64±3.45	-0.063	342.0±48.0
0.001458	0.082	124.94±3.45	-0.073	310.1±48.0
0.001782	0.100	125.51±2.82	-0.067	364.9±39.3
0.001782	0.100	125.13±2.82	-0.078	336.5±39.3
0.002094	0.119	124.56±2.40	-0.067	383.3±33.4
0.002094	0.119	124.65±2.40	-0.073	371.4±33.4
0.002094	0.116	126.16±2.40	-0.086	352.1±33.4

Table 6.5 Continued

0.002455	0.137	125.80±2.05	-0.128	303.1±28.5
0.002455	0.138	125.00±2.05	-0.121	312.7±28.5
0.001458	0.081	125.99±3.45	-0.069	324.4±48.0
0.001458	0.082	124.97±3.45	-0.051	372.2±48.0
0.001458	0.082	125.15±3.45	-0.055	363.3±48.0
0.001782	0.100	125.19±2.82	-0.081	330.6±39.3
0.001782	0.101	124.75±2.82	-0.077	338.1±39.3
0.001782	0.100	125.23±2.82	-0.063	372.4±39.3
0.002094	0.117	125.31±2.40	-0.087	346.9±33.4
0.002094	0.116	125.92±2.40	-0.075	372.9±33.4
0.002455	0.139	124.65±2.05	-0.094	358.1±28.5
0.002455	0.138	125.27±2.05	-0.117	319.9±25.5
0.002455	0.137	125.51±2.05	-0.117	322.6±28.5
0.002434	0.139	124.39±2.07	-0.119	311.0±28.8
0.002434	0.138	124.52±2.07	-0.098	348.2±28.8
0.002434	0.136	125.37±2.07	-0.112	328.6±28.8
0.002434	0.137	125.18±2.07	-0.100	347.8±28.8
0.002434	0.138	124.66±2.07	-0.096	352.2±28.8
0.002376	0.136	123.99±2.12	-0.099	340.2±29.5
0.002376	0.135	124.63±2.12	-0.110	323.2±29.5
0.002376	0.136	124.16±2.12	-0.102	335.7±29.5
0.002376	0.132	125.86±2.12	-0.108	332.3±29.5
0.002376	0.135	124.56±2.12	-0.097	347.5±29.5
0.002440	0.139	124.42±2.06	-0.120	311.1±28.7
0.002440	0.139	124.41±2.06	-0.139	277.0±28.7
0.002440	0.139	124.36±2.06	-0.124	303.1±28.7
0.002376	0.135	124.39±2.12	-0.119	306.3±29.5
0.002376	0.136	124.16±2.12	-0.111	320.7±29.5
0.002376	0.136	124.28±2.12	-0.112	319.2±29.5
0.002376	0.134	124.79±2.12	-0.116	314.4±29.5
0.002434	0.138	124.77±2.07	-0.111	327.3±28.8
0.002434	0.137	125.11±2.07	-0.101	346.8±28.8
0.002434	0.138	124.79±2.07	-0.105	337.7±28.8
0.002434	0.138	124.65±2.07	-0.097	351.5±28.8
0.002434	0.137	125.02±2.07	-0.123	308.2±28.8

Table 6.5 Continued

0.002434	0.139	124.31±2.07	-0.106	334.0±28.8
		T = 313.15 K		
0.001458	0.080	126.52±3.48	----	----
0.001458	0.080	126.63±3.48	----	----
0.001458	0.081	127.74±3.48	----	----
0.001782	0.096	128.06±2.85	----	----
0.001782	0.097	127.53±2.85	----	----
0.001782	0.095	128.60±2.85	----	----
0.002094	0.114	127.33±2.43	----	----
0.002094	0.112	128.23±2.43	----	----
0.002455	0.136	126.44±2.07	----	----
0.002455	0.136	126.43±2.07	----	----
0.002455	0.134	127.08±2.07	----	----
		T = 328.15 K		
0.001458	0.080	127.413.53	----	----
0.001458	0.080	127.233.53	----	----
0.001458	0.078	128.803.53	----	----
0.001782	0.093	130.012.89	----	----
0.001782	0.097	128.002.89	----	----
0.001782	0.097	127.802.89	----	----
0.002094	0.112	128.682.46	----	----
0.002094	0.115	127.522.46	----	----
0.002094	0.113	128.462.46	----	----
0.002455	0.131	128.832.10	----	----
0.002455	0.129	129.742.10	----	----
0.002455	0.129	129.702.10	----	----

With respect to L-tryptophan Kikuchi *et al.*'s (1995) values for $\bar{V}_2^o$ at 288.15 and 298.15 K are found to be slightly lower than our reported values. Both Jolicoeur *et al.* (1986) and Iqbal and Verrall (1989) have reported values which are slightly higher at 298.15 K, however, we note that Kharakoz's (1989) and Mishra and Ahluwalia's (1984)

Table 6.6. Partial molar volumes and heat capacities at infinite dilution, of L-dopa, L-phenylalanine, L-tryptophan, L-histidine, and L-tyrosine.

Temperature (K)	V_2^o (cm^3 mol^{-1})	S_V (cm^3 kg mol^{-2})	c_{p2}^o (J K^{-1} mol^{-1})	S_{Cp} (J kg K^{-1} mol^{-2})
		L-dopa		
288.15	124.10 ± 0.85	**	314.9 ± 11.3	**
298.15	126.35 ± 0.56	**	338.1 ± 9.1	**
313.15	126.34 ± 0.45	**	362.9 ± 21.3	**
328.15	128.71 ± 0.94	**		
		L-phenylalanine		
288.15	120.58 ± 0.05 [120.43[d], 120.3[e]]	1.06 ± 0.54	379.0 ± 0.8	-2.4 ± 7.7
298.15	122.03 ± 0.05 [121.50[d], 121.92[c], 121.48[a], 121.7[e], 122.2[f]]	0.33 ± 0.54	392.8 ± 0.8 [384[c]]	-16.3 ± 7.7
313.15	123.55 ± 0.14 [123.5[e]]	1.86 ± 1.26	401.6 ± 1.2	2.2 ± 10.7
328.15	125.49 ± 0.08 [124.9[e]]	-0.14 ± 0.78	428.3 ± 1.1	-169.7 ± 10.8
		L-tryptophan		
288.15	141.99 ± 0.12 [141.38[d], 141.6[e]]	2.39 ± 3.32	398.2 ± 3.1	-149.4 ± 88.8
298.15	143.78 ± 0.07 [143.38[d], 144.24[b], 144.0[c], 143.7[e], 143.7[f]]	-0.16 ± 1.99	407.3 ± 2.3 [420[c]]	-12.3 ± 66.3
313.15	146.23 ± 0.08 [145.6[e]]	-8.54 ± 2.28	431.5 ± 6.4	-167.0 ± 184.3
328.15	147.90 ± 0.09 [147.8[e]]	-3.82 ± 2.58	457.3 ± 8.2	-559.6 ± 223.9

Table 6.6 Continued

		L-histidine		
288.15	97.65 ± 0.02 [97.3e]	1.73 ± 0.12	212.2 ± 1.0	11.0 ± 4.9
298.15	98.98 ± 0.02 [99.14[c], 98.79[a] 98.8[e], 98.3[f]]	1.45 ± 0.09	232.9 ± 0.9 [241[c]]	23.9 ± 4.4
313.15	100.51 ± 0.03 [100.4[e]]	1.27 ± 0.13	258.1 ± 0.9	16.8 ± 4.7
328.15	101.58 ± 0.04 [101.6[e]]	1.32 ± 0.20	273.2 ± 1.9	15.2 ± 9.6
		L-tyrosine		
288.15	122.82 ± 1.20 [120.92[d]]	**	305.7 ± 27.2	**
298.15	125.02 ± 0.58 [124.33[d], 123[c] 124.3[f]]	**	335.4 ± 23.6 [299[c]]	**
313.15	127.33 ± 0.74	**		
328.15	128.52 ± 0.91	**		

** Apparent molar properties have been averaged to estimate the partial molar property at infinite dilution (uncertainties are standard deviations), [a](Millero *et al.*, 1978), [b](Iqbal & Verall, 1989), [c](Jolicoeur *et al.*, 1986), [d](Kikuchi *et al.*, 1995), [e](Kharakoz, 1989), [f](Mishra & Ahluwalia, 1984).

value of $\bar{V}_2^o$ = 143.7 cm^3 mol^{-1} are in excellent agreement with the value reported in the current study. It may be possible to attribute the small differences observed between our reported $\bar{V}_2^o$ data and several of those reported in the literature to differences in chemical purity or alternatively to the low solubility of L-tryptophan in water and hence to the signal to noise ratios of the various vibrating tube densimeters utilised in the reported investigations. As indicated by equation 3.12 uncertainties in apparent molar volumes increase as concentrations decrease. The agreement between our partial molar volumes at

infinite dilution and the volumes reported by Kharakoz (1989) is reasonable at all other temperatures investigated with the exception of 313.15 K where the disagreement is greater than the sum of the combined uncertainties. We are unable to explain this disagreement.

Our $\bar{V}_2^0$ value for aqueous L-histidine at 298.15 K (98.98 ± 0.02 cm^3 mol^{-1}) is in good agreement with the values of 99.14 cm^3 mol^{-1}, 98.79 cm^3 mol^{-1} and 98.8 cm^3 mol^{-1} reported by Jolicoeur *et al.* (1986), Millero *et al.* (1978) and Kharakoz (1989) respectively. However, we note that Mishra and Ahluwalia's (1984) value of $\bar{V}_2^0 = 98.3$ cm^3 mol^{-1} appears a little low when compared to these other values. Good agreement is observed between our data and those reported by Kharakoz (1989) at all of the other temperatures investigated in this study.

Given the extremely low solubility of L-tyrosine in water and the magnitude of the reported uncertainties in the partial molar volumes at infinite dilution, we observe acceptable agreement with all previously published values (Jolicoeur *et al.*, 1986; Kikuchi *et al.*, 1995; Mishra & Ahluwalia, 1984).

Literature values for partial molar heat capacities at infinite dilution could only be found at one temperature; 298.15 K. These are the data reported by Jolicoeur *et al.* (1986), in their comprehensive study of amino acids. Unfortunately, our data does not agree well with this work (Jolicoeur *et al.*, 1986). However, as indicated previously, the species investigated herein approach the limits of our measurement capabilities, where signal to noise ratios decrease dramatically and discrepancies can be expected. With the lack of reported $\bar{C}p_2^0$, in the literature it is difficult to attribute these discrepancies to any other cause. Even at the temperature of the human body, 310 K, reliable calorimetric data for aqueous solutions of biomolecules are scarce.

6.4 Discussion

The revised HKF equations of state (equations 2.54 to 2.58) have been discussed previously in Subsection 2.3.3 as a method of estimating molar entropies, enthalpies of

formation, Gibbs energies of formation, molar volumes, compressibilities, and molar heat capacities at infinite dilution. The equations use only seven adjustable solute dependent parameters; c_1, c_2, a_1, a_2, a_3, a_4, and an effective Born coefficient, ω_e (Shock & Helgeson, 1990). There are also two solvent dependent parameters; Ψ, θ, which for water are assigned values of 2600 bar and 228 K respectively.

In its simplest form the revised HKF equation for any partial molar property at infinite dilution may be written as

$$\bar{Y}_2^o = \Delta\bar{Y}_s^o + \Delta\bar{Y}_e^o, \tag{6.2}$$

where subscripts s and e are used to denote the structural and electrostatic contributions to the partial molar property. Structural and electrostatic contributions to partial molar heat capacities at infinite dilution are defined by equations 2.56 and 2.58. Values for the Born functions Q and X have been calculated using Johnson and Norton's (1991), equations for the dielectric constant for water ($Q = 6.49\cdot10^{-7}$, $6.69\cdot10^{-7}$, $7.17\cdot10^{-7}$, and $7.88\cdot10^{-7}$ bar^{-1}; $X = -3.16\cdot10^{-7}$, $-3.14\cdot10^{-7}$, $-3.12\cdot10^{-7}$, and $-3.17\cdot10^{-7}$ K^{-1} at 288.15, 298.15, 313.15, and 328.15 K respectively). A more detailed description of the revised HKF semi-empirical equations of state, containing equations for standard molar entropy, isothermal compressibility, enthalpy of formation, and Gibbs free energy of formation, has been reported by Amend and Helgeson (1997b).

For neutral organic species the effective Born parameter is assumed to be independent of temperature and pressure. Because all data within our model come from measurements made at atmospheric pressure (~0.1 MPa), equations for $\bar{C}p_2^o$ and $\bar{V}_2^o$ may be simplified:

$$\bar{C}p_2^o = c_1 + \frac{c_2}{(T - \theta)^2} + \omega_e T X \tag{6.3}$$

and

$$\bar{V}_2^o = \sigma + \frac{\zeta}{T - \theta} - \omega_e Q, \tag{6.4}$$

where

$$\sigma = a_1 + \frac{a_2}{\Psi + p} \tag{6.5}$$

and

$$\zeta = a_3 + \frac{a_4}{\Psi + p}. \tag{6.6}$$

These simplified equations serve as the basis of our model where the species dependent parameters of c_1, c_2, σ, and ζ can be treated as the sum of quantities for 13 functional groups, which in turn may be used to build the amino acid and peptide molecules utilised in our investigation. Thus, in terms of additivity, equations 6.3 and 6.4 can be expressed as

$$\Delta\bar{C}p^{o}_{2j} = \sum_i c_{1i} + \frac{\sum_i c_{2i}}{(T-\theta)^2} + \omega_{e,j}TX \tag{6.7}$$

and

$$\Delta\bar{V}^{o}_{2j} = \sum_i \sigma_i + \frac{\sum_i \zeta_i}{T-\theta} - \omega_{e,j}Q, \tag{6.8}$$

where i denotes any of the thirteen functional groups contained within a given molecule, j. These functional groups are found in table 6.7.

Following the procedure described in our previous functional group additivity schemes (Hakin *et al.*, 1994b, 1995), we have made two simplifying assumptions to increase the number of degrees of freedom in our analyses:

$$B_{CH3} = 1.5\ B_{CH2} \tag{6.9}$$

and

$$B_H = 0.5\ B_{CH2}, \tag{6.10}$$

where B denotes any of the additive parameters, c_1, c_2, σ, or ζ within the species of interest.

All amino acids contained within our data set were of the L stereo isomer form, except for methionine (Hakin *et al.*, 1997) for which the racemic mixture was used. All species were treated as zwitter ions; therefore, in our additivity scheme we define the amino

acid group as $(NH_3^+)CH(COO^-)$. To utilise this grouping for the peptide molecules included in our analyses it was necessary to artificially combine the terminal ends of the peptide molecule into one unit. While we still consider only one amino acid group in any peptide, we recognise that we have significantly altered the polarization of the molecule by this manipulation. To address this point, we treat the effective Born coefficients, which help to describe solvation effects, as non-additive parameters in our analyses. However, these coefficients remain variables, so that the fit of our model to the input volumetric and thermochemical data may be optimised.

Partial molar heat capacities at infinite dilution are more sensitive to the structures of solvated molecules than partial molar volumes at infinite dilution. Therefore, we have attempted to obtain optimised Born coefficients for each investigated solute using equation 6.7 instead of equation 6.8. As a first approximation, effective Born coefficients were estimated using the empirical correlation equation reported by Shock and Helgeson (1990). The combination of these Born coefficients and the experimental infinite dilution properties allows for functional group matrices to be fit to equations 6.7 and 6.8. This procedure yields first estimates of the functional group contributions to c_1, c_2, σ, and ζ parameters. New estimates for the effective Born coefficients were obtained using equation 6.8 and the newly calculated c_1 and c_2 parameters for each species at each temperature. Because the effective Born coefficients are assumed to be independent of temperature and pressure, a weighted average of the new Born coefficients was calculated, to produce a temperature independent coefficient for each species. Weights were determined as the reciprocals of the uncertainties in the reported partial molar heat capacities at infinite dilution. Following the procedure described above, in an iterative fashion, optimized group contributions to c_1, c_2, σ, and ζ and optimised ω_e values for each species were obtained. Group contributions for parameters c_1, c_2, σ, and ζ are reported in table 6.7 and optimized Born coefficients are reported in table 6.8.

Calculated residuals, $\bar{C}p^{\circ}_2(obs) - \bar{C}p^{\circ}_2(calc)$ and $\bar{V}^{\circ}_2(obs) - \bar{V}^{\circ}_2(calc)$, of our fitted

model are shown in Figures 6.1 and 6.2. Ninety five per cent confidence limits are shown at ± 9.4 J K^{-1} mol^{-1} for partial molar heat capacities at infinite dilution and ± 2.35 cm^3 mol^{-1} for partial molar volumes at infinite dilution.

Other authors (Amend & Helgeson, 1997a,b; Shock, 1992; Shock & Helgeson, 1990) have used either empirical correlation methods or additivity approaches to predict the c_1, c_2, σ, and ζ of the HKF equations. However, because of the manner in which we have handled the calculation of our effective Born coefficients, it is difficult to compare our values with those available in the literature. Amend and Helgeson (1997b) have predicted some group contributions to structural parameters which are common to our grouping scheme. In spite of the expected discrepancies, Amend and Helgeson's (1997b) predicted temperature dependence of the structural contributions to heat capacities and volumes for

Table 6.7. Functional group contributions to isobaric HKF parameters at 0.1 MPa.

Functional Group	σ (cm^3 mol^{-1})	ζ (cm^3 K mol^{-1})	c_1 (J K^{-1} mol^{-1})	10^{-5} c_2 (J K mol^{-1})
$CH(NH_3^+)COO^-$	38.81	-208.75	69.12	-2.908
CH_2	16.29	-53.91	72.19	0.2033
OH	9.78	-60.57	33.56	-0.8734
COOH	25.62	-295.03	43.08	-1.668
Phenyl	77.08	-493.03	275.08	0.2947
OH (phenyl)	1.03	55.84	-15.73	-0.5464
CH	7.14	-1.88	39.70	0.6475
$CONH_2$	28.58	-271.13	58.58	-2.344
CONH	19.19	-156.04	28.19	-2.383
S	17.21	-256.98	-5.74	0.2293
$NH_2C(NH)_2$	42.99	-211.87	76.32	-2.662
Imidazole	49.75	-276.14	135.45	-0.5821
Indole	101.15	-624.97	334.41	-0.5118

Figure. 6.1 Calculated residuals for partial molar volumes at infinite dilution, $\bar{V}_2^o$(obs)-$\bar{V}_2^o$(calc), for species used as input to our analyses.

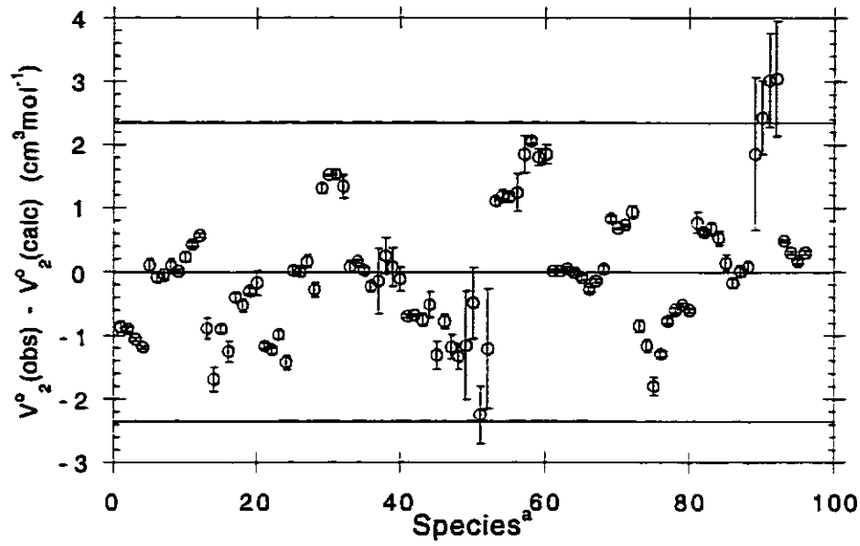

[a]Each species is shown in the order presented in table 6.8 at 288.15, 298.15, 313.15, and 328.15 K. Error bars represent the calculated experimental error on each data point.

Figure. 6.2 Calculated residuals for partial molar heat capacities at infinite dilution, $\bar{C}p_2^o$(obs)-$\bar{C}p_2^o$(calc) for species used as input to our analysis.

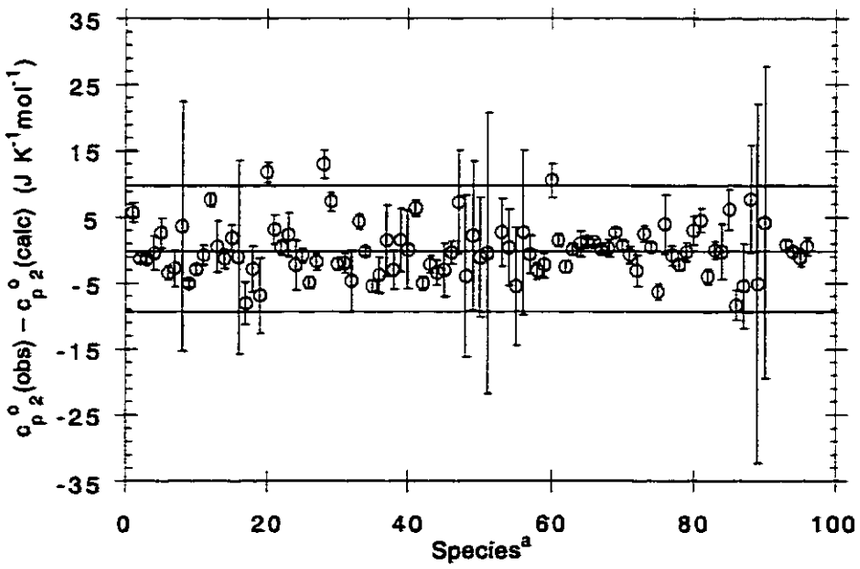

[a]Each species is shown in the order presented in table 6.8 at 288.15, 298.15, 313.15, and 328.15 K. Error bars represent the calculated experimental error on each data point.

the carboxyl (COOH) and the amide ($CONH_2$) groups are in modest agreement with those predicted by our model. These trends are illustrated in Figures 6.3 and 6.4.

Calculated and experimental $\bar{C}p_2^o$ and $\bar{V}_2^o$ values are shown in Figures 6.5 to 6.8 for the species measured in this study. These figures also show the predictions made by the model of Shock and Helgeson (1990) and that of Amend and Helgeson (1997a).

For histidine in water our experimental and calculated data are in reasonable agreement with Amend and Helgeson's model (1997a).

Figure. 6.3 Temperature dependence of the structural contribution to partial molar heat capacities at infinite dilution, $\bar{C}p_{2,s}^o$, of the COOH and $CONH_2$ functional groups at 0.1 MPa.

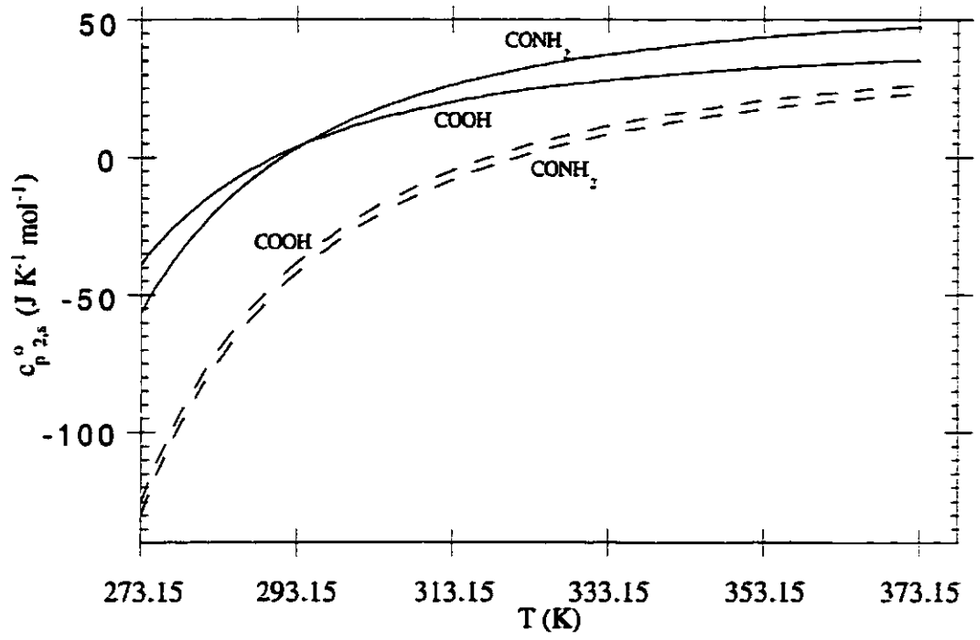

- - - (Amend & Helgeson, 1997a) —— this study.

Figure. 6.4 Temperature dependence of the structural contribution to partial molar volumes at infinite dilution, $\bar{V}^{o}_{2,s}$, of the COOH and $CONH_2$ functional groups at 0.1 MPa.

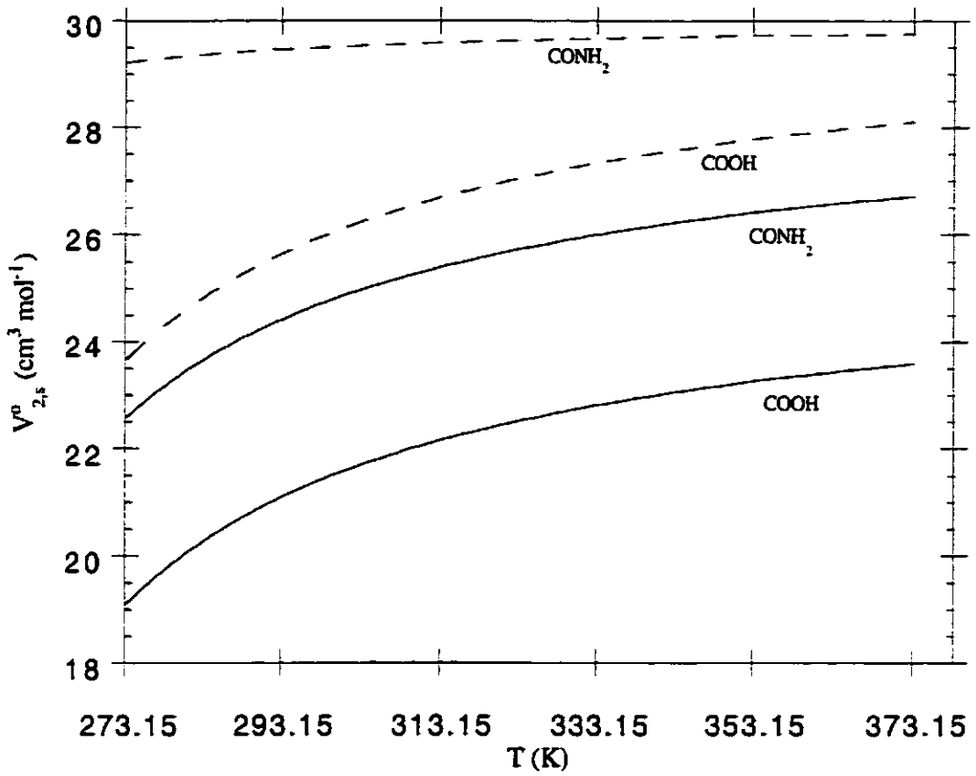

- - - (Amend & Helgeson, 1997a), —— this study.

There are no previous HKF parameters for aqueous L-dopa located within the literature.

For the remaining aromatic amino acids (L-phenylalanine, L-tryptophan, and L-tyrosine) our modelled temperature trends for partial molar heat capacities at infinite dilution agree with the general trends predicted by Amend and Helgeson (1997a), yet there are offsets at higher temperatures. The trends predicted by Shock and Helgeson (1990) do not follow our experimental data. All models agree with experimental values at, or near, 298.15 K for almost every species. Given the way in which the input data sets to the various models have been constructed, this is not surprising.

Figure. 6.5 Experimental and calculated standard partial molar volumes at infinite dilution, $\bar{V}_2^o$, of L-phenylalanine and its derivatives from 273.15 to 373.15 K at 0.1 MPa.

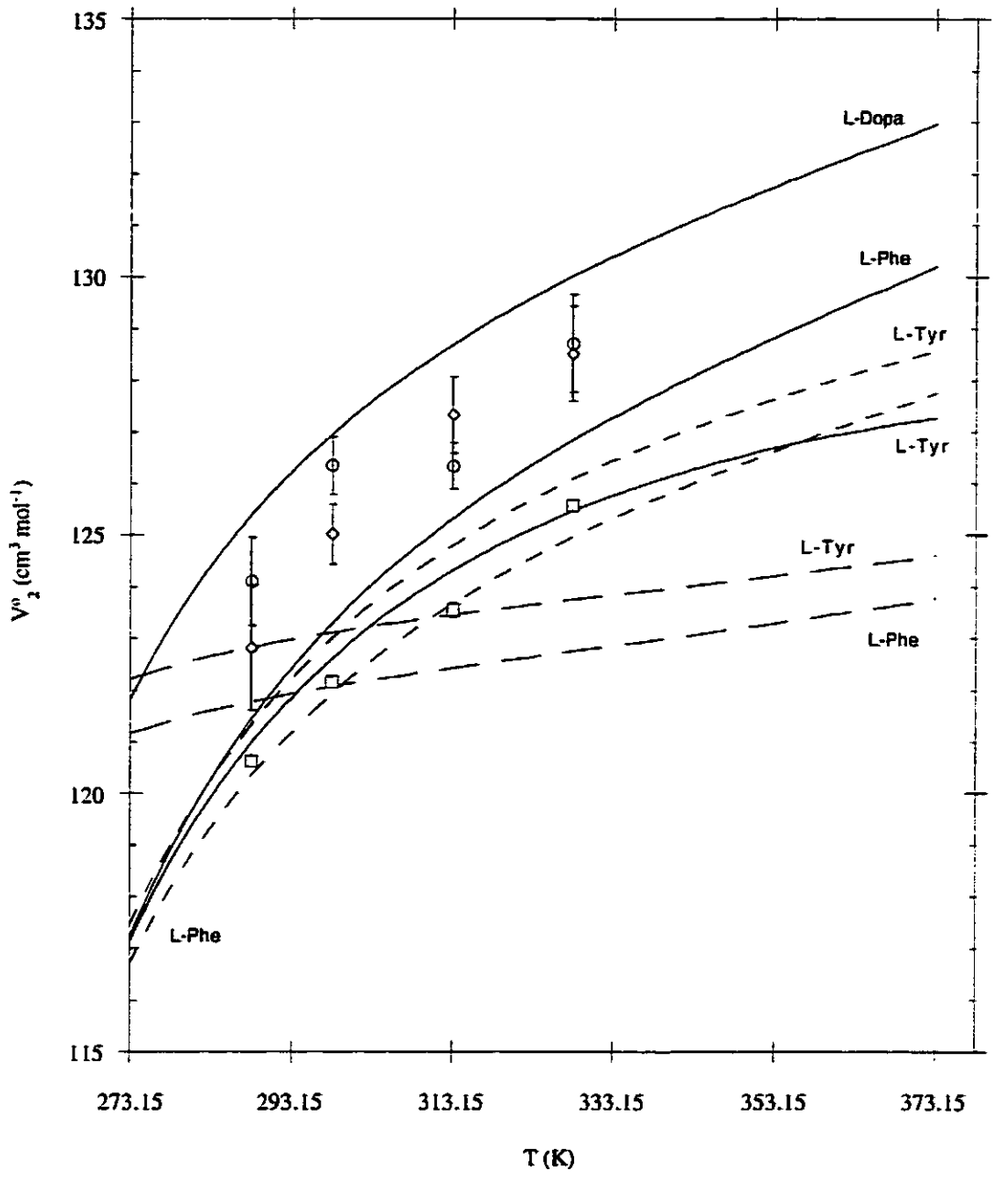

- - - (Amend & Helgeson, 1997a), ——— (Shock & Helgeson, 1990), —— this study, o L-dopa, ◇ L-tyrosine, □ L-phenylalanine.

Figure. 6.6 Partial molar volumes at infinite dilution, $\bar{V}_2^o$, of L-tryptophan (o experimental data) and L-histidine (● experimental data) over the temperature range 273.15 to 373.15 K at 0.1 MPa.

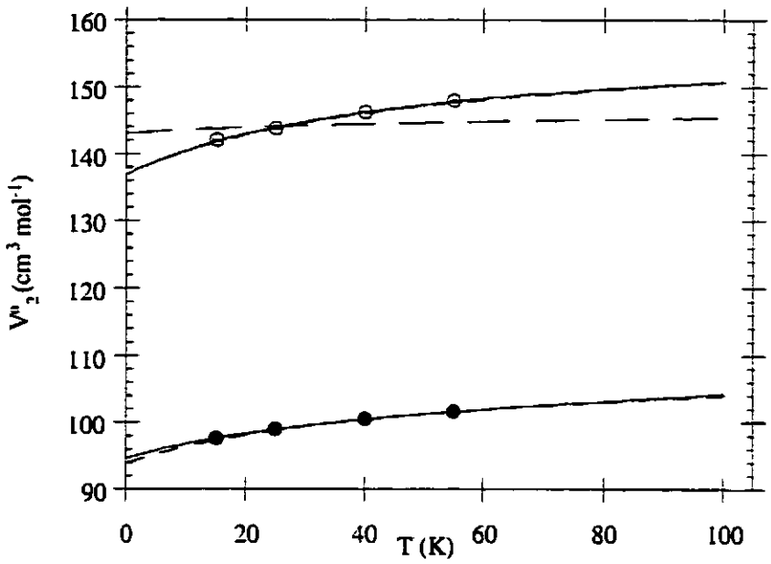

- - - (Amend & Helgeson, 1997a), ——— (Shock & Helgeson, 1990), —— this study.

Amend and Helgeson's (1997a) predicted trends for partial molar volumes at infinite dilution as a function of temperature are in good agreement with our model and our experimental data over the investigated temperature range. As shown in table 6.6, $\bar{V}_2^o$ values obtained over reasonable temperature ranges, are more commonly available in the literature than $\bar{C}p_2^o$ values. Shock and Helgeson's model (1990) is in reasonable agreement with the other models considering the limited volumetric data available for amino acid systems when the model was developed.

Several of the effective Born coefficients predicted by our model, reported in table 6.8, deviate significantly from those predicted by the empirical correlation predictions of Shock and Helgeson (1990). We have attempted to find correlations between our optimised effective Born coefficients and several possible thermodynamic indicators.

Figure. 6.7 Experimental and calculated partial molar heat capacities at infinite dilution, $\bar{C}p_2^o$, of L-phenylalanine and its derivatives from 273.15 to 373.15 K at 0.1 MPa.

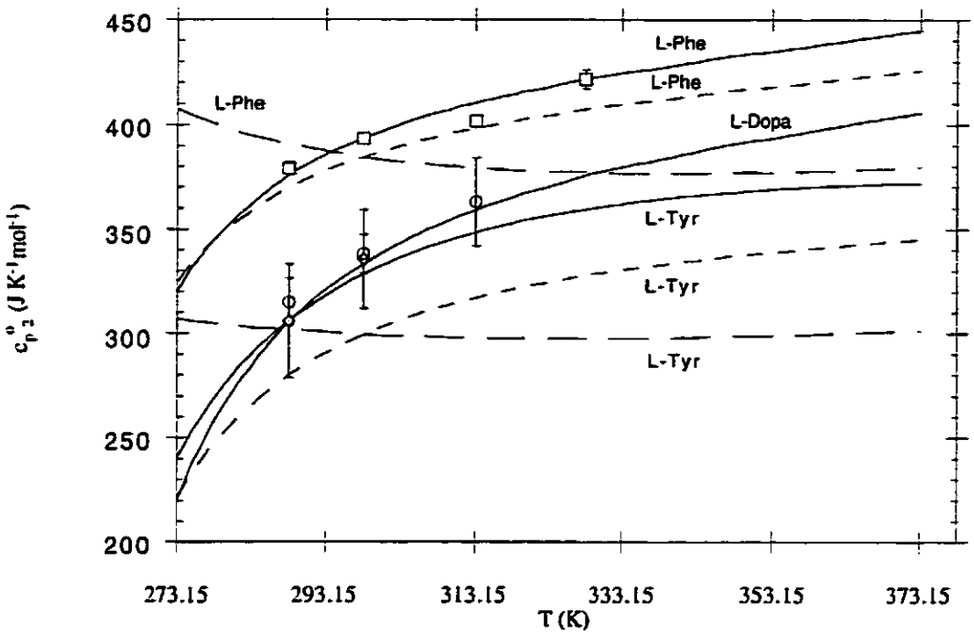

- - - (Amend & Helgeson, 1997a), ———(Shock & Helgeson, 1990), —— this study, o L-dopa, ◇ L-tyrosine, □ L-phenylalanine.

However, no empirical correlations affording good statistical confidence could be found. Since effective Born coefficients contribute more at higher temperatures (>398.15 K) it may be possible to find correlations when more high temperature and pressure data exists.

Most of our optimised effective Born coefficients are of the same sign and magnitude as those previously reported in the literature (Shock & Helgeson, 1990; Amend & Helgeson, 1997a), with the exception of values for glycine and L-tyrosine in which we observe a change in sign. With respect to L-tyrosine this observation may be the result of our inability to obtain high precision thermochemical data at temperatures greater than

Figure. 6.8 Partial molar heat capacities at infinite dilution, $\bar{C}p_2^o$, of L-tryptophan (o experimental data) and L-histidine (● experimental data) over the temperature range 273.15 to 373.15 K at 0.1 MPa.

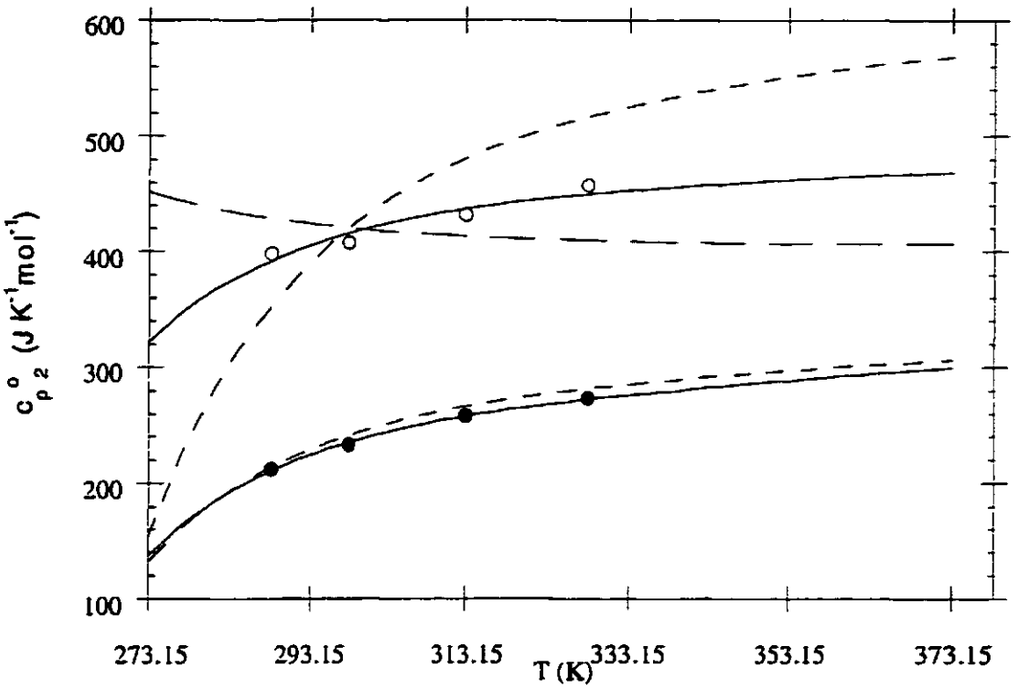

- - - (Amend & Helgeson, 1997a), — — — (Shock & Helgeson, 1990), —— this study.

298.15 K. Reasons for this were discussed previously. The same reasoning cannot be used to explain the positive optimised Born coefficient obtained for glycine.

In spite of what appear to be good quality input volumetric and thermochemical data sets, we have always found the modeling of $\bar{C}p_2^o$ and $\bar{V}_2^o$ data for glycine to be problematic (Hakin *et al.*, 1994b, 1995). In attempting to probe this problem in more detail we have completed a densimetric investigation of aqueous glycine at elevated temperature and pressures (Hakin *et al.*, 1998) (up to 473.15 K and 30 MPa). Included within the results of this study, is a fit of the appropriate form of the revised HKF equation (equations 2.55 and 2.57) to the reported partial molar volumes at infinite dilution. The effective Born

coefficient obtained from this fit was also found to be positive. This observation appears to explain the difficulties we experienced with predicting effective Born coefficients using data below 398.15 K and over a relatively narrow temperature range, 288.15-313.15 K. It appears that to extend predictive abilities of HKF equations, more high temperature and pressure volumetric and calorimetric studies must be performed on several aqueous amino acid and peptide systems.

The question now becomes, is it possible to extend this additivity model beyond the temperature (288.15 - 328.15 K) and pressure (0.1 MPa) limits of our input data set? To answer this question we must be able to estimate the HKF parameters which define the response to applied pressure; namely the a_2 and a_4 parameters of equations 6.5 and 6.6. Amend and Helgeson (1997a) have reported empirical correlation equations for the calculation of these parameters. Once the a_2 and a_4 parameters have been obtained it is possible to calculate values for the a_1 and a_3 parameters from our calculated σ and ζ terms. All of our calculated HKF parameters for the amino acids and peptides utilized within this additivity analysis are reported in table 6.8. Coefficients reported in table 6.8 may be used to estimate the temperature and pressure dependance of any Gibbs energy change; however, our uncertainty in these coefficients indicated the requirement for more conclusive studies, before these coefficients may be used for estimating higher derivative properties, such as partial molar volumes and heat capacities.

In conclusion, we have constructed an additivity model based on the revised HKF equations of state that have enabled us to predict, with confidence, the volumetric and thermochemical properties of many biologically important molecules in aqueous solution over a limited temperature range (288.15 - 328.15 K) at 0.1 MPa.

Although the theory behind HKF equations may not be directly related to aqueous neutral organic species, our study shows that HKF equations are useful as empirical equations for modeling partial molar thermodynamic properties at infinite dilution. The

Table 6.8. HKF parameters for investigated aqueous solutions of amino acids and peptides.

Species	a_1	a_2	a_3	$10^{-5}a_4$	σ	ζ	c_1	$10^{-5}c_2$	$10^{-5}\omega_e$
α-ABA	7.701	653.8	36.244	-1.8388	79.53	-344.51	249.58	-2.4018	-2.6786
DL-Met	10.539	1987.1	41.039	-2.7721	113.03	-655.40	316.03	-1.9692	-2.4121
Gly	5.000	-794.0	8.060	-0.8253	46.95	-236.70	105.21	-2.8084	0.8196
Gly-L-Asn	11.076	2181.5	37.337	-2.9082	119.15	-744.73	300.26	-7.2235	-4.0282
Gly-L-Leu	13.298	3535.1	84.518	-3.8557	146.57	-637.19	497.94	-3.6262	-4.0829
Gly-L-Val	11.970	2752.1	68.838	-3.3076	130.28	-583.29	425.75	-3.8294	-2.2610
Glygly	7.978	688.8	26.973	-1.8633	82.42	-446.64	205.58	-4.9851	-0.3521
Glyglygly	10.908	2294.7	49.196	-2.9874	117.90	-656.59	305.96	-7.1618	-2.9964
L-Ala	6.332	-21.4	23.463	-1.3661	63.24	-290.60	177.40	-2.6051	-1.8119
L-Arg	11.976	2836.1	71.092	-3.3664	130.66	-583.34	362.00	-4.9602	-2.2759
L-Asn	8.080	749.0	19.778	-1.9054	83.68	-534.78	199.88	-5.0467	-3.3816
L-Asp	7.833	621.0	13.945	-1.8158	80.72	-558.68	184.38	-4.3767	-4.1918
L-dopa	12.295	2936.2	68.267	-3.4364	134.24	-638.51	384.93	-3.7918	-2.7342
L-Glu	9.198	1307.0	27.015	-2.2960	97.01	-612.59	256.57	-4.1735	-0.8983
L-Gln	9.428	1479.4	34.045	-2.4167	99.96	-588.69	272.07	-4.8435	-0.4047
L-His	9.828	1707.4	45.073	-2.5763	104.85	-539.79	276.75	-3.2888	-2.7184
L-Ile	10.336	2011.8	64.518	-2.7894	111.10	-427.25	397.56	-1.4494	-1.5459
L-Leu	10.302	2100.3	66.899	-2.8513	111.10	-427.25	397.56	-1.4494	-3.0616
L-Phe	12.164	2742.3	51.332	-3.3007	132.18	-755.69	416.39	-2.4100	-2.8159
L-Ser	6.492	-12.9	20.331	-1.3721	64.88	-324.22	174.86	-3.5802	-1.5105
L-Thr	7.740	716.2	37.069	-1.8825	80.16	-353.05	250.66	-2.8311	-1.7260
L-Trp	14.195	3718.7	64.317	-3.9842	156.24	-888.62	475.71	-3.2185	-0.5704
L-Tyr	12.215	2876.5	60.801	-3.3947	133.21	-697.10	400.66	-3.1009	0.9842
L-Val	8.965	1340.2	51.834	-2.3193	94.81	-373.34	325.38	-1.6527	-1.5166

Units a_1 = J mol^{-1} bar^{-1}, a_2 = J mol^{-1}, a_3 = J K mol^{-1} bar^{-1}, a_4 = J K mol^{-1}, σ = cm^3 mol^{-1}, ζ = cm^3 K mol^{-1}, c_1 = J K^{-1} mol^{-1}, c_2 = J K mol^{-1}, ω_e = J mol^{-1}

present study concludes that HKF theory does indeed produce a model with a great deal of utility. However, the need for experimentally determined thermodynamic data for aqueous solutions of biologically significant species remains paramount. In response to this need we have measured apparent molar volumes for aqueous L-alanine, L-serine, and glycylglycine at elevated temperatures and pressures. Several aspects of these investigations are discussed in Chapter 7.

7) A HIGH TEMPERATURE AND PRESSURE VOLUMETRIC STUDY OF GLYCYLGLYCINE AND L-SERINE.

7.1 Introduction

Gurley *et al.* (1991) have successfully extracted proteins from 150 million year old fossil bones, indicating that some biomolecules may be stable over a wide range of temperature and pressure conditions for extended periods of time. Understanding the behaviour of these proteins and their precursors over this wide range of conditions, could increase our knowledge of the evolution of life and ancient environmental conditions. In addition, Haberstroth and Karl (1989) have discovered free aqueous amino acids within hydrothermal vent habitats of the Guaymas Basin, located in the Gulf of California, also indicating the possible stability of biochemicals under extreme conditions in aqueous environments. Concerning studies and discoveries similar to these, the behaviour of aqueous amino acids and peptides under extreme temperature and pressure conditions has been the focus of several recent investigations (Bada *et al.*, 1995; Hakin *et al.*, 1998, 1999a; Kohara *et al.*, 1997; Marshall, 1994; Simoneit *et al.*, 1998). Indeed many authors suggest that life may have originated in oceanic hydrothermal vents (Amend & Shock, 1998; Corliss *et al.*, 1981; Barloss & Hoffman, 1985). In this capacity, defining aqueous thermodynamic equilibria is paramount to understanding these biological indicators. Experimental investigations of thermodynamic properties for most biochemicals have been confined to temperatures close to 298.15 K and pressures of 0.10 MPa; therefore, there are few data to confirm models which extend over a large temperature and pressure surface (Amend & Helgeson, 1997a; Shock, 1992).

As discussed in the previous chapter, revised HKF theory has been used by many authors to gain insight into aqueous biochemical behaviour beyond the conditions of available data (Amend & Helgeson, 1997a; Amend & Shock, 1998; Shock, 1992). Very few studies dispute the utility of the revised HKF equations of state; however, the validity

of predicted coefficients for amino acids and peptides have been discussed, as these coefficients have been predicted using limited thermodynamic data from only a handful of aqueous organic chemicals (Amend & Helgeson, 1997a; Hakin *et al.*, 1998; Marriott *et al.*, 1998). Although predicted equilibrium constants for several hydrocarbon gas solubility reactions have supported the validity of these equations (Amend & Helgeson, 1997a; Shock & Helgeson, 1990), the assumption that amino acids and small peptides may be modelled by similar profiles may be premature. In addition, many conclusions and predictions have been drawn from investigations using these approximated HKF parameters for amino acids (Amend & Helgeson, 1997a; Amend & Shock, 1998; Shock, 1992; Shock, 1995). These include predicting amino acid dissociation constants at high temperature and pressure (Amend & Helgeson, 1997a) to suggesting the stability of peptides in extreme aqueous conditions (Shock, 1992).

Recently, Hakin *et al.* (1998, 1999a) have measured the volumetric properties of aqueous glycine and L-alanine up to 523 K and 30.00 MPa, where the volumetric temperature and pressure surfaces were found to be similar to those for inorganic electrolytes. Shock and Helgeson (1990) had previously predicted that the volumetric surface of glycine and other amino acids would resemble those of other aqueous neutral species, i.e., a reverse sigmoidal volumetric trend with respect to temperature. Although the volumetric profiles found by Hakin *et al.* (1998, 1999a) resembled other systems which have been modeled by the revised HKF equations of state, they did not resemble the volumetric curves shown by aqueous ethylene, argon, or other neutral species (Biggerstaff *et al.*, 1985; Biggerstaff & Wood, 1988a,b; Shock *et al.*, 1989). Shock *et al.* (1989) have suggested that at higher temperatures volatile neutral molecules cause a repulsion of water dipoles so that the effective Born coefficients are negative. These negative effective Born coefficients for amino acids cause the predicted thermodynamic profiles to resemble those of other volatile aqueous neutral species (Amend & Helgeson, 1997a; Shock, 1992; Shock & Helgeson, 1990). In the case of L-alanine and glycine, experimental data show that the

effective Born coefficients are positive. By the same justification, these species do not seem to disrupt the dipole electrostatic forces within the solvent (Hakin *et al.*, 1998, 1999a; Marriott *et al.*, 1998). Perhaps a simple explanation would be that amino acids exist in their zwitter ionic form and therefore exhibit substantial solute dipoles. Unlike hydrophobic species, i.e., aqueous ethylene and argon, small amino acids may increase solvent structure in water as the critical point is approached. Unfortunately, this behavior may not be assumed for all amino acids, because as the hydrophobicity of the amino acid side chain becomes significant, the volumetric and thermochemical temperature and pressure surfaces may change.

Experimentally, it is difficult to measure the thermodynamic properties of hydrophobic amino acids because of low solubilities. Thus it would seem that not all amino acid profiles may be known in the near future. As data become available, coefficients and methods of predicting coefficients for semi-empirical models must be modified and updated. In response to the limited number of experimental thermodynamic studies of amino acids removed from ambient conditions, we have embarked on a systematic study of their volumetric properties in water under elevated temperature and pressure conditions. Relative densities of aqueous glycine have been measured near 298 K at 0.10, 10.00, 20.00, and 30.00 MPa to extend our previous reported data (Hakin *et al.*, 1994a, 1998). These measurements have permitted an evaluation of the performance of our high temperature and pressure densimeter at temperatures close to ambient. In addition, relative densities of aqueous L-serine and glycylglycine have been measured from 298 to 423 K and at 10.00, 20.00, and 30.00 MPa respectively.

Calculated apparent molar volumes have been combined with previously measured volumetric and partial molar heat capacity data to obtain precise coefficients to the revised HKF equations of state (Tanger & Helgeson, 1988). The temperature and pressure dependence of volumes and heat capacities for these systems have been compared to those predicted in previous studies (Amend & Helgeson, 1997; Shock, 1992; Shock &

Helgeson, 1990; Marriott *et al.*, 1998). New HKF coefficients have also been used to investigate the apparent stability of aqueous glycylglycine and diketopiperazine in an elevated temperature and pressure region.

7.2 Experimental

The high temperature and pressure vibrating tube densimeter is described in detail in Section 3.5 of this thesis. The reference fluid utilised in these investigations was pure water and was obtained from an Osmonics model Aries High-Purity DI loop. Standard solutions of high purity sodium chloride (min. 99.5%), glycine (99%), L-serine (99%), and glycylglycine (99%) were prepared by weight on the molality concentration scale (Sigma® Cat. No. S-7653, G-7203, S-4500, and G-1002 respectively). Sodium chloride was dried at 383 K for over 24 hours before use with no further purification. Glycine, L-serine, and glycylglycine were purified by recrystallisation from ethanol+water and dried at 328 K under a vacuum over phosphorus pentoxide for over 48 hours. Calibration solutions were prepared at an average concentration of 5.3 mol kg^{-1}. All solutions were stored in sealable 100 mL Nalgene bottles. Infrared spectra of the amino acids and peptide were obtained using a Bomem BM100 series IR spectrophotometer. Proton NMR spectra were obtained using a Brüker 250 MHz instrument in which D_2O was used as an internal standard. All spectra were in good agreement with those reported in the literature.

Time period data obtained in the course of density measurements were analysed using the visual user specified baseline method discussed in Chapter 4. The densities of sodium chloride and water were calculated at the mean temperature and pressure of each peak using Archer's (1992) Pitzer Ion Interaction program for sodium chloride and Hill's (1990) equation of state for water. Uncertainties in relative densities were estimated using equation 4.2.

7.3 Results and discussion

Apparent molar volumes have been calculated from relative densities using equation 3.9. Uncertainties in calculated apparent molar volumes, $\delta V_{2,\phi}$, were estimated using equation 3.12 where $\delta\rho=\sigma\Delta\rho$ (equation 4.2). Uncertainties arising from errors in solution preparation, δm, have been considered to be negligible. Relative densities, apparent molar volumes, and uncertainties are reported in tables 7.1 to 7.9.

Equation 6.1 was found to produce a good fit of apparent molar volumes for all species investigated at constant temperature and pressure. The partial molar volume at infinite dilution for aqueous glycine at 298.08±0.80 K and 0.10 MPa (43.18±0.04 cm^3 mol^{-1}) is in good agreement with our previously published value of 43.26 cm^3 mol^{-1} at 298.15 K and 0.10 MPa (Hakin *et al.*, 1994a). This previously published value was obtained using the higher precision Sodev O2D densimeter described in Section 3.3 and has been shown to agree with other investigations within the literature (Cabani *et al.*, 1981; DiPaola & Belleau, 1978; Jolicoeur & Boileau, 1978; Kharakoz, 1989; Millero *et al.*, 1978; Mishra & Ahluwalia, 1984; Wadi & Goyal, 1992). In comparison to our commercial Sodev O2D densimeter, controlling temperature is more problematic for the high temperature and pressure densimeter. However the results of this investigation indicate that the latter instrument is capable of precise density measurements near 298 K.

Through best subset regression analyses of all S_V coefficients obtained for L-alanine (Hakin *et al.*, 1994b, 1999a), glycine (Hakin *et al.*, 1994a, 1998), glycylglycine (Hakin *et al.*, 1995), and L-serine (Hakin *et al.*, 1994a) it was found that equation 7.1 provided a good model of S_V over a wide temperature and pressure range:

$$S_V = a_5pT^2 + a_6T + \frac{a_7}{T} + a_8T^2. \qquad (7.1)$$

Table 7.1 Relative densities and apparent molar volumes of aqueous glycine at 297.61±0.96 K and 0.10, 10, 20, and 30 MPa.

T (K)	m (mol kg^{-1})	ρ_o [(a)] (kg m^{-3})	$\rho - \rho_o$ (kg m^{-3})	$\sigma\Delta\rho$ (kg m^{-3})	$V_{2,\phi}$ (cm^3 mol^{-1})
		p = 0.10 MPa			
297.73	0.5463	997.148	16.805	0.044	43.61±0.08
297.72	0.5463	997.150	16.787	0.044	43.64±0.08
297.71	0.8737	997.153	26.176	0.092	44.00±0.11
297.71	0.8737	997.154	26.264	0.092	43.89±0.11
297.71	1.126	997.154	33.120	0.117	44.22±0.11
297.74	1.126	997.146	33.235	0.117	44.12±0.11
297.78	1.528	997.137	43.841	0.120	44.48±0.08
297.77	1.528	997.137	43.960	0.120	44.40±0.08
298.47	0.2916	996.959	9.104	0.055	43.49±0.19
298.52	0.2916	996.946	9.157	0.055	43.30±0.19
298.52	0.2751	996.946	8.631	0.033	43.35±0.12
298.53	0.2751	996.942	8.602	0.033	43.46±0.12
298.58	0.2336	996.929	7.256	0.097	43.73±0.42
298.59	0.2336	996.927	7.352	0.097	43.31±0.42
		p = 10.00 ± 0.01 MPa			
297.35	2.450	1001.674	65.866	0.239	45.18±0.10
297.33	2.450	1001.679	65.634	0.239	45.28±0.10
297.27	2.159	1001.698	59.013	0.118	45.05±0.06
297.25	2.159	1001.703	59.091	0.118	45.01±0.06
297.24	1.889	1001.703	52.548	0.161	44.86±0.09
297.21	1.889	1001.711	52.617	0.161	44.82±0.09
297.15	1.528	1001.724	43.557	0.050	44.60±0.03
297.16	1.528	1001.723	43.539	0.050	44.61±0.03
297.17	1.126	1001.724	32.809	0.055	44.44±0.05
297.16	1.126	1001.726	32.864	0.055	44.39±0.05
297.14	0.8737	1001.730	25.960	0.047	44.19±0.05
297.11	0.8737	1001.739	26.007	0.047	44.13±0.05
297.08	0.5463	1001.743	16.592	0.038	43.95±0.07
297.07	0.5463	1001.749	16.606	0.038	43.92±0.07
298.02	0.2147	1001.496	6.613	0.179	43.96±0.83

Table 7.1 Continued

297.99	0.2147	1001.504	6.613	0.179	43.12±0.83
		p = 20.00 ± 0.01 MPa			
297.07	2.450	1006.131	65.645	0.344	45.20±0.14
297.07	2.450	1006.128	65.325	0.344	45.33±0.14
297.00	2.159	1006.151	58.336	0.162	45.30±0.08
296.96	2.159	1006.161	58.495	0.162	45.22±0.08
297.03	1.889	1006.141	52.329	0.295	44.91±0.16
297.04	1.889	1006.141	52.037	0.295	45.06±0.16
297.02	1.528	1006.145	43.210	0.091	44.76±0.06
297.02	1.528	1006.146	43.122	0.091	44.82±0.06
297.02	1.126	1006.146	32.627	0.031	44.54±0.03
296.98	1.126	1006.154	32.605	0.031	44.56±0.03
296.99	0.8737	1006.156	25.779	0.448	44.33±0.51
296.99	0.8737	1006.156	25.332	0.448	44.84±0.51
297.00	0.5463	1006.153	16.473	0.095	44.10±0.17
297.02	0.5463	1006.149	16.381	0.095	44.27±0.17
297.03	0.2181	1006.147	6.899	0.289	43.07±1.31
297.01	0.2181	1006.151	6.610	0.289	44.38±1.31
297.88	0.2147	1005.907	6.601	0.016	43.95±0.08
297.89	0.2147	1005.906	6.586	0.016	44.02±0.08
297.86	0.2827	1005.914	8.553	0.131	44.35±0.46
297.84	0.2827	1005.916	8.684	0.131	43.89±0.46
		p = 30.00 ± 0.01 MPa			
298.00	2.450	1010.160	64.835	0.026	45.47±0.01
298.00	2.450	1010.160	64.848	0.026	45.46±0.01
298.02	2.159	1010.153	58.359	0.072	45.22±0.03
298.01	2.159	1010.150	58.305	0.072	45.24±0.03
298.02	1.889	1010.143	51.718	0.116	45.17±0.06
298.02	1.889	1010.163	51.834	0.116	45.10±0.06
297.98	1.528	1010.165	42.768	0.169	44.99±0.11
297.97	1.528	1010.168	42.930	0.169	44.88±0.11
298.01	1.126	1010.161	32.381	0.027	44.69±0.02
298.01	1.126	1010.161	32.403	0.027	44.67±0.02

Table 7.1 Continued

298.02	0.8737	1010.150	25.503	0.024	44.58±0.03
298.01	0.8737	1010.152	25.480	0.024	44.61±0.03
297.99	0.2181	1010.162	6.682	0.015	44.00±0.07
297.96	0.2181	1010.170	6.697	0.015	43.93±0.07
297.95	0.5463	1010.176	16.281	0.106	44.39±0.19
297.94	0.5463	1010.172	16.383	0.106	44.21±0.19
297.89	0.2147	1010.193	6.552	0.051	44.12±0.23
297.88	0.2147	1010.197	6.603	0.051	43.88±0.23
297.84	0.2827	1010.208	8.415	0.354	44.77±1.23
297.83	0.2827	1010.209	8.769	0.354	43.54±1.23

(a) Calculated from Hill's (1990) equation of state for water.

Table 7.2 Relative densities and apparent molar volumes of aqueous L-serine at 298.62±0.55 K and 10, 20, and 30 MPa.

T (K)	m (mol kg^{-1})	ρ_o [(a)] ($kg\ m^{-3}$)	$\rho - \rho_o$ ($kg\ m^{-3}$)	$\sigma\Delta\rho$ ($kg\ m^{-3}$)	$V_{2,\phi}$ ($cm^3\ mol^{-1}$)
		p = 10.01 ± 0.01 MPa			
298.10	2.569	1001.477	90.074	0.329	64.21±0.14
298.09	2.569	1001.479	90.089	0.329	64.20±0.14
298.13	3.088	1001.470	104.158	0.359	64.59±0.13
298.15	3.088	1001.465	104.379	0.359	64.51±0.13
298.15	3.694	1001.462	119.934	0.122	64.80±0.04
298.15	3.694	1001.464	120.051	0.122	64.77±0.04
298.18	2.004	1001.456	73.247	0.142	63.83±0.07
298.19	2.004	1001.454	73.115	0.142	63.90±0.07
298.27	1.656	1001.433	61.999	0.081	63.67±0.05
298.29	1.656	1001.425	62.075	0.081	63.62±0.05
298.23	1.292	1001.417	49.687	0.271	63.44±0.22
298.36	1.292	1001.409	49.651	0.271	63.23±0.22
298.39	0.5991	1001.401	24.539	0.081	62.56±0.14
298.39	0.5991	1001.403	24.619	0.081	62.43±0.14
298.38	0.1752	1001.402	7.394	0.095	62.39±0.54
298.39	0.1752	1001.399	7.488	0.095	61.85±0.54

Table 7.2 Continued

		p = 20.01 ± 0.01 MPa			
298.74	3.694	1005.665	118.862	0.229	65.00±0.07
298.78	3.694	1005.655	119.091	0.229	64.93±0.07
298.83	3.088	1005.641	103.812	0.195	64.59±0.07
298.83	3.088	1005.639	103.706	0.195	64.63±0.07
298.81	2.569	1005.644	89.361	0.211	64.39±0.09
298.82	2.569	1005.646	89.564	0.211	64.31±0.09
298.87	2.004	1005.633	72.706	0.150	64.01±0.08
298.89	2.004	1005.627	72.606	0.150	64.06±0.08
298.92	1.656	1005.616	61.519	0.065	63.86±0.04
298.92	1.656	1005.618	61.570	0.065	63.83±0.04
298.90	1.292	1005.621	49.183	1.370	63.74±1.08
298.91	1.292	1005.622	50.553	1.370	62.66±1.08
298.88	0.5991	1005.628	24.318	0.067	62.84±0.11
298.85	0.5991	1005.635	24.253	0.067	62.95±0.11
298.82	0.1752	1005.645	7.514	0.152	61.63±0.86
298.83	0.1752	1005.643	7.361	0.152	62.49±0.86
		p = 30.00 ± 0.01 MPa			
298.81	3.694	1009.927	118.120	0.253	65.09±0.07
298.79	3.694	1009.933	118.344	0.253	65.02±0.07
298.77	3.088	1009.942	103.457	0.514	64.59±0.18
298.77	3.088	1009.942	103.687	0.514	64.51±0.18
298.77	2.569	1009.936	88.236	1.579	64.73±0.65
297.76	2.569	1009.940	89.729	1.579	64.12±0.65
298.73	2.004	1009.949	72.314	0.077	64.09±0.04
297.73	2.004	1009.947	72.381	0.077	64.06±0.04
297.74	1.656	1009.944	61.083	0.361	64.02±0.22
298.74	1.656	1009.946	61.031	0.361	64.05±0.22
298.75	1.292	1009.941	49.113	0.222	63.69±0.17
298.74	1.292	1009.944	49.064	0.222	63.72±0.17
298.74	0.5991	1009.945	23.960	0.241	63.34±0.40
298.76	0.5991	1009.939	24.194	0.241	62.95±0.40
298.88	0.1752	1009.905	7.164	0.029	63.51±0.16
298.93	0.1752	1009.887	7.144	0.029	63.62±0.16

(a) Calculated from Hill's (1990) equation of state for water.

Table 7.3 Relative densities and apparent molar volumes of aqueous L-serine at 374.50±0.85 K and 10, 20, and 30 MPa.

T (K)	m (mol kg^{-1})	ρ_o [(a)] (kg m^{-3})	$\rho - \rho_o$ (kg m^{-3})	$\sigma\Delta\rho$ (kg m^{-3})	$V_{2,\phi}$ (cm^3 mol^{-1})
		p = 10.00 ± 0.01 MPa			
373.60	3.798	962.637	121.640	0.479	66.25±0.15
373.65	3.798	962.601	121.845	0.479	66.18±0.15
373.73	3.257	962.544	107.955	0.276	66.01±0.10
373.77	3.257	962.518	108.171	0.276	65.93±0.10
373.80	2.670	962.497	91.772	0.351	65.82±0.15
373.81	2.670	962.485	91.790	0.351	65.81±0.15
373.87	2.222	962.442	78.610	0.521	65.64±0.27
373.91	2.222	962.413	79.112	0.521	65.38±0.27
373.98	1.574	962.363	58.554	0.129	65.09±0.09
374.01	1.574	962.348	58.681	0.129	65.00±0.09
374.02	1.142	962.338	43.688	0.128	64.97±0.12
374.02	1.142	962.341	43.815	0.128	64.84±0.12
374.03	0.5694	962.331	22.781	0.028	64.48±0.05
374.05	0.5694	962.313	22.777	0.028	64.49±0.05
374.13	0.1682	962.258	6.849	0.207	64.80±1.33
374.16	0.1682	962.240	7.056	0.207	63.47±1.33
		p = 20.00 ± 0.01 MPa			
374.63	3.792	966.426	119.431	0.647	66.78±0.20
374.66	3.792	966.406	119.905	0.647	66.63±0.20
374.70	3.228	966.372	105.285	0.032	66.57±0.01
374.72	3.228	966.359	105.298	0.032	66.57±0.01
374.78	2.736	966.320	92.453	0.487	66.24±0.20
374.79	2.736	966.312	92.432	0.487	66.25±0.20
374.82	2.224	966.290	77.700	0.074	66.04±0.04
374.83	2.224	966.287	77.636	0.074	66.07±0.04
374.85	1.500	966.273	55.174	0.097	65.63±0.07
374.86	1.500	966.270	55.079	0.097	65.71±0.07
374.90	1.136	966.238	43.265	0.831	65.06±0.80
374.92	1.136	966.226	42.434	0.831	65.86±0.80

Table 7.3 Continued

374.96	0.5705	966.194	22.540	0.135	64.94±0.26
374.97	0.5705	966.185	22.410	0.135	65.19±0.26
375.02	0.1643	966.156	6.658	0.032	64.92±0.21
375.01	0.1643	966.157	6.686	0.032	64.74±0.21
		p = 30.00 ± 0.01 MPa			
374.61	3.792	970.837	119.142	0.312	66.73±0.10
374.64	3.792	970.823	118.835	0.312	66.83±0.10
374.70	3.228	970.778	104.422	0.278	66.75±0.10
374.71	3.228	970.773	104.563	0.278	66.70±0.10
374.76	2.736	970.738	91.067	0.195	66.69±0.08
374.77	2.736	970.729	91.257	0.195	66.61±0.08
374.78	2.224	970.726	76.544	0.265	66.50±0.13
374.77	2.224	970.725	76.646	0.265	66.45±0.13
374.75	1.500	970.740	53.955	0.287	66.41±0.21
374.75	1.500	970.740	54.235	0.287	66.21±0.21
374.78	1.136	970.720	41.962	0.129	66.20±0.12
374.77	1.136	970.727	41.998	0.129	66.17±0.12
374.76	0.5705	970.733	21.767	0.143	66.29±0.27
374.77	0.5705	970.725	21.908	0.143	66.02±0.27
374.79	0.1643	970.716	6.474	0.019	66.01±0.12
374.79	0.1643	970.717	6.457	0.019	66.12±0.12

(a) Calculated from Hill's (1990) equation of state for water.

Table 7.4 Relative densities and apparent molar volumes of aqueous L-serine at 398.29±0.96 K and 10, 20, and 30 MPa.

T (K)	m (mol kg^{-1})	ρ_o [a] (kg m^{-3})	$\rho - \rho_o$ (kg m^{-3})	$\sigma\Delta\rho$ (kg m^{-3})	$V_{2,\phi}$ (cm^3 mol^{-1})
		p = 10.00 ± 0.01 MPa			
398.62	3.798	943.571	122.954	0.406	66.37±0.13
398.65	3.798	943.552	123.313	0.406	66.25±0.13
398.63	3.257	943.568	109.235	0.243	66.05±0.09
398.59	3.257	943.593	109.478	0.243	65.96±0.09
398.64	2.670	943.560	93.152	0.226	65.70±0.10

Table 7.4 Continued

398.69	2.670	943.518	93.360	0.226	65.61±0.10
398.86	2.222	943.375	80.019	0.142	65.38±0.08
398.80	2.222	943.428	80.161	0.142	65.31±0.08
398.79	1.574	943.433	59.553	0.180	64.80±0.13
398.84	1.574	943.396	59.417	0.180	64.90±0.13
399.13	0.5694	943.159	23.255	0.019	63.93±0.04
399.11	0.5694	943.170	23.255	0.019	63.93±0.04
399.17	0.1682	943.128	7.088	0.047	63.59±0.32
399.20	0.1682	943.098	7.042	0.047	63.90±0.32
		p = 20.00 ± 0.01 MPa			
398.12	3.798	948.839	122.236	1.031	66.45±0.33
398.13	3.798	948.828	121.417	1.029	66.71±0.33
398.19	3.257	948.782	108.058	0.227	66.35±0.08
398.17	3.257	948.794	108.256	0.227	66.27±0.08
398.17	2.670	948.798	93.201	0.247	65.54±0.11
398.18	2.670	948.789	93.446	0.247	65.44±0.11
398.14	2.222	948.824	78.656	0.864	65.97±0.45
398.11	2.222	948.840	79.519	0.894	65.51±0.45
398.19	1.574	948.781	58.748	0.578	65.27±0.42
398.26	1.574	948.729	59.316	0.578	64.86±0.42
398.36	1.142	948.642	45.061	0.760	63.91±0.75
398.32	1.142	948.674	44.433	0.760	64.53±0.75
398.14	0.5694	948.822	22.880	0.206	64.57±0.41
398.08	0.5694	948.870	22.754	0.206	64.81±0.41
398.09	0.1682	948.857	7.021	0.137	63.93±0.91
398.15	0.1682	948.812	7.158	0.137	63.03±0.91
		p = 30.00 ± 0.01 MPa			
397.33	3.798	954.164	121.795	1.172	66.43±0.37
397.47	3.798	954.052	120.770	1.695	66.76±0.37
397.25	3.257	954.223	106.448	0.767	66.78±0.28
397.24	3.257	954.232	105.730	0.766	67.05±0.28
397.39	2.670	954.108	91.301	0.436	66.24±0.19
397.47	2.670	954.051	91.539	0.437	66.14±0.19
397.86	2.222	953.752	78.415	0.407	65.96±0.21

Table 7.4 Continued

397.96	2.222	953.669	78.016	0.407	66.17±0.21
398.04	1.574	953.614	58.601	0.676	65.26±0.49
398.08	1.574	953.576	57.926	0.676	65.75±0.49
398.21	1.142	953.478	43.548	0.106	65.30±0.10
398.32	1.142	953.387	43.454	0.106	65.40±0.10
398.53	0.5694	953.221	23.183	0.060	63.88±0.12
398.48	0.5694	953.265	23.172	0.060	63.90±0.12
398.55	0.1682	953.213	7.626	0.495	59.88±3.24
398.58	0.1682	953.187	7.131	0.495	63.13±3.24

(a) Calculated from Hill's (1990) equation of state for water.

Table 7.5 Relative densities and apparent molar volumes of aqueous L-serine at 421.90±2.05 K and 10, 20, and 30 MPa.

T (K)	m (mol kg^{-1})	ρ_o [(a)] (kg m^{-3})	$\rho - \rho_o$ (kg m^{-3})	$\sigma\Delta\rho$ (kg m^{-3})	$V_{2,\phi}$ (cm^3 mol^{-1})
		p = 10.00 ± 0.01 MPa			
420.60	3.873	924.685	126.980	0.823	66.21±0.27
420.61	3.873	924.670	126.843	0.822	66.25±0.27
420.60	3.267	924.680	111.178	0.002	65.93±0.01
420.60	3.267	924.681	111.160	0.002	65.93±0.01
420.61	2.779	924.668	98.205	0.962	65.37±0.43
420.60	2.779	924.676	99.167	0.962	64.95±0.43
420.58	2.232	924.702	81.996	0.146	64.93±0.08
420.59	2.319	924.688	82.125	0.146	64.86±0.08
420.60	1.765	924.677	66.964	0.407	64.60±0.28
420.59	1.765	924.691	66.582	0.407	64.86±0.28
420.55	1.235	924.720	48.600	0.329	64.24±0.32
420.55	1.235	924.723	48.271	0.329	64.56±0.32
420.56	0.9614	924.715	38.762	1.083	63.82±1.34
420.55	0.9614	924.727	37.875	1.075	64.92±1.33
420.56	0.5647	924.712	23.151	0.647	64.10±1.35
420.56	0.5647	924.714	22.603	0.643	65.24±1.34
420.61	0.1825	924.671	7.807	0.037	63.09±1.33

Table 7.5 Continued

420.61	0.1825	924.676	8.010	0.037	61.78±1.33
420.71	0.9614	924.576	38.785	0.128	63.79±0.23
420.70	0.9614	924.591	38.652	0.127	63.96±0.23
420.65	0.5647	924.636	23.664	0.009	63.03±0.10
420.57	0.5647	924.704	23.712	0.009	62.92±0.10
		p = 20.00 ± 0.01 MPa			
422.64	2.232	928.178	81.049	0.259	65.37±0.14
422.64	2.232	928.172	81.305	0.259	65.23±0.14
422.73	1.765	928.100	66.121	0.360	65.11±0.24
422.75	1.765	928.075	66.458	0.360	64.88±0.24
422.75	1.235	928.075	48.029	0.476	64.74±0.46
422.72	1.235	928.105	48.503	0.476	64.28±0.46
422.68	0.9614	928.139	38.722	0.269	63.82±0.33
422.64	0.9614	928.168	38.459	0.269	64.14±0.33
422.76	0.5647	928.060	23.555	0.158	63.21±0.33
422.87	0.5647	927.970	23.399	0.158	63.54±0.33
423.13	0.2824	927.745	11.869	0.187	63.64±0.77
423.25	0.2824	927.626	12.055	0.187	62.88±0.77
423.28	0.1825	927.607	7.957	0.038	62.10±0.24
423.19	0.1825	927.689	7.995	0.038	61.85±0.24
422.45	2.779	928.340	97.372	0.240	65.66±0.11
422.48	2.779	928.318	97.608	0.240	65.56±0.11
422.54	3.267	928.265	110.466	0.711	66.12±0.27
422.60	3.267	928.216	111.128	0.711	65.87±0.27
		p = 30.00 ± 0.01 MPa			
421.71	3.873	934.134	122.258	1.211	67.49±0.39
422.00	3.873	933.887	121.293	1.208	67.81±0.39
422.20	3.267	933.720	110.953	1.741	65.78±0.66
422.37	3.267	933.566	109.480	1.735	66.34±0.66
422.51	2.779	933.447	96.175	0.676	66.05±0.30
422.55	2.779	933.408	96.322	0.677	65.99±0.30
422.61	2.232	933.358	79.622	0.202	66.01±0.11
422.61	2.232	933.359	79.776	0.202	65.93±0.11
422.67	1.765	933.302	65.914	0.280	65.13±0.19

Table 7.5 Continued

422.76	1.765	933.231	66.161	0.280	64.96±0.19
422.80	1.235	933.187	47.697	0.210	64.94±0.20
422.83	1.235	933.165	47.894	0.210	64.75±0.20
422.82	0.9614	933.181	38.277	0.161	64.26±0.19
422.84	0.9614	933.157	38.124	0.161	64.45±0.19
422.94	0.5647	933.073	23.349	0.179	63.54±0.37
422.98	0.5647	933.035	23.180	0.179	63.89±0.37
422.93	0.1825	933.079	7.939	0.158	62.14±0.99
422.86	0.1825	933.144	8.091	0.158	62.18±1.00

(a) Calculated from Hill's (1990) equation of state for water.

Table 7.6 Relative densities and apparent molar volumes of aqueous glycylglycine at 298.43±0.21 K and 10, 20, and 30 MPa.

T (K)	m (mol kg^{-1})	ρ_o [a] (kg m^{-3})	$\rho - \rho_o$ (kg m^{-3})	$\sigma\Delta\rho$ (kg m^{-3})	$V_{2,\phi}$ (cm^3 mol^{-1})
		p = 10.00 ± 0.01 MPa			
298.36	0.9502	1001.404	47.570	0.315	78.27±0.34
298.36	0.9502	1001.404	47.672	0.315	78.16±0.34
298.33	0.8172	1001.413	41.298	0.382	78.29±0.48
298.35	0.8172	1001.407	41.627	0.382	77.88±0.48
298.32	0.6797	1001.415	34.961	0.243	77.90±0.36
298.28	0.6797	1001.425	35.150	0.243	77.62±0.36
298.30	0.5661	1001.421	29.763	0.196	77.19±0.35
298.36	0.5661	1001.408	29.568	0.196	77.54±0.35
298.48	0.4435	1001.374	22.987	0.213	78.43±0.49
298.50	0.4435	1001.369	23.200	0.213	77.94±0.49
298.57	0.3320	1001.346	17.751	0.331	77.23±1.00
298.57	0.3320	1001.346	17.584	0.331	77.74±1.00
298.56	0.2227	1001.351	11.946	0.274	77.50±1.23
298.57	0.2227	1001.347	11.673	0.274	78.73±1.23
298.66	0.1248	1001.324	6.557	0.252	78.99±2.02
298.68	0.1248	1001.318	6.806	0.252	76.99±2.02
298.29	0.9502	1001.421	47.401	0.212	78.45±0.23

Table 7.6 Continued

298.32	0.9502	1001.414	47.189	0.212	78.68±0.23
298.32	0.8172	1001.415	41.386	0.249	78.18±0.31
298.33	0.8172	1001.411	41.634	0.249	77.87±0.31
298.46	0.5661	1001.374	29.087	0.540	78.40±0.97
298.46	0.5661	1001.374	29.619	0.540	77.45±0.97
298.46	0.4435	1001.373	23.302	0.363	77.71±0.83
298.48	0.4435	1001.373	23.101	0.363	78.17±0.83
		p = 20.00 ± 0.01 MPa			
298.41	0.9502	1005.759	46.105	0.330	79.72±0.35
298.39	0.9502	1005.765	46.424	0.330	79.38±0.35
298.37	0.8172	1005.771	40.329	0.151	79.37±0.19
298.38	0.8172	1005.771	40.480	0.151	79.19±0.19
298.38	0.6797	1005.769	34.246	0.155	78.85±0.23
298.36	0.6797	1005.774	34.103	0.155	79.06±0.23
298.35	0.5661	1005.775	28.720	0.129	78.93±0.23
298.38	0.5661	1005.769	28.651	0.129	79.06±0.23
298.49	0.5661	1005.738	28.672	0.575	79.02±1.02
298.51	0.5661	1005.731	29.235	0.575	78.02±1.02
298.50	0.3320	1005.735	16.968	0.347	79.48±1.04
298.52	0.3320	1005.730	17.302	0.347	78.48±1.04
298.58	0.2227	1005.714	11.622	0.262	78.84±1.17
298.59	0.2227	1005.708	11.884	0.262	77.68±1.17
298.63	0.1248	1005.697	6.517	0.255	79.19±2.03
298.64	0.1248	1005.695	6.772	0.255	77.17±2.03
		p = 30.01 ± 0.01 MPa			
298.20	0.9502	1010.106	45.989	0.205	79.71±0.22
298.30	0.9502	1010.075	46.188	0.205	79.50±0.22
298.38	0.8172	1010.052	40.193	0.453	79.41±0.56
298.40	0.8172	1010.046	39.742	0.453	79.97±0.56
298.45	0.6797	1010.033	33.117	0.722	80.39±1.06
298.46	0.6797	1010.031	33.838	0.722	79.33±1.06
298.49	0.5661	1010.022	28.337	0.213	79.49±0.38
298.48	0.5661	1010.022	28.540	0.213	79.13±0.38
298.48	0.4435	1010.022	22.672	0.146	78.90±0.33

Table 7.6 Continued

298.46	0.4435	1010.027	22.816	0.146	78.58±0.33
298.39	0.2227	1010.047	11.291	0.199	80.20±0.88
298.37	0.2227	1010.054	11.490	0.199	79.31±0.88
298.34	0.1248	1010.064	6.347	0.268	80.41±2.11
298.35	0.1248	1010.063	6.615	0.268	78.30±2.11

(a) Calculated from Hill's (1990) equation of state for water.

Table 7.7 Relative densities and apparent molar volumes of aqueous glycylglycine at 376.83±0.50 K and 10, 20, and 30 MPa.

T (K)	m (mol kg^{-1})	ρ_o [(a)] ($kg\ m^{-3}$)	$\rho - \rho_o$ ($kg\ m^{-3}$)	$\sigma\Delta\rho$ ($kg\ m^{-3}$)	$V_{2,\phi}$ ($cm^3\ mol^{-1}$)
		p = 10.00 ± 0.01 MPa			
376.76	1.174	960.373	56.042	0.261	81.05±0.25
376.81	1.174	960.335	56.217	0.261	80.89±0.25
376.93	0.9485	960.252	46.686	0.342	80.29±0.40
376.98	0.9485	960.212	46.346	0.342	80.68±0.40
377.03	0.8026	960.181	39.923	0.238	80.28±0.33
377.03	0.8026	960.180	39.695	0.238	80.60±0.33
377.10	0.6745	960.128	33.915	0.260	80.21±0.43
377.16	0.6745	960.085	34.171	0.260	79.79±0.43
377.26	0.5302	960.010	27.120	0.073	79.84±0.15
377.27	0.5302	960.004	27.059	0.073	79.97±0.15
377.28	0.3882	959.998	20.195	0.020	79.48±0.06
377.27	0.3882	960.008	20.190	0.020	79.49±0.06
377.24	0.2777	960.029	14.664	0.116	79.10±0.46
377.22	0.2777	960.039	14.549	0.116	79.56±0.46
377.23	0.1401	960.040	7.294	0.285	80.50±2.21
377.23	0.1401	960.038	7.579	0.285	78.29±2.21
		p = 20.00 ± 0.01 MPa			
376.29	1.174	960.373	56.246	0.064	80.86±0.06
376.34	1.174	960.335	56.275	0.064	80.83±0.06
376.48	0.9485	960.252	46.388	0.114	80.63±0.13
376.53	0.9485	960.212	46.502	0.114	80.50±0.13

Table 7.7 Continued

376.61	0.8026	960.181	39.972	0.092	80.22±0.13
376.62	0.8026	960.180	39.889	0.092	80.33±0.13
376.69	0.6745	960.128	34.025	0.059	80.03±0.10
376.72	0.6745	960.085	33.974	0.059	80.12±0.10
376.76	0.5302	960.010	27.013	0.049	80.07±0.10
376.76	0.5302	960.004	27.059	0.049	79.97±0.10
376.72	0.3882	959.998	20.115	0.038	79.70±0.11
376.70	0.3882	960.008	20.133	0.038	79.65±0.11
376.71	0.2777	960.029	14.609	0.011	79.32±0.04
376.73	0.2777	960.039	14.619	0.011	79.28±0.04
376.76	0.1401	960.040	7.472	0.041	79.12±0.32
376.76	0.1401	960.038	7.430	0.041	79.44±0.32
		p = 30.00 ± 0.01 MPa			
376.38	1.174	969.616	54.850	0.129	81.90±0.12
376.47	1.174	969.553	54.977	0.129	81.78±0.12
376.61	0.9485	969.451	45.141	0.156	81.82±0.18
376.64	0.9485	969.428	44.995	0.156	81.98±0.18
376.77	0.8026	969.338	38.695	0.175	81.70±0.24
376.77	0.8026	969.341	38.730	0.175	81.66±0.24
376.77	0.6745	969.339	32.854	0.250	81.68±0.40
376.76	0.6745	969.345	33.100	0.250	81.28±0.40
376.79	0.5302	969.327	26.190	0.020	81.51±0.04
376.79	0.5302	969.327	26.210	0.020	81.46±0.04
376.83	0.3882	969.301	19.616	0.042	80.86±0.12
376.83	0.3882	969.298	19.574	0.042	80.98±0.12
376.84	0.2777	969.285	14.185	0.068	80.74±0.26
376.85	0.2777	969.284	14.235	0.068	80.55±0.26
376.85	0.1401	969.282	7.271	0.142	80.44±1.08
376.83	0.1401	969.293	7.133	0.142	81.49±1.08

(a) Calculated from Hill's (1990) equation of state for water.

Table 7.8 Relative densities and apparent molar volumes of aqueous glycylglycine at 397.91±0.55 K and 10, 20, and 30 MPa.

T (K)	m (mol kg^{-1})	ρ_o [(a)] (kg m^{-3})	$\rho - \rho_o$ (kg m^{-3})	$\sigma\Delta\rho$ (kg m^{-3})	$V_{2,\phi}$ (cm^3 mol^{-1})
		p = 10.00 ± 0.01 MPa			
398.29	1.302	943.844	62.334	0.611	80.89±0.54
398.32	1.302	943.821	62.245	0.610	80.97±0.54
398.24	1.122	943.878	54.746	0.150	80.54±0.15
398.16	1.122	943.947	54.839	0.150	80.44±0.15
398.02	0.9176	944.066	45.477	0.314	80.45±0.39
397.95	0.9176	944.120	45.772	0.314	80.08±0.39
397.83	0.7382	944.215	36.532	0.843	81.25±1.30
397.86	0.7382	944.192	37.375	0.843	79.95±1.30
397.72	0.5946	944.301	30.355	0.355	80.07±0.68
397.68	0.5946	944.339	30.684	0.356	79.44±0.68
397.71	0.4425	944.314	23.822	0.755	77.56±1.93
397.73	0.4425	944.299	23.078	0.754	79.46±1.93
397.63	0.2882	944.378	15.249	0.090	79.28±0.35
397.55	0.2882	944.439	15.187	0.090	79.52±0.35
397.44	0.1334	944.527	6.994	0.537	80.48±4.53
397.41	0.1334	944.550	7.505	0.540	76.18±4.53
		p = 20.00 ± 0.01 MPa			
397.64	1.302	949.222	61.928	0.096	81.10±0.08
397.78	1.302	949.110	61.848	0.098	81.18±0.08
397.91	1.122	949.007	53.845	0.522	81.32±0.53
398.00	1.122	948.937	54.347	0.523	80.81±0.53
398.00	0.9176	948.929	45.233	0.118	80.62±0.15
398.06	0.9176	948.883	45.244	0.118	80.61±0.15
397.92	0.7382	949.001	37.125	0.195	80.22±0.30
397.88	0.7382	949.027	37.309	0.195	79.94±0.30
397.84	0.5946	949.057	30.257	0.141	80.14±0.27
397.78	0.5946	949.107	30.397	0.141	79.88±0.27
397.81	0.4425	949.086	22.774	0.172	80.13±0.44
397.73	0.4425	949.151	22.609	0.172	80.54±0.44

Table 7.8 Continued

397.54	0.2882	949.304	15.034	0.084	80.01±0.03
397.47	0.2882	949.358	15.042	0.084	79.98±0.03
397.49	0.1334	949.337	7.254	0.162	78.20±1.35
397.49	0.1334	949.337	7.106	0.162	79.44±1.35
		p = 30.00 ± 0.01 MPa			
398.34	1.302	953.371	61.503	0.134	81.36±0.12
398.37	1.302	953.352	61.443	0.134	81.41±0.12
398.31	1.122	953.394	54.001	0.075	81.04±0.08
398.33	1.122	953.383	53.932	0.075	81.11±0.08
398.42	0.9176	953.311	44.232	1.026	81.74±1.26
398.37	0.9176	953.353	45.258	1.026	80.48±1.26
398.23	0.7382	953.460	37.042	0.189	80.23±0.29
398.24	0.7382	953.448	36.861	0.189	80.51±0.29
398.10	0.5946	953.558	30.131	0.073	80.27±0.14
398.08	0.5946	953.567	30.200	0.073	80.14±0.14
397.93	0.4425	953.687	22.396	0.121	80.97±0.30
397.91	0.4425	953.709	22.517	0.121	80.66±0.30
397.83	0.2882	953.776	15.152	0.147	79.45±0.56
397.84	0.2882	953.768	15.299	0.147	78.89±0.56
397.72	0.1334	953.861	7.179	0.018	78.74±0.15
397.71	0.1334	953.872	7.161	0.018	78.88±0.15

(a) Calculated from Hill's (1990) equation of state for water.

Table 7.9 Relative densities and apparent molar volumes of aqueous glycylglycine at 423.14±0.41 K and 10, 20, and 30 MPa.

T (K)	m (mol kg^{-1})	ρ_o [(a)] (kg m^{-3})	$\rho - \rho_o$ (kg m^{-3})	$\sigma\Delta\rho$ (kg m^{-3})	$V_{2,\phi}$ (cm^3 mol^{-1})
		p = 10.00 ± 0.01 MPa			
422.78	1.294	922.699	62.418	0.113	81.05±0.11
422.86	1.294	922.624	62.531	0.113	80.94±0.11
423.08	1.124	922.423	55.125	0.063	80.72±0.07
423.17	1.124	922.340	55.184	0.063	80.66±0.07
423.29	0.9113	922.229	45.534	0.260	80.51±0.34

Table 7.9 Continued

423.26	0.9113	922.261	45.794	0.260	80.17±0.34
423.07	0.7294	922.437	37.192	0.113	80.05±0.18
423.01	0.7294	922.492	37.305	0.113	79.87±0.18
423.00	0.5960	922.496	30.914	0.048	79.59±0.10
423.03	0.5960	922.473	30.866	0.048	79.68±0.10
423.06	0.4527	922.443	23.764	0.020	79.47±0.05
423.10	0.4527	922.399	23.744	0.020	79.52±0.05
423.21	0.2718	922.304	14.548	0.091	79.05±0.39
423.24	0.2718	922.278	14.639	0.091	78.66±0.39
423.32	0.1361	922.203	7.443	0.101	78.29±0.87
423.35	0.1361	922.170	7.342	0.101	79.16±0.87
		p = 20.00 ± 0.01 MPa			
423.35	1.294	927.544	62.272	0.273	81.06±0.25
423.33	1.294	927.562	62.000	0.273	81.31±0.25
423.32	1.124	927.565	54.666	0.207	81.09±0.22
423.32	1.124	927.569	54.863	0.207	80.88±0.22
423.30	0.9113	927.583	45.246	0.032	80.77±0.01
423.28	0.9113	927.607	45.245	0.032	80.77±0.01
423.26	0.7294	927.619	36.871	0.061	80.46±0.10
423.24	0.7294	927.640	36.826	0.061	80.54±0.10
423.20	0.5960	927.677	30.696	0.050	79.91±0.10
423.19	0.5960	927.685	30.647	0.050	80.01±0.10
423.19	0.4527	927.687	23.731	0.042	79.46±0.11
423.20	0.4527	927.676	23.770	0.042	79.36±0.11
423.27	0.2718	927.616	14.561	0.050	78.91±0.21
423.26	0.2718	927.625	14.611	0.050	78.69±0.21
423.16	0.1361	927.710	7.304	0.150	79.39±1.28
423.19	0.1361	927.682	7.454	0.150	78.11±1.28
		p = 30.01 ± 0.01 MPa			
422.59	1.279	933.378	61.395	0.096	81.11±0.09
422.66	1.279	933.317	61.315	0.096	81.18±0.09
422.89	1.072	933.115	53.938	0.350	79.21±0.38
422.96	1.072	933.052	54.284	0.350	78.83±0.38
422.82	0.8822	933.187	44.878	0.153	79.33±0.20

Table 7.9 Continued

422.79	0.8822	933.202	45.026	0.153	79.13±0.20
422.82	0.7230	933.180	36.544	0.189	80.37±0.30
422.84	0.7230	933.159	36.733	0.189	80.06±0.30
423.09	0.5834	932.943	30.352	0.037	79.25±0.07
423.15	0.5834	932.885	30.337	0.037	79.28±0.07
423.25	0.4290	932.803	23.479	0.032	76.79±0.09
423.31	0.4290	932.755	23.449	0.032	76.87±0.09
423.40	0.2723	932.678	14.488	0.071	79.24±0.30
423.41	0.2723	932.665	14.418	0.071	79.54±0.30
423.44	0.1351	932.638	7.423	0.021	77.87±0.18
423.45	0.1351	932.629	7.403	0.021	78.04±0.18

(a) Calculated from Hill's (1990) equation of state for water.

Combining equation 7.1 with the HKF equation for the partial molar volume at infinite dilution (equation 6.4), results in equation 7.2:

$$V_{2,\phi} = \bar{V}_2^o + S_V m$$

therefore

$$V_{2,\phi} = a_1 + \frac{a_2}{\Psi+p} + \frac{a_3}{T-\Theta} + \frac{a_4}{(T-\Theta)(\Psi+p)} - \omega_e Q + (a_5 pT^2 + a_6 T + \frac{a_7}{T} + a_8 T^2)m \,. \qquad (7.2).$$

Equation 7.2 was fitted to apparent molar volumes to obtain the HKF parameters, a_1, a_2, a_3, a_4, and ω_e and concentration descriptive parameters a_5 through a_8. Born functions Q, X, and Y for all HKF equations in this investigation were calculated using a program utilising the procedures described by Helgeson and Kirkham (1974, 1976) and the equations for the dielectric constant for water reported by Johnson and Norton (1991). Data used in the fitting of equation 7.2 included a combination of data from tables 7.1 through 7.9 and previously published volumetric data at 288.15, 298.15, 313.15, and 328.15 K and 0.10 MPa (Hakin *et al.*, 1994a, 1995). The glycine data set also included previously published high temperature and pressure volumetric data reported by Hakin *et al.* (1998). Because previously published data obtained using the Sodev O2D densimeter

Table 7.10 HKF coefficients for equation 6.3 and 7.2 for aqueous L-serine, glycine, and glycylglycine.

Coefficient	L-serine	Glycine	Glycylglycine
a_1 (cm^3 mol^{-1})	75.24±3.57	59.08±2.60	73.89±4.29
10^{-4} a_2 (cm^3 bar mol^{-1})	-1.481±0.927	-2.088±0.690	2.808±1.162
a_3 (cm^3 K mol^{-1})	408.6±296.7	-617.3±198.9	2095±344
10^{-5} a_4 (cm^3 K bar mol^{-1})	-23.13±7.782	6.247±5.303	-66.57±9.28
10^{9} a_5 (cm^3 kg K^{-2} bar^{-1} mol^{-2})	-6.047±2.208	-8.027±2.046	-12.74±8.17
10^{2} a_6 (cm^3 kg K^{-1} mol^{-2})	-1.520±0.591	-2.614±0.338	0.858±0.163
a_7 (cm^3 kg K mol^{-2})	747.7±239.8	1168±150	-462.9±184.5
10^{5} a_8 (cm^3 kg K^{-2} mol^{-2})	3.273±1.116	5.360±0.608	*****
c_1 (J K^{-1} mol^{-1})	225.1±4.10	148.1±5.6	134.2±5.2
10^{-5} c_2 (J K mol^{-1})	-4.068±0.214	-3.636±0.290	-3.549±0.269
10^{-5} ω_e (J mol^{-1})	2.791±0.261	3.746±0.091	2.463±0.237

are more precise than data collected using the high temperature and pressure densimeter, these data were weighted by a factor of two in all regression fits.

Calculated apparent molar volumes at all concentrations are plotted against experimental values in figures 7.1 to 7.3, where solid lines indicate the 95% confidence interval limits for equation 7.2. Effective Born coefficients obtained by regression with experimental data were positive for all species.

Isobaric volumetric curves at 0.10, 10.00, 20.00, and 30.00 MPa are shown in figures 7.4 to 7.6 and compared with those of Amend and Helgeson (1997a), Shock and Helgeson (1990), Shock (1992), and Marriott *et al.* (1998). These curves show large discrepancies as the temperature approaches the critical point of water. Because all investigations contain data at 298.15 K, it comes as no surprise that they all agree at this temperature.

Figure 7.1 Experimental apparent molar volumes for aqueous glycine versus predicted apparent molar volumes from equation 7.2 at temperatures from 288.15 to 473 K and pressures of 0.10, 10.00, 20.00, and 30.00 MPa.

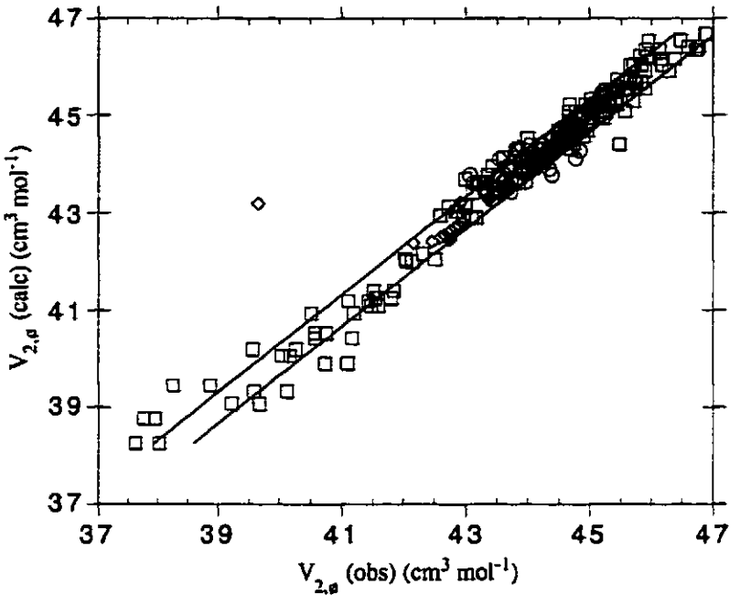

o this investigation, ◇ Hakin *et al.* (1994), □ Hakin *et al.* (1998), — 95 % confidence interval limits.

Figure 7.2 Experimental apparent molar volumes for aqueous L-serine versus predicted apparent molar volumes from equation 7.2 at temperatures from 288.15 to 421.90 K and pressures of 0.10, 10.00, 20.00, and 30.00 MPa.

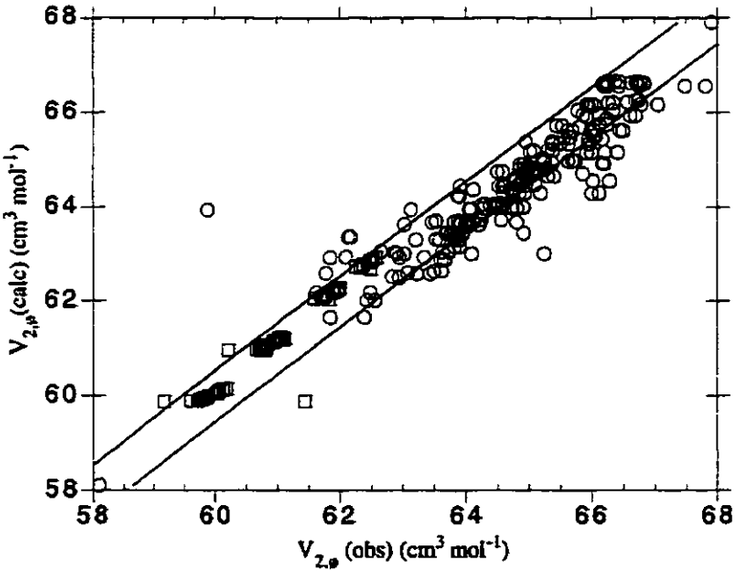

o this investigation, □ Hakin *et al.* (1994), — 95 % confidence interval limits.

Figure 7.3 Experimental apparent molar volumes for aqueous glycylglycine versus predicted apparent molar volumes from equation 7.2 at temperatures from 288.15 to 423.14 K and pressures of 0.10, 10.00, 20.00, and 30.00 MPa.

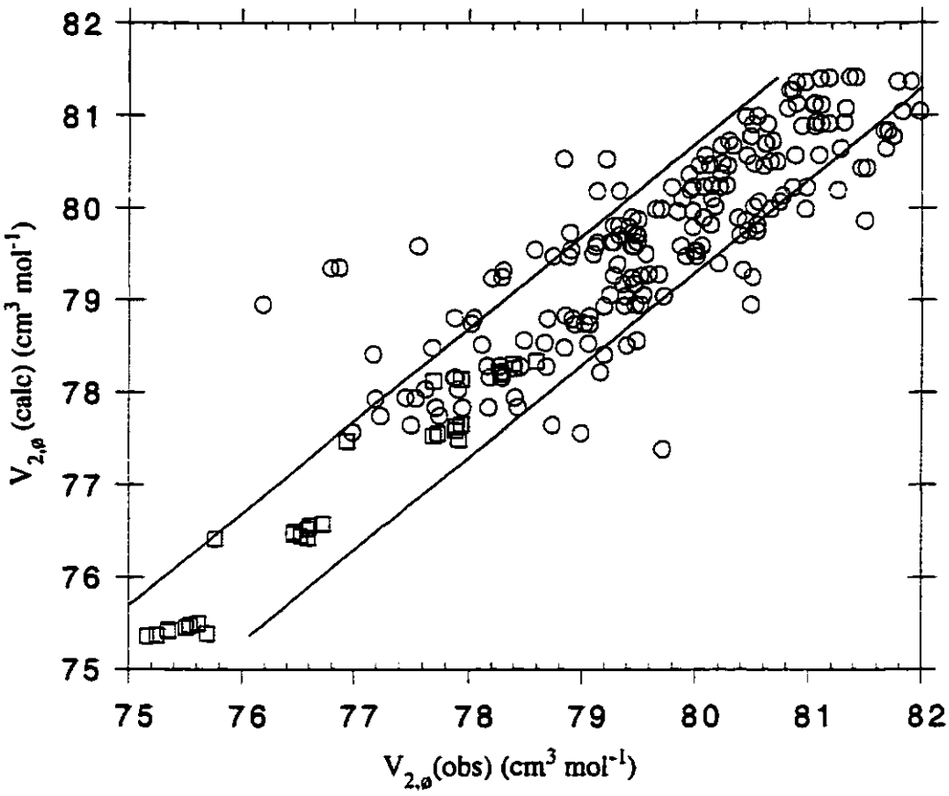

o this investigation, □ Hakin *et al.* (1995), — 95 % confidence interval limits.

In figures 7.4 to 7.6 the isobaric volume curves stopping at 373.15 K correspond to the 0.10 MPa isobar. In all cases Shock and Helgeson (1990) and Shock (1992) show trends where the partial molar volume decreases with increasing pressure. This trend differs from our investigation and those of Amend and Helgeson (1997a). Although Shock and Helgeson (1990) note that their coefficients are a first estimate, these first estimates show drastically different results at any temperature or pressure beyond ambient. Our partial molar volume data at infinite dilution are in good agreement with the pressure trends

Figure 7.4 Temperature dependence of calculated partial molar volumes at infinite dilution for aqueous L-serine from 273.15 K to 470 K and 0.10, 10.00, 20.00, and 30.00 MPa.

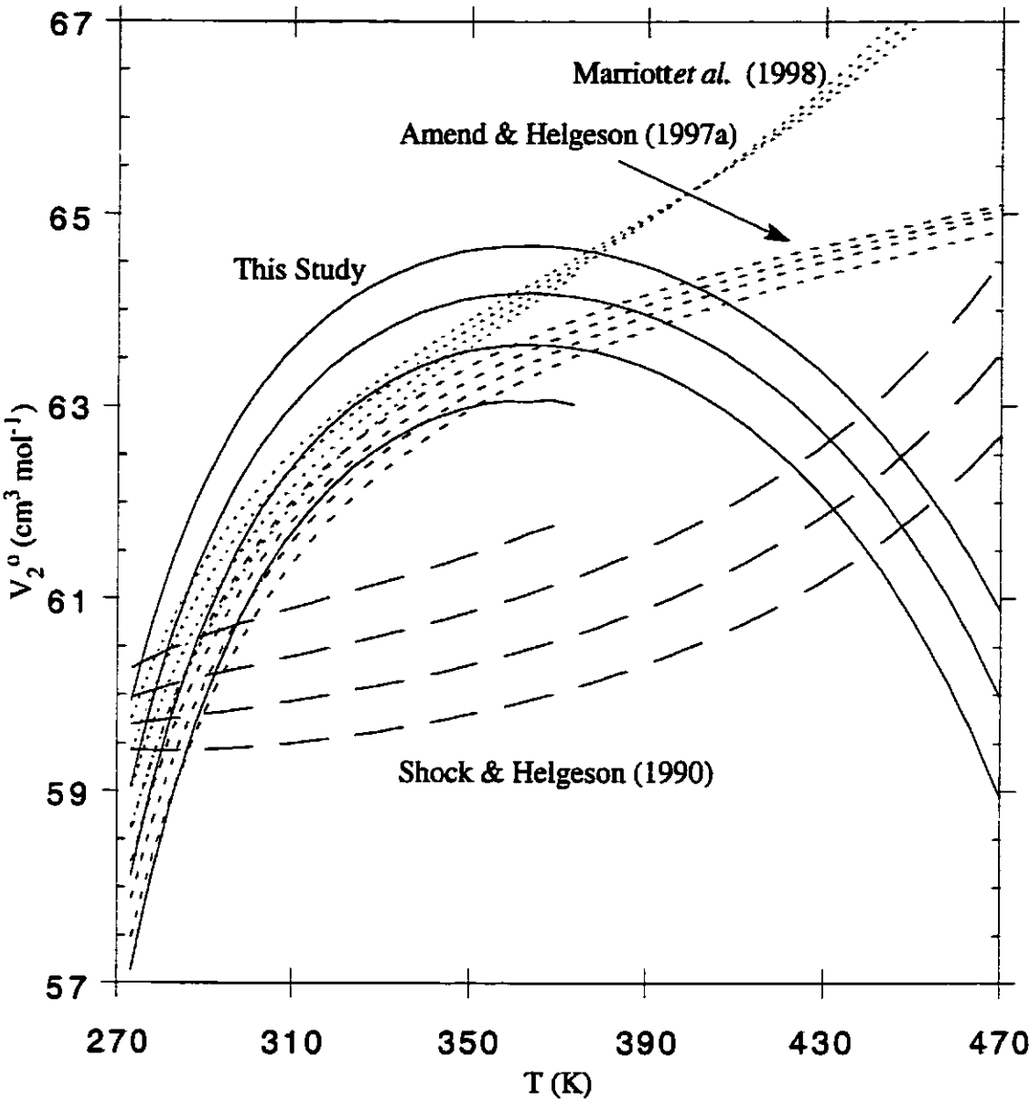

Figure 7.5 Temperature dependence of calculated partial molar volumes at infinite dilution for aqueous glycine from 273.15 K to 470 K and 0.10, 10.00, 20.00, and 30.00 MPa.

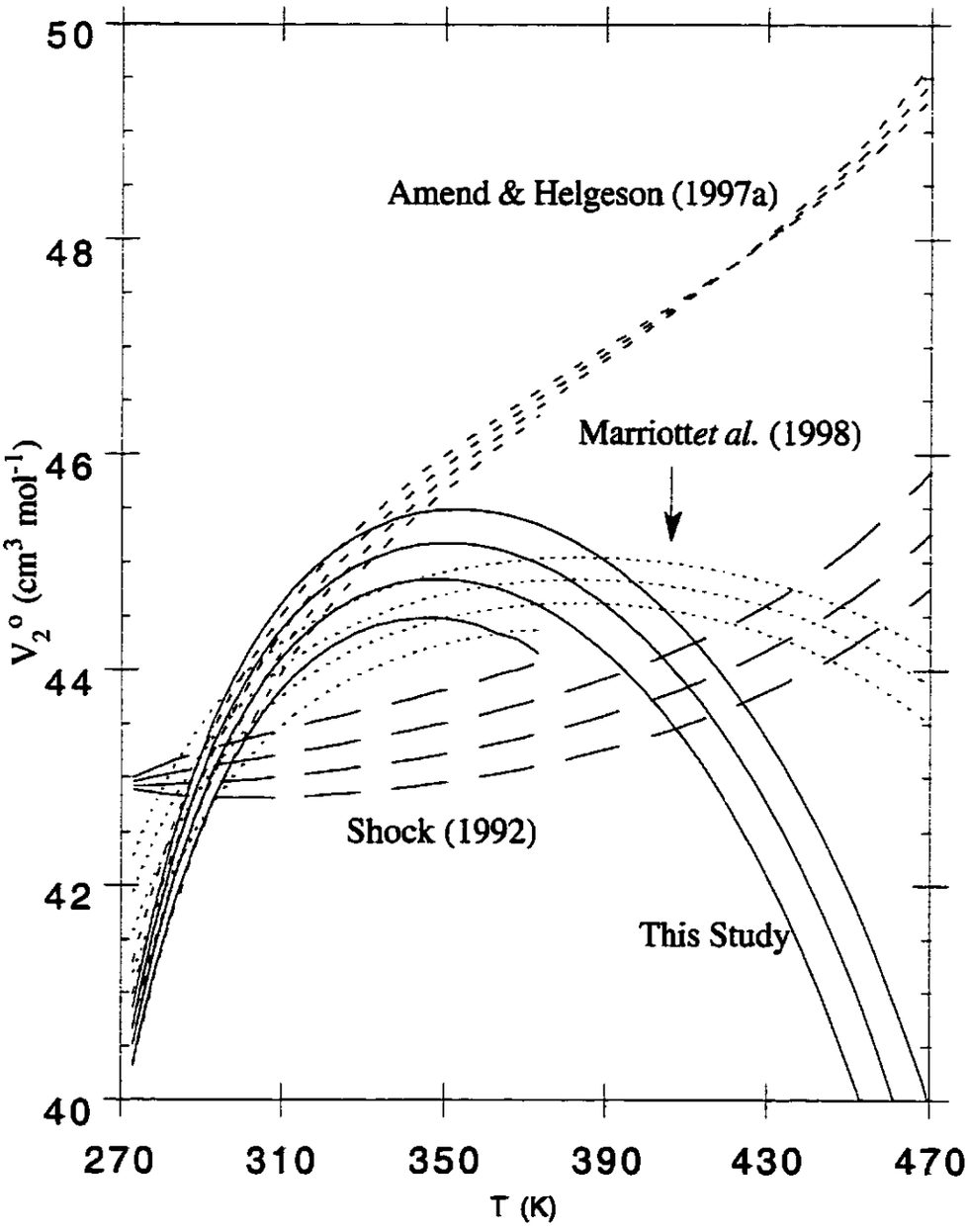

Figure 7.6 Temperature dependence of calculated partial molar volumes at infinite dilution for aqueous glycylglycine from 273.15 K to 470 K and 0.10, 10.00, 20.00, and 30.00 MPa.

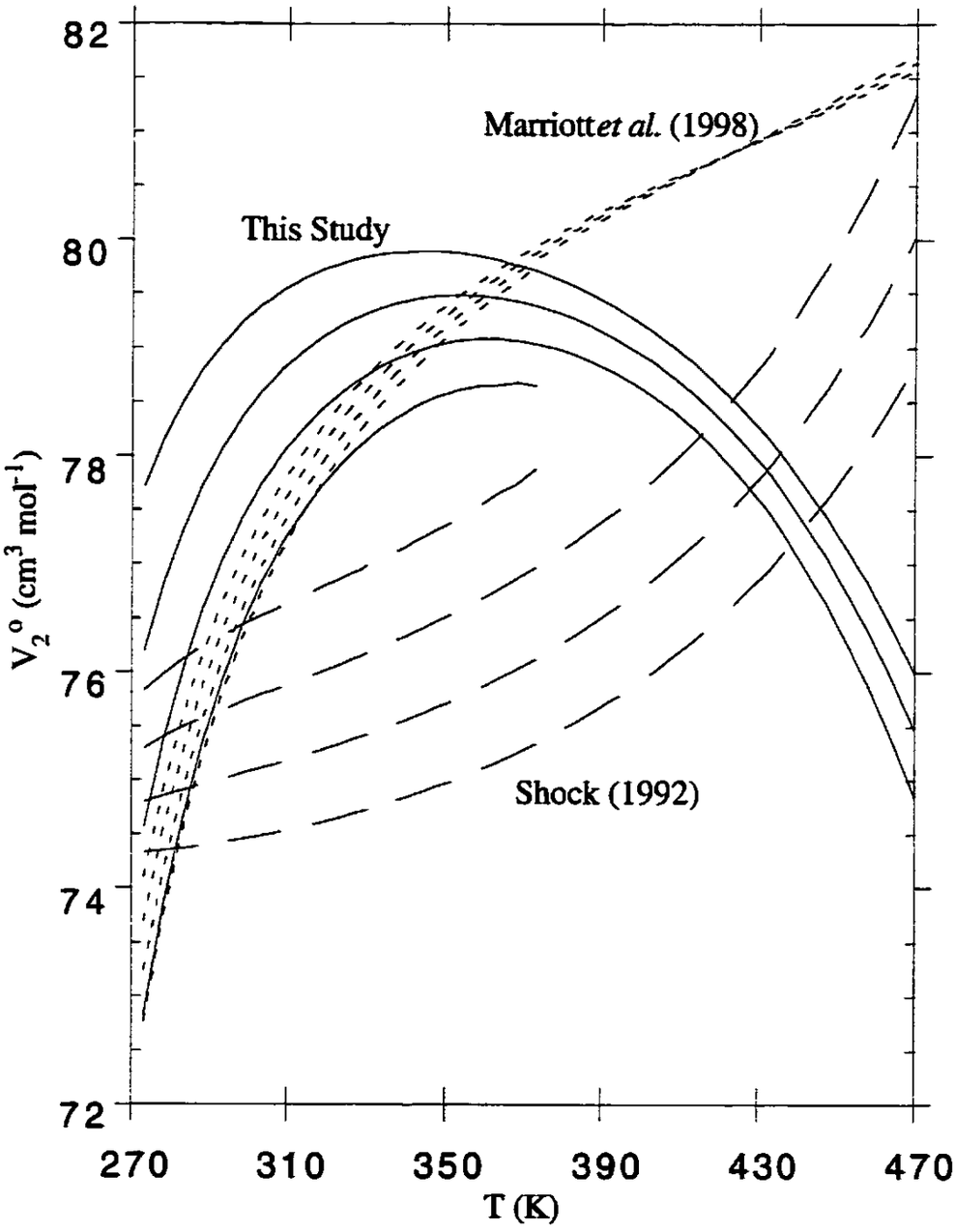

of Amend and Helgeson (1997a). However, the magnitude of the pressure effect is more consistent with Shock (1992) and Shock and Helgeson (1990). Amend and Helgeson (1997a) used experimental compressibility data to obtain information about the pressure effect on partial molar volume; therefore, greater precision in their prediction of trends is expected.

The effect of temperature on partial molar properties is dominated by the effective Born solvation term as the temperature approaches the critical point of water. Although effective Born coefficients predicted from the additivity scheme of Marriott *et al.* (1998) are negative for aqueous glycylglycine and L-serine, good agreement is observed up to approximately 360 K. This is considered reasonable since the lower temperature apparent molar heat capacities and volumes used for the input set in Marriott *et al.*'s (1998) additivity scheme are the same as those used in this study. With respect to glycine, Amend and Helgeson (1997a) also show good agreement with our study up to approximately 350 K. The temperature dependence of partial molar volumes for all species investigated in this study did not agree with those reported by Shock (1992) and Shock and Helgeson (1990). However, as previously mentioned predictions at 298.15 K and 0.10 MPa do agree.

In light of the drastically different effective Born coefficients obtained from fitting high temperature and pressure experimental volumes, previous predictions at high temperature and pressure may be reevaluated. In particular, Shock (1992) has discussed the implication of peptide stability through thermodynamic equilibrium calculations using the HKF equations of state. Although Shock's (1992) equilibrium calculations may be correct with respect to the synthesis and hydrolysis of peptides, our evidence of imprecise evaluations of volumetric temperature and pressure surfaces, indicate these calculations are wrong. Thus effective Born coefficients were utilised with previously published heat capacities at 288.15, 298.15, 313.15, and 328.15 K and 0.10 MPa in fitting the equation 6.3. The coefficients c_1 and c_2 obtained from fitting equation 6.3 are also reported in table 7.10, thereby completing the prediction of coefficients required in a full utilisation of the

HKF equations of state. All uncertainties reported in table 7.10 are reported at the 95% confidence level.

7.4 Aqueous peptide stability at elevated temperatures and pressures.

The calculated coefficients reported in table 7.10 permit us to estimate the thermodynamic properties of some biologically important aqueous species. These estimates allow for the prediction of equilibria among peptides and free amino acids.

Two possible reactions,

$$\text{glycine} + \text{glycine} \rightleftharpoons \text{glycylglycine} + H_2O \qquad (7.3)$$

and

$$\text{glycine} + \text{glycine} \rightleftharpoons \text{diketopiperazine} + 2H_2O\,, \qquad (7.4)$$

have been investigated by Shock (1992) to question the degradation of the dipeptide glycylglycine in aqueous solution. In the current study, attempts were made to measure the densities of several aqueous glycylglycine solutions at 523 K and 10.00 MPa. These attempts were unsuccessful as a low solubility organic compound was formed in our instrument. Sample solutions of glycylglycine at these temperatures were collected and the solvent was removed. The solid waste was redissolved in D_2O standard and an NMR spectrum was obtained. This NMR analysis of aqueous glycylglycine sample after being exposed to high temperatures indicated the presence of aqueous glycylglycine, glycine, and diketopiperazine.

Aqueous glycylglycine was also sealed in thick wall glass ampoules and placed in an oven at several temperatures of 423 K and greater. Oven tests of these glycylglycine solutions indicated visible degradation at temperatures above 423 K and saturation pressure. Visible degradation of glycylglycine solutions near 473 K took approximately one half hour. the residence time in our vibrating tube densimeter is only 5 minutes. Therefore degradation must be at a much faster rate at 523 K than at 473 K. Measurements at 473 K and 448 K did not show any irregularity in time period data nor was the solution

visually different upon exiting the instrument. We have assumed that with a slow degradation rate and the short residence time in our instrument that data obtained at 423 K are representative of aqueous glycylglycine. Although, due to the short residence time, density measurements above 423 K could be reasonably precise, we did not include these data in our analysis. We do note however that partial molar volumes at infinite dilution near 473 K obtained by extrapolation from experimental data are slightly greater than those predicted using our HKF coefficients for aqueous glycylglycine.

Our experimentally determined apparent molar volumes have allowed us to obtain HKF coefficients for aqueous glycine and glycylglycine solutions. However, there are no volumetric data for diketopiperazine at elevated temperatures and pressures reported in the literature. Therefore, we have investigated possible correlations among the reported thermodynamic properties of L-serine, L-alanine, glycine, and glycylglycine and their respective HKF coefficients (Hakin *et al.*, 1999a).

Although Shock and Helgeson (1990) and Amend and Helgeson (1997a) found reasonable correlation for the prediction of effective Born coefficients using standard partial molar entropies, $\bar{S}^{o}_{2}$, our investigations indicate a good correlation with partial molar heat capacities at infinite dilution, 298.15 K, and 0.10 MPa. Since partial molar heat capacities at these conditions are readily available within the literature, we chose to use equation 7.5 to predict an effective Born coefficient for diketopiperazine:

$$\omega_e \text{ (cm}^3 \text{ bar mol}^{-1}) = 4.378 \cdot 10^6 - 1.666 \cdot 10^4 \, \bar{C}p^{o}_{2,\ 298.15K,\ 0.10\ MPa} \qquad (7.5)$$

Equation 7.5 is shown in figure 7.7. Recently we measured the apparent molar volumes and heat capacities of some cyclic dipeptides in water. Infinite dilution partial molar volumes and heat capacities at 288.15, 298.15, 313.15, and 328.15 K and 0.10 MPa were obtained from these studies (Hakin et al., 1999b). The partial molar heat capacity at infinite

Figure 7.7 Correlation equation 7.5 for the prediction of effective Born coefficients from partial molar heat capacities at infinite dilution at 298.15 K and 0.10 MPa.

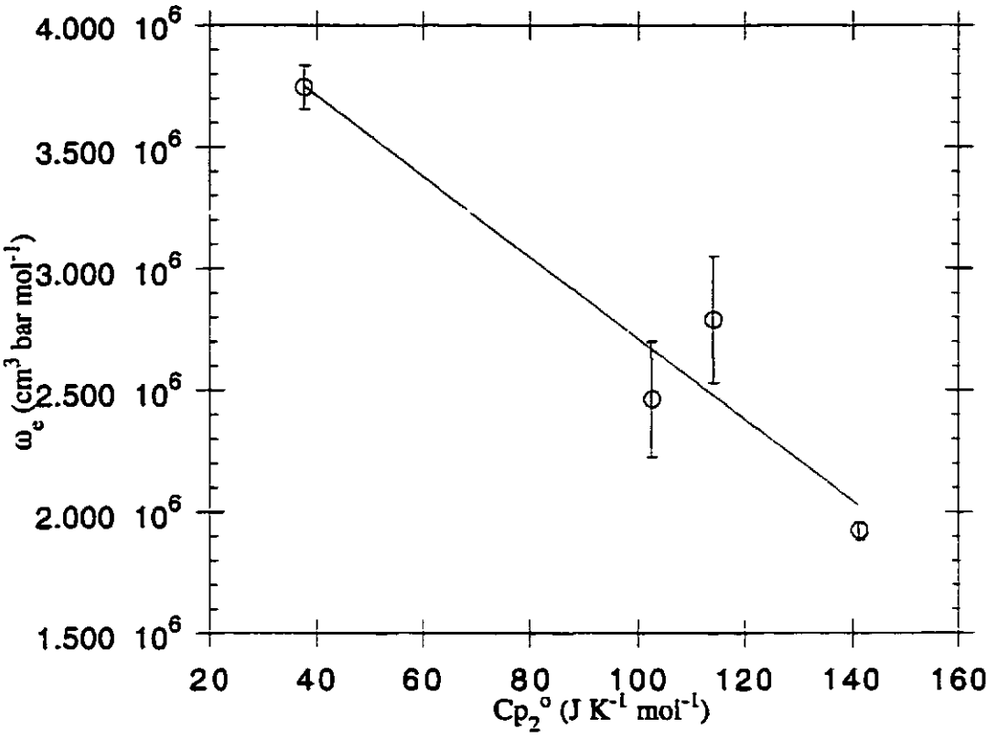

dilution of diketopiperazine was calculated to be 141.8±0.9 J K^{-1} mol^{-1}, hence using equation 7.5, a predicted Born coefficient was estimated to be $2.015 \cdot 10^5$ J mol^{-1}. This value is in poor agreement with the value of $-1.967 \cdot 10^5$ J mol^{-1} reported by Shock *et al.* (1992).

Using the predicted Born coefficient above, equations 6.3 and 6.4 were fit to the partial molar volumes and heat capacities at infinite dilution to obtain coefficients c_1, c_2, σ, and ζ. For aqueous diketopiperazine these were estimated to be 234.9±4.3 J K^{-1} mol^{-1}, $-3.486 \cdot 10^5 \pm 0.225 \cdot 10^5$ J K mol^{-1}, 87.05±0.56 cm^3 K mol^{-1}, and -610.7±41.9 cm^3 K mol^{-1} respectively. Previous studies have used the correlation equations of Shock and Helgeson (1990) to predict coefficients a_2 and a_4 which describe the pressure dependencies of HKF equations of state (Amend & Helgeson, 1997a; Marriott

et al., 1998; Shock, 1992). These correlation equations describe a correlation of a_2 coefficients with partial molar volumes at infinite dilution obtained at ambient conditions. An additional correlation equation describes the correlation of a_2 coefficients with a_4 coefficients. This study has found that the a_4 coefficients may be better estimated through correlation with partial molar volumes at infinite dilution obtained at ambient conditions. Reasonable correlation was also found between a_2 and a_4. Therefore, we have used equations 7.6 and 7.7 to predict these two HKF coefficients:

$$a_4 \text{ (cm}^3 \text{ K bar mol}^{-1}) = 9.959 \cdot 10^6 - 2.208 \cdot 10^5 \, \bar{V}^{o}_{2,\,298.15K,\,0.10\ MPa} \qquad (7.6)$$

and

$$a_2 \text{ (cm}^3 \text{ bar mol}^{-1}) = -2.185 \cdot 10^4 - 6.997 \cdot 10^{-3} \, a_4 \,. \qquad (7.7)$$

Correlation equations 7.6 and 7.7 are shown in figures 7.8 and 7.9. Experimental data obtained for aqueous diketopiperazine provided a partial molar volume at infinite dilution of 76.85±0.04 cm^3 mol^{-1} at 298.15 K and 0.10 MPa. Using equations 6.5, 6.6, 7.6, and 7.7 and this value for partial molar volume, the remainder of the HKF coefficients have been predicted; a_1=76.61 cm^3 mol^{-1}, a_2=2.717·10^4 cm^3 bar mol^{-1}, a_3=2083 cm^3 K mol^{-1}, and a_4=-7.007·10^6 cm^3 K bar mol^{-1}.

All of the predicted coefficients for diketopiperazine were found to be very similar to those of L-alanine. It should be noted that these correlation equations were obtained from a very small set of data and therefore should only be used in the case where not all HKF coefficients can be obtained. It would be more satisfying to obtain HKF coefficients for aqueous diketopiperazine directly from experimental data, since diketopiperazine does not have the two local charges of an amino acid zwitter ion. However, currently these equations for the prediction of HKF coefficient represent our best option.

The partial molar Gibbs energy at infinite dilution, $\Delta\bar{G}^o$, or chemical potential has been defined in Section 2.1 with its relationship to equilibrium being defined by equation 2.3. Partial molar Gibbs energy of formation of a single species at any temperature and

Figure 7.8 Correlation equation 7.6 for the prediction of the a_4 coefficient from partial molar volume data at infinite dilution at 298.15 K and 0.10 MPa.

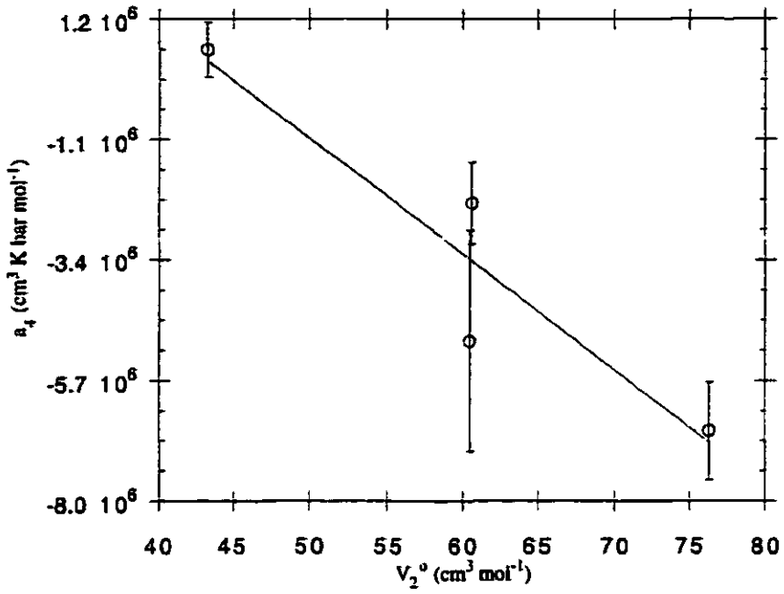

Figure 7.9 Correlation equation 7.7 for the prediction of the a_2 coefficient from a known a_4 coefficient.

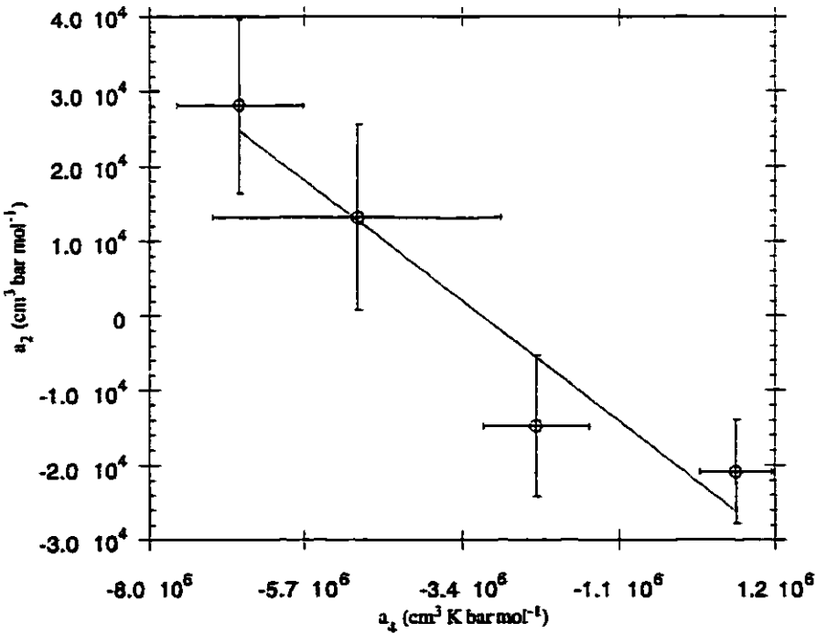

pressure, $\Delta\bar{G}^{o}_{T,p}$, can be defined by

$$\Delta\bar{G}^{o}_{T,p} = \Delta\bar{G}^{o}_{f} + (\bar{G}^{o}_{T,p} - \bar{G}^{o}_{T_r,p_r}), \tag{7.8}$$

where $\Delta\bar{G}^{o}_{f}$ is the partial molar Gibbs energy of formation at some reference temperature and pressure, T_r and p_r, and $(\bar{G}^{o}_{T,p} - \bar{G}^{o}_{T_r,p_r})$ is the difference in the partial molar Gibbs energy for a change from the reference state to the temperature and pressure of interest, T and P. For this study the reference state was chosen to be 298.15 K and 0.10 MPa. According to Chapter 2 and equation 2.50, if expressions describing pressure and temperature effects on the partial molar volume and heat capacity are known, then expressions describing the same effects for $\Delta\bar{S}^{o}$, $\Delta\bar{H}^{o}$, and $\Delta\bar{G}^{o}$ can be derived through integration. Thus, according to the revised HKF equations of state, $(\bar{G}^{o}_{T,p} - \bar{G}^{o}_{T_r,p_r})$ may be defined by equation 7.9 (Tanger and Helgeson, 1988):

$$\begin{aligned}(\bar{G}^{o}_{T,p} - \bar{G}^{o}_{T_r,p_r}) &= -\bar{S}^{o}_{T_r,p_r}(T - T_r) + \int_{T_r}^{T}\bar{C}^{o}_{p}dT - \int_{T_r}^{T}\frac{\bar{C}^{o}_{p}}{T}dT + \int_{P_r}^{P}d\bar{V}_{j}T_r n_o dp \\ &= -\bar{S}^{o}_{T_r,p_r}(T - T_r) - c_1\left[T\ln\left(\frac{T}{T_r}\right) - T + T_r\right] + a_1(p-p_r) + a_2\ln\left(\frac{\Psi+p}{\Psi+p_r}\right) \\ &\quad - c_2\left\{\left[\left(\frac{1}{T-\Theta}\right) - \left(\frac{1}{T_r-\Theta}\right)\right]\left(\frac{\Theta-T}{\Theta}\right) - \frac{T}{\Theta^2}\ln\left(\frac{T_r(T-\Theta)}{T(T_r-\Theta)}\right)\right\} \\ &\quad + \left(\frac{1}{T-\Theta}\right)\left[a_3(p-p_r) + a_4\ln\left(\frac{\Psi+p}{\Psi+p_r}\right)\right] + \omega_e\left[Y(T-T_r) + \frac{1}{\varepsilon} - \frac{1}{\varepsilon_{T_r p_r}}\right]. \end{aligned} \tag{7.9}$$

Using equations 7.8 and 7.9 the partial molar Gibbs energies for the formation of aqueous glycine, glycylglycine, and diketopiperazine at infinite dilution have been calculated from 273.15 to 608.15 K and 0.10, 10.00, 20.00, and 30.00 MPa. These energies of formation are compared to those predicted by Shock (1992) in figures 7.10 to 7.12. For a consistent comparison, our calculations have used the partial molar Gibbs energies of formation at the reference state of 298.15 K and 0.10 MPa which have been reported by Shock (1992).

Although the partial molar volume and partial molar heat capacity profiles of glycine predicted through these coefficients and those reported by Shock (1992) show poor agreement, the predicted partial molar Gibbs energy of formation is within 0.5% up to ~570 K. Volumes and heat capacities, being first and second derivative properties of the Gibbs energy (equations 2.4 and 2.8), are more sensitive to changes in temperature and pressure. Thus, by integrating back to any Gibbs energy property, temperature and pressure dependent information becomes less susceptible to error. Therefore, because equation 7.9 has been derived through these derivative relationships, there is little disagreement shown until the temperature is sufficiently large for the contribution of the effective Born term to be significant. Figures 7.10 and 7.13 show the percent deviation of

Figure 7.10 The calculated percent deviation between partial molar Gibbs energies of formation for aqueous glycine up to 608.15 K.

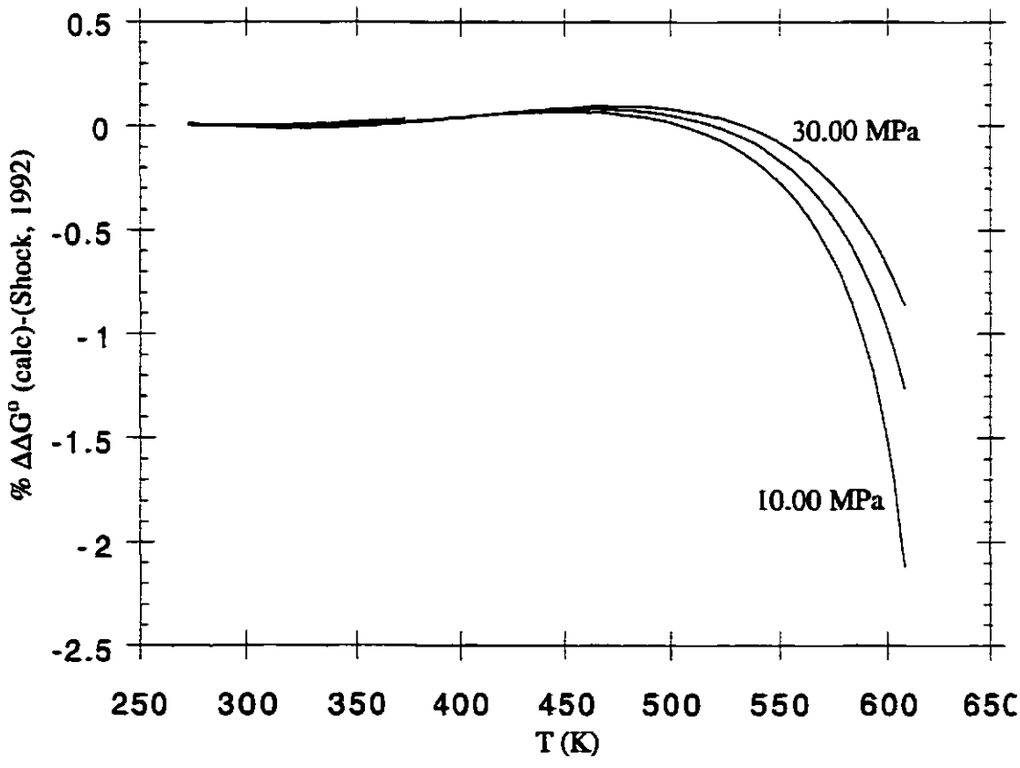

Figure 7.11 The calculated percent deviation between partial molar Gibbs energies of formation for aqueous glycylglycine up to 608.15 K.

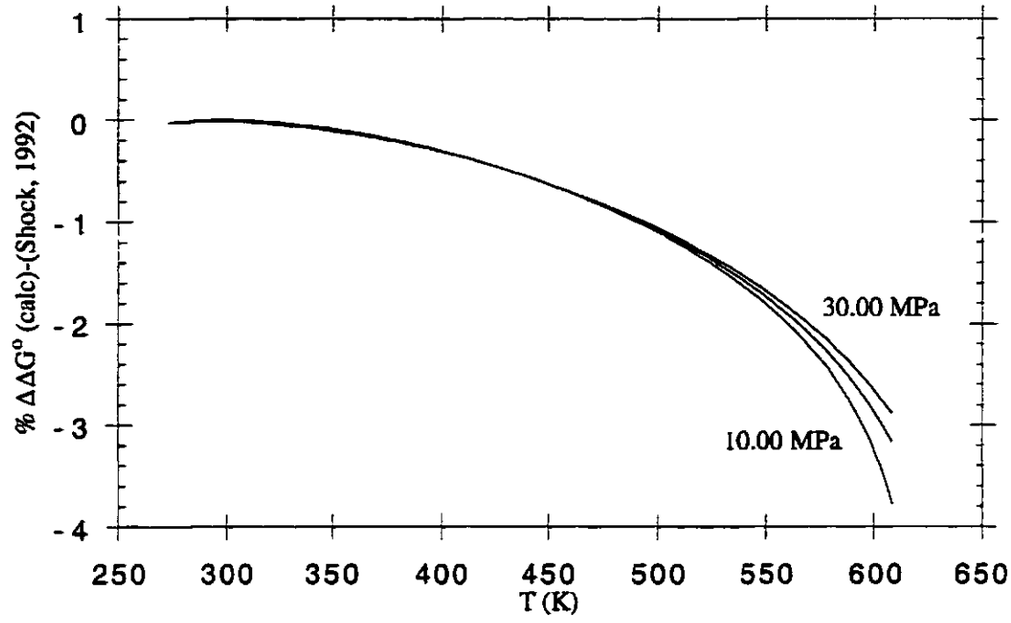

Figure 7.12 The calculated percent deviation between partial molar Gibbs energies of formation for aqueous diketopiperazine up to 608.15 K.

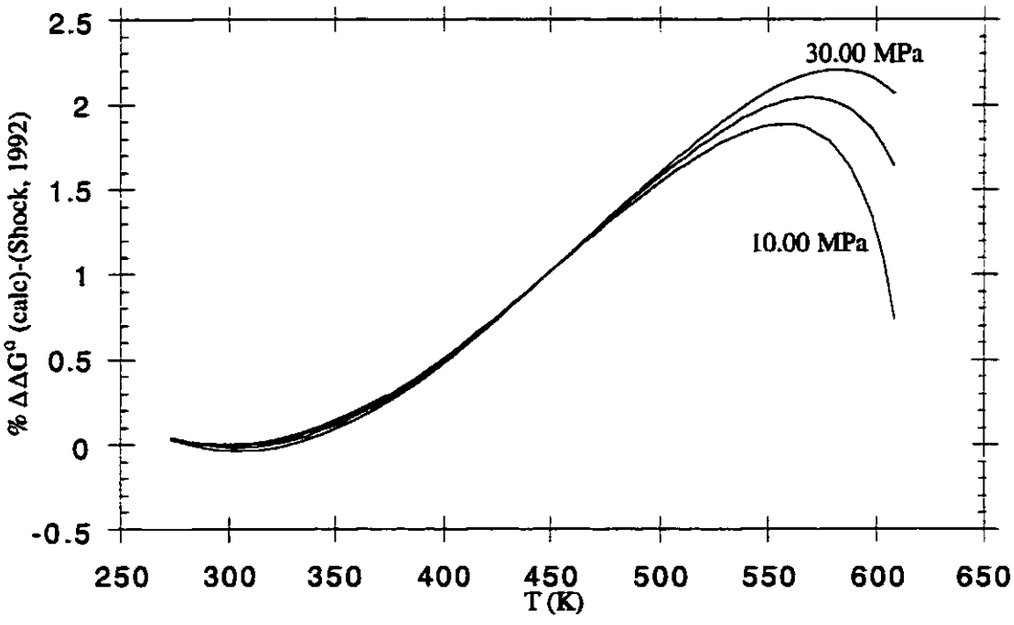

predicted Gibbs energies of formation for aqueous species involved in reactions 7.3 and 7.4. The results of our comparison show that while the HKF coefficients predicted by Shock (1992) and Shock and Helgeson (1990) may be robust for lower temperature (<400 K) Gibbs energy predictions, they may not be suited for predicting higher derivative properties. In addition it seems that first approximation predictions by Shock (1992) and Shock and Helgeson (1990) may not be suited for investigating equilibrium constants above 400 K. In general, results of empirically predicted equilibrium studies in this temperature range must be cautiously interpreted.

Using the partial molar Gibbs energy for the formation of water, as predicted by Helgeson & Kirkham (1974) and calculated partial molar Gibbs energies for the formation of aqueous glycine, glycylglycine, and diketopiperazine, we have calculated the Gibbs energy change for synthesis reactions 7.3 and 7.4. Figures 7.13 and 7.14 show the logarithm of the respective equilibrium constant as a function of temperature in the range of 273.15 to 608.15 K. These equilibrium constants have been calculated with the HKF coefficients from this investigation and those previously reported by Shock (1992). Both Shock (1992) and this investigation show an increase in dipeptide stability and cyclic dipeptide stability as temperature is increased. Our study also seems to indicate a larger pressure dependence on the equilibrium potential at high temperatures.

Figure 7.15 indicates that there is a Gibbs energy drive for the hydrolysis degradation of glycylglycine at all temperatures investigated within this study. As aqueous glycylglycine is not known to undergo fast hydrolysis in water at ambient temperature this hydrolysis reaction must be kinetically slow. Also, while kinetic rates for any reaction become faster at higher temperatures, the thermodynamic equilibrium for the formation of glycylglycine becomes more favourable at higher temperatures.

Figure 7.13 Temperature dependence of the equilibrium constant for the formation of aqueous glycylglycine up to 608.15 K and 0.10, 10.00, 20.00, and 30.00 MPa.

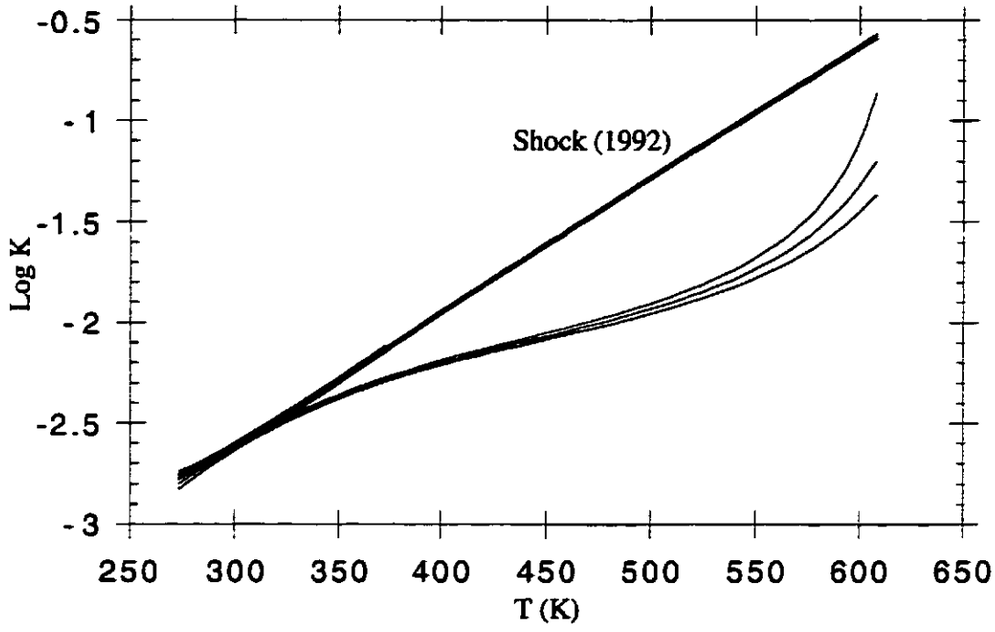

Figure 7.14 Temperature dependence of the equilibrium constant for the formation of aqueous diketopiperazine up to 608.15 K and 0.10, 10.00, 20.00, and 30.00 MPa.

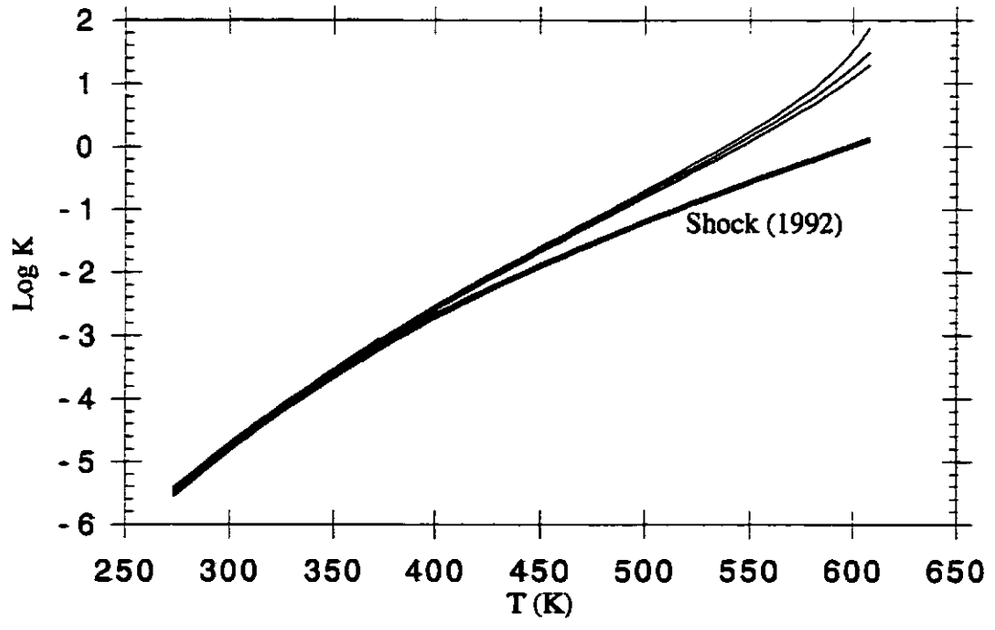

Figure 7.15 Change in Gibbs energy for the formation of aqueous glycylglycine and diketopiperazine from 273.15 to 608.15 K and at 0.10, 10.00, 20.00, and 30.00 MPa.

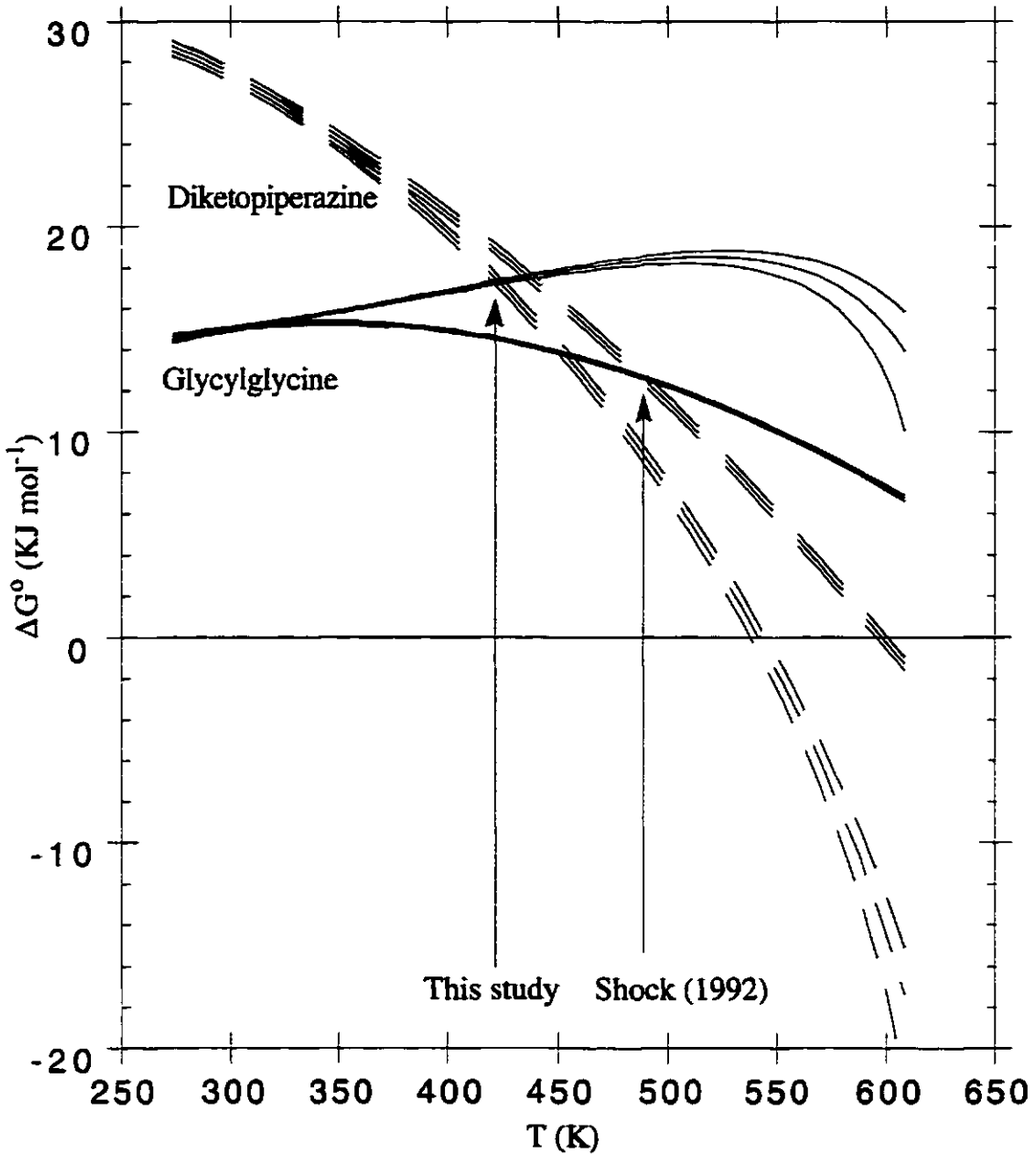

Glycylglycine may also survive to high temperatures since as figure 7.15 shows, the thermodynamic stability of diketopiperazine increases even faster than that of glycylglycine. Above ~420 K, the Gibbs energy change for the two diglycine polymers begins to favour diketopiperazine. Instead of a hydrolysis degradation to aqueous glycine

(the reverse of reaction 7.3), glycylglycine may simply form the more stable diketopiperazine in one step. Since at these higher temperatures thermodynamic equilibrium favours both the formation of aqueous diketopiperazine and free aqueous glycine, the reactions must be determined by kinetics. Because elementary reaction rates approach a maximum limit as temperature is increased, these results do not disagree with our previous discussion of aqueous glycylglycine degradation within our densimeter at 523 K. This apparent cyclic thermodynamic preference is also observed by Shock (1992). However, Shock (1992) predicts the point of thermodynamic preference change is at or near 590 K.

In concluding this study, we have found that equations which have maxima at the singular (228 K) point and the critical point of water are successful at modeling aqueous zwitter ionic amino acids and peptides over a large temperature and pressure range. Since the semi-empirical HKF equations of state exhibit these maxima and have been successful with modeling aqueous electrolytes, they are a fair choice for extrapolation beyond experimental data. However, extrapolations for higher derivative thermodynamic properties which are more sensitive to temperature and pressure are still poor, due to the lack of experimental data at higher temperatures and pressures.

Kohara *et al.* (1997) have shown that amino acid degradation at elevated temperatures and pressures is decreased dramatically by transfer from an aqueous solution to an aqueous solution with a high fugacity of hydrogen. High fugacities of hydrogen are indicative of hydrothermal vent environments. Therefore, the results of this study cannot implicate the thermodynamic stability of peptides in hydrothermal vent habitats. To draw such conclusions we would need to obtain measurements for a solvent environment similar to those of hydrothermal vents. Nevertheless our research is a necessary step to a more complete understanding of biochemical interactions within such unique environmental conditions.

8) CONCLUSIONS AND POSSIBLE FUTURE DIRECTIONS

The various studies presented within this thesis have indicated how more detailed and precise thermodynamic data can improve our understanding of the equilibrium properties of solutions beyond 298.15 K and 0.10 MPa. All conclusions have indicated that as theories within thermodynamics evolve with the availability of experimental data, investigators should cautiously interpret conclusions drawn from models which do not include the latest and most complete set of data. Unfortunately these selected investigations have also shown that the availability of experimental thermodynamic data is limited.

8.1 Aqueous electrolyte investigations

Although single ion partial molar volumes are fairly well defined for most electrolyte solutions at 298.15 K, there exists a need for more heat capacity data for the trivalent rare earth ions in water. The precision of infinite dilution extrapolations can be improved with modern measurements, since most previous heat capacity investigations were completed when calorimetric measurements lacked the necessary precision at lower concentrations. The data reported for the aqueous rare earth sulphates in this thesis may now be used by future investigators to understand how similar unstudied species may equilibrate with their environment.

Future studies could include measuring completely associated rare earth sulphates by addition of excess sulphate. Using a Picker microflow calorimeter, or a newer differential scanning calorimeter, these data could provide more precise heat capacity changes for the association reactions. In addition, current investigations could be complemented by the addition of data at temperatures removed from ambient. With respect to more detailed speciation investigations, which have been shown to be necessary for the interpretation of thermodynamic parameters, Raman spectroscopy could be utilised. With more investigations it may be possible to obtain good estimates of Pitzer ion interaction

coefficients,thus providing equations to calculate several thermodynamic properties over a wide temperature and pressure range.

8.1 Aqueous non-electrolyte investigations

The additivity analysis presented in Chapter 6 may be used as an aid to predicting thermodynamic properties for several uncharacterised aqueous species. A future direction in this area could be to increase the input data set to include high temperature and pressure data. In other words, although the additivity scheme may be robust at temperatures below 328 K, Chapter 7 has shown that the HKF equations may model higher temperature data as well. Since electrostatic Born solvation theory is prominent in the higher temperature region and these terms were not treated as being additive, another future project could include reevaluating the same additivity scheme with new predictions for effective Born coefficients.

With respect to the investigation described in Chapter 7, as kinetic impedance on biological reactions becomes less of a factor at high temperature, thermodynamic characterisation becomes even more important to understanding high temperature aqueous biochemical behavior. While the general conclusions of equilibrium investigations obtained using first approximations of semi-empirical models may be consistent with experimental data, extrapolations have been shown to fail at higher temperatures. Although these equations should be robust for temperatures in excess of 400 K, they must be reevaluated on a regular basis. As some conclusions made from studies using these semi-empirical equations have been the source of controversy, e.g., amino acid stability (Bada *et al.*, 1995), more experimental investigations are required to defend claims. With respect to amino acid stability, several studies conclude that amino acids decompose to aliphatic amines and carbon dioxide. Others have reported that this amino acid instability may be reversed in hydrothermal vent conditions where the salinity is higher and the pH is different from that of pure water. To address the need for further investigations of these claims,

volumetric and heat capacity data could be obtained for some aliphatic amines. In addition, all species could be measured in sea water and appropriate thermodynamic transfer properties could be calculated. Finally it is noted that high temperature and pressure apparent molar heat capacity investigations for aqueous glycine solutions are currently underway.

APPENDIX A. C++ CODE FOR AUTOMATED ANALYSIS PROGRAM DISCUSSED IN CHAPTER 4

A.1 1 The program tubeopt

```
#include <stdlib.h>
#include <fstream.h>
#include <string.h>
#include <iostream.h>
#include "vtdsr.h"

// Tubeopt goes through spectra using the stacker package to bring in data
// and finds the derivative using the VTDSR package. Each group of points
// or window is brought in and regressed linearly with time. The slopes are
// tested with a standard students t tests for a null hypothesis of zero.
// The p value (tolerance) is reduced untill the proper number of peaks
// are found. Once the tolerance is optimised for the spectrum, the data
// file is opened again, and squared time period differences are calculated
// by the peak points and moveing baseline equation, which correlates
// temperature variance with time period variance. A further explanation
can
// be found in the Vibrating Tube Peak Analysis manual.

// Window width is the number of data points in the derivative window at a
time.
int width =4;
// Width2 is the width of the temperature correlation window.
int width2 = 151;
// Width and width2 must be odd numbers greater than one.
// A peak buffer region is the number of datum that are idnored on each
corner of
// a peak.
int pbuff=9;
// Add back numbers are a carry over from human analysis using spectra
calc.
// Untill this program is used permanently, add backs will be used due to
// the data colection program.
double add_back;

// Ncolumns is the amount of columns in the file of data
char file_enter[80];
int ncolumns = 3;
double tolerance = 0.005;

compute_derivative();

// Class special is a special type of comp_vector unique to this program.
```

```
// The special vector uses another vector which is coded to label base line
// points.  Only these baseline points are included in the special vector.
class special : public comp_vector
{
  public:
    special(window &n, power* CHECK, unsigned int colum, int a)
   {
       long double *temp_vector = new long double[int(CHECK->_length())];
      int i;
      node *term = n.head;
      int r=0;
      for(i=0; i<(CHECK->_length()); i++)
      {
         term = term->next;
         if((int(CHECK->value(i))==0)&&(int(CHECK->value(i-4))==0))
         {
             temp_vector[r]=pow(((*term)[colum]),a);
            r++;
         }
      }
      length = r;
      vector = new long double[length];
      for(i=0; i<length; i++){vector[i]=temp_vector[i];}
      delete temp_vector;
   }
};

main()
{
   // Obtaining the file name in order to open and read.
   cout << "Please enter the spectrum file root name? ";
   cin >> file_enter;
   cout << "Please enter the number of peaks (100 MAX.) for derivative
optimization? ";
   int peak_count;
   cin >> peak_count;
   cout << "Please enter the `add back' period for this run?";
   cin >> add_back;
   cout.setf(ios::fixed,ios::floatfield);
   cout.precision(3);

   // Lower tolerance or alpha level until number of peaks matches the
   // number of peaks which should be in the spectrum.
   int count_peaks = peak_count*2+2;
  do
  {
     if(tolerance<0.000009)
     {
          cerr << "The spectrum is too messy for statistical analysis with\n";
```

```
        cerr << "the current parameters.  Either the increase the
window\n";
        cerr << "width within the program or choose peaks and
baselines\n";
       cerr << "by observation." << endl;
        exit(EXIT_FAILURE);
    }
    if(tolerance>0.00009){tolerance -= 0.00005;}
    else{tolerance -= 0.000005;}
     count_peaks=compute_derivative();
 }
  while(peak_count<(count_peaks/2));

 // Check that all peaks are in spectrum
 if (((peak_count*2)>count_peaks))
 {
    cerr << "Not enough peaks or some speaks too small.\n";
    cerr << "Must choose peaks and baselines by observation or reduce ";
    cerr << "the number of peaks.\n" << endl;
    exit(EXIT_FAILURE);
 }

 double *difference = new double[peak_count];
 double *diffsquare = new double[peak_count];
 double *temperature = new double[peak_count];
 double *temphigh = new double[peak_count];
 double *templow = new double[peak_count];
 int *peak_points = new int[peak_count];

 int r;
 for(r=0; r<peak_count; r++)
 {
    difference[r]=0;
    diffsquare[r]=0;
    temperature[r]=0;
    temphigh[r]=0;
    templow[r]=1000;
    peak_points[r]=0;
 }

 // open windows for the derivative file and the data file.
 // Output a report file (more detailed than screen output.)
 char file_name[80], file_dp[80], file_rep[80];
 for (r=0;r<80;r++)
 {
     file_name[r] = file_enter[r];
    file_dp[r] = file_enter[r];
    file_rep[r] = file_enter[r];
 }
```

```
 strcat(file_name,".prn");
 strcat(file_dp,".dt");
 strcat(file_rep,".rep");
 ofstream orfile(file_rep);
 orfile.setf(ios::fixed,ios::floatfield);
 orfile.precision(3);
 ifstream *ifile = new ifstream(file_name);
 ifstream *idpfile = new ifstream(file_dp);

 // Testing whether the files were opened for reading.
 if ((!(*ifile).good()) | | (!(*idpfile).good()))
 {
    cerr << "The file " << file_name
         << " could not be opened for reading." << endl;
    exit(EXIT_FAILURE);
 }

  window temp_corr(*ifile, width2, ncolumns);
  window peak_choice(*idpfile, width2, 4);
 do
 {
    power *CHECK = new power(peak_choice, width2, 3, 1);
   if(((CHECK->value((width2-1)/2))>0)&&((CHECK->value((width2-
1)/2+pbuff))>0)
      &&((CHECK->value((width2-1)/2-pbuff))>0))
   {
      power *PERIOD = new power(temp_corr, width2, 1, 1);
      power *TEMP = new power(temp_corr, width2, 2, 1);
      special *REF_PERIOD = new special(temp_corr, CHECK, 1, 1);
      special *REF_TEMP = new special(temp_corr, CHECK, 2, 1);
      special *REF_TEMP2 = new special(temp_corr, CHECK, 2, 2);

       comp_vector *intercept = new comp_vector(temp_corr,
                              (REF_PERIOD->_length()));
      equation *temp_quad = new equation(3, *REF_PERIOD);
      temp_quad->take(0, *intercept);
      temp_quad->take(1, *REF_TEMP);
      temp_quad->take(2, *REF_TEMP2);
        temp_quad->solve_gauss_jordan_reduction();

      // compution of the difference in squared time periods
      double temp_point = (TEMP->value((width2-1)/2));
      double P_peak = (PERIOD->value((width2-1)/2));
      P_peak += add_back;
      int peak_no = (CHECK->value((width2-1)/2));
      double P_not=0;
      P_not += (temp_quad->coeff(0));
       P_not += (temp_quad->coeff(1))*temp_point;
        P_not += (temp_quad->coeff(2))*temp_point*temp_point;
```

```
        P_not += add_back;
         difference[peak_no-1] += ((pow(P_peak,2))-(pow(P_not,2)));
         diffsquare[peak_no-1] += pow(((pow(P_peak,2))-(pow(P_not,2))),2);
         temperature[peak_no-1] += temp_point;
         if((temphigh[peak_no-1])<(TEMP->max()))
        {
            temphigh[peak_no-1] = (TEMP->max());
        }
         if(templow[peak_no-1]>(TEMP->min()))
        {
            templow[peak_no-1] = (TEMP->min());
        }
         peak_points[peak_no-1]++;
        orfile << peak_no << "\t";
        orfile << temp_point << "\t";
        orfile << P_not << "\t";
        orfile << P_peak << "\t";
        orfile << ((pow(P_peak,2))-(pow(P_not,2))) << "\t";
         orfile << (temphigh[peak_no-1]-templow[peak_no-1]) << "\t";
         orfile << peak_points[peak_no-1] << "\n";
       delete PERIOD;
       delete TEMP;
       delete REF_PERIOD;
       delete REF_TEMP2;
       delete intercept;
       delete temp_quad;
    }
    delete CHECK;
      temp_corr.move(*ifile, ncolumns);
     peak_choice.move(*idpfile, 4);
}
while ((!(*idpfile).eof())&&(!(*ifile).eof()));

// compute mean peak differences and report

cout << "\n\n\t\t\tVIBRATING TUBE SPECTRUM ANALYSIS\n"
   <<"\t\t\t\t    1997\n\n"
     << "Spectrum file was `" << file_enter << ".prn'.\n\n"
     << "Analysis was looking for " << peak_count << " peaks.\n\n"
     << "The derivative required a " << (1-tolerance)*100 << "% confidence"
     << " level for the isolation of " << peak_count << " peaks.\n\n\n"
    << "Peak No. \tTemp (K) \tT Drift \tDiff. \t\t(95%)SE Diff. \n";
orfile << "\n\n\t\t\tVIBRATING TUBE SPECTRUM ANALYSIS\n"
    <<"\t\t\t\t    1997\n\n"
      << "Spectrum file was `" << file_enter << ".prn'.\n\n"
      << "Analysis was looking for " << peak_count << " peaks.\n\n"
      << "The derivative required a " << (1-tolerance)*100 << "% confidence"
      << " level for the isolation of " << peak_count << " peaks.\n\n\n"
     << "Peak No. \tTemp (K) \tT Drift \tDiff. \t\t(95%)SE Diff. \n";
```

```
    double t_factor, sd_dev, var;
    for(r=0; r<peak_count; r++)
    {
       cout << (r+1) << "\t\t"
            << temperature[r]/peak_points[r] << "\t\t"
            << (temphigh[r]-templow[r]) << "\t\t"
            << difference[r]/peak_points[r] << "\t";
       orfile << (r+1) << "\t\t"
            << temperature[r]/peak_points[r] << "\t\t"
            << (temphigh[r]-templow[r]) << "\t\t"
            << difference[r]/peak_points[r] << "\t";
       t_factor = 2;
        // (alpha_t_dist(0.05, (peak_points[r]-1)));
        if((temphigh[r]-templow[r])<0){cout << "false peak" << "\n";}
        var = (diffsquare[r]-(difference[r])*(difference[r])/peak_points[r]);
       var /= (peak_points[r]-1);
       sd_dev = sqrt(var);
       cout << (t_factor*sd_dev) << "\n";
       orfile << (t_factor*sd_dev) << "\n";
    }
    delete ifile;
    delete idpfile;
    delete difference;
    delete diffsquare;
    delete temperature;
    delete temphigh;
    delete templow;
    delete peak_points;
    return (EXIT_SUCCESS);
}

compute_derivative()
{
    // A `.dt' file is a file containing derivative information.
    char file_name[80], file_out[80];
    int r;
    for (r=0;r<80;r++)
    {
        file_name[r] = file_enter[r];
        file_out[r] = file_enter[r];
    }
     strcat(file_name,".prn");
     strcat(file_out,".dt");
     ofstream ofile(file_out);
     ofile.setf(ios::fixed,ios::floatfield);
     ofile.precision(3);
     cout << tolerance*100 << endl;
     ifstream *ifile = new ifstream(file_name);
```

```
// Testing whether the file was opened for reading.
if (!(*ifile).good())
{
    cerr << "The file " << file_name
         << " could not be opened for reading." << endl;
    exit(EXIT_FAILURE);
}

 window range(*ifile, width, ncolumns);
int count_peaks = 0;
int true_null = 0;
int false_null = 0;
double old_slope = 0;
double base_se=0.005;
int choice=0;
do
{
    // Vector containing y data is PERIOD.
    power *PERIOD = new power(range, width, 1, 1);
     comp_vector *intercept = new comp_vector(range, width);
    power *TIME = new power(range, width, 0, 1);

   equation *dperioddt = new equation(2, *PERIOD);
   dperioddt->take(0,*intercept);
   dperioddt->take(1,*TIME);

    // Computing values for regression analysis
     dperioddt->solve_gauss_jordan_reduction();
   dperioddt->uncertainties();

   double dTdt;
   dTdt = (dperioddt->coeff(1));

   // Choices are 0 for baseline, 0> for peaks, and -1 for slopes.
   // Test for slope by t-test at alpha level according to tolerance.
   double stat_t=0, p_value_t=0;
   stat_t=(dTdt)/(base_se);
    p_value_t = 1-(t_probability(stat_t, dperioddt->df_res()));
     if (p_value_t<tolerance){false_null++;true_null=0;}
     else{true_null++;false_null=0;base_se=(.001);}

   if((false_null==3)&&(choice!=-1))
  {
     choice=-1;
     count_peaks++;
     old_slope=dTdt;
  }
  if((true_null==3)&&(choice==-1)&&(old_slope>0))
  {
```

```
        choice=(count_peaks+1)/2;
      }
      if((true_null==3)&&(choice==-1)&&(old_slope<0)){choice=0;}

      // Print info to dt file
      ofile << TIME->value((width-1)/2) << "\t";
      ofile << PERIOD->value((width-1)/2)+add_back << "\t";
      ofile << dTdt << "\t";
      // ofile << (base_se) << "\t";
      // ofile << stat_t << "\t";
      // ofile << p_value_t << "\t";
      ofile << choice << "\n";

      // move window
      delete PERIOD;
      delete intercept;
      delete TIME;
      delete dperioddt;
       range.move(*ifile, ncolumns);
   }
   while (!(*ifile).eof());
   delete ifile;
    return(count_peaks);
}
```

A.2 Object and subroutine libraries VTDSR and STACKER

VTDSR.H

```
#ifndef __vtdsr__
#define __vtdsr__
#include <math.h>
#include "stacker.h"

double t_probability(long double, int);
double alpha_t_dist(long double, int);
double F_probability(long double, int, int);
double alpha_F_dist(long double, int, int);
long double betai(long double, double, double);
long double betacf(long double, double, double);

class equation;

// comp_vector is a base class for all function component vectors.
// The idea is that future functions may be complicated, therefore, functions
// are defined by derived classes.  comp_vector is constant or a possible
// future unit vector where f(x) = 1
class  comp_vector
{
 protected:
   unsigned int length;
   long double* vector;
 public:
   friend ostream& operator << (ostream &, comp_vector &);
   friend node;
   friend equation;
   comp_vector() {};
   comp_vector(window &, unsigned int);
   long double dot_product(comp_vector &);
   int _length();
   long double mean();
   long double stdev();
   double min();
   double max();
   double value(unsigned int);
   virtual ostream& info(ostream &);
   ~comp_vector();
};

// Class power is a function component vector where the function is a x^n
class power : public comp_vector
{
    unsigned colum_no;
```

```
   int power1;
  public:
    power(window &, unsigned int, unsigned int, int);
    ostream& info(ostream &);
};

// Class cross is a function component vector where the function is a
// multiplication of another variable within the node data. e.g., x1^n*x2^m
// This would be a dot product of colums.
class cross : public comp_vector
{
     unsigned int colum_no, colum_no2;
    int power1, power2;
  public:
    cross(window &, unsigned int, unsigned int, int, unsigned int, int);
    ostream& info(ostream &);
};

// Class equation forms a system of singular type matrix equation Mx=b to
be
// solved by Gaussian Elimination (Gauss-Jordan). Equation takes its
values
// from function vectors which have already been specified as independent
// variables. This allows for the system of equations to be solved by equation
// multiplication with a vector, b, containing the dependent variable.
class equation
{
    unsigned int dimension;
    long double **A, SSres, SSreg, SSy;
    comp_vector** input_vectors;
    comp_vector* y;
  public:

    // creating a single matrix equation to be solved.
    equation(unsigned int, comp_vector &);
    // assigning component vectors to input into the equation
    void take(unsigned int, comp_vector &);
    void full();
    // Solve_gauss_jordan_reduction solves a single matrix set of equations
    // with full pivoting, by scaning for large matrix elements.
     void solve_gauss_jordan_reduction();
    // Computing the SSreg, SSres, and SSy to be used for error calculations.
    void uncertainties();
    long double R_squared();
    long double adj_R_squared();
    unsigned int df_res();
    unsigned int df_reg();
    long double sum_square_reg();
    long double sum_square_res();
```

```
    long double mean_square_reg();
    long double mean_square_res();
   long double F_factor();
   double equation::coeff(int);
    double equation::se_coeff(int);
  void test();
  ~equation();
};


equation::equation(unsigned int i, comp_vector &where_is_y)
{
   dimension = i;
   A = new long double*[dimension];
   y = &where_is_y;
  int j;
    input_vectors = new comp_vector*[dimension];
    for (j=0;j<dimension;j++)
  {
      A[j]=new long double[(2*dimension+1)];
     int z;
      for (z=0;z<=(2*dimension);z++) {A[j][z]=NULL;}
      input_vectors[j]=NULL;
  }
}

equation::~equation()
{
  int j;
   for (j=0;j<dimension;j++){delete [] A[j];}
  delete [] A;
  delete [] input_vectors;
}

void equation::take(unsigned int i, comp_vector &vectori)
{
  input_vectors[i] = &vectori;
  int j;
  unsigned int fill=0;
   for (j=0;j<dimension;j++)
  {
      if ((input_vectors[j]!=NULL) {fill++;}
  }
   if (fill==dimension) {full();}
   return;
}

void equation::full()
{
```

```
   int n, j;
   for (j=0;j<dimension; j++)
   {
      for (n=0;n<dimension; n++)
      {

         A[j][n]=(*(input_vectors[n])).dot_product(*(input_vectors[j]));
        if(j==n) {A[j][dimension+j]=1;}
      }
       A[j][2*dimension]=(*input_vectors[j]).dot_product(*y);
   }
}

void  equation::solve_gauss_jordan_reduction()
{
   // Forward elimination with partial pivot
   int z, j, k, max;
   long double t;
   for (z=0; z<dimension; z++)
   {
      // Partial Pivot
      // scan for largest value in colum z
      max = z;
      for (j = z+1; j<dimension; j++)
      {
         if (abs(A[j][z]) > abs(A[max][z])) {max = j;}
      }
      // swap row with largest z colum value for row z in A and b.
      for (k = z; k<=2*dimension; k++)
      {
         t = A[z][k];
         A[z][k] = A[max][k];
         A[max][k] = t;
      }
      // Forward Elimination
      for (j = z+1; j<dimension; j++)
      {
         for (k = 2*dimension; k>=z; k--)
         {
            A[j][k] -= A[z][k]*A[j][z]/A[z][z];
         }
      }
   }
   // Back elimination
   for (z=dimension-1; z>=0; z--)
   {
      for (j = z-1; j>=0; j--)
      {
         for (k=2*dimension; k>=0; k--)
```

```
        {
            A[j][k] -= A[z][k]*A[j][z]/A[z][z];
        }
      }
   }
    for (z=0;z<dimension;z++)
   {
      for (j=2*dimension; j>=0; j--){A[z][j]/=A[z][z];}
   }
}

void equation::uncertainties()
{
   // SSres
   int j,k;
    for (j=0;j<y->length;j++)
   {
      long double est= (-1)*y->vector[j];
       for (k=0;k<dimension;k++)
      {
          est+= ((input_vectors[k])->vector[j])*A[k][2*dimension];
      }
      SSres+=pow(est, 2);
   }
   // calc of SSy
   SSy = pow(((*y).stdev()),2)*(y->length-1);
   // calc of SSreg
   SSreg = SSy - SSres;
}

long double equation::sum_square_reg(){return (SSreg);}
long double equation::sum_square_res(){return (SSres);}
long double equation::mean_square_reg(){return (SSreg/df_reg());}
long double equation::mean_square_res(){return (SSres/df_res());}
unsigned int equation::df_res(){return (y->length-df_reg()-1);}
unsigned int equation::df_reg(){return (dimension-1);}
long double equation::F_factor()
{
    return(R_squared()/(df_reg())/((1-R_squared())/(df_res())));
}
long double equation::R_squared(){return (1-SSres/SSy);}
long double equation::adj_R_squared()
{
    return(1-mean_square_res()/(SSy/(df_reg()+df_res())));
}


double equation::coeff(int x)
{
```

```
    return (A[x][dimension+dimension]);
}

double equation::se_coeff(int x)
{
    return (sqrt(A[x][x+dimension]*mean_square_res()));
}

void equation::test()
{
   int j, k;
    for (j=0;j<dimension; j++)
   {
      cout << "Function vector " << j << "\n" << *(input_vectors[j]);
   }
   cout << "\n The equation looks like \n";
    for (j=0;j<dimension; j++)
   {
       for (k=0;k<dimension; k++) {cout << (A[j])[k] << "\t";}
      cout << "\n";
   }
    for (j=0;j<dimension; j++)
   {
       for (k=0;k<=dimension; k++) {cout << (A[j])[k+dimension] << "\t";}
      cout << "\n" << endl;
   }
   cout << "Sum Square Regression= " << SSreg << "  df= " << df_reg() <<
"\n";
   cout << "Sum Square Residuals= " << SSres<< "  df= " << df_res() << endl;
    cout << "Mean Square Regression= " << mean_square_reg() << "\n";
    cout << "Mean Square Residuals= " << mean_square_res() << endl;
   cout << "SE= " << sqrt(mean_square_res()) << endl;
   cout << "Unadjusted R Squared= " << R_squared() << endl;
    cout << "Adjusted R Squared= " << adj_R_squared() << endl;
   cout << "F factor= " << F_factor() << endl;
   cout << t_probability(2.131,15) << endl;
   cout << alpha_t_dist(0.05,15) << endl;
   cout << F_probability(3.09,6,11) << endl;
   cout << alpha_F_dist(0.05,6,11) << endl;
}

comp_vector::comp_vector(window &n, unsigned int l)
{
   length = l;
   vector = new long double[length];
   int i;
   for (i=0; i<length; i++){vector[i] = 1;}
}
```

```
comp_vector::~comp_vector()
{
   delete [] vector;
}

long double comp_vector::dot_product(comp_vector &B1)
{
   if ((length)!=(B1.length))
   {
      cerr << "Function only handles vectors of same length." << endl;
      exit(EXIT_FAILURE);
   }
   int j;
   long double product = 0;
   for (j=0;((j<(length))&&(j<(B1.length)));j++)
   {
      product = product + (vector[j]) * (B1.vector[j]);
   }
   return product;
}

power::power(window &n, unsigned int l, unsigned int colum, int a)
{
   length = l;
    colum_no=colum;
   power1 = a;
   vector = new long double[length];
   int i;
   node *term = n.head;
   for (i=0; i<length; i++)
   {
      term = term->next;
       vector[i] = pow (((*term)[colum_no]),(power1));
   }
}

cross::cross(window &n, unsigned int l, unsigned int colum, int a1,
unsigned int
         colum2, int a2)
{
   length = l;
    colum_no = colum;
    colum_no2 = colum2;
   power1 = a1;
   power2 = a2;
   vector = new long double[length];
   int i;
   node *term = n.head;
   for (i=0; i<length; i++)
```

```
  {
     term = term->next;
     vector[i] =

pow(((*term)[colum_no]),((power1)))*pow(((*term)[colum_no2]),(power2));
  }
}

int comp_vector::_length(){return(length);}

long double comp_vector::mean()
{
   int j;
   long double tmp = 0;
    for (j=0;j<length;j++){tmp+=vector[j];}
   tmp/=length;
   return tmp;
}

long double comp_vector::stdev()
{
   long double tmp = 0;
   long double avg = mean();
   int j;
    for (j=0;j<length;j++){tmp += pow((vector[j]-avg),2);}
   tmp/=(length-1);
   tmp = sqrt(tmp);
   return tmp;
}

double comp_vector::min()
{
   int j;
   long double m = vector[0];
    for (j=1;j<length;j++)
   {
      if (vector[j]<m) {m=vector[j];}
   }
    return m;
}

double comp_vector::max()
{
   int j;
   long double m = vector[0];
    for (j=1;j<length;j++)
   {
      if (vector[j]>m) {m=vector[j];}
   }
```

```
    return m;
}

double comp_vector::value(unsigned int r) {return vector[r];}

ostream& comp_vector::info(ostream &printing)
{
    printing << "Constant" << "\n";
    return(printing);
}

ostream& power::info(ostream &printing)
{
    printing << "Data from colum " << colum_no << " f(x)=x^" << power1 <<
"\n";
    return(printing);
}

ostream& cross::info(ostream &printing)
{
    printing << "Data from colums " << colum_no << " & " << colum_no2;
    printing << "   f(x)=x1^" << power1 << "x2^" << power2 << "\n";
    return(printing);
}

ostream& operator << (ostream &printing, comp_vector &n)
{
   int i;
    printing << n.info(printing);
    return(printing);
}

// Returns a two tailed probability corresponding to a given t
double t_probability(long double t, int v)
{
   long double x= double(v)/double(v+t*t);
   return(1-betai(x,double(v)/double(2),0.5));
}

// Returns a t value corresponding to given two tailed alpha level
// good for + or - 0.000001 alpha level
double alpha_t_dist(long double alpha, int v)
{
   long double eps = 0.5;
   long double prob = 1-alpha;
   long double est;
   long double t = 0.000001;
   while (fabs(eps)>0.000001)
   {
```

```
      est = t_probability(t,v);
      if (fabs(est-prob)<fabs(eps)*1.000001) {eps/=2;}
      if ((est-prob)<0) {t+=eps;}
      if ((est-prob)>0) {t-=eps;}
   }
   return (t-eps);
}

// Returns a given alpha corresponding to a given F
double F_probability(long double F, int v1, int v2)
{
   long double x= double(v2)/double(v2+v1*F);
   return(betai(x,double(v2)/2,double(v1)/2));
}
// Returns a given F value corresponding to a given alpha level
// good for + or - 0.000001 alpha level
double alpha_F_dist(long double alpha, int v1, int v2)
{
   long double eps = 0.5;
   long double est;
   long double F = 0.000001;
   while (fabs(eps)>0.000001)
   {
      est = F_probability(F,v1,v2);
      if (fabs(est-alpha)<fabs(eps)*1.000001) {eps/=2;}
      if ((est-alpha)<0) {F-=eps;}
      if ((est-alpha)>0) {F+=eps;}
   }
   return (F-eps);
}
// Incomplete beta function for t-distribution and F-distribution.
// Algorithym taken almost directly from Numerical Recipies, 1987,
// P-166-168
long double betai(long double x, double a, double b)
{
   long double BT;
   if ((x<0)||(x>1))
   {
      cerr << "Bad argument in beta" << endl;
      exit(EXIT_FAILURE);
   }
   if ((x==0)||(x==1)) {BT=0;}
   else
   {
      // factor in front of continued fraction
       BT=(exp(lgamma(a+b)-lgamma(a)-lgamma(b))*pow(x,a)*pow((1-x),b));
   }
   if(x<((a+1)/(a+b+2)))
   {
```

```
      // continued fraction
      return (BT*betacf(x,a,b)/a);
   }
   else
   {
      // continued fraction after symetry transformation
      return (1-BT*betacf((1-x),b,a)/b);
   }
}
// Continued fraction evaluation routine used for betai function
// Source is in notes for betai
long double betacf(long double x, double a, double b)
{
   int M;
   int itmax=100;
   double eps = 0.0000003;
   long double D, AP, BP, APP, BPP, AOLD;
   long double AM =1;
   long double BM =1;
   long double AZ =1;
   // first two factors 1 and d1
   long double BZ = 1-(a+b)*x/(a+1);
   // continued fraction
   for (M=1; M<itmax; M++)
   {
      // even factor
      D=M*(b-M)*x/((a+2*M-1)*(a+2*M));
      // one step (even) of recurrence
      AP=AZ+D*AM;
      BP=BZ+D*BM;
      // odd factor
      D=-(a+M)*(a+b+M)*x/((a+2*M)*(a+2*M+1));
      // next step in (odd) of recurrence
      APP = AP+D*AZ;
      BPP = BP+D*BZ;
      // save old answer
      AOLD = AZ;
      // renormalize
      AM = AP / BPP;
      BM = BP / BPP;
      AZ = APP / BPP;
      BZ = 1;
      // check for end of iteration
      if ((fabs(AZ-AOLD))<(eps*fabs(AZ))) {M=itmax;}
   }
   return AZ;
}
#endif //  __vtdsr__
```

STACKER.H

```
#ifndef __stacker__
#define __stacker__

#include <stdlib.h>
#include <new.h>
#include <iostream.h>

class window;
class comp_vector;
class power;
class cross;
class special;

class node
{
   int n;
    double* data_num;
   node *next;
  public:
    friend ostream& operator << (ostream &, node &);
    friend ostream& operator << (ostream &, window &);
    friend window;
    friend comp_vector;
    friend power;
    friend cross;
    friend special;

    node(){data_num = NULL;};
    ~node(){delete [] data_num;};
    node(double*, int);
    node(const node &);
    node & operator = (const node & );
    double operator[] (unsigned int s);
};

class window
{
    node *head, *z;
    unsigned int width;
 public:
    friend ostream& operator << (ostream &, window &);
    friend ifstream ifile(char);
    friend comp_vector;
    friend power;
    friend cross;
    friend special;
    window(ifstream &, int, int);
```

```
    ~window();

    void pop();
    void push(ifstream &, int);
    void move(ifstream &, int);

    // int empty;
};

node::node(double data_entry[], int a)
{
    n = a;
    data_num = new double[n];
    int i;
    for (i=0; i<n; i++) {data_num[i] = data_entry[i];}
}
node::node(const node &dumy)
{
    data_num = new double[n];
    n = dumy.n;
    int i;
    if (dumy.data_num!=NULL)
    {
        for (i=0; i<n; i++) {data_num[i] = dumy.data_num[i];}
    }
}
node & node::operator = (const node &dumy)
{
    n = dumy.n;
    int i;
    data_num = new double[n];
    if (dumy.data_num!=NULL)
    {
        for (i=0; i<n; i++) {data_num[i] = dumy.data_num[i];}
    }
    return(*this);
}
double node::operator[] (unsigned int s)
{
    if (s>n) {cerr << "Node does not have colum " << s;}
    return (data_num[s]);
}
ostream& operator << (ostream &printing, node &dumy)
{
    int i;
    for (i=0; i<dumy.n; i++)
    {
        printing << dumy.data_num[i] << "\t";
    }
```

```
    return(printing);
}

window::window(ifstream &ifile, int max, int data_colum)
{
   head = new node;
   z = new node;
   head->next = z;
   z->next = z;
   width = max;

   // When a window is opened it is filled with the first max data points.
   int i;
    for (i=1;i<=max;i++)
   {
      // test file for enough data to fill at least one window
      if (ifile.eof())
      {
          cerr << "This file does not have enough data." << endl;
          exit(EXIT_FAILURE);
      }

       push(ifile, data_colum);
   }
}
window::~window()
{
   node *t = head;
   while (t != z)
   {
      head = t;
      t = t->next;
      delete head;
   }
}
void window::push(ifstream &ifile, int data_colum)
{
    double *data_in = new double[data_colum];
   // Read in a node from the ifile and then insert it into the linked list
   // just after the head.

   int i;
    for (i=0; i<data_colum; i++)
   {
      ifile >> data_in[i];
   }
    node v(data_in, data_colum);

   delete [] data_in;
```

```
    node *t = new node;
    *t = v;

    t->next = head->next;
    head->next = t;
}
void window::pop()
{
    // This function removes the first node into a full window.
    // 'term' is node which will be just before z and 'terminate' is node to be
    // removed from the tail ie FIFO
    // pop must be used before push
    int i;
    node *term = head;
    for (i=1;i<width;i++){term = term->next;}
    node *terminate = term->next;
    term->next = terminate->next;
    delete terminate;
}
void window::move(ifstream &ifile, int data_colum)
{
    // test file for next data point
    if (ifile.eof())
    {
        cerr << "This file does not have any more data." << endl;
        exit(EXIT_FAILURE);
    }
    pop();
     push(ifile, data_colum);
}

ostream& operator << (ostream &printing, window &n)
{
    int i;
    node *term = n.head;
    for (i=1;i<=n.width;i++)
    {
        term = term->next;
        printing << *term << "\n";
    }
     return(printing);
}
#endif //   __stacker__
```

APPENDIX B. SPECIATION CALCULATION RESULTS FOR THE AQUEOUS RARE EARTH SULPHATES.

The following relationships and equations were required for equilibrium speciation calculations.

Equilibrium relationships:

$$R^{3+} + SO_4^{2-} \rightleftharpoons RSO_4^+$$

$$K\{RSO_4^+\} = \frac{[RSO_4^+]\gamma_{RSO_4^+}}{[SO_4^{2-}]\gamma_{SO_4^{2-}}[R^{3+}]\gamma_{R^{3+}}} \quad \text{(B.1)}$$

$$RSO_4^+ + SO_4^{2-} \rightleftharpoons R(SO_4)_2^-$$

$$K\{R(SO_4)_2^-\} = \frac{[R(SO_4)_2^-]\gamma_{R(SO_4)_2^-}}{[RSO_4^+]\gamma_{RSO_4^+}[SO_4^{2-}]\gamma_{SO_4^{2-}}} \quad \text{(B.2)}$$

$$H^+ + SO_4^{2-} \rightleftharpoons HSO_4^-$$

$$K_a = \frac{[HSO_4^-]\gamma_{HSO_4^-}}{[H^+]\gamma_{H^+}[SO_4^{2-}]\gamma_{SO_4^{2-}}} \quad \text{(B.3)}$$

$$H^+ + OH^- \rightleftharpoons H_2O$$

$$K_w = [H^+]\gamma_{H^+}[OH^-]\gamma_{OH^-} \quad \text{(B.4)}$$

Mass balance:

$$m\{R^{3+}{}_{Total}\} = \frac{m\{R_2(SO_4)_3\}}{2}$$

$$= [R^{3+}] + [RSO_4^+] + [R(SO_4)_2^-] \quad \text{(B.5)}$$

$$m\{SO_4^{2-}{}_{Total}\} = \frac{m\{R_2(SO_4)_3\}}{3}$$

$$= [SO_4^{2-}] + [HSO_4^-] + [RSO_4^+] + 2[R(SO_4)_2^-] \quad \text{(B.6)}$$

Charge balance:

$$[H^+] + 3[R^{3+}] + [RSO_4^+] = 2[SO_4^{2-}] + [HSO_4^-] + [R(SO_4)_2^-] + [OH^-] \quad \text{(B.7)}$$

Ionic acitivity coefficients:

$$\log \gamma_i = -\frac{z^2 A_\gamma \sqrt{I}}{1 + \sqrt{I}} + 0.2\, z^2 A_\gamma I \quad \text{(B.8)}$$

Table B.1 Calculated ion concentrations for aqueous $Y_2(SO_4)_3$ at 298.15 K.

$\{Y_2(SO_4)_3\}$ (mol kg^{-1})	Y^{3+} (mol kg^{-1})	YSO_4^+ (mol kg^{-1})	$Y(SO_4)_2^-$ (mol kg^{-1})	SO_4^{2-} (mol kg^{-1})	Other ions (mol kg^{-1})10^7
0.01346	0.006842	0.01307	0.007012	0.01329	2.479
0.01594	0.008011	0.01508	0.008790	0.01516	2.516
0.04031	0.01938	0.03230	0.02895	0.03074	2.754
0.04097	0.01968	0.03273	0.02955	0.03110	2.759
0.05437	0.02554	0.04120	0.04200	0.03791	2.842
0.07087	0.03230	0.05124	0.05821	0.04496	2.923
0.06878	0.03147	0.04998	0.05610	0.04414	2.914
0.08035	0.03595	0.05689	0.06786	0.04844	2.962
0.09120	0.03994	0.06329	0.07917	0.05197	3.001
0.09910	0.04273	0.06793	0.08755	0.05428	3.026

Table B.2 Calculated ion concentrations for aqueous $La_2(SO_4)_3$ at 298.15 K.

$\{La_2(SO_4)_3\}$ (mol kg^{-1})	La^{3+} (mol kg^{-1})	$LaSO_4^+$ (mol kg^{-1})	$La(SO_4)_2^-$ (mol kg^{-1})	SO_4^{2-} (mol kg^{-1})	Other ions (mol kg^{-1})10^7
0.005332	0.002369	0.006747	0.001549	0.006153	2.302
0.009481	0.003853	0.01148	0.003626	0.009708	2.405
0.01355	0.005326	0.01577	0.006002	0.01287	2.480
0.02025	0.007794	0.02233	0.01038	0.01767	2.574
0.02591	0.009908	0.02752	0.01439	0.02143	2.637
0.03226	0.01228	0.03307	0.01916	0.02537	2.697
0.02871	0.01096	0.03000	0.01647	0.02320	2.665
0.04052	0.01534	0.03999	0.02571	0.03014	2.763
0.04378	0.01653	0.04265	0.02839	0.03192	2.786
0.04896	0.01840	0.04679	0.03273	0.03463	2.820

Table B.3 Calculated ion concentrations for aqueous $Pr_2(SO_4)_3$ at 298.15 K.

$\{Pr_2(SO_4)_3\}$ (mol kg^{-1})	Pr^{3+} (mol kg^{-1})	$PrSO_4^+$ (mol kg^{-1})	$Pr(SO_4)_2^-$ (mol kg^{-1})	SO_4^{2-} (mol kg^{-1})	Other ions (mol kg^{-1})10^7
0.008265	0.002947	0.01055	0.003038	0.008174	2.364
0.01522	0.005099	0.01817	0.007175	0.01315	2.486
0.02543	0.008371	0.02823	0.01425	0.01954	2.605
0.03568	0.01172	0.03753	0.02212	0.02528	2.693
0.04408	0.01445	0.04475	0.02896	0.02958	2.752
0.05133	0.01678	0.05078	0.03509	0.03301	2.796
0.05990	0.01947	0.05774	0.04258	0.03679	2.841
0.06762	0.02184	0.06387	0.04953	0.03993	2.878
0.07876	0.02514	0.07255	0.05983	0.04408	2.924
0.08830	0.02786	0.07987	0.06887	0.04730	2.960

Table B.4 Calculated ion concentrations for aqueous $Nd_2(SO_4)_3$ at 298.15 K.

$\{Nd_2(SO_4)_3\}$ (mol kg^{-1})	Nd^{3+} (mol kg^{-1})	$NdSO_4^+$ (mol kg^{-1})	$Nd(SO_4)_2^-$ (mol kg^{-1})	SO_4^{2-} (mol kg^{-1})	Other ions (mol kg^{-1})10^7
0.01843	0.008207	0.02076	0.007887	0.01875	2.604
0.02642	0.01162	0.02831	0.01291	0.02512	2.705
0.03244	0.01416	0.03371	0.01701	0.02959	2.770
0.04646	0.01987	0.04568	0.02737	0.03896	2.892
0.06140	0.02553	0.05787	0.03940	0.04753	2.993
0.07260	0.02948	0.06677	0.04896	0.05313	3.056
0.08045	0.03210	0.07292	0.05587	0.05667	3.095
0.08983	0.03508	0.08021	0.06437	0.06054	3.137
0.09836	0.03766	0.08679	0.07227	0.06375	3.172
0.1175	0.04303	0.1014	0.09050	0.06998	3.264

Table B.5 Calculated ion concentrations for aqueous $Eu_2(SO_4)_3$ at 298.15 K.

$\{Eu_2(SO_4)_3\}$ (mol kg^{-1})	Eu^{3+} (mol kg^{-1})	$EuSO_4^+$ (mol kg^{-1})	$Eu(SO_4)_2^-$ (mol kg^{-1})	SO_4^{2-} (mol kg^{-1})	Other ions (mol kg^{-1})10^7
0.006817	0.002713	0.008901	0.002019	0.007510	2.346
0.008558	0.003293	0.01099	0.002833	0.009018	2.390
0.01024	0.003854	0.01294	0.003678	0.01041	2.426
0.01321	0.004859	0.01627	0.005296	0.01278	2.482
0.01455	0.005316	0.01773	0.006067	0.01380	2.504
0.01641	0.005951	0.01970	0.007167	0.01519	2.533
0.01851	0.006679	0.02188	0.008464	0.01673	2.563
0.02116	0.007599	0.02457	0.01016	0.01861	2.597
0.02267	0.008126	0.02607	0.01115	0.01965	2.615
0.02513	0.008985	0.02847	0.01280	0.02131	2.643

Table B.6 Calculated ion concentrations for aqueous $Dy_2(SO_4)_3$ at 298.15 K.

$\{Dy_2(SO_4)_3\}$ (mol kg^{-1})	Dy^{3+} (mol kg^{-1})	$DySO_4^+$ (mol kg^{-1})	$Dy(SO_4)_2^-$ (mol kg^{-1})	SO_4^{2-} (mol kg^{-1})	Other ions (mol kg^{-1})10^7
0.005773	0.002879	0.007198	0.001470	0.007182	2.335
0.01054	0.004864	0.01260	0.003624	0.01179	2.459
0.01762	0.007850	0.01987	0.007508	0.01796	2.586
0.02218	0.009794	0.02425	0.01031	0.02166	2.650
0.03044	0.01330	0.03177	0.01581	0.02793	2.746
0.03660	0.01586	0.03713	0.02020	0.03226	2.805
0.04586	0.01961	0.04492	0.02719	0.03828	2.882
0.04420	0.01895	0.04354	0.02590	0.03724	2.869
0.05176	0.02191	0.04976	0.03185	0.04182	2.925
0.05988	0.02496	0.05630	0.03851	0.04634	2.977

Table B.7 Calculated ion concentrations for aqueous $Ho_2(SO_4)_3$ at 298.15 K.

$\{Ho_2(SO_4)_3\}$ (mol kg^{-1})	Ho^{3+} (mol kg^{-1})	$HoSO_4^+$ (mol kg^{-1})	$Ho(SO_4)_2^-$ (mol kg^{-1})	SO_4^{2-} (mol kg^{-1})	Other ions (mol kg^{-1})10^7
0.009765	0.005049	0.01196	0.002524	0.01229	2.474
0.01566	0.007849	0.01840	0.005072	0.01844	2.602
0.02263	0.01118	0.02549	0.008582	0.02522	2.717
0.03116	0.01519	0.03370	0.01343	0.03292	2.829
0.03807	0.01832	0.04011	0.01772	0.03868	2.905
0.04680	0.02210	0.04799	0.02352	0.04539	2.987
0.05072	0.02373	0.05147	0.02624	0.04821	3.020
0.06501	0.02929	0.06396	0.03677	0.05753	3.127
0.06855	0.03059	0.06701	0.03951	0.05963	3.150
0.07327	0.03226	0.07107	0.04322	0.06231	3.180
0.07875	0.03413	0.07575	0.04763	0.06525	3.212

Table B.8 Calculated ion concentrations for aqueous $Lu_2(SO_4)_3$ at 298.15 K.

$\{Lu_2(SO_4)_3\}$ (mol kg^{-1})	Lu^{3+} (mol kg^{-1})	$LuSO_4^+$ (mol kg^{-1})	$Lu(SO_4)_2^-$ (mol kg^{-1})	SO_4^{2-} (mol kg^{-1})	Other ions (mol kg^{-1})10^7
0.007321	0.003150	0.009186	0.002305	0.008166	2.365
0.01374	0.005525	0.01623	0.005721	0.01354	2.497
0.02424	0.009506	0.02653	0.01244	0.02131	2.640
0.03752	0.01455	0.03836	0.02213	0.02994	2.767
0.05301	0.02022	0.05123	0.03458	0.03865	2.877
0.07570	0.02787	0.06913	0.05440	0.04916	2.998
0.1161	0.03961	0.09974	0.09290	0.06283	3.147
0.1551	0.04910	0.1286	0.1326	0.07169	3.245
0.2010	0.05860	0.1624	0.1811	0.07851	3.327
0.2617	0.06914	0.2071	0.2473	0.08362	3.401
0.3858	0.08592	0.3003	0.3855	0.09629	3.484
0.4345	0.09122	0.3377	0.4400	0.08571	3.501

APPENDIX C. STRUCTURES OF NEUTRAL ORGANIC SPECIES STUDIED IN CHAPTERS 6 AND 7.

For reference, this appendix contains simple diagrams of structures for the amino acids and peptides investigated in Chapters 6 and 7.

ALIPHATIC AMINO ACIDS

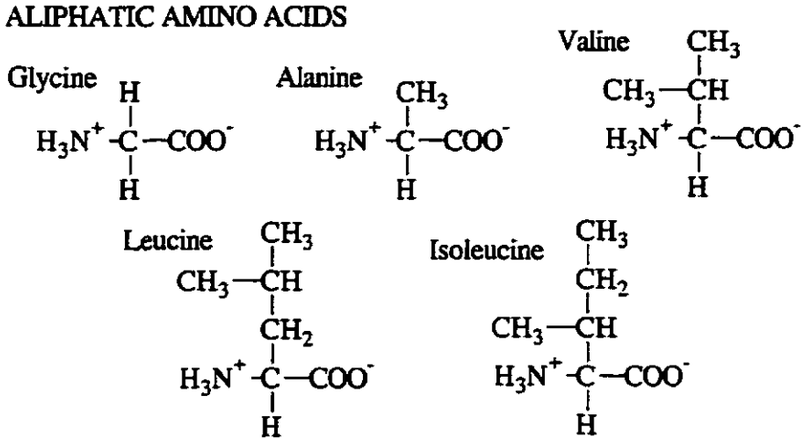

HYDROXYL OR SULPHUR CONTAINING AMINO ACID SIDE CHAINS

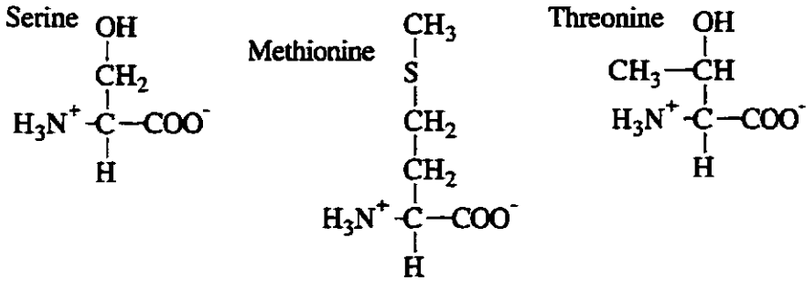

AROMATIC AMINO ACIDS

Phenylalanine

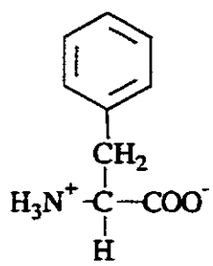

Tryptophan

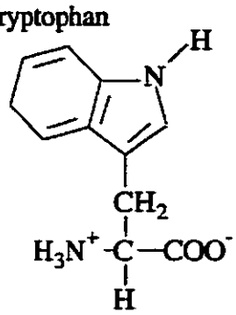

Tyrosine

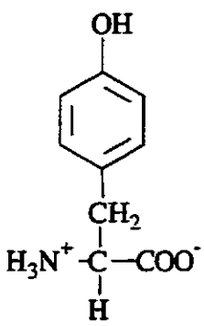

2,3-dihyroxyphenylalanine
(dopa)

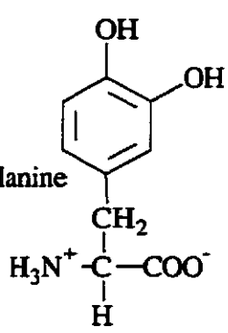

ACIDIC AMINO ACIDS

Aspartic Acid

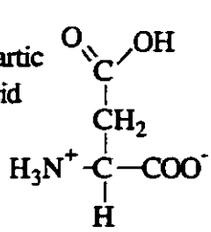

Asparagine

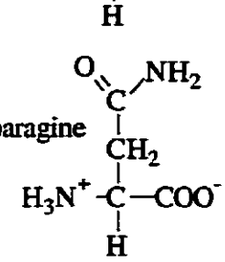

Glutamic Acid

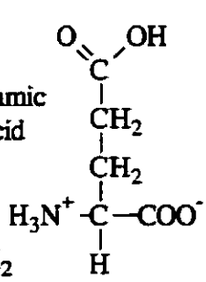

Glutamine

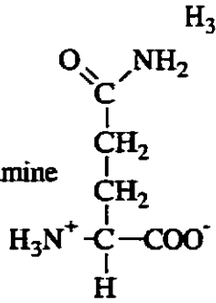

BASIC AMINO ACIDS

Histidine

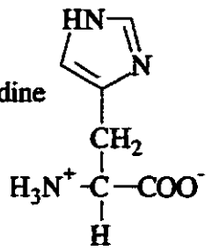

Arginine

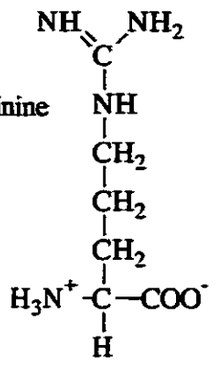

PEPTIDES

Glycylasparagine
(gly-asn)

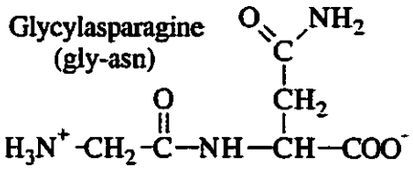

Glycyl-leucine
(gly-leu)

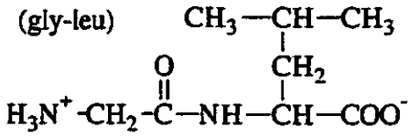

Glycylvaline
(gly-val)

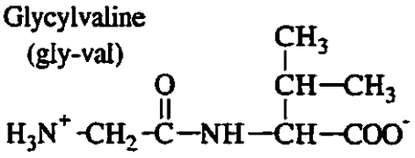

Diketopiperazine
(Cyclic gly-gly)

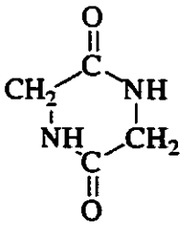

Glycylglycine
(gly-gly)

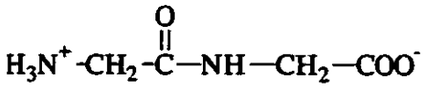

Glycylglycylglycine
(gly-gly-gly)

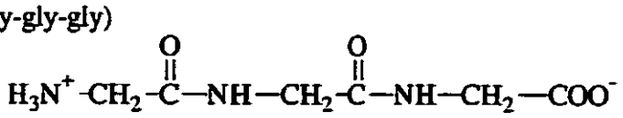

REFERENCES

Albert H. J. and Wood R. H. (1984) High-precision flow densimeter for fluids at temperatures to 700 K and pressures to 40 MPa. *Rev Sci. Instrum.* **55**, 589-593.

Amend J. P. and Helgeson H. C. (1997a) Calculation of the standard molal thermodynamic properties of aqueous biomolecules at elevated temperatures and pressures Part 1. L-α-amino acids. *J. Chem. Soc. Faraday Trans.* **93**, 1927-1941.

Amend J. P. and Helgeson H. C. (1997b) Group additivity equations of state for calculating the standard molal thermodynamic properties of aqueous organic species at elevated temperatures and pressures. *Geochim. Cosmochim. Acta* **61**, 11-46.

Amend J. P. and Shock E. L. (1998) Energetics of amino acid synthesis in hyrothermal ecosystems. *Science* **281**, 1659-1662.

Anderson G. M. and Crerar D. A. (1993) *Thermodynamics in geochemistry: The equilibrium model* Oxford University Press, New York.

Ananthaswamy J. and Atkinson G. (1984) Thermodynamics of concentrated electrolyte mixtures. 4. Pitzer-Debye-Hückel limiting slopes for water from 0 to 100 °C and from 1 atm to 1 kbar. *J. Chem. Eng. Data* **29**, 81-87.

Aono S., Bryant F. O., and Adams M. W. W. (1989) A novel and remarkably thermostable ferredoxin from the hyperthermophilic archaebacterium pyrococcus furiosus. *J. Bacteriol.* **171**, 3433-3439.

Archer D. G. (1991) Thermodynamic properties of the NaBr + H_2O system. *J. Phys. Chem. Ref. Data* **20**, 509-555.

Archer D. G. (1992) Thermodynamic properties of the sodium chloride + water system. II. Thermodynamic properties of NaCl (aq), NaCl·$2H_2O$ (cr), and phase equilibria. *J. Phys. Chem. Ref. Data* **21**, 793-829.

Archer D. G. and Wang P. (1990) The dielectric constant of water and Debye-Hückel limiting law slopes. *J. Phys. Chem. Ref. Data* **19**, 371-411.

Arrhenius S. (1887) Über die Dissociation der in Wasser gelösten Stoffe. *Z. physik. Chem.* **1**, 631-648.

Bada J. L., Miller S. L., and Zhao M. (1995) The stability of amino acids at submarine hydrothermal vent temperatures. *Origins Life Evol. Biosphere* **25**, 111-118.

Baes C. F. and Mesmer R. E. (1976) *The hydrolysis of cations.* Wiley-Interscience, New York.

Baross J. A. and Deming J. W. (1995) *Microbiology of deep sea hydrothermal vent environments* vol 1. Plenum, New York.

Barloss J. A. and Hoffman S. E. (1985) Submarine hydrothermal vents and associated gradient environments as sites for the origin of life. *Origins of Life* **15**, 327-345.

Biggerstaff D. R., White D. E., and Wood R. H. (1985) Heat capacities of aqueous argon from 306 to 578 K. *J. Phys. Chem.* **89**, 4378-4381.

Biggerstaff D. R. and Wood R. H. (1988a) Apparent molar volumes of aqueous argon, ethylene, and xenon from 300 to 716 K. *J. Phys. Chem.* **92**, 1988-1994.

Biggerstaff D. R. and Wood R. H. (1988b) Apparent molar heat capacities of aqueous argon, ethylene, and xenon at temperatures up to 720 K and pressures to 33 MPa. *J. Phys. Chem.* **92**, 1994-2000.

Born M. (1920) Volumen und hydratationswärm der ionen. *Z. Phys.* **1**, 45-48.

Brown S. H. and Kelly R. M. (1989) Cultivation techniques for hyperthermophilic archaebacteria: Continuous culture of Pyrococcus furiosus at temperatures near 100 °C. *Appl. Environ. Microbiol.* **55**, 2086-2088.

Burggraf S., Jannasch H. W., Nicolaus B., and Stetter K. O. (1990) Archaeoglobus profundus sp.nov., represents a new species within the sulfate-reducing archaebacteria. *Syst. Appl. Microbiol.* **13**, 24-28.

Cabani S., Conti G., Matteoli E., and Tiné M. R. (1981) Volumetric properties of amphionic molecules in water. *J. Chem. Soc. Faraday Trans.* 1 **77**, 2385-2394.

Chalikian T. V., Sarazyan A. P., Funck T., and Breslauer K. J. (1994) Partial molar volumes, expansibilities, adn compressibilities of oligoglycines in aqueous solutions at 18-55 °C. *Biopolymers* **34**, 541-553.

Chen C.-T., Emmett R. T., and Millero F. J. (1977) The apparent molal volumes of aqueous solutions of NaCl, KCl, $MgCl_2$, Na_2SO_4, and $MgSO_4$ from 0 to 1000 bars at 0, 25, and 50 °C. *J. Chem. Eng. Data* **22**, 201-207.

Chen C.-T. and Millero F. J. (1977) The volume and compressibility change for the formation of the $LaSO_4^+$ ion pair at 25 °C. *J. Sol. Chem.* **6**, 589-607.

Chiu H-C (1997) Stable baseline correction of digital strong-motion data. *Bull. Seism. Soc. Am.* **87**, 932-944.

Clifton D. K. and Steiner R. A. (1983) Cycle detection: A technique for estimating the frequency and amplitude of episodic fluctuations in blood hormone and substrate concentrations. *Endocrinology* **112**, 1057-1064.

Connaughton L. M., Hershey J. P., and Millero F. J. (1986) PVT properties of concentrated aqueous electrolytes: V. Densities and apparent molal volumes of the four major sea salts from dilute solution to saturation and from 0 to 100 °C. *J. Sol. Chem.* **15**, 989-1002.

Corliss J. B., Baross J. A., and Hoffman S. E. (1981) An hyothesis concerning the relationship between submarine hot springs and the origin of life on earth. Proceedings 26th International Geological Conference, *Oceanologica Acta* **4**, 59-69.

Debye P. and Hückel E. (1923) The theory of electrolytes. I. Lowering the freezing point and related phenomena. *Physik. Z.* **24**, 185-206.

Debye P. and Hückel E. (1924) Remarks on a theorem on the cataphorical migration velocity of suspended particles. *Physik. Z.* **25**, 49-52.

Desnoyers J. E., DeVisser C., Perron G., and Picker P. (1976) Reexamination of the heat capacities obtained by flow microcalorimetry. Recomendation for the use of a chemical standard. *J. Sol. Chem.* **5**, 605-616.

Dessauges G., Miljevic N., and Van Hook W. A. (1980) Isotope effects in aqueous systems. 9. Partial molar volumes af NaCl/H_2O and NaCl/D_2O solutions at 15, 30, and 45 °C. *J. Phys. Chem.* **84**, 2587-2595.

DiPaola G. and Belleau B. (1978) Apparent molal heat capacities and volumes of amino acids in aqueous polyol solutions. *Can. J. Chem.* **56**, 1827-1831.

Drude P. and Nernst W. (1894) Über Elektrostriktion durch freie Ionen. *Z. Phys. Chem.* **15**, 79-85.

Duke M. M., Hakin A. W., McKay R. M., and Preuss K. E. (1994) The volumetric and thermochemical properties of aqueous solutions of L-valine, L-leucine, and L-isoleucine at 288.15, 298.15, 313.15, and 328.15 K. *Can. J. Chem.* **72**, 1489-1494.

Dunn L. A. (1968) Apparent molar volumes of elevtrolytes. III. Some 1-1 and 2-1 electrolytes in aqueous solution at 0, 5, 15, 35, 45, 55, and 65°C. *Trans. Faraday Soc.* **64**, 2951-2961.

Fay D. P. and Purdie N. (1969) Calorimetric determination of the heats of complexation of the lanthanide monosulphates $LnSO_4^+$. *J. Phys. Chem.* **73**, 3462-3467.

Fay D. P. and Purdie N. (1970) Ultrasonic absorption in aqueous salts of the lanthanides. III. Temperature dependence of $LnSO_4$ complexation. *J. Phys. Chem.* **74**, 1160-1166.

Farrow M. F. and Purdie N. (1973) The conductance of lanthanide (III) sulphate solutions in D_2O. *J. Sol. Chem.* **2**, 503-511.

Fisher F. H. and Davis D. F. (1967) Effect of pressure on the dissociation of the $(LaSO_4)^+$ complex ion. *J. Phys. Chem.* **71**, 819-822.

Güntelberg E. (1926) Untersuchungen über Ioneninteraktion. *Z. Phys. Chem.* **123**, 199-247.

Gurley L. R., Valdez J. G., Spall W. D., Smith B. F., and Gillette D. D. (1991) Proteins in the fossil bone of the dinosaur, Seismosaurus. *J. of Protein Chem.* **10**, 75-90.

Haberstroth P. R. and Karl D. M. (1989) Dissolved free amino acids in hydrothermal vent habitats of the Guaymas Basin. *Geochim. Cosmochim. Acta* **53**, 2937-2945.

Hakin A. W. and Beswick C. L. (1991) Single-ion enthalpies and entropies of transfer from water to aqueous urea solutions at 298.15 K. *Can. J. Chem.* **70**, 1666-1670.

Hakin A. W., Duke M. M., Klassen S. A., McKay R. M., and Preuss K. E. (1994a) Apparent molar heat capacities and volumes of some aqueous solutions of aliphatic amino acids at 288.15, 298.15, 313.15, and 328.15 K. *Can. J. Chem.* **72**, 362-368.

Hakin A. W., Duke M. M., Marty J. L., and Preuss K. E. (1994b) Some thermodynamic properties of aqueous amino acid systems at 288.15, 298.15, 313.15, and 328.15 K: Group additivity analyses of standard-state volumes and heat capacities. *J. Chem. Soc. Faraday Trans.* **90**, 2027-2035.

Hakin A. W., Duke M. M., Groft L. L., Marty J. L., and Rushfeldt M. L. (1995) Calorimetric investigations of aqueous amino acid and dipeptide systems from 288.15 to 328.15 K. *Can. J. Chem.* **73**, 725-734.

Hakin A. W., Copeland A. K., Liu J. L., Marriott R. A., and Preuss K. E. (1997) Densities, apparent molar volumes, and apparent molar heat capacities of l-arginine, l-proline, and d,l-methionine in water at 288.15, 298.15, 313.15, and 328.15 K. *J. Chem. Eng. Data* **42**, 84-89.

Hakin A. W., Daisley D. C., Delgado L., Liu J. L., Marriott R. A., Marty J. L., and Tompkins G. (1998) Volumetric properties of glycine in water at elevated temperatures and pressures measured with a new optically driven vibrating-tube densimeter. *J. Chem. Thermodyn.* **30**, 583-606.

Hakin A. W., Liu J. L., and Marriott R. A. (1999a) Investigation of the elevated temperature and pressure volumetric surfaces of L-alanine and NaBr in water. In preparation.

Hakin A. W., Liu J. L., Kowalchuck M., and Cavilla B. (1999b) Thermodynamics of protein model compounds: A thermochemical and volumetric investigation of the thermodynamics of several cyclic dipeptides in water. In preparation.

Helgeson H. C. and Kirkham D. H. (1974) Theoretical prediction of the thermodynamic behavior of aqueous electrolytes at high pressures and temperatures: I. Summary of the thermodynamic/electrostatic properties of the solvent. *Am. J. Sci.* **274**, 1089-1198.

Helgeson H. C. and Kirkham D. H. (1976) Theoretical prediction of the thermodynamic properties of aqueous electrolytes at high pressures and temperatures: III. Equation of state for aqueous species at infinite dilution. *Am. J. Sci.* **276**, 97-240.

Helgeson H. C., Kirkham D. H., and Flowers G. C. (1981) Theoretical prediction of the thermodynamic properties of aqueous electrolytes at high pressures and temperatures: IV. Calculation of activity coefficients, osmotic coefficients, and apparent molal and standard and relative partial molal properties to 600°C and 5 kb. *Am. J. Sci.* **281**, 1249-1516.

Hill P. G. (1990) A unified fundamental equation for the thermodynamic properties of H_2O. *J. Phys. Chem. Ref. Data* **19**, 1233-1275.

Hill T. L. (1960) *An introduction to statistical thermodynamics*. Addison-Wesley, Reading, MA.

Hovey J. K. (1988) *Thermodynamics of aqueous solutions*. Ph.D. Thesis. University of Alberta, Edmonton, Aberta, Canada.

Hovey J. K., Hepler L. G., and Tremaine P. R. (1988) Thermodynamics of aqueous EDTA systems: Apparent and partial molar heat capacities and volumes of aqueous $EDTA^{4-}$, $HEDTA^{3-}$, H_2EDTA^{2-}, $NaEDTA^{3-}$, and $KEDTA^{3-}$ at 25°C. Relaxation

effects in mixed aqueous electrolyte solutions and calculations of temperature dependent equalibrium constants. *Can. J. Chem.* **66**, 881-896.

Iqbal M. and Verrall R. E. (1989) Apparent molar volume and adiabatic compressibility studies of aqueous solutions of some drug compounds at 25°C. *Can. J. Chem.* **67**, 727-735.

Izatt R. M., Eatough D., Christensen J. J., and Bartholomew C. H. (1969) Calorimetrically determined log K, ΔH^o, and ΔS^o values for the interaction of sulphate ion with several bi- and ter-valent metal ions. *J. Chem Soc. A Inorg. Phys. Chem.*, 47-53.

Johnson J. W. and Norton D. (1991) Critical phenomena in hydrothermal systems: State, thermodynamic, electrostatic, and transport properties of H_2O in the critical region. *Am. J. Sci.* **291**, 541-648.

Jolicoeur C. and Boileau J. (1978) Apparent molal volumes and heat capacities of low molecular weight peptides in water at 25 °C. *Can J. Chem.* **56**, 2707-2713.

Jolicoeur C., Reidl B., Desrochers D., Lemelin L. L., Zamojska R., and Enea O. (1986) Solvation of amino acid residues in water and urea-water mixtures: Volumes and heat capacities of 20 amino acids in water and 8 molar urea at 25 °C. *J. Sol. Chem.* **15**, 109-128.

Kell G. S. (1967) Precise representation of volume properties of water at one atmosphere. *J. Chem. Eng. Data* **12**, 66-69.

Kell G. S. (1972) *Water - a comprehensive treatise.* Vol. 1 page 363 Plenum, New York.

Kharakoz D. P. (1989) Volumetric properties of proteins and their analogs in diluted water solutions 1. Partial volumes of amino acids at 15-55 °C. *Biophys. Chem.* **34**, 115-125.

Kikuchi M., Sakurai M., and Nitta K. (1995) Partial molar volumes and adiabatic compressibilities of amino acids in dilute aqueous solutions at 5, 15, 25, 35, and 45 °C. *J. Chem. Eng. Data* **40**, 935-942.

Kohara M., Gamo T., Tanagawa H., and Kobayashi (1997) Stability of amino acids in simulated hydrothermal vent environments. *Chem. Lett.* **10**, 1053-1054.

Kratky O., Leopold H., and Stabinger H. (1969) Dichtemessungen an Flüssigkeiten und glassen auf 10^{-6} g/cm^3 pröparat volumen. *Z.Angew. Phys.* **27**, 273-277.

Leipziger F. D. and Roberts J. E. (1958) The apparent molar refraction of some aqueous rare earth nitrates. *J. Phys. Chem.* **62**, 1014-1016.

Lombardi D. R., Wang C., Sun B., Fountain A. W. III, Vickers T. J., Mann C. K., Reich F. R., Douglas J. G., Crawford B. A., and Kohlasch F. L. (1994) Quantitative and qualitative analysis of some inorganic compounds by Raman spectroscopy. *Appl. Spectroscopy* **48**, 875-883.

Lo Surdo A., Alzola E. M., and Millero F. J. (1982) The (p,V,T) properties of concentrated aqueous electrolytes I. Densities and apparent molar volumes of NaCl, Na_2SO_4, $MgCl_2$, and $MgSO_4$ solutions from 0.1 mol kg^{-1} to saturation and from 273.15 to 323.15 K. *J. Chem. Thermodyn.* **14**, 649-662.

Marcus Y. (1991) Thermodynamics of solvation ions. Part 5.-Gibbs free energy of hydration at 298.15 K. *J. Chem. Soc. Faraday Trans.* **87**, 2995-2999.

Marriott R. A., Hakin A. W., and Liu J. L. (1998) Modeling of thermodynamic properties of amino acids and peptides using additivity and HKF theory. *J. Sol. Chem.* **27**, 771-802.

Marsh K. N. and O'Hare P. A. G. (1994) *Solution calorimetry. Experimental thermodynamics Vol IV.* Blackwell Scientific, Oxford.

Marshall L. W. (1994) Hydrothermal synthesis of amino acids. *Geochim. Cosmochim. Acta* **58**, 2099-2106.

Majer V., Crovetto R., and Wood R. H. (1991) A new version of vibrating-tube flow densimeter for measurements at temperatures up to 730 K. *J. Chem. Thermodyn.* **23**, 333-344.

Millero F. J. (1970) The apparent and partial molal volume of aqueous sodium chloride solutions at various temperatures. *J. Phys. Chem.* **74**, 356-362.

Millero F. J. (1971) The molal volumes of electrolytes. *Chem. Rev.* **71**, 147-176.

Millero F. J., Lo Surdo A., and Shin C. (1978) The apparent molar volumes and adiabatic compressibilities of aqueous amino acids *J. Phys. Chem.* **82**, 784-792.

Miodushi T. (1998) Identification of saturating solid phases in aqueous solutions of lanthanide(III) sulfates from the solubility data. *Chem. Anal. (Warsaw)* **43**, 457-462.

Mishra A. K. and Ahluwalia J. C. (1984) Apparent molal volumes of amino acids, N-acetylamino acids, and peptides in aqueous solutions. *J. Phys. Chem.* **88**, 86-92.

Okabe N., Sagimori Y., and Hokaze M. (1991) Binding characteristics of DOPA (3,4-dihydroxyphenylalanine) and its metabolites to bovine serum albumin measured by ultrafiltration technique. *Chem. Pharm. Bull.* **39**, 2115-2216.

Olofsson I. V. (1979) Apparent molar heat capacities and volumes of aqueous NaCl, KCl, and KNO_3 at 298.15 K. Comparison of Picker flow calorimeter with other calorimeters. *J. Chem. Thermodyn.* **11**, 1005-1014.

O'Sullivan F. (1986) A statistical perspective on III-posed inverse problems. *Statistical Science* **1**, 502-527.

Perron G., Fortier J.-L., and Desnoyers J. E. (1975) The apparent molar heat capacities and volumes of aqueous NaCl from 0.1 to 3 mol kg^{-1} in the temperature range 274.65 to 318.15 K. *J. Chem. Thermodyn.* **7**, 1177-1184.

Phillips A. J. and Hamilton P. A. (1996) Improved detection limits in fourier transform spectroscopy from a maximum entropy approach to baseline estimation. *Anal. Chem.* **68**, 4020-4025.

Picker P., Tremblay E., and Jolicoeur C. (1974) High-precision digital readout flow densimeter for liquids. *J. Sol. Chem.* **3**, 377-384.

Picker P., Leduc P.-A., Philip P. R., and Desnoyers J. E. (1971) Heat capacity of solutions by flow microcalorimetry. *J. Chem. Thermodyn.* **3**, 631-642.

Pitzer K. S. and Brewer L. (1961) Revised edition of *Thermodynamics* by G. N. Lewis and M. Randall, 2nd ed. McGraw-Hill, New York.

Pitzer K. S. (1979) Theory: ion interaction approach, in Pytkowicz (1979)

Pitzer K. S. ed. (1991) *Activity coefficients in electrolyte solutions.* vol 2. CRC Press, Boca Raton.

Pouchert C. J. (1981) *The Aldrich library of infrared spectra* 3rd. edition. Aldrich Chemical Co. Inc., Milwaukee, Wis..

Pouchert C. J. and Cambell J. R. (1974) *The Aldrich library of NMR spectra* vol 3. Aldrich Chemical Co. Inc., Milwaukee, Wis..

Puigdomench I., Rard J. A., Plyasunov A. V., and Grenthe I. (1997) Temperature corrections to thermodynamic data, in: *Modelling in aquatic chemistry*, Nuclear Energy Agency, Organisation for Economic Co-operation and Development, Paris, France.

Pytkowicz R. M ed. (1979) *Activity coefficients in electrolyte solutions.* vol 1. CRC Press, Boca Raton.

Rao G. N., Kumari V. M. Ch. V., Ramana K. V., and Rao R. S. (1989) Computer-augmented modelling of complexes of amino acids in aquo-organic mixtures: Part II-acedo-basic equalibria of L-alanine and L-dopa in aquo-DMF media. *Indian J. Chem.* **28A**, 709-712.

Rard J. A. (1988) Aqueous solubilities of praseodymium, europium, and lutetium sulfates. *J. Sol. Chem.* **17**, 499-517.

Rard J. A. (1996) Isopiestic determination of the osmotic coefficients of $Lu_2(SO_4)_3$(aq) and H_2SO_4(aq) at the termperature T=298.15 K, and review and revision of the thermodynamic properties of $Lu_2(SO_4)_3$(aq) and $Lu_2(SO_4)_3 \cdot 8H_2O$(cr). *J. Chem. Thermodyn.***28**, 83-110.

Rard J. A. and Spedding F. H. (1982) Isopiestic determination fo the activity coefficients of some aqueous rare-earth electrolyte solutions at 25 °C. 6. $Eu(NO_3)_3$, $Y(NO_3)_3$, and YCl_3. *J. Chem. Eng. Data* **27**, 454-461.

Robinson R. A. and Stokes R. H. (1965) *Electrolyte solutions*. Butterworths, London.

Shock E. L. (1990) Do amino acids equilibriate in hydrothermal fluids? *Geochim. Cosmochim. Acta* **54**, 1185-1189.

Shock E. L. (1992) Stability of peptides in high temperature aqueous solutions. *Geochim. Cosmochim. Acta* **56**, 3481-3491.

Shock E. L. (1993) Hydrothermal organic synthesis experiment. *Origins Life Evol. Biosphere* **22**, 135-146.

Shock E. L. and Helgeson H. C. (1990) Calculation of the thermodynamic and transport properties of aqueous species at high pressures and temperatures: Standard partial molal properties of organic species. *Geochim. Cosmochim. Acta* **54**, 915-945.

Shock E. L., Helgeson H. C., and Sverjensky D. A. (1989) Calculation of the thermodynamic and transport properties of aqueous species at high pressures and temperatures: Standard partial molal properties of inorganic neutral species. *Geochim. Cosmochim. Acta* **53**, 2157-2183.

Shock E. L., Oelkers E. H., Johnson J. W., Sverjensky D. A., and Helgeson H. C. (1992) Calculation of the thermodynamic properties of aqueous species at high pressures and temperatures: Effective electrostatic radii, dissociation constants, and standard partial molar properties to 1000 °C and 5 kb. *J. Chem. Soc. Faraday Trans.* **88**, 803-826.

Simoneit B. R. T., Summons R. E., and Jahnke L. L. (1998) Biomarkers as tracers for life on early Earth and Mars. *Origins of Life Evol. Biosphere* **28**, 475-483.

Simonson J. M., Oakes C. S., and Bodnar R. J. (1994) Densities of NaCl (aq) to the temperature 523 K at pressures to 40 MPa measured with a new vibrating-tube densimeter. *J. Chem. Thermodyn.* **26**, 345-359.

Singh P.P, Woolley E. M., McKurdy K. G., and Hepler L. G. (1976) Heat capacities of aqueous electrolytes: eight 1:1 electrolytes and ΔC_p^o for ionization of water at 298 K. *Can. J. Chem.* **54**, 3315-3318.

Spedding F. H. and Jaffe S. (1954) Conductances, solubilities and ionization constants of some rare earth sulphates in aqueous solutions at 25°C. *J. Amer. Chem. Soc.* **76**, 882-884.

Spedding F. H., Cullen P. F., and Habenschuss A. (1974) Apparent molal volumes of some dilute aqueous rare earth salt solutions at 25 °. *J. Phys. Chem.* **78**, 1106-1110.

Spedding F. H., Pikal M. J., and Ayers B. O. (1966) Apparent molar volumes of some aqueous rare earth chloride and nitrate solutions at 25 °. *J. Phys. Chem.* **70**, 2440-2449.

Spedding F. H., Shiers L. E., Brown M. A., Baker J. L., Guitierrez L., McDowell L. S., and Habenschuss A. (1975a) Densities and apparent molar volumes of some aqueous rare earth solutions at 25 °C. III. Rare earth nitrates. *J. Phys. Chem.* 79, 1087-1096.

Spedding F. H., Seager V. W., Gray K. A., Boneau P. K., Brown M. A., DeKock C. W., Baker J. L., Shiers L. E., Weber H. O., and Habenschuss A. (1975b) Densities and apparent molar volumes of some aqueous rare earth solutions at 25°C. I. Rare earth chlorides. *J. Chem. Eng. Data* **20**, 72-81.

Spitzer J. J., Olofsson I. V., Singh P. P., and Hepler L. G. (1979) Apparent molar heat capacities and volumes of aqueous electrolytes at 25 °C: $LaCl_3$, $K_3(CN)_6$, and $K_4Fe(CN)_6$. *Can J. Chem.* **57**, 2798-2803.

Strunk D. H., Hamman J. W., and Timmel B. M. (1979) Determination of proof of distilled alcoholic beverages, using an oscillating U-tube density meter. *J. Assoc. Off. Anal. Chem.* **62**, 653-658.

Tammann G. (1895) Über die Volumänderungen bei der Neutralisation verdünnter Lösungen *Z. Phys. Chem.* **16**, 91-96.

Tanger J. C. and Helgeson H. C. (1988) Calculation of the thermodynamics and transport properties of aqueous species at high pressures and temperatures. Revised equations of state for the standard partial molar properties of ions and electrolytes. *Amer. Jour. Sci.* **288**, 19-98.

Vaslow R. (1966) The apparent molal volumes of the alkali metal chlorides in aqueous solution and evidence for salt-induced structure transitions. *J. Phys. Chem.* **70**, 2286-2294.

Wadi R. K. and Goyal R. K. (1992) Temperature dependence of apparent molar volumes and viscosity B-coefficients of amino acids in aqueous potassium thiocyanate solutions from 15 to 35 °C. *J. Solution Chem.* **21**, 163-170.

Weast R. C., Ed. (1970) *Handbook of Chemistry and Physics.* The Chemical Rubber Co., Cleveland, Ohio.

Webb T. J. (1926) The free energy of hydration of ions and the electrostriction of the solvent. *J. Am. Chem. Soc.* **48**, 2589-2603.

Woolley E. M and Hepler L. G. (1977) Heat capacities of weak electrolytes and ion association reactions: method and application to aqueous $MgSO_4$ and HIO_3 at 298 K. *Can. J. Chem.* **55**, 158-163.

Xiao C. and Tremaine R. (1996) Apparent molar heat capacities and volumes of $LaCl_3$ (aq), $La(ClO_4)_3$ (aq), and $Gd(ClO_4)_3$ (aq) between the temperatures 283 K and 328 K. *J. Chem. Thermodyn.* **28**, 43-66.

Xiao C. and Tremaine R. (1997) The thermodynamics of aqueous trivalent rare earth elements. Apparent molar heat capacities and volumes of $Nd(ClO_4)_3$ (aq), $Eu(ClO_4)_3$ (aq), $Er(ClO_4)_3$ (aq), and $Yb(ClO_4)_3$ (aq) from the temperatures 283 K to 328 K. *J. Chem. Thermodyn.* **29**, 827-852.

Young T. F. and Smith M. B. (1954) Thermodynamic properties of mixtures of electrolytes in aqueous solutions. *J. Phys. Chem.* **58**, 716-724.

Zana R. and Yeager E. (1966) Determination of ionic partial molar volumes from ionic vibration potentials. *J. Phys. Chem.* **70**, 954-956.

Zana R. and Yeager E. (1967) Ultrasonic vibration potentials and their use in the determination of ionic partial molal volumes. *J. Phys. Chem.* **71**, 521-536.